Predictive Control, Estimation and Sensor Placement of Large-Scale Transport-Reaction Systems

by

Lu Zhang

A thesis submitted in partial fulfillment of the requirements for the degree of

Doctor of Philosophy

in

Process Control

Department of Chemical and Materials Engineering

University of Alberta

Abstract

Advanced process control and monitoring rely on the accurate description of complex processes and their dynamic behaviors. Typically, numerous industrial processes are characterized by either partial differential equations (PDEs) or ordinary differential equations (ODEs), depending on whether their dynamics evolve spatiotemporally or temporally. Consequently, these processes are classified as distributed parameter systems (DPS) or lumped parameter systems (LPS). The underlying fact is that most of the large-scale chemical and petrochemical processes are influenced by both temporal and spatial factors, and the existence of the spatial variable in the mathematical model rises challenges in the controller and estimator designs. The focus of this thesis is to develop advanced controllers and observers for the improvement of control performance and reliable monitoring realizations for large-scale DPS processes.

Continuous-time DPS can be considered an important representation of complex industrial processes, while it is more valuable to obtain discrete-time models for the design of controllers and observers when it comes to practical implementation in digital devices. This thesis provides a discrete-time infinite-dimensional modelling framework specifically designed for large-scale DPS while preserving essential model properties (such as stability, observability, input-output mapping and etc.), where no model spatial discretization or spatial model reduction is required.

Considering the inherent complexity and numerous constraints involved in chemical and petrochemical industry processes, the utilization of model predictive control (MPC) offers significant advantages. This thesis introduces an MPC design based on developed discrete-time infinite-dimensional models, aiming to achieve satisfac-

tory performance while handling input and output constraints and addressing the constrained stabilization of disturbed DPS. Additionally, a tracking MPC scheme is formulated for a class of large-scale DPS in a late lumping manner, with the objective of achieving the desired target set-points while accommodating system constraints. Furthermore, to address scenarios where an accurate model of the underlying dynamical system is unavailable, a robust MPC scheme is proposed, incorporating multiple DPS models to ensure system stabilization.

Due to the difficulties in obtaining state information in DPS, state estimation techniques are employed to incorporate controller design. To estimate the spatiotemporal state, the discrete-time Luenberger observer and Kalman filter are proposed for the considered large-scale DPS. To account for the constrained actuator and parameter in the estimation, moving horizon estimation (MHE) is developed by extending the MHE theory of LPS. Additionally, the distributed nature of DPS introduces complexity in terms of sensor placement. This thesis explores the sensor location selection problem along with estimator design accounting for the delayed measurements by minimizing the variance of estimation error.

The effectiveness of the developed discrete-time controllers and estimators are demonstrated by numerical simulations of various large-scale DPS, including tubular reactor, pipeline system, and continuous pulp digester.

Preface

This thesis is an original work conducted by Lu Zhang under the supervision of Prof. Stevan Dubljevic and Prof. Charles Robert (Bob) Koch. Portions of the thesis have been published in peer-reviewed journals.

- Chapter 2 of this thesis has been published as: L. Zhang, J. Xie, C.R. Koch, and S. Dubljevic. "Model predictive control of jacket tubular reactors with a reversible exothermic reaction." *Industrial & Engineering Chemistry Research*, 59, no. 42: 18921-18936, 2020. I was responsible for the formulation, simulation, and analysis as well as the manuscript composition. J. Xie was responsible for the formulation, simulation, and analysis. C. R. Koch and S. Dubljevic were the supervisory authors and were involved with concept formation and manuscript composition.

- Chapter 3 of this thesis has been submitted as: L. Zhang, J. Xie, and S. Dubljevic. "Tracking model predictive control and moving horizon estimation design of distributed parameter pipeline systems." *Computers & Chemical Engineering*, 2023. I was responsible for the formulation, simulation, and analysis as well as the manuscript composition. J. Xie was responsible for the formulation and analysis. S. Dubljevic was the supervisory author and was involved with concept formation and manuscript composition.

- Chapter 4 of this thesis has been published as: L. Zhang, J. Xie, and S. Dubljevic. "Dynamic modeling and model predictive control of a continuous pulp digester." *AIChE Journal*, 68, no. 3: e17534, 2022. I was responsible for the formulation, simulation, and analysis as well as the manuscript composition. J. Xie was responsible for the formulation and analysis. S. Dubljevic was the

supervisory author and was involved with concept formation and manuscript composition.

- Chapter 5 of this thesis has been published as: L. Zhang, J. Xie, and S. Dubljevic, 2022. "Sensor location selection for continuous pulp digesters with delayed measurements." *AIChE Journal*, 68(12), p.e17862, 2022. I was responsible for the formulation, simulation, and analysis as well as the manuscript composition. J. Xie was responsible for the formulation and analysis. S. Dubljevic was the supervisory author and was involved with concept formation and manuscript composition.

- Chapter 6 of this thesis will be submitted as: L. Zhang, J. Xie, S. Dubljevic. "A robust model predictive control strategy for multi-model infinite-dimensional transport-reaction systems". I was responsible for the formulation, simulation, and analysis as well as the manuscript composition. J. Xie was responsible for the formulation and analysis. S. Dubljevic was the supervisory author and was involved with concept formation and manuscript composition.

To my parents, for their love, encouragement and support.

Acknowledgements

With my deepest appreciation, I acknowledge my supervisor, Prof. Stevan Dubljevic, for his support, inspiration, and intellectual guidance throughout my graduate studies. I express my gratitude to Prof. Dubljevic for providing me with the valuable opportunity to join the DPS group, and giving me consistent motivation and encouragement. I would also like to acknowledge my co-supervisor Prof. Charles Robert (Bob) Koch. I sincerely appreciate the help and support from Prof. Koch and the time that he invested in guiding my research and revising the papers. I am very fortunate to have them as the supervisors of my doctoral studies. I am truly thankful for their guidance, help, support and patience, without which this thesis would not have been possible.

Besides my supervisors, I would like to thank my committee members Prof. Zukui Li, Prof. Jinfeng Liu, and Prof. Milana Trifkovic for their participation in my doctoral examination, and their valuable comments and corrections of my thesis.

I would like to express my deepest gratitude to Dr. Junyao for mentoring, engaging in discussions, and providing numerous valuable comments. I would also like to extend my thanks to my fellow friends in the DPS Group, especially Dr. Guilherme and Dr. Jukka-Pekka, for their guidance and fruitful discussions. Additionally, I am grateful to my group of friends on Campus for contributing to making my graduate student life a truly enriching and enjoyable experience. I sincerely wish you all the best future and success in your career development.

I would like to thank the Natural Sciences and Engineering Research Council of Canada (NSERC) and Alberta Upstream Petroleum Research Fund (AUPRF) for the financial support, and the department of Chemical and Materials Engineering at the University of Alberta for providing a pleasant environment to pursue my PhD.

To my beloved family, I am truly grateful for the boundless love, support, and

profound understanding. I extend my heartfelt gratitude to my father, Jingwu, and my mother, Nan, for their unwavering commitment to supporting me in every decision I have made throughout my life. No matter what I do, they are always proud of me and give me the courage to pursue my dreams. My deep appreciation also goes to my boyfriend for his understanding and support, and constant encouragement in becoming the best version of myself. I would also like to express my deepest gratitude to my friend Weiwei for encouraging me spiritually in times of happiness and sadness.

Contents

List of Tables

List of Figures

Chapter 1

Introduction

In this chapter, the motivations of this thesis are introduced first. Subsequently, existing works on dynamic modeling, optimal control, and estimation of DPSs are briefly reviewed and summarized. Lastly, the research contributions and outline of the thesis are provided.

1.1 Motivation

In industrial practice, especially in chemical and petrochemical engineering processes, the states, inputs, and outputs of a mathematical model that describe the dynamic systems may depend on both temporal and spatial variables. Among these models, PDEs are commonly employed to capture transport (transport-reaction) phenomena, offering a more precise representation by considering temporal and spatial derivatives. Research in this field remains active, combining classical mathematical analysis techniques with modern computational techniques to facilitate process simulation and numerical studies of complex problems [5, 6, 7].

Tubular reactors encompass a broad range of processes within the fields of chemical and biochemical engineering, as discussed in references [8, 9, 10]. For example, there exist various simple and/or complex reversible reactions in tubular reactor systems in the chemical and biological processes, such as polymerization and isomerization, and general esterification. Another representative application is the continuous pulp digester, which is a large vertical tubular reactor in which wood chips react with an aqueous solution, referred to as white liquor, to remove the lignin from the cellulose fibers. The product of the digesting process is cellulose fibers, or pulp, which are

used to make paper products. The reacting flow dynamics in the above industrial processes are usually described by nonlinear PDEs derived from conservation laws, originating from mass and energy balances, and which belong to the class of DPS.

As one of the most representative and cost-effective ways for material transportation, pipelines have been widely utilized in the oil, gas and water distribution industry. Non-reacting flow dynamics in long-range pipeline systems can be also modelled as the DPS as their dynamics depend both on time and space. The real-time transient model, constructed based on the conservation of mass, momentum, and energy balance laws, has gained widespread utilization as a prominent example of first principle modelling [6], [11]. More specifically, it can be characterized by the Euler equations in one dimension, constituting a system of nonlinear coupled hyperbolic PDEs.

The majority of research has been conducted for the above industrial processes within the framework of continuous-time infinite-dimensional settings or discretizing the original PDEs to a set of ODEs. However, this raises concerns regarding the performance of controllers designed for continuous-time DPS when implemented numerically. Moreover, with the increasing utilization of digital technology in modern control systems, it becomes necessary to transform the overall system into a discrete version to enable controller implementation while ensuring the performance of discretization. In such cases, bilinear transform techniques can be employed to circumvent the need for repetitive and laborious derivations when similar results obtained for continuous systems are required for discrete systems [12]. Specifically, Cayley transformation has been widely utilized for establishing 1-1 correspondences of continuous-time and discrete-time PDE systems in terms of energy-preserving, reachability, stability, stabilizability, controllability and observability, and optimality [13, 14]. Motivated by this, in this thesis, the conversions of the continuous-time infinite-dimensional system representation to the discrete-time infinite-dimensional model for a class of complex DPS, are done by the application of Cayley-Tustin transformation.

Advanced process control, monitoring, and decision-making in the context of DPS usually require the advanced control realization which is usually constrained by physical limitations of well-built plants or natural limits on the actuator power. Among these, MPC is a representative algorithm used for synthesizing optimal control strategies. This approach involves solving an open-loop optimal control problem over a

finite horizon at each sampling instant. By utilizing an optimization algorithm, a sequence of optimal control moves is determined, and the first move in the sequence is applied to the process. The research area of MPC of linear and nonlinear LPS has flourished over the past decades [15, 16, 17, 18]. However, MPC design for complex large-scale infinite-dimensional systems has not been fully investigated. This thesis is devoted to exploring advanced controller design to improve the processes operations of the above DPS, accounting for distributed parameter nature for optimal process performance characteristics, and satisfying the constraints and/or limitations.

As the system state of DPS is distributed over a region in space and only a finite number of sensors can be installed, measurement of the entire state is never possible for systems described by PDE. In this case, state estimation is often necessary for control problems and/or for monitoring purposes. In addition, the knowledge of the system state variables might be limited by the time delay in obtaining the measurements, the disturbance corrupting the data, which leads to a more complex problem. Compared to LPS, it is more demanding for DPS settings to account for the effects that sensors or actuators have on spatially and time-varying states. Thus, the need arises to develop a range of state estimators that are specifically designed for infinite-dimensional systems in various scenarios. This thesis presents several observer designs based on extensions of Luenberger observer, Kalman filter, and moving horizon estimator theories, aiming to enhance control and monitoring performance for complex DPS in various scenarios within the framework of discrete-time infinite-dimensional systems.

Furthermore, practical applications often involve time-varying operating conditions. For instance, in a pipeline system, batch transportation introduces changes in several parameters of the mathematical model. Similarly, variations in the properties of wood entering the digester, such as softwood and hardwood, impact the parameters and operation of the continuous pulp digester system. In such cases, accurate model parameters are often unavailable or unknown, and hence a robust controller is typically required. To tackle this challenge, this thesis investigates a robust model predictive controller capable of handling the multi-model infinite-dimensional system and satisfying the system constraints.

1.2 Literature Review

1.2.1 Distributed parameter systems

The representation of systems using linear ODEs typically involves expressing them as a collection of n first-order differential equations, where the solution resides in the real-valued space $\mathbb{R}^n$. In contrast, DPS is characterized by PDEs, which can also be formulated in a similar manner. However, there is a notable distinction: the state space is no longer defined in $\mathbb{R}^n$ but expands to an infinite-dimensional Hilbert space. Likewise, the matrix A, which was previously used in the finite-dimensional case, is replaced by an operator that operates within this infinite-dimensional space. As a result, systems modeled with PDEs are often referred to as infinite-dimensional systems. The majority of DPS models can be derived from the first principles, which include conservation laws of continuity, momentum, and energy. Given these physical conservation laws, the well-defined inputs, states, and outputs can be identified with a corresponding physical meaning. For different purposes (such as state estimation or control), different types of inputs and outputs of interest can be considered. To complete a physical realization by DPS, corresponding boundary conditions (BCs) and initial conditions (ICs) need to be given.

Typical distributed parameter systems are characterized by prominent spatial variations along which temporal and spatial evolution of physical properties takes place. A general second-order DPS model is formulated as follows:

$$\frac{\partial^2 x(\zeta,t)}{\partial t^2} = f\left(x(\zeta,t), u(t), \frac{\partial x(\zeta,t)}{\partial \zeta}, \frac{\partial x(\zeta,t)}{\partial t}, \frac{\partial^2 x(\zeta,t)}{\partial t \partial \zeta}, \frac{\partial^2 x(\zeta,t)}{\partial \zeta^2}\right) \tag{1.1a}$$

$$y(t) = g(x(\zeta,t), u(t)) \tag{1.1b}$$

with initial condition and boundary conditions given as:

$$x(\zeta,0) = x_0(\zeta) \tag{1.2a}$$

$$\frac{\partial x(0,t)}{\partial \zeta} + qx(0,t) = 0 \tag{1.2b}$$

where $x(\zeta,t)$, $u(t)$ and $y(t)$ are the state, input and output of interest, and ζ and t stand for spatial coordinate and time. f and g are two nonlinear or linear functions of state x, input u, first-order spatial derivative of state $\frac{\partial x(\zeta,t)}{\partial \zeta}$ and second-order spatial

derivative of state $\frac{\partial^2 x(\zeta,t)}{\partial \zeta^2}$. In addition, $\frac{\partial x(\zeta,t)}{\partial t}$ represents temporal derivative of state and we assume $\frac{\partial^2 x(\zeta,t)}{\partial t \partial \zeta} = \frac{\partial^2 x(\zeta,t)}{\partial \zeta \partial t}$. In the formulation of LPS, there are no spatial derivative terms in Eq.(1.1a). The spatial characteristics make DPSs more difficult for control, estimation and stabilization realization, compared to LPSs.

As for the initial condition, it is provided as a spatial function given by Eq.(1.2a). In addition, a general mixd Robin boundary condition at $\zeta = 0$ is described as Eq.(1.2b), which is more physically realistic for in-situ processes. When the parameter $q = 0$, it can lead to the well-known Neumann boundary condition with flux of state equal to zero. In contrast, one attains the Dirichlet boundary condition when $x(0,t) = 0$.

To classify the above DPS model, one can arrange Eq.(1.1a) into the following expression:

$$A\frac{\partial^2 x(\zeta,t)}{\partial t^2} + 2B\frac{\partial^2 x(\zeta,t)}{\partial t \partial \zeta} + C\frac{\partial^2 x(\zeta,t)}{\partial \zeta^2} = F\left(x(\zeta,t), u(t), \frac{\partial x(\zeta,t)}{\partial \zeta}, \frac{\partial x(\zeta,t)}{\partial t}\right) \quad (1.3a)$$

Then, the above equation is referred as:

- Parabolic PDE, if $B^2 - AC = 0$, for reaction-diffusion and conduction problems.
- Hyperbolic PDE, if $B^2 - AC > 0$, for vibration and wave motion problems.
- Elliptic PDE, if $B^2 - AC < 0$, for steady-state, potential-type problems.

There is only a single state $x(\zeta,t)$ in the DPS Eq.(1.1a), and the state varies in one spatial dimension ζ. In real industrial processes, models often tend to be multi-states described, and states or BC are coupled, which poses a significant challenge in state estimation, control, and output regulation.

1.2.2 Discretization of distributed parameter systems

Continuous-time DPSs can envision as good representatives of complex industrial processes, while it is more practical and valuable for designers to obtain discrete-time models for the sake of digital controllers and observers design. Since most of the control systems used in industry are embedded control systems, it is quite common to implement discrete-time control strategies with just a digital-to-analog converter. Thus the discretization of a model before designing a controller is necessary. Hence,

this section will summarize a brief review of discretization methods for DPS and compare the pros and cons associated with different discretization techniques.

The finite difference method (FDM) is the most widely utilized approach for the discretization of PDE modelling, which is quite simple to understand and implement in a large class of PDE models in one dimensional. Forward Euler discretization (explicit Euler) and backward Euler discretization (implicit Euler) have a wide range of applications when it comes to FDM for PDEs. Both the explicit and implicit Euler discretization methods can be easily implemented on digital devices. However, explicit Euler discretization in space and in time is not numerically stable, while implicit Euler in both time and space is unconditionally numerically stable despite the original instability [19, 20]. Moreover, the implicit Euler discretization method might cause computation inefficiency and lead to the inversion of large matrices which may be typically ill-posed. Hence, some researchers apply explicit Euler in time and implicit Euler in space, which is computationally effective compared to implicit Euler both in time and space and is numerically stable if Lax conditions are satisfied. On the other hand, the obtained numerical model can only provide estimation of states at the spatial discretization points instead of spatial states between discretized points.

To address these, the finite element model (FEM) is proposed and applied in many engineering areas, which is suitable for numerical simulation of nontrivial structures or shapes [21]. With the rapid advances in computing technology, increasingly advanced grid techniques have been developed and applied for FEM computation with higher precision and efficiency while the computing time and storage requirement are very high. Since nontrivial geometries are not focused in this thesis proposal, FEM will not be of interest in this proposal.

Along this line, in order to ensure energy and guarantee structure preservation, a set of significant efforts were presented. In particular, the Cayley-Tustin time discretization framework was proposed by Havu, V. and Malinen, J [13, 14], which was demonstrated to be a symmetric and symplectic integration scheme. Another novel energy-preserving approach was introduced by L. Lefevre and coworkers [22, 23]. Their method of spatial discretization for infinite-dimensional systems can preserve the model structure during the model reduction. The main difference is that the Cayley-Tustin time discretization method does not alter the system theoretic proper-

ties (such as stability, controllability, and observability) which play a significant role in the controller design [24]. However, the implication of Cayley-Tustin approach for control and estimator designs of large-scale DPS has not been fully investigated.

Motivated by the aforementioned considerations, the Cayley-Tustin method will be utilized for the time discretization of continuous-time PDEs, which avoids changing the nature of the transformed system when implementing the designed controller and estimator.

1.2.3 Optimal control and estimation of distributed parameter systems

In general, there are two classes of controller and estimator design methodologies that have been proposed to represent infinite-dimensional systems, called *early lumping* and *late lumping* [8]. The early lumping approximates the DPS to LPS by applying some type of spatial approximation to a continuous model to arrive at a discrete model, which is used for the controller design. The main advantage of early lumping approaches is that it is simpler to be conducted by exploring finite-dimensional control theories and methods. However, it is worth noting that through early lumping, the fundamental control theoretical properties (controllability, observability, and stabilizability) might be lost and/or altered significantly, see [8, 25]. Moreover, high-accuracy control usually requires that the PDEs be approximated with a large number of ODEs, which dramatically increases the complexity of the calculations and implementation. In contrast, the late lumping uses the PDEs model for the controller design without spatial approximation. The approximation is performed only for implementation purposes of the controller. Late lumping allows the control designer to avoid losing the distributed nature of the DPS and to take full advantage of their natural properties. The design procedure of early lumping and late lumping is shown in Fig. 1.1.

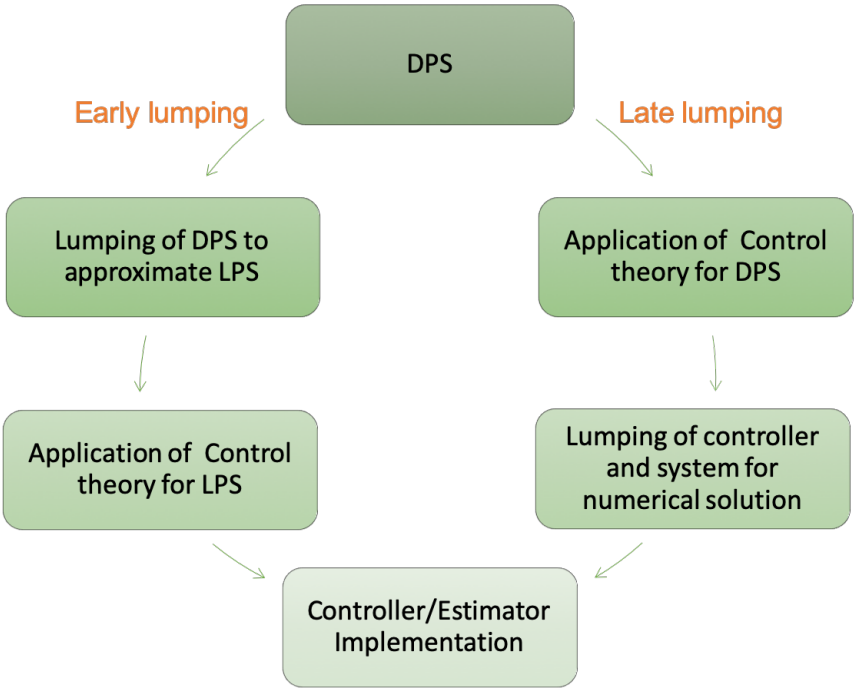

Figure 1.1: Design procedure via early lumping and late lumping

Over the past decades, a number of researchers have explored many problems related to control of a system described by PDEs, such as optimal control [26, 27, 28], internal model control [29, 30, 31, 32], nonlinear and robust control [25, 33, 34], predictive control [35, 36, 37, 11, 38], and adaptive control [39, 40]. Among these, MPC as a popular and widely deployed methodology in the chemical process control, pipeline control and pulp and paper industries is capable of handling such requirements [6, 7, 36]. The main idea of MPC can be traced its origins back to the optimal linear quadratic regulator (LQR) developed by Kalman in 1960 [41, 42] and application of it originated in the chemical industry and petroleum refineries in the 1970s [43, 44]. It is an online-optimization based method, and can take physical constrains of inputs, states and outputs into account. Given that, there are a lot of applications of MPC for chemical process controls [15, 17, 43]. When it comes to MPC design for infinite-dimensional systems, some significant works have proposed and extended the framework of distributed and boundary actuation with states and outputs constraints [45, 46]. Most of these contributions have been developed based on continuous-time infinite-dimensional models or continuous-time finite-dimensional models through model reductions or spatial discretization techniques. Therefore, the

design of MPC for discrete-time infinite-dimensional models carries great importance from both theoretical and practical perspectives.

The standard formulations of MPC minimize a nominal objective function using a single linear time-invariant model to predict future plant behavior. However, the main shortcoming is that such control techniques that provide optimal performance for a particular model may perform very poorly when implemented on a physical system which is not exactly described by the model [47]. Therefore, the robust control strategies are considered which concern that the systems are uncertain in some sense. A robust controller indicates that it is able to guarantee the closed-loop stability for different operating conditions of the process. The design of optimization-based robust controller for lumped parameter system has received plentiful attention and can be grouped into four main categories, including min-max control formulations, stabilizing state-feedback schemes, control Lyapunov functions, and cost-contracting constraints [48]. For the robustness of state-of-the-art model predictive controller design of distributed parameter systems, there are limited references available. One work conducted by Miriam and coworkers is that an order-reduced continuous-time DPS model by proper orthogonal decomposition (POD) is developed for robust nonlinear MPC design [49]. However, there are not extensive research addressing the robust MPC design for discrete-time DPS without model reduction.

Most control schemes are derived under the assumption that the state of the system is known explicitly. However the state is often not measured directly in real-world applications due to the physical constraints of sensor installation, and/or the prohibitive expense of implementing spatially-distributed sensors, so estimates of the actual state based on output measurements must be used instead. Studies focusing on the estimation of state/output and parameters for infinite-dimensional systems have received relatively less attention compared to the aforementioned contributions on controller designs and model stabilization. The estimation theory was initially developed with seminal contributions of Luenberger [50, 51] and Kalman [42] who introduced basic concepts of state Luenberger observer and Kalman filter designs from the deterministic and stochastic point of view, respectively. In addition, the existing finite-dimensional concepts of the observer design was extended to the infinite-dimensional setting, in the case of continuous models [52]. In recent studies, the

Luenberger observer and Kalman filter were extended for linear discrete-time infinite-dimensional systems [53]. However, these two classical estimators are commonly employed for estimation purposes but fall short in accounting for system constraints [54]. An alternative tool, MHE, has emerged as a superior estimation technique [55]. MHE is an optimization-based state estimation method that utilizes a sequence of recent measurements to estimate the current state of a system, which has gained significant attention in the research community, particularly for LPS [56, 57, 58], but has been rarely explored for DPS modelled by PDEs [59, 60].

The accuracy of the estimation depends not only on the type of estimator but also on the location of the sensors, especially for DPS. The sensor placement problem has been considered by many researchers in the area of chemical process control, and a number of different performance criteria for sensor placement have been taken into account. One of the earliest approaches is to maximize the observability through a choice of the sensor locations to improve the degree of complete observability for the deterministic state reconstruction problem [61, 62]. For the system with stochastic disturbances, unmeasured states can be estimated with the Kalman filter, and the optimal selection of measurements can be determined by minimizing the average variance of the state estimates [63] or the steady-state error variance [64]. There are also some other criteria to evaluate the performance of sensor locations including detection of load disturbances and location for optimal control [61]. These approaches have mature applications on the lumped parameter systems which are described by ordinary differential equations, and have been gradually extended and applied to the DPS in recent years. For example, the modal observability and controllability measures was utilized to determine optimal sensor and actuator locations of parabolic PDEs [65]. The optimal area for sensing or actuation in advective PDEs was determined by maximizing the support of the observability or controllability Gramian, respectively [66]. It was demonstrated that the nuclear norm of the solution to the operator Riccati equation is the steady-state minimum error variance of an estimate for DPS [67]. The placement of a single sensor and/or a single actuator in advection-diffusion equations with proportional feedback control was addressed [68]. Most of the previous contributions of the sensor selection for DPS mainly consider the spectral systems described by parabolic PDEs, which can be addressed by means of model reduction techniques

also known in estimation and control theory as the early lumping approach. However, for non-spectral systems (e.g., first order hyperbolic PDEs), where the slow-fast dynamic separation does not hold there are less contributions in the literature.

1.3 Main Contributions

There is now fairly extensive theory extending the common approaches to controller and estimation design for lumped systems to DPS. However, for most contributions, a finite-dimensional approximation of the system is first obtained and controller design is based on this finite-dimensional approximation. The major challenge is to account for the characteristics of infinite-dimensional systems when extending the application of optimal control and estimation techniques for lumped parameter systems. Additionally, if the systems of interest are non-spectral systems, which implies that does not have eigenvalues and corresponding eigenvectors, all previous designs which rely on spectral decomposition of dynamics can not be used. Thirdly, disturbances, constraints and uncertainties issues widely presented in industrial process system engineering pose another layer of technical challenge to the estimation and control of DPS.

The objective of this thesis is to explore advanced and robust optimal controller designs to improve the performance of large-scale distributed parameter chemical and petrochemical systems and provide reliable monitoring realizations in process systems without the need of finite-dimensional approximation.

The main contributions of the thesis are summarized as follows:

- Discrete-time dynamic modeling of large-scale distributed parameter chemical and petrochemical systems, including a spatially varying jacket tubular reactor, a pipeline network system, and a continuous pulp digester. The obtained discrete-time systems preserve the infinite-dimensional properties and can facilitate the controller and estimator design without any approximation or lumping in the spatial domain.

- Development and deployment of optimization-based predictive controllers for discrete-time large-scale distributed parameter systems to achieve stabilization

and/or set-point tracking while accounting for the system constraints.

- Designs of discrete-time infinite-dimensional Luenberger, Kalman filter, and moving horizon estimator for spatio-temporal state estimation under deterministic and stochastic conditions, and state/parameter estimation under the consideration of physical constraints, respectively.

- Investigation of selection of sensor location for first-order hyperbolic PDE systems by minimizing the variance of estimation error while accounting for the delayed measurements.

- Design of robust MPC for a class of discrete-time distributed parameter systems with multiple models, where the robustness is guaranteed based on restricting the future behavior of the controller cost function for each plant in the uncertainty description.

1.4 Thesis Outline

The outline of the thesis is organized as follows:

Chapter 2 addresses the model predictive controller design for a jacket tubular reactor with a simple reversible exothermic reaction (A $\rightleftharpoons$ B). Using energy and mass balance laws, four nonlinear hyperbolic partial differential equations are derived to model the tubular reactor dynamics in terms of two concentrations, the reactor temperature, and the spatially varying jacket temperature. The nonlinear continuous-time model is linearized and discretized in time by the use of the Cayley-Tustin transform without spatial discretization or model reduction. Along these lines, a state-feedback model predictive controller is formulated to realize model stabilization with respect to input and output constraints. To account for the state estimation, a Luenberger observer-based model predictive control frame is further developed, and observer gains are obtained as solutions of an operator Riccati equation. Finally, two numerical examples are provided to demonstrate the feasibility and applicability of the proposed MPC designs.

Chapter 3 proposes an optimization-based control, state, and parameter estimation strategy for distributed parameter pipeline systems with boundary actuation.

The spatial-temporal pressure and velocity model dynamics within the pipelines are described by a system of six coupled one-dimensional first-order nonlinear hyperbolic PDEs. To address the discrete-time modelling challenge and preserve the infinite-dimensional nature of the pipeline system, the Cayley-Tustin transformation is deployed for model time discretization without any spatial discretization or model reduction. Considering the lack of full state information across entire pipelines, unknown states and uncertain parameters are estimated using MHE. Based on the estimated states and parameters, a tracking MPC strategy for the discrete-time infinite-dimensional pipeline system is proposed, which enables specific operation while ensuring physical constraint satisfaction. The performance of the control and estimation is assessed via numerical examples.

Chapter 4 explores the design of a model predictive controller of the continuous pulp digester process consisting of the co-current zone and counter-current zone modeled by a set of nonlinear coupled hyperbolic PDEs. The distributed parameter system of interest is not spectral, and slow–fast dynamic separation does not hold. To address this challenge, the nonlinear continuous-time model is linearized and discretized in time utilizing the Cayley-Tustin discretization framework, which ensures system theoretic properties and structure preservation without spatial discretization or model reduction. The discrete model is used in the full state model predictive controller design, which is augmented by the Luenberger observer design to achieve the output constrained regulation. Finally, a numerical example is provided to demonstrate the feasibility and applicability of the proposed controller designs.

Chapter 5 investigates the state estimation and sensor placement for a continuous pulp digester with delayed measurements. The underlying model of interest is heat transfer in a pulp digester modeled by two coupled hyperbolic partial differential equations and an ordinary differential equation. Output measurements are considered with delay due to the possible low sampling rate. The Cayley-Tustin transformation is utilized to realize model time discretization in a late lumping manner which does not account for any type of spatial approximation or model reduction. The discrete Kalman filter is applied to estimate the system states using the delayed measurements. The selection of sensor location is addressed along with estimator design accounting for the delayed measurements and investigated by minimizing the variance of esti-

mation error. The performance of the state estimator is evaluated, and the sensor placement is analyzed through simulation studies, which offers a planning view of sensor location in industrial applications.

Chapter 6 proposes a robust model predictive control strategy for a class of linear infinite-dimensional transport-reaction models emerging from chemical engineering practice. The model uncertainty is assumed to be described by a discrete set of linear models (multi-plant uncertainty), and the robustness is achieved by assembling cost-contracting constraints for all the possible models in the uncertainty domain. The properties of the closed-loop system are analyzed, and the effectiveness of the proposed approach is demonstrated through a comparison with the nominal stabilizing MPC.

Chapter 7 summarizes the main results of this thesis and discusses future research directions.

Chapter 2

Model Predictive Control of Jacket Tubular Reactor with Reversible Exothermic Reaction

2.1 Introduction

Tubular reactors play a significant role in chemical engineering practice. Models of various types of tubular reactors are usually described by nonlinear partial differential equations (PDEs) derived from conservation laws, originated from mass and energy balances and which belong to the class of distributed parameter systems (DPS) [8]. The salient feature of these models is temporal and spatial state dependence that captures the kinetics properties within the reactors and can be connected with the phase change, generation, and/or consumption of chemical species [69].

Due to the numerous industrial applications of tubular reactors, the corresponding issues of modelling and controlling are of great importance for the safety and economic operations [70, 71, 72, 73], and hence have been explored in many studies over the years. For instance, a series of contributions were focused on the first-order exothermic irreversible reaction $A \rightarrow bB$ within the uniform jacket tubular reactors [74, 75, 76]. An ideal plug-flow tubular reactor having a simple exothermic consecutive reaction $A \rightarrow B \rightarrow C$ with the co-current cooling [77] and $A + B \rightarrow C$ with advection and axial diffusion were further investigated [78]. In addition, the reversible reactions $aA \rightleftharpoons rR$ were widely studied especially in chemical and biological proceses, such as polymerization and isomerization, enzyme kinetics and racemization of molecules with mirror-image structures [79, 80, 81]. Based on the mathematical models of various

reaction systems, significant research efforts have been made towards control designs [82, 83]. In particular, a globally stabilizing boundary feedback control law was developed to stabilize the unstable steady states of temperature and concentration on the inlet side of the tubular reactor [84]. Furthermore, the backstepping-based infinite-dimensional observers were proposed for a class of linear parabolic PDEs [85]. Along the same line, the dynamic analysis and linear quadratic optimal control had extensively developed for a class of tubular reactors [74, 86, 87]. However, when it comes to the controller design for reversible reaction systems, there are limited attention in research literature [88, 79, 89, 90]. The inevitable difficulty comes from the infinite-dimensional nature of heterodirectional hyperbolic systems, which is a limiting factor when controller designs and monitoring realizations are considered. Motivated by these observations, the objective of this chapter is the simple reversible reaction which is described by the nonlinear coupled 4×4 hyperbolic PDEs.

Considering the typical requirements for operation of tubular reactors in practice, such as the temperature and concentration of reactants not exceeding certain ranges, as well as the physical limits of actuators or sensors, MPC as a popular and widely deployed methodology in the process industry is capable of handling such requirements. The main idea of MPC can be dated back to the 1960s and application of it originated in chemical industry in the 1970s [91]. Basically, a model of interest is implemented as an optimization problem, which is then solved to determine the best set of inputs for decisions. The optimization problem needs to be reformulated iteratively as time increase, and only the first input is implemented every time. Over the past two decades, MPC has been extensively used in linear and nonlinear finite-dimensional systems [16, 17]. MPC theory is now a mature body of knowledge encompassing stability and robustness of linear and nonlinear models, which has significant impact on industrial process control and has been extended to the control of the infinite-dimensional systems, and especially tubular reactor systems [92, 93]. More specifically, a nonlinear MPC for a tubular reactor was developed by combining data-driven and model reduction approaches, where the proper orthogonal decomposition (POD) and finite element Galerkin projection methods were applied to approximate the PDE system [5]. Similar methods (POD and Galerkin projection) were utilized to derive the low-order linear model that captures the dominant dynamics of the

PDEs, which were subsequently used for MPC design of distributed reactor models with axial and radial diffusion [94]. An economic MPC framework was proposed for a tubular reactor and the reduced-order model was constructed based on the basis of historical data-based empirical eigenfunctions and Galerkin's method [95]. However, those approaches are only applicable for the Riesz spectral systems (parabolic, and higher order dissipative PDEs) and not suitable for non-spectral systems, such as the hyperbolic PDEs. There are other extensions in this area, for instance, a nonlinear MPC scheme for continuous emulsion co-polymerization in a tubular reactor was presented [96], where the PDEs were converted to a system of ODEs using the method of lines. A general nonlinear MPC framework for low-density polyethylene tubular reactors was developed [97], where the cascade PDEs-ODEs system were discretized in space and time for implementation by using the implicit Euler and finite element scheme. In addition, there are some other works on linear model predictive controller designs of transport reaction systems based on online model reduction [98, 99] and structure-preserving discretization framework [76, 36, 38].

Most of the aforementioned works depend on spatial approximation (discretization) in the controller design stage. However, the main drawback of these approaches lies in that the spatial discretization might induce numerical instability and/or the fundamental control theoretical properties (controllability, observability, and stabilizability) might be lost and/or altered significantly [8, 19]. On the other hand, the obtained discrete model can only provide approximate states at the spatial discretization points instead of the spatial states between discretized point. In general, these approaches belong to early lumping, since spatial discretization needs to preformed in the design stage. In contrast, late lumping takes full advantage of the available distributed parameter control theory and utilizes the infinite-dimensional setting for controller design, and only performs lumping along some spatial approximation for the purpose of implementation.

In a late lumping manner, the Cayley-Tustin time discretization framework was proposed by Havu, V. and Malinen, J [14, 13], which was demonstrated to be a symmetric and symplectic integration scheme that ensures energy and structure preservation. Another novel energy-preserving approach was introduced by L. Lefevre and coworkers [22, 24, 23]. Their method of spatial discretization for infinite-dimensional

systems can preserve the model structure during the model reduction, and consist in splitting the initial structured infinite-dimensional model into N finite-dimensional sub-models with the same energetic behavior [22]. Comparing with the Cayley-Tustin time discretization method, the main similarity is that both approaches guarantee structure preserving numerical integration. The main difference is that the Cayley-Tustin time discretization method does not alter the system theoretic properties (such as stability, controllability, and observability) which play a significant role in the controller design [24, 100]. However, this perspective is not investigated when using the framework [22, 24, 23].

Motivated by the aforementioned considerations, we extend the finite-dimensional MPC setting to the jacket tubular reactor with a simple reversible reaction modeled by the 4×4 hyperbolic PDEs, and in particular the Cayley-Tustin method is utilized for time discretization of continuous hyperbolic PDEs model, and in the linear MPC controller design in a late lumping manner, which achieves satisfactory performance with respect to input and output constraints and accounts for constrained stabilization of the disturbed system.

The five contributions of this work are summerized next: 1). A partial differential equation model is established for a jacked tubular reactor with consideration of a simple reversible reaction ($A \rightleftharpoons B$), which is a common practice in chemical engineering but has not been fully investigated in the literature since it accounts for the heterodirectional hyperbolic systems. 2). A spatially varying jacket temperature is considered instead of uniformly distributed jacket temperature along with the concentration of reactants and products, and the temperature of the reactor to reflect the spatiotemporal dynamics of the reactor system. 3). Cayley-Tustin time discretization is utilized to preserve system properties (such as stability, controllability, observability). 4). A full state feedback MPC controller is designed and implemented to address the physical constraints in actuators and sensors. 5). Considering the common scenario of unavailability of full state information and the existence of disturbance, an observer-based MPC is designed using the state estimated by the Luenberger observer and finding the observer gain by solving an operator Riccati equation.

The organization of this chapter is described next. In Section 2.2, the infinite-dimensional state space model is introduced. Furthermore, the linearized model and

Cayley-Tustin time discretization for the tubular reactor are provided. In Section 2.3, the model predictive controllers are designed including state feedback MPC and observer-based MPC. Finally, in Section 2.4, the performance of the presented state feedback MPC and observer-based MPC are demonstrated by two numerical examples, where the influence of constraints, penalty weights and disturbances on the MPC performance is further analyzed. Concluding remarks are drawn in Section 2.5.

2.2 Problem Formulation

In this section, we introduce the problem formulation. First, the mathematical model of the jacketed tubular reactor is presented with a simple reversible reaction taking place. Second, the model linearization around the equilibrium point is proposed to construct a linearized model. Finally, the discrete-time infinite-dimensional model is obtained utilizing the Cayley-Tustin transform framework.

2.2.1 Model description

Figure 2.1 shows a schematic of a tubular reactor. This tubular reactor is a non-isothermal reactor where an elementary, exothermic first-order reversible reaction takes place ($A \rightleftharpoons B$).

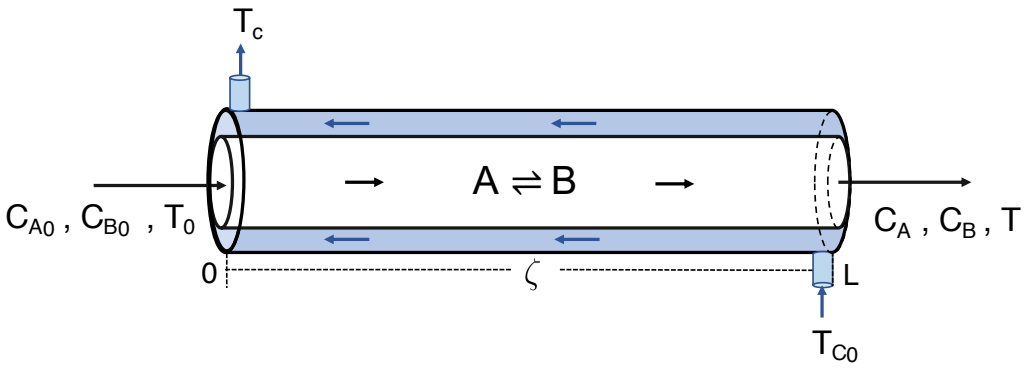

Figure 2.1: Jacket tubular reactor representation.

The mathematical model for the considered tubular reactor is based on the following assumptions. 1) Uniform radial velocity and distribution. 2) Uniform radial temperature and concentration distribution. 3) Constant density and volume of the

liquid within the reactor. The heat capacity of the reactant, diffusion, and dispersion are neglected.

Under these simplifying assumptions, the dynamics of the process are typically described by the following four nonlinear PDEs which are derived from energy and mass balance principles [101, 92, 102]. In particular, one considers the spatially varying jacket temperature that can be described by another hyperbolic PDE.

$$\begin{aligned}
\frac{\partial C_A(\zeta,t)}{\partial t} &= -v\frac{\partial C_A(\zeta,t)}{\partial \zeta} - k_1 e^{-\frac{E_1}{T(\zeta,t)R}} C_A(\zeta,t) + k_2 e^{-\frac{E_2}{T(\zeta,t)R}} C_B(\zeta,t) \\
\frac{\partial C_B(\zeta,t)}{\partial t} &= -v\frac{\partial C_B(\zeta,t)}{\partial \zeta} + k_1 e^{-\frac{E_1}{T(\zeta,t)R}} C_A(\zeta,t) - k_2 e^{-\frac{E_2}{T(\zeta,t)R}} C_B(\zeta,t) \\
\frac{\partial T(\zeta,t)}{\partial t} &= -v\frac{\partial T(\zeta,t)}{\partial \zeta} + \frac{-\Delta H}{\rho C_p} k_1 e^{-\frac{E_1}{T(\zeta,t)R}} C_A(\zeta,t) - \frac{-\Delta H}{\rho C_p} k_2 e^{-\frac{E_2}{T(\zeta,t)R}} C_B(\zeta,t) \\
&\quad + \frac{U}{\rho C_p V}(T_c(\zeta,t) - T(\zeta,t)) \\
\frac{\partial T_c(\zeta,t)}{\partial t} &= v_c\frac{\partial T_c(\zeta,t)}{\partial \zeta} - \frac{U}{\rho C_p V}(T_c(\zeta,t) - T(\zeta,t)) + b(\zeta)\bar{u}(t)
\end{aligned} \tag{2.1}$$

In these equations, C_A, C_B denote the concentration of reactant and product, respectively. The temperature inside of the reactor is T and T_c is the temperature of cooling medium flowing around the wall of the tubular reactor. The symbols $v, v_c, E_1, E_2, k_1, k_2, R, \Delta H, \rho C_p, U, V$ denote the superficial fluid velocity, the velocity of cooling fluid, the activation energy of reactant and product, the kinetic constant of A and B, the ideal gas constant, the enthalpy, constant heat capacity, product of the density and heat capacity of the fluid in the reactor, the heat transfer coefficient, the volume of reactor, respectively [103]. Parameters of the reactor considered are shown in Table 2.1 .

Table 2.1: Notation and values of parameters

Process parameters	Notations	Numerical Values
Fluid velocity in reactor	v	0.025m/s
Fluid velocity in jacket	v_c	0.1m/s
Length of the reactor	L	1m
Activation energy of reactant	E_1	46.15kJ/mol
Activation energy of product	E_2	209.29 kJ/mol
Heat transfer parameter	$\frac{U}{\rho C_p V}$	$0.2s^{-1}$
Idea gas constant	R	8.314J/(mol.K)
Stoichiometric coefficient	$\frac{-\Delta H}{\rho C_p}$	−4250 K.L/mol

In addition, ζ ($\zeta \in [0, L]$) and t ($t \in [0, \infty)$) denote the spatial variable and temporal variable, respectively. The boundary actuation is $\bar{u}(t)$ and it is characterized by $b(\zeta)$, which is given as $b(\zeta) = \frac{1}{2\bar{\zeta}_L} 1_{[\zeta_L - \bar{\zeta}_L, \zeta_L + \bar{\zeta}_L]}(\zeta)$. In summary, the controlled variables are the concentration C_A, C_B and the temperature T of the reactor, and the corresponding manipulated variable is the inlet flow temperature of the jacket. The mathematical model in Eq.(2.1), represents a nonlinear relation between controlled variables and manipulated variables.

Correspondingly, the following boundary conditions are considered for $t \in [0, \infty)$:

$$C_A(0,t) = C_{A_0}, C_B(0,t) = 0, T(0,t) = T_0, T_c(L,t) = T_{C_0} \tag{2.2}$$

with the given initial conditions for $\zeta \in [0, L]$:

$$C_A(\zeta,0) = C_A(\zeta), C_B(\zeta,0) = 0, T(\zeta,0) = T(\zeta), T_c(\zeta,0) = T_c(\zeta) \tag{2.3}$$

The output is taken as the following form:

$$y(t) = C \begin{bmatrix} C_A(\zeta,t) \\ C_B(\zeta,t) \\ T(\zeta,t) \\ T_c(\zeta,t) \end{bmatrix} \tag{2.4}$$

where $C(\cdot) = \text{diag}\{\int_0^L (\cdot)\delta(\zeta - L)d\zeta, \int_0^L (\cdot)\delta(\zeta - L)d\zeta, \int_0^L (\cdot)\delta(\zeta - L)d\zeta, \int_0^L (\cdot)\delta(\zeta)d\zeta\}$ and $\delta(\zeta)$ is the Dirac function which can capture spatial measurement points of interest.

2.2.2 System linearization

The mathematical model described above is composed of a set of PDEs that accurately describe the dynamics of the tubular reactor from spatial and temporal dimensional. It is however a fully coupled and nonlinear PDEs model that is difficult to solve directly and analyze further. Linearizing this system around some steady states of interest is one way to proceed [76].

Firstly, the steady-state model of Eq.(2.1) can be simply obtained as the time

$t \to \infty$, which means that all derivatives with respect to time are equal to zero.

$$
\begin{aligned}
&-v\frac{\partial C_{A_{ss}}}{\partial \zeta} - k_1 e^{-\frac{E_1}{T_{ss}R}} C_{A_{ss}} + k_2 e^{-\frac{E_2}{T_{ss}R}} C_{B_{ss}} = 0 \\
&-v\frac{\partial C_{B_{ss}}}{\partial \zeta} + k_1 e^{-\frac{E_1}{T_{ss}R}} C_{A_{ss}} - k_2 e^{-\frac{E_2}{T_{ss}R}} C_{B_{ss}} = 0 \\
&-v\frac{\partial T_{ss}}{\partial \zeta} + \frac{-\Delta H}{\rho C_p} k_1 e^{-\frac{E_1}{T_{ss}R}} C_{A_{ss}} - \frac{-\Delta H}{\rho C_p} k_2 e^{-\frac{E_2}{T_{ss}R}} C_{B_{ss}} + \frac{U}{\rho C_p V}(T_{c_{ss}} - T_{ss}) = 0 \\
&v_c\frac{\partial T_{c_{ss}}}{\partial \zeta} - \frac{U}{\rho C_p V}(T_{c_{ss}} - T_{ss}) = 0
\end{aligned}
\tag{2.5}
$$

The steady states can be solved numerically by the finite difference method. More specifically, the derivatives with respect to the axial variable can be replaced by the first-order backward and the first-order forward differences. As a result, the corresponding steady states profiles are illustrated in Figure 2.2.

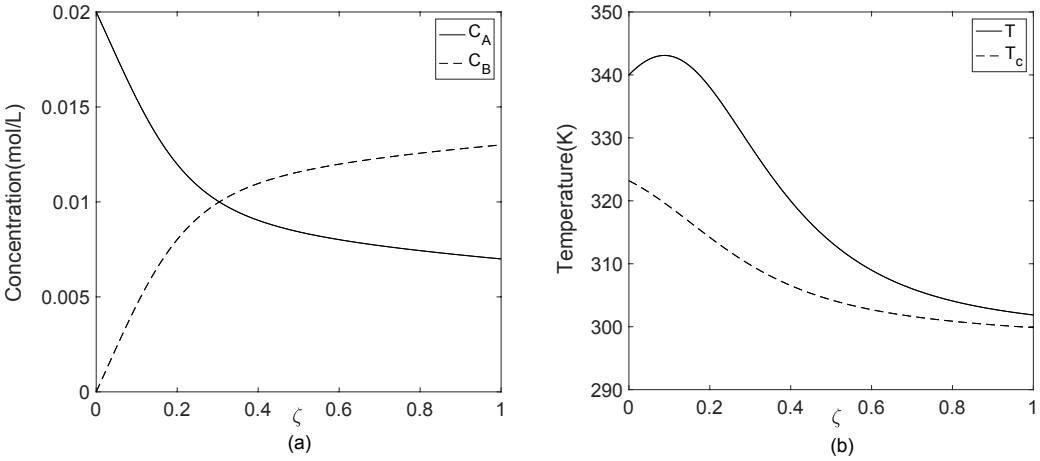

Figure 2.2: Steady-states profiles of the tubular reactor.

By applying the state transformation and linearization, the original nonlinear PDEs in Eq.(2.1) can be linearized around the steady states.

$$
X = \begin{bmatrix} x_1(\zeta,t) \\ x_2(\zeta,t) \\ x_3(\zeta,t) \\ x_4(\zeta,t) \end{bmatrix} = \begin{bmatrix} C_A(\zeta,t) - C_{A_{ss}}(\zeta,t) \\ C_B(\zeta,t) - C_{B_{ss}}(\zeta,t) \\ T(\zeta,t) - T_{ss}(\zeta,t) \\ T_c(\zeta,t) - T_{c_{ss}}(\zeta,t) \end{bmatrix} \tag{2.6}
$$

Moreover, the steady states $C_{A_{ss}}, C_{B_{ss}}, T_{ss}, T_{c_{ss}}$ need to satisfy their corresponding boundary conditions indicated in Eq.(2.2) respectively. Therefore, the linearized infinite-dimensional model is obtained as the following form:

$$
\frac{\partial X(\zeta,t)}{\partial t} = V\frac{\partial X(\zeta,t)}{\partial \zeta} + A(\zeta)X(\zeta,t) + B(\zeta)u(t) \tag{2.7}
$$

where $u(t)$ is the corresponding input action of the linearized system and the following notations are used in this equation.

$$V = \text{diag}\{-v, -v, -v, v_c\}, A(\zeta) = \begin{bmatrix} -N_1 & N_2 & -G_1 & 0 \\ N_1 & -N_2 & G_1 & 0 \\ \beta N_1 & -\beta N_2 & G_2 & \alpha \\ 0 & 0 & \alpha & -\alpha \end{bmatrix}, B(\zeta) = [0; 0; 0; b(\zeta)]$$
$$\alpha = \frac{U}{\rho C_p V}, \beta = \frac{-\Delta H}{\rho C_p}, \mu_1 = \frac{E_1}{R}, \mu_2 = \frac{E_2}{R}, N_1 = k_1 e^{-\frac{\mu_1}{T_{ss}}}, N_2 = k_2 e^{-\frac{\mu_2}{T_{ss}}}$$
$$G_1 = N_1 \mu_1 \frac{C_{Ass}}{T_{ss}^2} - N_2 \mu_2 \frac{C_{Bss}}{T_{ss}^2}, G_2 = \beta N_1 \mu_1 \frac{C_{Ass}}{T_{ss}^2} - \beta N_2 \mu_2 \frac{C_{Bss}}{T_{ss}^2} - \alpha \tag{2.8}$$

The linearized system has the corresponding boundary conditions of

$$x_1(0,t) = 0, x_2(0,t) = 0, x_3(0,t) = 0, x_4(L,t) = 0 \tag{2.9}$$

and the initial conditions:

$$\begin{aligned} x_1(\zeta,0) &= C_A(\zeta) - C_{A_{ss}}(\zeta), x_2(\zeta,0) = C_B(\zeta) - C_{B_{ss}}(\zeta) \\ x_3(\zeta,0) &= T(\zeta) - T_{ss}(\zeta), x_4(\zeta,0) = T_c(\zeta) - T_{c_{ss}}(\zeta) \end{aligned} \tag{2.10}$$

The linearized jacket tubular reactor model is now complete and the standard infinite-dimensional continuous-time state-space model can be formulated as:

$$\begin{aligned} \dot{X}(\zeta,t) &= \mathcal{A}X(\zeta,t) + \mathcal{B}u(t) \\ Y(t) &= CX(\zeta,t) \end{aligned} \tag{2.11}$$

subject to the boundary conditions Eq.(2.9) and the initial conditions Eq.(2.10). The state $X(\zeta,t) \in \mathcal{X}$, with $\mathcal{X} = L^2((0,L),\mathbb{R}^4)$ being defined as a real separable Hilbert space with inner product $\langle \cdot, \cdot \rangle$. The input $u(t) \in L^2_{loc}([0,\infty),\mathcal{U})$ and output $y(t) \in L^2_{loc}([0,\infty),\mathcal{Y})$, where $\mathcal{U}$ and $\mathcal{Y}$ are real separable Hilbert spaces.

In this form, one can define the operator $\mathcal{A}(\cdot) = V\frac{\partial(\cdot)}{\partial\zeta} + A(\zeta)(\cdot)$ on its domain $\mathcal{D}(\mathcal{A}) = \{\psi_i(\zeta) \in L_2(0,1) | \psi_i(\zeta)$ is absolutely continuous, $\frac{d\psi_i}{d\zeta} \in L_2(0,1)$, with $i = 1,2,3,4$, and $\psi_1(0) = 0, \psi_2(0) = 0, \psi_3(0) = 0, \psi_4(1) = 0\}$. $\mathcal{A}$ is the infinitesimal generator of a C_0-semigroup on $\mathcal{X}$. Also, the input operator $\mathcal{B}$ is defined as a bounded operator $\mathcal{B} = [\ 0;\ 0;\ 0;\ b(\zeta)]$. The operator $\mathcal{B}$ can approximate "point actuation" by using a small interval shape function [52]. To construct the model predictive controller in the next section, the adjoint operator of $\mathcal{A}$ needs to be predetermined. For this system, the adjoint operator $\mathcal{A}^*$ is easily found using the inner product formula,

$\langle \mathcal{A}\varphi_i, \phi_i \rangle = \langle \varphi_i, \mathcal{A}^* \phi_i \rangle, i = 1,2,3,4$, and is:

$$\mathcal{A}^*(\cdot) = -V\frac{\partial(\cdot)}{\partial \zeta} + A^*(\zeta)(\cdot) \tag{2.12}$$

with its domain defined as $\mathcal{D}(\mathcal{A}^*) = \{\phi_i(\zeta) \in L_2(0,1),\ \phi_i(\zeta)$ is absolutely continuous, $\frac{d\phi_i}{d\zeta} \in L_2(0,1),$ with $i = 1,2,3,4,$ and $\phi_1(1) = 0, \phi_2(1) = 0, \phi_3(1) = 0, \phi_4(0) = 0\}$.

The output is obtained:

$$Y(t) = C\begin{bmatrix} x_1(\zeta,t) + C_{A_{ss}}(\zeta) \\ x_2(\zeta,t) + C_{B_{ss}}(\zeta) \\ x_3(\zeta,t) + T_{ss}(\zeta) \\ x_4(\zeta,t) + T_{c_{ss}}(\zeta) \end{bmatrix} = C\begin{bmatrix} x_1 \\ x_2 \\ x_3 \\ x_4 \end{bmatrix} + \begin{bmatrix} C_{Ass}(L) \\ C_{Bss}(L) \\ T_{ss}(L) \\ T_{css}(0) \end{bmatrix}, \tag{2.13}$$

In an analogous manner, by $\langle C\varphi_i, \phi_i \rangle = \langle \varphi_i, C^* \phi_i \rangle, i = 1,2,3,4,$ C^* operator is determined as:

$$C^*(\cdot) = \text{diag}\{\delta(\zeta - L)\int_0^L (\cdot)d\eta, \delta(\zeta - L)\int_0^L (\cdot)d\eta, \delta(\zeta - L)\int_0^L (\cdot)d\eta, \delta(\zeta)\int_0^L (\cdot)d\eta\} \tag{2.14}$$

The detailed manipulation of the adjoint operator $\mathcal{A}^*$ and C^* refer to the Appendix A.1 and A.2.

2.2.3 Model discretization

Based on the linearized infinite-dimensional system, we introduce the Cayley-Tustin discretization framework to transform the continuous system to the discrete-time one. Let us consider the above linear system in Eq.(2.11) and a given a time discretization $h > 0$, and the Cayley-Tustin discretization is given by

$$\begin{aligned} \frac{X(jh) - X((j-1)h)}{h} &\approx \mathcal{A}\frac{X(jh) + X((j-1)h)}{2} + \mathcal{B}u(jh), X(0) = X_0 \\ Y(jh) &\approx C\frac{X(jh) + X((j-1)h)}{2} \end{aligned} \tag{2.15}$$

for $j \geq 1$, where we omit the spatial dependence of x for brevity. Then let $\frac{u_j^{(h)}}{\sqrt{h}}$ be an approximation of $u(jh)$ by the mean value within a given sampling time, $\frac{u_j^{(h)}}{\sqrt{h}} = \frac{1}{h}\int_{(j-1)h}^{jh} u(t)dt$. It has been shown in [14] that $\frac{u_j^{(h)}}{\sqrt{h}}$ converges to $u(jh)$ as $h \to 0$ in several different ways, similar for $Y(jh)$. Further, rewriting Eq.(2.15) gives the discrete time dynamics Eq.(2.16). It is frequently called Tustin discretization in the

engineering literature, which is discovered in 1940s by Tustin and referred as Tustin transform in digital and sample-data control literature [19].

$$\begin{aligned} \frac{X_j^{(h)} - X_{j-1}^{(h)}}{h} &\approx \mathcal{A}\frac{X_j^{(h)} + X_{j-1}^{(h)}}{2} + \mathcal{B}\frac{u_j^{(h)}}{\sqrt{h}}, X_0^{(h)} = X_0 \\ \frac{Y_j^{(h)}}{\sqrt{h}} &\approx \mathcal{C}\frac{X_j^{(h)} + X_{j-1}^{(h)}}{2} \end{aligned} \tag{2.16}$$

Through some basic computations, the following infinite-dimensional discrete-time state space model is obtained:

$$\begin{aligned} X_j^{(h)} &= \mathcal{A}_d X_{j-1}^{(h)} + \mathcal{B}_d u_j^{(h)} \\ Y_j^{(h)} &= \mathcal{C}_d X_{j-1}^{(h)} + \mathcal{D}_d u_j^{(h)} \end{aligned} \tag{2.17}$$

where $\mathcal{A}_d$, $\mathcal{B}_d$, $\mathcal{C}_d$, $\mathcal{D}_d$ are the discrete-time spatial operators and we denote:

$$\begin{pmatrix} \mathcal{A}_d & \mathcal{B}_d \\ \mathcal{C}_d & \mathcal{D}_d \end{pmatrix} = \begin{pmatrix} [\delta - \mathcal{A}]^{-1}[\delta - \mathcal{A}] & \sqrt{2\delta}[\delta - \mathcal{A}]^{-1}\mathcal{B} \\ \sqrt{2\delta}\mathcal{C}[\delta - \mathcal{A}]^{-1} & \mathcal{C}[\delta - \mathcal{A}]^{-1}\mathcal{B} \end{pmatrix} \tag{2.18}$$

where $\delta = 2/h$ and the resolvent is $\mathcal{R}(\delta, \mathcal{A})(\cdot) = (\delta I - \mathcal{A})^{-1}(\cdot)$. Clearly, one must satisfy $\delta \in \rho(\mathcal{A})$ so that the resolvent operator is well-defined. In particular, $\mathcal{C}(\delta - \mathcal{A})^{-1}\mathcal{B}$ denotes the transfer function of the linearized continuous model. The unbounded operators $\mathcal{A}$ of the continuous-time system are mapped into bounded operators $\mathcal{A}_d$ in the discrete-time counterpart through Cayley transform. In addition, it has been demonstrated that the controllability and stability are invariant under this transformation [76]. The continuous state evolutional operator $\mathcal{A}$ is discretized in time and $\mathcal{A}_d$ can be described by the resolvent operator with $\mathcal{A}_d(\cdot) = [\delta I - \mathcal{A}]^{-1}[\delta I + \mathcal{A}](\cdot) = -I(\cdot) + 2\delta[\delta I - \mathcal{A}]^{-1}(\cdot) = -I(\cdot) + 2\delta\mathcal{R}(\delta, \mathcal{A})(\cdot)$, where I is an identity operator.

2.2.4 Resolvent operator

In order to obtain the above discrete-time spatial operators which are generated by the Cayley-Tustin discretization, the resolvent operator needs to be determined. In general, there is a link between the resolvent operator and the analytical solution in Laplace-domain for the continuous-time model, such as $\mathcal{R}(s, \mathcal{A})(\cdot) = [sI - \mathcal{A}]^{-1}(\cdot)$, which means one can obtain the resolvent operator by applying the Laplace transform. To better understand the resolvent operator, let us consider the following model:

$$\dot{z}(\zeta, t) = \mathcal{A}z(\zeta, t), z(\zeta, 0) = z_0(\zeta) \tag{2.19}$$

where $\mathcal{A}$ is defined as a spatial derivative operator. Through applying the Laplace transform, one attains the associated resolvent operator $\mathcal{R}(s,\mathcal{A})$ as follows:

$$z(\zeta,s) = [sI - \mathcal{A}]^{-1} z_0(\zeta) = \mathcal{R}(s,\mathcal{A}) z_0(\zeta) \tag{2.20}$$

This illustrates that the resolvent operator is mapping the initial condition $z_0(\zeta)$ to the solution $z(\zeta,s)$ in Laplace-domain.

Following this line, for the linearized hyperbolic PDEs in Eq.(2.7), the Laplace transform is applied giving:

$$\frac{\partial X(\zeta,s)}{\partial \zeta} = FX(\zeta,s) - V^{-1}X(\zeta,0) \tag{2.21}$$

where

$$F = V^{-1}[(SI - A(\zeta)] = \begin{bmatrix} -\frac{s+N_1}{v} & \frac{N_2}{v} & -\frac{G_1}{v} & 0 \\ \frac{N_1}{v} & -\frac{s+N_2}{v} & \frac{G_1}{v} & 0 \\ \frac{\beta N_1}{v} & -\frac{\beta N_2}{v} & \frac{s+G_2}{v} & \frac{\alpha}{v} \\ 0 & 0 & -\frac{\alpha}{v_c} & \frac{s+\alpha}{v_c} \end{bmatrix}$$

and V is defined in Eq.(2.8). Because of the diagonal form of V, it is clear that V is invertible, which means the well-posedness is guaranteed. Based on the semigroup operator theory [52], a frequency-domain solution is generated under the zero-input condition as follows:

$$\begin{bmatrix} x_1(\zeta,s) \\ x_2(\zeta,s) \\ x_3(\zeta,s) \\ x_4(\zeta,s) \end{bmatrix} = e^{F\zeta} \begin{bmatrix} x_1(0,s) \\ x_2(0,s) \\ x_3(0,s) \\ x_4(0,s) \end{bmatrix} - \int_0^{\zeta} e^{F(\zeta-\eta)} V^{-1} \begin{bmatrix} x_1(\eta,0) \\ x_2(\eta,0) \\ x_3(\eta,0) \\ x_4(\eta,0) \end{bmatrix} d\eta \tag{2.22}$$

For notational simplicity, $e^{F\zeta}$ can be denoted as $e^{F\zeta} = [F_{ij}(\zeta,s)]_{4\times4}$ with $i,j = 1,2,3,4$. The frequency-domain solution of the distributed parameter system is:

$$\begin{bmatrix} x_1(\zeta,s) \\ x_2(\zeta,s) \\ x_3(\zeta,s) \\ x_4(\zeta,s) \end{bmatrix} = \begin{bmatrix} F_{11}(\zeta,s) & F_{12}(\zeta,s) & F_{13}(\zeta,s) & F_{14}(\zeta,s) \\ F_{21}(\zeta,s) & F_{22}(\zeta,s) & F_{23}(\zeta,s) & F_{24}(\zeta,s) \\ F_{31}(\zeta,s) & F_{32}(\zeta,s) & F_{33}(\zeta,s) & F_{34}(\zeta,s) \\ F_{41}(\zeta,s) & F_{42}(\zeta,s) & F_{43}(\zeta,s) & F_{44}(\zeta,s) \end{bmatrix} \begin{bmatrix} x_1(0,s) \\ x_2(0,s) \\ x_3(0,s) \\ x_4(0,s) \end{bmatrix} +$$
$$\int_0^{\zeta} \begin{bmatrix} F_{11}(\zeta-\eta,s) & F_{12}(\zeta-\eta,s) & F_{13}(\zeta-\eta,s) & F_{14}(\zeta-\eta,s) \\ F_{21}(\zeta-\eta,s) & F_{22}(\zeta-\eta,s) & F_{23}(\zeta-\eta,s) & F_{24}(\zeta-\eta,s) \\ F_{31}(\zeta-\eta,s) & F_{32}(\zeta-\eta,s) & F_{33}(\zeta-\eta,s) & F_{34}(\zeta-\eta,s) \\ F_{41}(\zeta-\eta,s) & F_{42}(\zeta-\eta,s) & F_{43}(\zeta-\eta,s) & F_{44}(\zeta-\eta,s) \end{bmatrix} \begin{bmatrix} \frac{1}{v} & 0 & 0 & 0 \\ 0 & \frac{1}{v} & 0 & 0 \\ 0 & 0 & \frac{1}{v} & 0 \\ 0 & 0 & 0 & -\frac{1}{v_c} \end{bmatrix} \begin{bmatrix} x_1(\eta,0) \\ x_2(\eta,0) \\ x_3(\eta,0) \\ x_4(\eta,0) \end{bmatrix} d\eta \tag{2.23}$$

Considering that the corresponding boundary conditions Eq.(2.9) are bidirectional, one needs to convert them to one side in order to determine the resolvent operator as

follows:

(1) At $\zeta = 0$, one can substitute $x_1(0,s) = 0$, $x_2(0,s) = 0$, $x_3(0,s) = 0$ into Eq.(2.23) which results in $F_{14}(0,s) = 0$, $F_{24}(0,s) = 0$, $F_{34}(0,s) = 0$.

(2) At $\zeta = L$, one can substitute $x_4(L,s) = 0$ into Eq.(2.23) which yields

$$\begin{aligned} x_4(0,s) = -\frac{1}{F_{44}(L,s)} \int_0^L [\frac{1}{v} F_{41}(L-\eta,s)x_1(\eta,0) + \frac{1}{v} F_{42}(L-\eta,s)x_2(\eta,0) + \\ \frac{1}{v} F_{43}(L-\eta,s)x_3(\eta,0) - \frac{1}{v_c} F_{44}(L-\eta,s)x_4(\eta,0)]d\eta \end{aligned} \tag{2.24}$$

Consequently, the resolvent operator can be determined utilizing Eq.(2.23) and Eq.(2.24) in the following form:

$$\begin{bmatrix} x_1(\zeta,s) \\ x_2(\zeta,s) \\ x_3(\zeta,s) \\ x_4(\zeta,s) \end{bmatrix} = \begin{bmatrix} \mathcal{R}_{11}(F,s) & \mathcal{R}_{12}(F,s) & \mathcal{R}_{13}(F,s) & \mathcal{R}_{14}(F,s) \\ \mathcal{R}_{21}(F,s) & \mathcal{R}_{22}(F,s) & \mathcal{R}_{23}(F,s) & \mathcal{R}_{24}(F,s) \\ \mathcal{R}_{31}(F,s) & \mathcal{R}_{32}(F,s) & \mathcal{R}_{33}(F,s) & \mathcal{R}_{34}(F,s) \\ \mathcal{R}_{41}(F,s) & \mathcal{R}_{42}(F,s) & \mathcal{R}_{43}(F,s) & \mathcal{R}_{44}(F,s) \end{bmatrix} \begin{bmatrix} x_1(\eta,0) \\ x_2(\eta,0) \\ x_3(\eta,0) \\ x_4(\eta,0) \end{bmatrix} \tag{2.25}$$

The associated resolvent operators can be expressed as

$$\begin{cases} \mathcal{R}_{i1}(F,s)(\cdot) = -\frac{F_{i4}(\zeta,s)}{F_{44}(L,s)} \int_0^L \frac{1}{v} F_{41}(L-\varepsilon,s)(\cdot)d\varepsilon + \int_0^\zeta \frac{1}{v} F_{i1}(\zeta-\eta,s)(\cdot)d\eta, i = 1,2,3,4 \\ \mathcal{R}_{i2}(F,s)(\cdot) = -\frac{F_{i4}(\zeta,s)}{F_{44}(L,s)} \int_0^L \frac{1}{v} F_{42}(L-\varepsilon,s)(\cdot)d\varepsilon + \int_0^\zeta \frac{1}{v} F_{i2}(\zeta-\eta,s)(\cdot)d\eta, i = 1,2,3,4 \\ \mathcal{R}_{i3}(F,s)(\cdot) = -\frac{F_{i4}(\zeta,s)}{F_{44}(L,s)} \int_0^L \frac{1}{v} F_{43}(L-\varepsilon,s)(\cdot)d\varepsilon + \int_0^\zeta \frac{1}{v} F_{i3}(\zeta-\eta,s)(\cdot)d\eta, i = 1,2,3,4 \\ \mathcal{R}_{i4}(F,s)(\cdot) = \frac{F_{i4}(\zeta,s)}{F_{44}(L,s)} \int_0^L \frac{1}{v_c} F_{44}(L-\varepsilon,s)(\cdot)d\varepsilon - \int_0^\zeta \frac{1}{v_c} F_{i4}(\zeta-\eta,s)(\cdot)d\eta, i = 1,2,3,4 \end{cases} \tag{2.26}$$

Now, the discrete-time operators in Eq.(2.18) can be solved by straightforwardly substituting the above resolvent operators. Afterwards, the discrete-time linear model is obtained:

$$\begin{aligned} X(\zeta,k) &= \mathcal{A}_d X(\zeta,k-1) + \mathcal{B}_d u(k) \\ Y(k) &= C_d X(\zeta,k-1) + \mathcal{D}_d u(k) \end{aligned} \tag{2.27}$$

with the boundary conditions Eq.(2.9) and the initial conditions Eq.(2.10).

2.3 MPC Formulation

The formulation of the model predictive controller is developed for the discrete-time PDE model Eq.(2.27). In particular, the constrained optimal controller design for the finite-dimensional system theory is extended and deployed for the infinite-dimensional system. Two cases to demonstrate the performance of the controller: one, including

the state feedback MPC with the assumption that full states are available, and two a Luenberger observer-based MPC to reconstruct the state from the available output measurements. These two cases are shown schematically in Figure 2.3. One notes that, in the MPC formulation, the state and output are denoted as $Z(\zeta, k)$ and $V(k)$ to avoid the confusion in the notation.

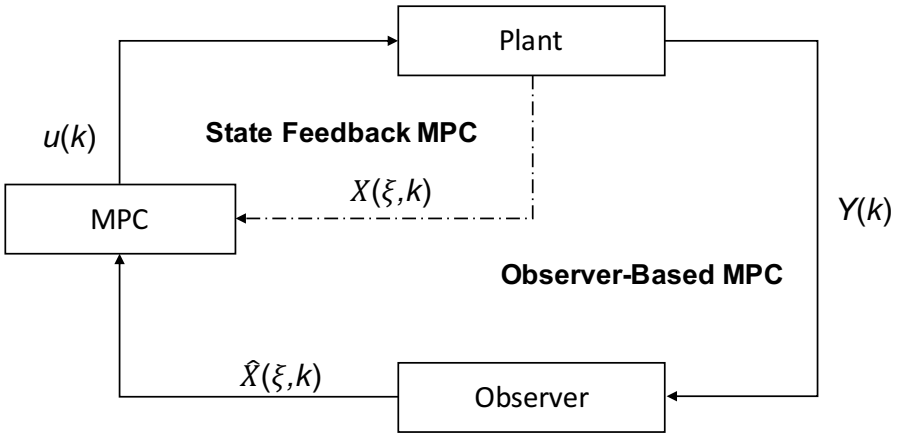

Figure 2.3: Scheme of state feedback MPC and observer-based MPC.

2.3.1 State feedback MPC

In this section, the MPC design for the finite-dimensional system is extended to the discrete-time infinite-dimensional tubular reactor model based on the previous contributions [18, 76, 36]. The predictive controller is founded as the solution of an optimization problem such that the following open-loop objective function on an infinite horizon is minimized at a given sampling time k:

$$\min_{u^N} \sum_{j=0}^{\infty} V_{k+j|k}^T Q V_{k+j|k} + u_{k+j|k}^T R u_{k+j|k} + \Delta u_{k+j|k}^T \bar{S} \Delta u_{k+j|k} \tag{2.28}$$

where Q is a symmetric positive semidefinite spatial operator, and R is a symmetric positive definite spatial operator. $V_{k+j|k}$ and $u_{k+j|k}$ represent the output and input variables at future time $k+j$ predicted at current time k, and the term $\Delta u_{k+j|k}$ denotes the change of an input vector at time $k+j$ as $\Delta u_{k+j|k} = u_{k+j|k} - u_{k+j-1|k}$. The vector u^N includes the control sequence $\{u_{k|k}, u_{k+1|k}, u_{k+2|k}, ..., u_{k+N-1|k}\}$ and the first element $u_{k|k}$ will be injected to the plant as the future control action.

A typical feature in MPC is that the infinite-horizon objective function can be cast into a finite-horizon objective function by assuming that the inputs are zero

beyond the control horizon N, i.e., $u_{k+N|k} = 0, j \geq N$. In addition, one penalty term needs to be added to the objective function in order to approximate the inputs and outputs beyond the horizon [104]. In this case, under the assumption of observability, the terminal output penalty term can be written as the corresponding state penalty term. Since the state is a spatio-temporal variable, the penalty term is given in the form of the inner product. Therefore, the finite horizon objective function with input and output constraints can be formulated as follows:

$$\begin{aligned}
&\min_{u^N} \sum_{j=0}^{N-1} V_{k+j|k}^T Q V_{k+j|k} + u_{k+j|k}^T R u_{k+j|k} + \langle Z_{k+N-1|k}, \bar{Q} Z_{k+N-1|k} \rangle \\
&\text{s.t. } Z_{\zeta,k-1|k} = X_{\zeta,k-1|k} \\
&\quad Z_{k+j|k} = \mathcal{A}_d Z_{k+j-1|k} + \mathcal{B}_d u_{k+j|k} \\
&\quad V_{k+j|k} = C_d Z_{k+j-1|k} + \mathcal{D}_d u_{k+j|k} \\
&\quad u_{\min} \leq u_{k+j|k} \leq u_{\max} \\
&\quad V_{\min} \leq V_{k+j|k} \leq V_{\max}
\end{aligned} \tag{2.29}$$

where N is the prediction horizon, $\bar{Q}$ is the spatial operator to penalize the terminal state which depends on the stability of the given model. u_{min} and u_{max} are the lower and upper bound vectors of the manipulated input $u(t)$. Moreover, V_{min} and V_{max} are lower and upper output constraints, respectively. It is important to note that the input and output constraints are imposed for two fundamentally different reasons. The input constraint usually represents physical limits of the control actuator or available control actuation, such as the limitation of the flow valve. For the output constraint, it usually represents the typical requirements among operation of tubular reactors in practice, such as the temperature of product not exceeding certain ranges, as well as the physical limits of actuators or sensors.

According to the nature of transport reaction systems, one can define $\bar{Q}$ as the infinite sum $\bar{Q} = \sum_{i=0}^{\infty} \mathcal{A}_d^{*i} C_d^* Q C_d \mathcal{A}_d^i$ which can be determined from the solution of the following discrete Lyapunov equation [104]:

$$\mathcal{A}_d^* \bar{Q} \mathcal{A}_d + C_d^* Q C_d = \bar{Q} \tag{2.30}$$

In particular, it can be demonstrated that the unique solution of the discrete Lyapunov equation is directly related to the continuous one which is shown as follows

[52]:

$$\mathcal{A}^*\bar{Q} + \bar{Q}\mathcal{A} = -C^*QC \tag{2.31}$$

The assumption of C being infinite-time admissible for $\mathcal{A}$ is required which denotes the continuous-time Lyapunov equation having solutions [105]. By multiplying a spatial function $X(\zeta)$ and substituting operator $\mathcal{A}$ on both sides, we can obtain:

$$\begin{aligned}
&\mathcal{A}^*\bar{Q}X + \bar{Q}\mathcal{A}X = -C^*QCX \\
&-V\frac{\partial \bar{Q}X}{\partial \zeta} + \mathcal{A}^T\bar{Q}X + \bar{Q}\left(V\frac{\partial X}{\partial \zeta} + \mathcal{A}X\right) = -C^*QCX \\
&-V\bar{Q}\frac{\partial X}{\partial \zeta} - V\frac{\partial \bar{Q}}{\partial \zeta}X + \mathcal{A}^T\bar{Q}X + V\bar{Q}\frac{\partial X}{\partial \zeta} + \bar{Q}\mathcal{A}X = -C^*QCX \\
&\frac{\partial \bar{Q}}{\partial \zeta} = V^{-1}\mathcal{A}^T\bar{Q} + V^{-1}\bar{Q}\mathcal{A} + V^{-1}C^*QC
\end{aligned}$$

where $\bar{Q} \in \mathcal{D}(\mathcal{A}^*)$. As a result, the straightforward algebraic manipulation of the objective function presented in Eq.(2.29) leads to the following quadratic programming optimization problem.

$$\begin{aligned}
&\min_U J = \frac{1}{2}U^THU + U^T\langle I, FZ_{\zeta,k-1|k}\rangle + \langle Z_{\zeta,k-1|k}, \bar{Q}Z_{\zeta,k-1|k}\rangle \\
&\text{s.t. } U_{\min} \le U \le U_{\max} \\
&\qquad V_{\min} \le GU + SZ_{\zeta,k-1|k} \le V_{\max}
\end{aligned} \tag{2.32}$$

where $U = \{u_{k+n}\}_{n=1}^N$ and $H \in \mathcal{L}(U)$ is positive and self-adjoint. By direct calculation, it is straightforward to find:

$$h_{i,j} = \begin{cases} \mathcal{D}_d^*Q\mathcal{D}_d + \mathcal{B}_d^*\bar{Q}\mathcal{B}_d + R & \text{for } i = j \\ \mathcal{D}_d^*QC_d\mathcal{A}_d^{i-j-1}\mathcal{B}_d + \mathcal{B}_d^*\bar{Q}\mathcal{A}_d^{i-j}\mathcal{B}_d & \text{for } i > j \\ h_{j,i}^* & \text{for } i < j \end{cases} \tag{2.33}$$

with F given by $F = \{\mathcal{D}_d^*QC_d\mathcal{A}_d^{k-1} + \mathcal{B}_d^*\bar{Q}\mathcal{A}_d^k\}_{k=1}^{N-1}$.

The constraints of Eq.(2.32) can be written in the form:

$$\begin{bmatrix} I \\ -I \\ G \\ -G \end{bmatrix} U \le \begin{bmatrix} U_{\max} \\ -U_{\min} \\ V_{\max} - SZ_{\zeta,k-1|k} \\ -V_{\min} + SZ_{\zeta,k-1|k} \end{bmatrix} \tag{2.34}$$

where G is a lower triangular matrix given by

$$g_{i,j} = \begin{cases} \mathcal{D}_d & \text{for } i = j \\ C_d\mathcal{A}_d^{i-j-1}\mathcal{B}_d & \text{for } i > j \\ 0 & \text{for } i < j \end{cases}$$

and $S = \{C_d\mathcal{A}_d^{k-1}\}_{k=1}^N$.

2.3.2 Observer-based MPC

In the previous section, we assumed that the states are available at each sample time k. In other words, it requires knowledge of the current state of the system in order to compute the solution of optimal input formulated at each interval. However, in most applications, state information is not always known. Therefore, for output feedback, a Luenberger observer which can reconstruct the states based on the output measurements is needed. In general, there are two ways to design the Luenberger observer, including the continuous-time observer based on the continuous system model and discrete one under the discrete setting.

Firstly, let us recall the linearized continuous-time model:

$$\begin{aligned} \dot{X}(\zeta,t) &= \mathcal{A}X(\zeta,t) + \mathcal{B}u(t) \\ Y(t) &= CX(\zeta,t) \end{aligned} \tag{2.35}$$

The Luenberger observer is presented by the following equations:

$$\begin{aligned} \dot{\hat{X}}(\zeta,t) &= \mathcal{A}\hat{X}(\zeta,t) + \mathcal{B}u(t) + L_c(Y(t) - \hat{Y}(t)) \\ \hat{Y}(t) &= C\hat{X}(\zeta,t) \end{aligned} \tag{2.36}$$

where L_c is the continuous observer gain to be designed. Stability of the observer implies that the state estimation error, $e(\zeta,t) = X(\zeta,t) - \hat{X}(\zeta,t)$, converges to zero within a certain time. The error dynamic equation is shown as follows:

$$\dot{e}(\zeta,t) = (\mathcal{A} - L_cC)e(\zeta,t) \tag{2.37}$$

The design problem is to choose an appropriate observer gain L_c such that the operator $\mathcal{A}_c = \mathcal{A} - L_cC$ is stable which guarantees the stability of the error dynamics. According to the infinite-dimensional features, the observer gain L_c can be obtained by solving the following Lyapunov equation:

$$\langle Q_cX, \mathcal{A}_c^*X\rangle + \langle \mathcal{A}_c^*X, Q_cX\rangle = -\langle MX, X\rangle, X \in \mathcal{D}(\mathcal{A}_c^*) \tag{2.38}$$

where M is positive definite design parameter and Q_c is a nonnegative self-adjoint operator which maps from $\mathcal{D}(\mathcal{A}_c^*)$ to $\mathcal{D}(\mathcal{A}_c)$. Let us assume that the pair $(\mathcal{A}, C)$ is exponential detectable, then if there exists a nonnegative self-adjoint operator Q_c which is the solution of the following operator Riccati equation [53]:

$$\mathcal{A}Q_c + Q_c\mathcal{A}^* - 2Q_cC^*CQ_c + M = 0, \text{on } \mathcal{D}(\mathcal{A}^*) \tag{2.39}$$

The observer gain $L_c = Q_c C^*$ is an exponentially stabilizing gain which guarantees the exponentially stability of $\mathcal{A}_c = \mathcal{A} - L_c C$.

In a similar manner, one can design a discrete Luenberger observer based on the following discrete-time model:

$$\begin{aligned} X(\zeta, k) &= \mathcal{A}_d X(\zeta, k-1) + \mathcal{B}_d u(k) \\ Y(k) &= C_d X(\zeta, k-1) + \mathcal{D}_d u(k) \end{aligned} \tag{2.40}$$

The observer is constructed by the following equations:

$$\begin{aligned} \hat{X}(\zeta, k) &= \mathcal{A}_d \hat{X}(\zeta, k-1) + \mathcal{B}_d u(k) + L_d(Y(k) - \hat{Y}(k)) \\ \hat{Y}(k) &= C_d \hat{X}(\zeta, k-1) + \mathcal{D}_d u(k) \end{aligned} \tag{2.41}$$

where L_d is the discrete observer gain to be designed. Similarly, we can obtain the error dynamic as $e_k = (\mathcal{A}_d - L_d C_d) e_{k-1}$. To obtain a stabilizing observer gain $L_d = Q_d C_d^*$, Q_d which is nonnegative self-adjoint operator must be found by solving the following Discrete Lyapunov equation:

$$\langle X, [\tilde{\mathcal{A}}_d^* Q_d \tilde{\mathcal{A}}_d - Q_d] X \rangle = -\langle X, [\tilde{C}_d^* N \tilde{C}_d] X \rangle \tag{2.42}$$

where $\tilde{\mathcal{A}}_d = \mathcal{A}_d - L_d C_d = -I(\cdot) + 2\delta[\delta I - \mathcal{A}_c]^{-1}$ and $\tilde{C}_d = \sqrt{2\delta} C[\delta - \tilde{\mathcal{A}}_d]^{-1}$. It can be demonstrated that the solution of the discrete Lyapunov equation is also the solution of the continuous Lyapunov equation under the Cayley-Tustin time discretization setting [53, 106]. Therefore, the discrete Luenberger observer gain can be obtained by constructing the continuous observer gain.

According to the principle of predictive control, the state estimated by the observer at the current moment will be used as the starting point for predicting the future dynamics of the system. Hence, the observer-based MPC can be reconstructed by setting the initial state equal to the estimate of the current state at each time k, i.e., $Z_{\zeta,k-1|k} = \hat{X}_{\zeta,k-1|k}$. One can obtain the estimate of the current state from Luenberger observer, from which one can reconstruct the entire state trajectory [107]. In this

case, the observer-based MPC is directly formulated as follows :

$$
\begin{aligned}
\min_{u^N} \quad & \sum_{j=0}^{N-1} V_{k+j|k}^T Q V_{k+j|k} + u_{k+j|k}^T R u_{k+j|k} + \langle Z_{k+N-1|k}, \bar{Q} Z_{k+N-1|k} \rangle \\
\text{s.t.} \quad & Z_{\zeta,k-1|k} = \hat{X}_{\zeta,k-1|k} \\
& Z_{k+j|k} = \mathcal{A}_d Z_{k+j-1|k} + \mathcal{B}_d u_{k+j|k} \\
& V_{k+j|k} = \mathcal{C}_d Z_{k+j-1|k} + \mathcal{D}_d u_{k+j|k} \\
& u_{\min} \leq u_{k+j|k} \leq u_{\max} \\
& V_{\min} \leq V_{k+j|k} \leq V_{\max}
\end{aligned}
\tag{2.43}
$$

where $u^N, N, Q, R, \bar{Q}$ are as in Eq.(2.29). As for implementation, the Luenberger observer design and MPC must be performed iteratively until the performance is acceptable.

2.4 Simulation Study

In this section, the performance of the two MPC formulations developed in the previous section is demonstrated through two case studies. Case study 1 illustrates the state feedback MPC design where all states of the system are assume to be available or measurable. The sensitivity analysis of input and output weights and constraints of MPC formulation is given. Considering the unavailability of state measurements in realistic tubular reactors, the observer is designed to reconstruct the states, based on which an observer-based MPC is simulated as Case study 2. Both of the controllers are designed to satisfy the input and output constraints requirements and achieve system stabilization at the same time. The resulting constrained optimization problems become quadratic programming problems which are solved using the MATLAB subroutine QuadProg.

The parameter values used in Eq.(2.32) and for simulations are listed in Table 2.1. For the initial conditions of the dynamic system, we consider $x_1(\zeta, 0) = 0.019\zeta, x_2(\zeta, 0) = 0.03\zeta, x_3(\zeta, 0) = 0.02\zeta, x_4(\zeta, 0) = 0.02(1 - \zeta)$. In addition, $\bar{\zeta}_L = 0.15$ is chosen for the input operator. In both cases, the horizon of $N = 15$ is selected with the terminal constraint formulation. The input and output weights are chosen as $R = 5$ and $Q = \text{diag}\{0.5, 0.5, 0.5, 0.5\}$ for MPC implementation, respectively. The input

and output constraints are considered as $u_{min} = -0.5$, $u_{max} = 0.05$, $V_{min} = -0.5$ and $V_{max} = 9$ with respect to state perturbation. As for the Cayley-Tustin time discretization, we choose $h = 2$ at the time discretization interval which implies $\delta = 1$. The spatial discretization interval is taken as $d\zeta = 0.01$.

As shown in Figure 2.4, the open-loop states converge to their corresponding steady states rapidly which indicates the original plant is intrinsically stable. By implementing the proposed MPC frameworks, we aim to steer the convergence rate without violating the physical constraints of actuators and sensors. In order to clearly show the perturbation of each state, the linearized states are depicted in Figure 2.5, where it is apparent that all states go to close zero within the considered time range.

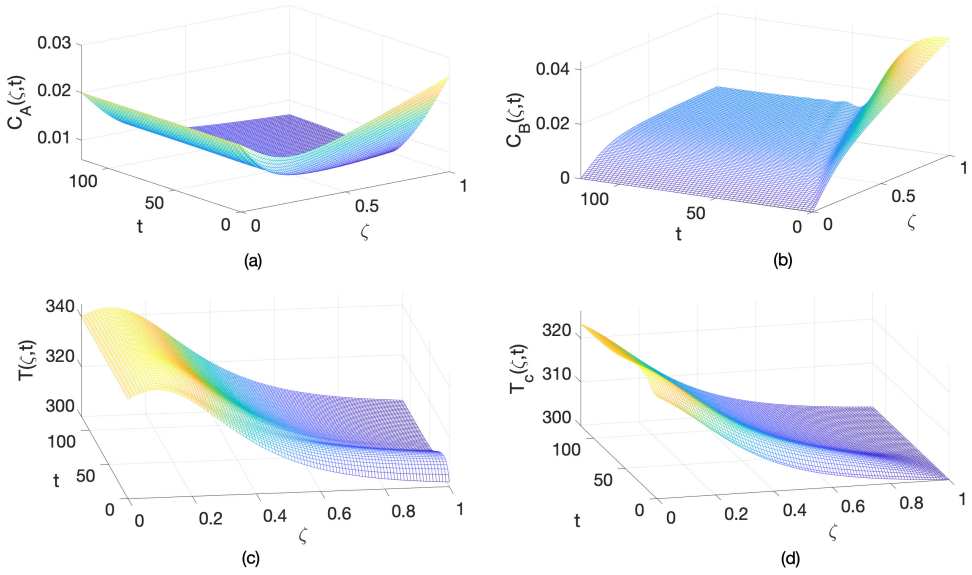

Figure 2.4: Open-loop steady state profiles of the tubular reactor.

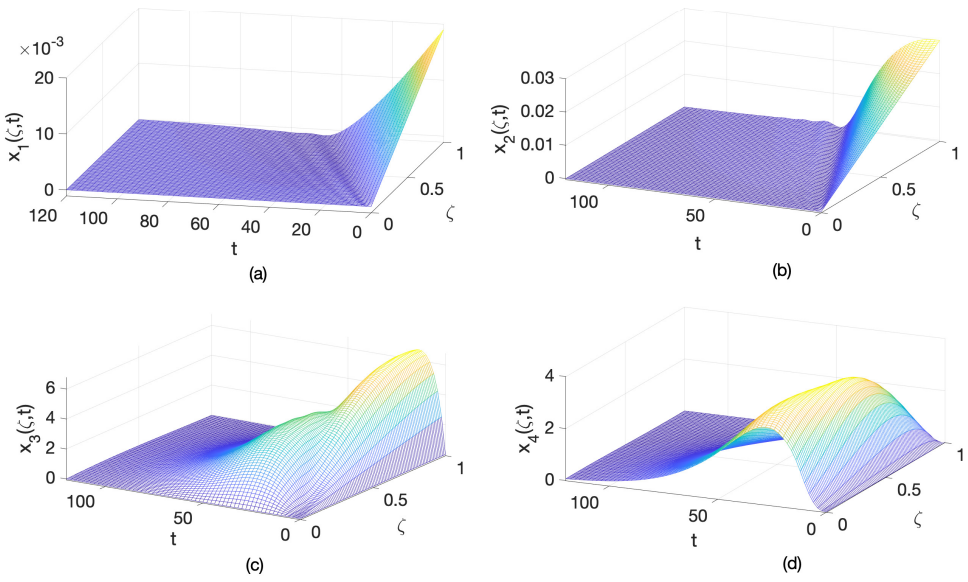

Figure 2.5: Perturbations of open-loop state profiles of the tubular reactor from Eq.(2.27).

2.4.1 Case study 1: State feedback MPC

By implementing the optimal control input on the plant model, the states of the closed-loop system under the MPC law given by Eq.(2.32) are obtained and shown in Figure 2.6. The closed-loop system is stabilized because all of the states go to zero with a faster convergence rate compared with the open-loop states shown in Figure 2.5. This can also be verified from the output profiles shown in Figure 2.7, where the four outputs under the state feedback MPC law converge to steady states which are faster than the corresponding open-loop profiles. In this case, we aim to steer the temperature of the reactor without exceeding its corresponding physical constraint. It can be observed from Figure 2.8(a), compared with the open-loop temperature profiles, the closed-loop profile converge to steady state at a faster rate and satisfy the constraints simultaneously. The corresponding manipulated input is given in Figure 2.8(b). The control effort is required on the half of the time horizon to keep the output inside the range of set limits and after that, the requirement for input control is not obvious.

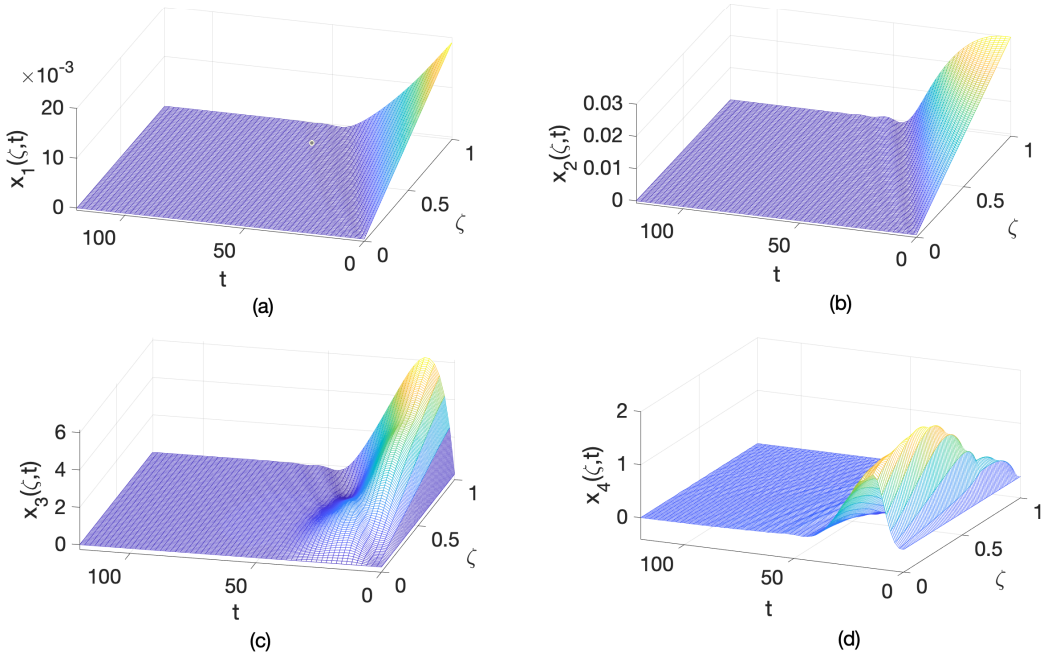

Figure 2.6: Perturbations of closed-loop state profiles of the tubular reactor under the state feedback MPC law from Eq.(2.32).

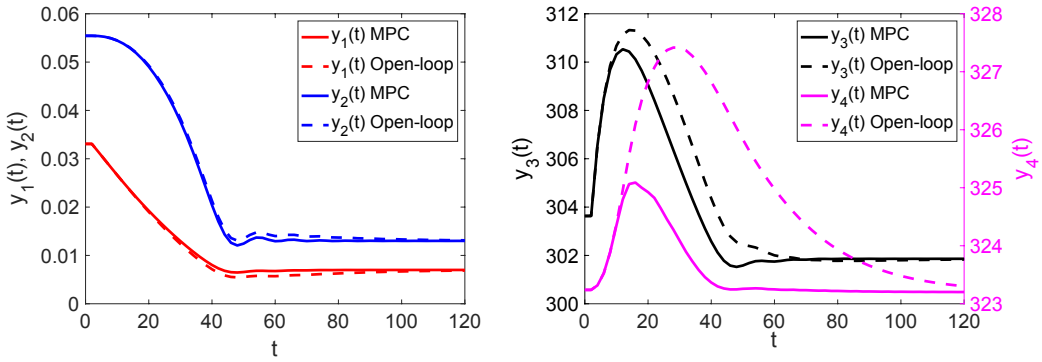

Figure 2.7: Performance comparison of open-loop and closed-loop output profiles under the state feedback MPC law from Eq.(2.32).

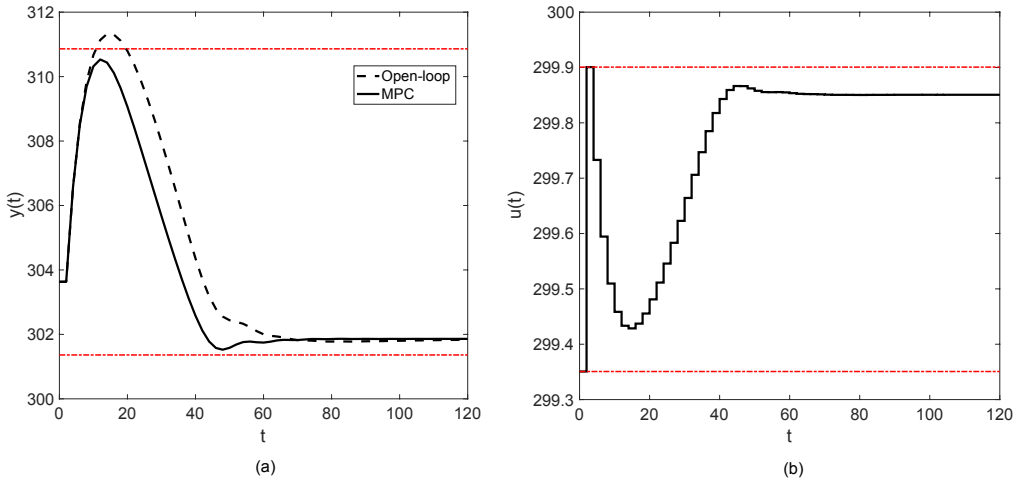

Figure 2.8: (a) Comparison between profiles of the open-loop and closed-loop outputs (y_3) using the state feedback MPC from Eq.(2.32). (b) Input profile calculated in the state feedback MPC case from Eq.(2.32).

In addition, the influence of the choice of the input and output weights (Q and R) on the state feedback MPC performance is investigated below, where the average absolute error is taken as the evaluation index. With the same objective function and horizon, different input and output constraints (with ±5% and ±10% based on the chosen case $u_{min} = -0.5$, $u_{max} = 0.05$, $V_{min} = -0.5$ and $V_{max} = 9$) are implemented. As illustrated in Table 2.2, it is apparent that the state feedback MPC generally presents a very small average absolute error which stays within a reasonable range (4.46×10^{-5} to 1.00×10^{-3}) under these conditions considered. In particular, when the input and output weights are chosen as $R = 5$ and $Q = \text{diag}\{0.5, 0.5, 0.5, 0.5\}$ for MPC implementation, the average absolute error is smallest and which is the case considered in this chapter.

Table 2.2: Performance comparison of the state feedback MPC with different input and output weights and constraints

Weights		+10%	+5%	base case	-5%	-10%
Q=diag {0.5,	R=5	1.00×10^{-3}	1.00×10^{-3}	1.00×10^{-3}	7.91×10^{-4}	4.46×10^{-5}
0.5, 0.5, 0.5}	R=10	5.03×10^{-3}	5.03×10^{-3}	5.03×10^{-3}	4.51×10^{-3}	3.51×10^{-3}
Q=diag {5,5	R=5	1.32×10^{-3}	1.51×10^{-3}	1.67×10^{-3}	1.83×10^{-3}	2.14×10^{-3}
5,5}	R=10	5.71×10^{-4}	8.53×10^{-4}	8.79×10^{-4}	9.95×10^{-4}	1.77×10^{-3}

2.4.2 Case study 2: Observer-based MPC

The performance of observer-based MPC is now described. Compared with the implementation of state feedback MPC, the MPC is now implemented based on the estimate states. Firstly, in order to obtained the estimate states, the observer design implies that the expression in Eq.(2.39) is applied, with a arbitrary choice of the design parameter $M(\zeta)$ and $\Psi(\zeta)$ in the domain of $\mathcal{D}(\mathcal{A}^*)$, which leads to the following equations:

$$\mathcal{A}Q_c\Psi(\zeta) + Q_c\mathcal{A}^*\Psi(\zeta) + M\Psi(\zeta) - 2Q_cC^*CQ_c\Psi(\zeta) = 0$$

$$V\frac{\partial Q_c}{\partial \zeta}\Psi(\zeta) + VQ_c\frac{\partial \Psi}{\partial \zeta} + A(\zeta)Q_c\Psi(\zeta) + Q_c[-V\frac{\partial \Psi}{\partial \zeta} + A(\zeta)^*\Psi(\zeta)] + M\Psi(\zeta) - 2Q_cC^*CQ_c\Psi(\zeta) = 0$$

$$V\frac{\partial Q_c}{\partial \zeta}\Psi(\zeta) + A(\zeta)Q_c\Psi(\zeta) + Q_cA(\zeta)^*\Psi(\zeta) + M\Psi(\zeta) - 2Q_cC^*CQ_c\Psi(\zeta) = 0$$

which yields

$$\frac{\mathrm{d}Q_c}{\mathrm{d}\zeta} = V^{-1}[2Q_cC^*CQ_c - 2A(\zeta)Q_c - M]$$

Therefore, one needs to choose Q_c which in the domain of $\mathcal{A}$ and positive function M to ensure the nonnegative definiteness of Q_c. Choosing M to be 0.001, Q_c can be solved numerically and then the observer gain is found $L = Q_cC^*$. As shown in Figure 2.9, the estimation error of the designed Luenberger observer converges to zero with time increasing.

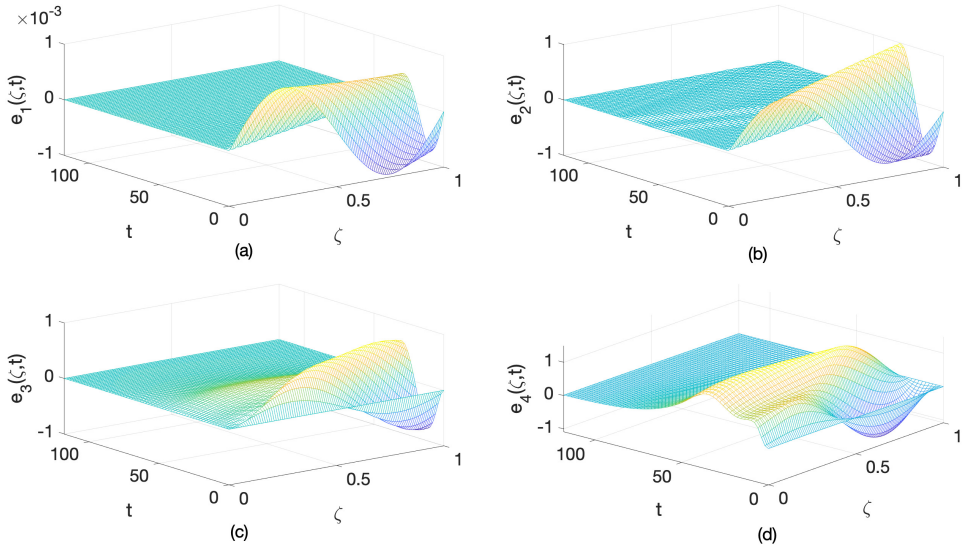

Figure 2.9: Evolution of the observer error $e(\zeta, t)$.

As shown in Figure 2.10, output profiles under the observer-based MPC law converge to steady states that are similar to the corresponding state feedback output profiles as shown in Figure 2.7. The third output under the observer-based MPC law has a faster convergency rate than the open-loop profile. The obvious difference between them is that the observer-based MPC keeps the output within the given constraints to satisfy the requirements. The input manipulation obtained from the observer-based MPC, which is the solution of the constrained optimization problem in Eq.(2.43) as shown in Figure 2.11. The comparison of plant outputs and observer outputs are shown in Figure 2.12. The estimated outputs have a slight overshoot compared with plant outputs but there are no obvious differences in terms of convergency rates.

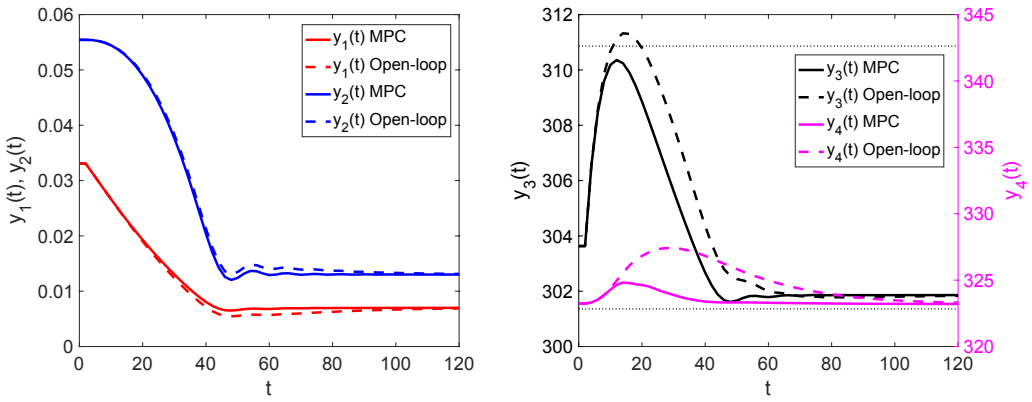

Figure 2.10: Performance comparison of open-loop and closed-loop output profiles under the observer-based MPC law from Eq.(2.43).

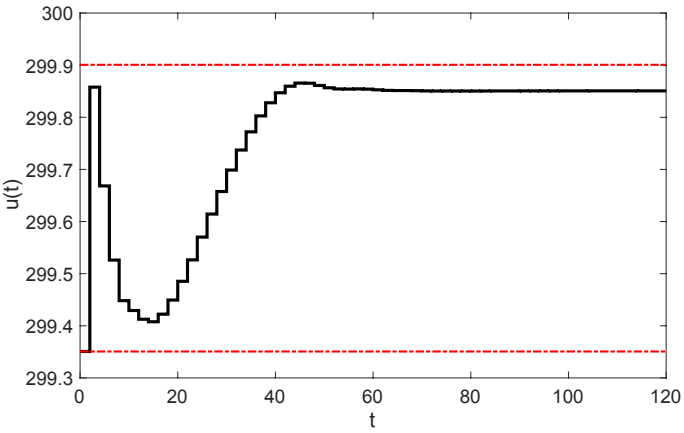

Figure 2.11: Input profile computed by the observer-based MPC in Eq.(2.43).

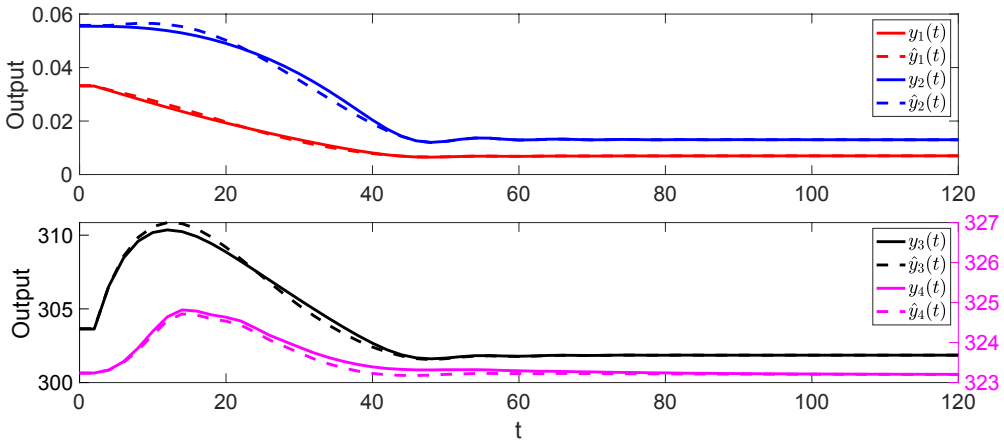

Figure 2.12: Estimated output profiles using the Luenberger observer.

In order to further investigate the performance of the proposed MPC design, we consider two truly unknown disturbances which makes the open-loop system potentially unstable. In addition, we assumed the addition of disturbance does not affect the feasibility of input and output constraints. Specifically, two types of disturbance including input disturbance and distributed disturbance were injected to the system.

In this first scenario, we consider the input disturbance, $d(t) = 0.0005\sin(0.06t)$. The perturbations of open-loop state profiles shown in Figure 2.13 have shown the sinusoidal trend given by the disturbance signal considered here, and the proposed MPC design can stabilize the unstable modes as illustrated in Figure 2.14. As shown in Figure 2.15, it is apparent that the open-loop output responses oscillate due to input disturbance injection. The MPC controller is able to simultaneously realize disturbance rejection and converge to steady states in a short time, and satisfies the given constraints. The corresponding manipulated input is given in Figure 2.16. Therefore, it can be clearly seen that under the consideration of input disturbance, the proposed MPC achieves a good control performance.

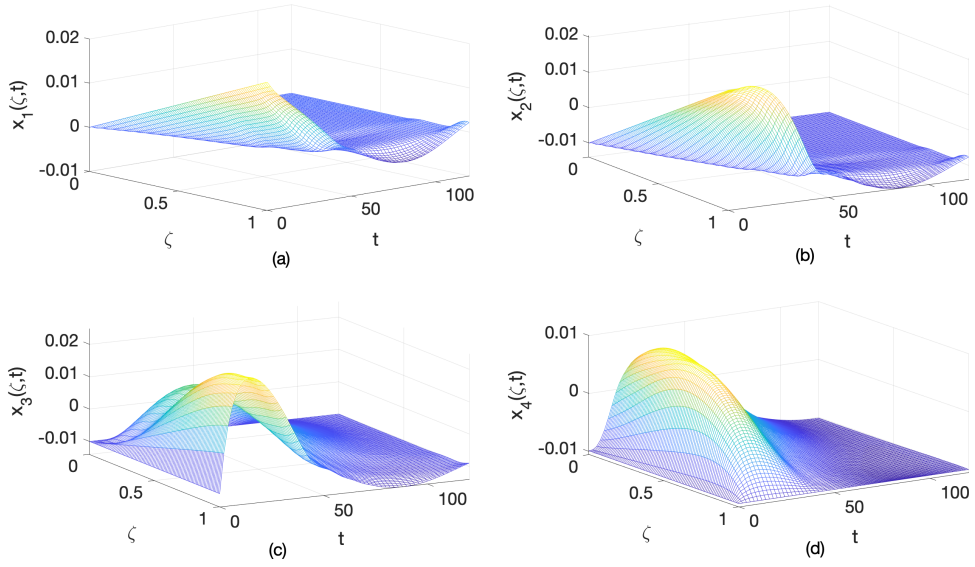

Figure 2.13: Perturbations of open-loop state profiles under the consideration of input disturbance.

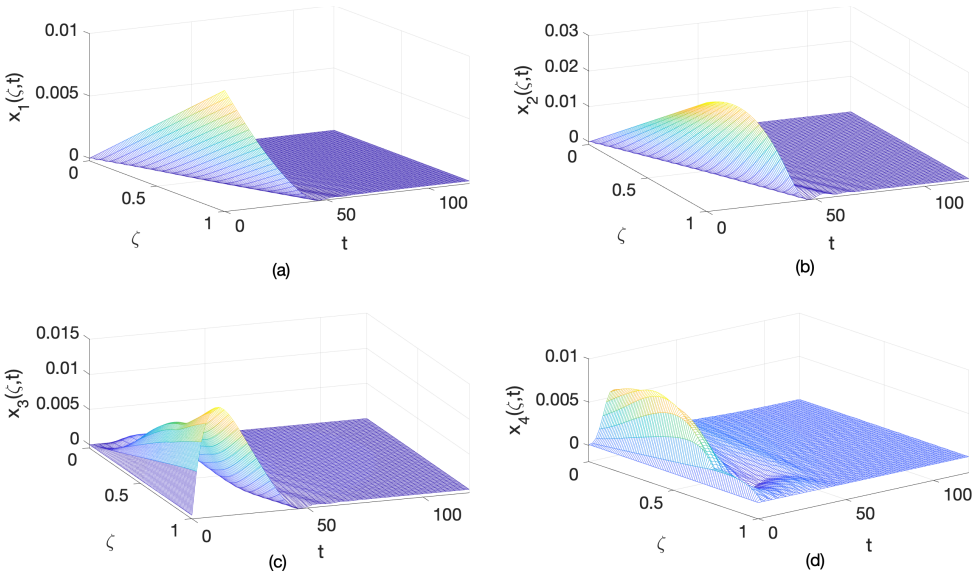

Figure 2.14: Perturbations of closed-loop state profiles under the consideration of input disturbance with the observer-based MPC law from Eq.(2.43).

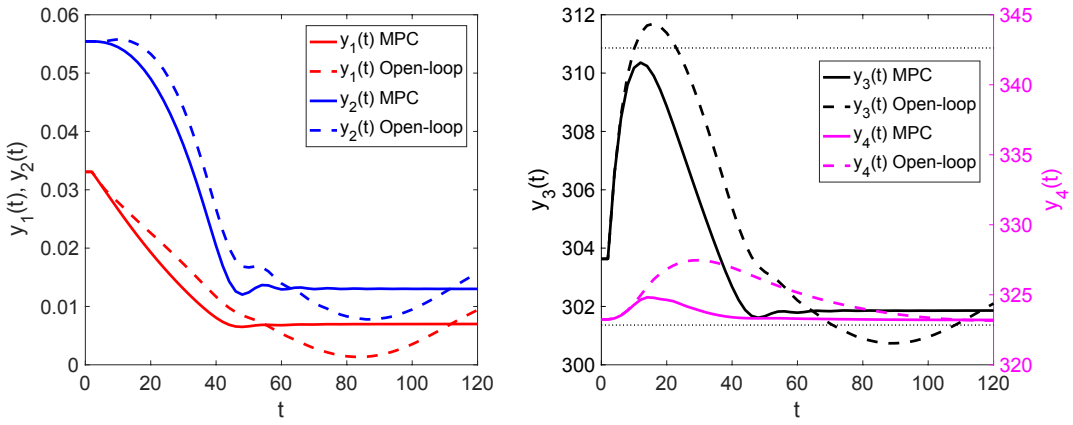

Figure 2.15: Closed-loop output profiles under the consideration of input disturbance with the observer-based MPC law from Eq.(2.43).

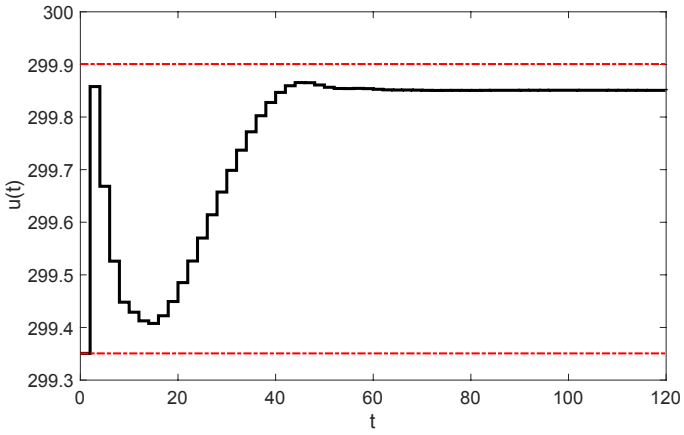

Figure 2.16: Input profile calculated in the observer-based MPC case from Eq.(2.43).

In this second scenario, we consider the distributed disturbance which is expressed by a step signal, $d(t) = \begin{cases} 0.0001, & t \in [32, 62] \\ 0 & \text{otherwise} \end{cases}$. As shown in Figure 2.17, the open-loop outputs show significantly oscillation when the step disturbance is applied. The closed-loop output profiles show that the disturbance does not affect the designed control law because of the fast convergency rate and good disturbance rejection. The corresponding manipulated input is given in Figure 2.18. It is apparent that the control actions become more reliable and the system converges faster.

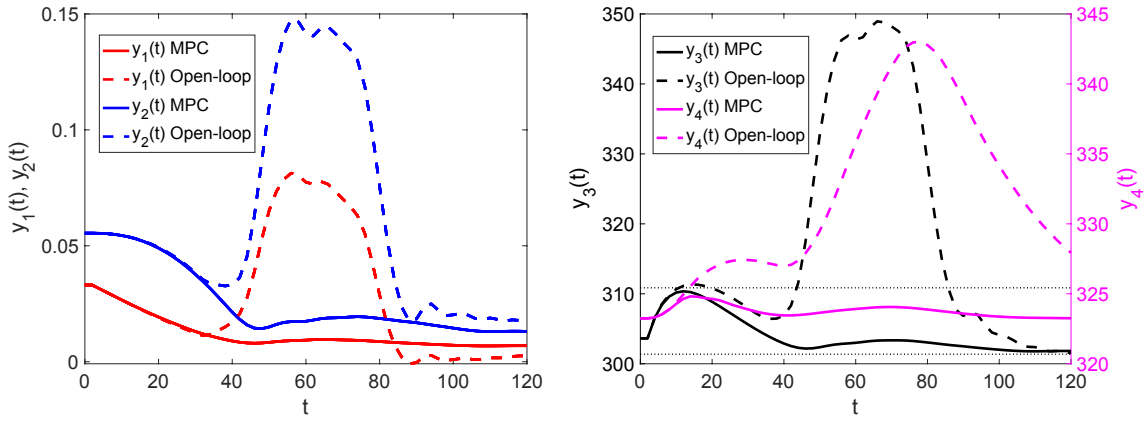

Figure 2.17: Closed-loop output profiles considering the distributed disturbance under the observer-based MPC law from Eq.(2.43).

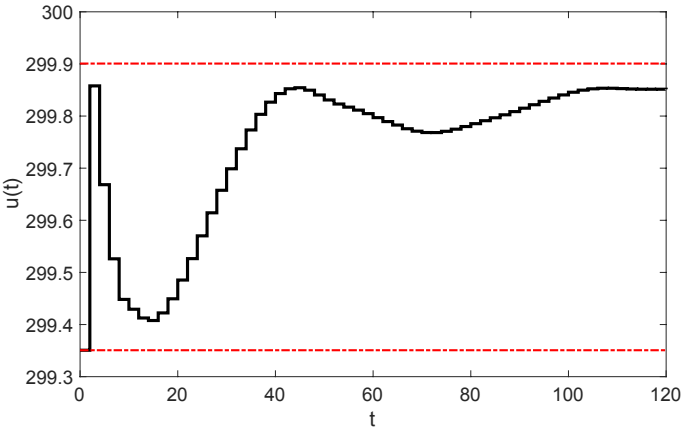

Figure 2.18: Input profile generated by the observer-based MPC from Eq.(2.43).

Finally, the performance of open-loop, state feedback MPC and observer-based MPC are compared from the perspectives of average settling time and absolute error under the consideration of two types of disturbances with the same overall simulation time of 120 seconds. More specifically, the settling time is calculated as the time taken by the outputs response to reach the steady states with 2% tolerance in this case. The absolute error is defined as the absolute difference of the controlled outputs and the outputs according to steady states at 120s. The average settling time and absolute error are calculated by taking average of all outputs. For the disturbance signals, we consider two same types of disturbance including input disturbance and

distributed disturbance.

Table 2.3: Performance comparison of open-loop and closed-loop systems with different types of disturbance.

Types of disturbance	Input disturbance		Distributed disturbance	
Specifications	Settling time	Abs. error	Settling time	Abs. error
Open-loop	- -	5.13×10^{-2}	75.5s	1.10
State feedback MPC	42s	3.73×10^{-4}	67s	4.33×10^{-3}
Observer-based MPC	45s	9.75×10^{-4}	68s	4.93×10^{-3}

As illustrated in Table 2.3, it is apparent that the settling time of state feedback MPC is slightly smaller than the observer-based MPC under the consideration of input sinusoidal disturbance, while the open-loop system the settling time is not achieved during the overall simulation. The average absolute error of open-loop system is 5.13×10^{-2}, which is worse than the error of two strategies controller (9.75×10^{-4} and 3.73×10^{-4} respectively) where the observer-based MPC shows a competitive performance to the state feedback MPC. Under the proposed distributed disturbance consideration, the overall trend is similar to the input disturbance but the open-loop system shows a worse absolute error than other cases. Through the simulation studies, it can be seen that the feasibility and applicability for MPC design are valid. As expected, the two constrained predictive controllers developed in this chapter are able to minimize the energy cost and/or prevent damage to equipment (sensors and actuators) in order to improve the safety and efficiency of the system.

The novelty of the proposed design method lies in the combination of Cayley-Tustin time discretization of PDE model with MPC application in tubular reactor with reversible reaction. Therefore, the proposed design outperforms other numerical simulation methods by using Cayley-Tustin time discretization because of numerical stability, energy-preserving, theoretic properties (such as stability, controllability, and observability) preserving in a late lumping manner. The construction of the model predictive controller of infinite-dimensional system leads to a finite-dimensional constrained quadratic optimization problem which is easily solvable by using standard numerical optimization methods.

2.5 Conclusions

In this chapter, the model predictive control algorithms were developed for a jacket tubular reactor as the distributed parameters system, considering the input and state constraints. The plant was described by a set of nonlinear coupled hyperbolic PDEs considering a simple reversible exothermic reaction taking place in the reactor ($A \rightleftharpoons B$). In particular, a spatially varying jacket temperature was considered in this chapter instead of a constant one. After applying linearization around a given equilibrium operating point of interest, a linearized PDE model was obtained for the modelling tubular reactor dynamics. For model time-discretization, the Cayley-Tustin transform was utilized to map the continuous-time system to the discrete-time model representation without spatial discretization and model reduction which preserves the input-output stability of the plant. Model predictive controllers were formulated on that basis to realize model stabilization and account for input and output constraints. For state estimation, an observer-based MPC realization was proposed and realized by solving the corresponding operator Riccati equation which was utilized in the construction of Luenberger observer gains. Finally, two numerical examples were provided to demonstrate the feasibility of the proposed MPC design. They show that for the tubular reactor, the proposed MPC was capable of steering the original dynamics to steady states at a faster convergence rate without violating physical constraints and made a good performance in the presence of disturbances.

Chapter 3

Tracking Model Predictive Control and Moving Horizon Estimation Design of Distributed Parameter Pipeline Systems

3.1 Introduction

Pipelines have emerged as a highly economical and efficient means of transporting different hydrocarbons, including petroleum, crude oil, and diesel fuel. To meet the growing demands of energy transportation, extensive pipeline networks spanning long distances have been constructed to efficiently distribute various oil and gas commodities from reservoirs to markets and chemical plants. The ensuing challenge is the realization of energy scheduling under the complicated configurations of distributed pipeline networks and operational requirements. Consequently, advanced control and estimation methodologies are required to be tailored to pipeline transportation systems to realize robust, efficient, and safe operations.

Long-range pipeline systems belong to the distributed parameter system (DPS) as their dynamics depend both on time and space. Compared to the lumped parameter system (LPS), commonly characterized by ordinary differential equations (ODEs), DPS is often modelled by PDEs derived from first principles. DPS models are capable of describing the flow dynamics of transported fluid/gas within the pipeline system systematically [108]. The real-time transient model, constructed based on the conservation of mass, momentum, and energy balance laws, has gained widespread

utilization as a prominent example of first principle modelling [6], [11]. More specifically, it can be characterized by the Euler equations in one dimension, constituting a system of nonlinear coupled hyperbolic PDEs.

In the realm of controller design for distributed parameter pipeline systems, an extensive range of model-based control techniques have been explored. For instance, the design of discrete-time output regulators has been investigated to accommodate various operational requirements for different configurations of gas pipeline networks [109]. The backstepping technique has been applied to address the estimation and control of different topologies of pipeline systems [110, 111]. In order to fulfill the varying operational demands and satisfy the constraints associated with pipeline systems, there has been significant interest in exploring a variety of optimization-based approaches. Among these, a representative approach is MPC, commonly referred to as receding horizon control, which aims to determine the optimal control action by minimizing cost functions of interest while simultaneously adhering to various constraints. For example, a formulation of nonlinear MPC was introduced to minimize the operational expenses of gas pipeline networks [112] and was further extended and incorporated with a robust optimization strategy to address parametric uncertainty within the dynamic model [113]. A receding horizon optimal control algorithm was developed specifically for continuous-time hydraulic pipeline systems [11]. The optimal control design scheme considered sufficient conditions to ensure the global asymptotic stability of the system. A nonlinear MPC was proposed with the aim of facilitating fast closed-loop dynamics while ensuring compliance with all major constraints within the pipeline system [114]. A novel optimization strategy was presented to improve economic performance by coordinated dispatch, which took into account the spatio-temporal interactions between gas and electric transmission networks [115].

Achieving reliable control in pipeline systems typically relies on accurate information about the system's state. However, the compact installation of pressure and flow meters is often cost-prohibitive and impractical when it comes to long-range pipeline networks. This challenge has spurred the application of state and parameter estimation techniques which are based on the sensor's measurements at a limited number of locations along the pipeline system. Classical estimators like the Kalman filter or the Luenberger observer are commonly employed for estimation purposes but fall short

in accounting for system constraints [54]. An alternative tool, MHE, has emerged as a superior estimation technique [55]. MHE is an optimization-based state estimation method that utilizes a sequence of recent measurements to estimate the current state of a system, which has gained significant attention in the research community, particularly for LPS [56, 57, 58], but has been rarely explored for DPS modelled by PDEs. As an illustration, a moving horizon estimator was proposed to realize the tracking of internal space-time flow and pressure profiles specifically during dynamic transients in pipeline systems [59]. Two estimation problems were formulated for state estimation and joint state and parameter estimation utilizing a reduced model of a natural gas system [60].

Most of the existing contributions on MPC and MHE designs of DPS are based on early lumped methods, which first approximate the spatial variables by utilizing finite difference methods, spectral approaches, and/or finite element techniques, and then apply finite-dimensional state estimation and control methods to the resulting lumped parameter systems. These early lumping approaches are simpler to conduct by exploring finite-dimensional control theories and methods but may cause stability inconsistency and result in the loss of important system properties [116]. In contrast, late lumping approaches refer to that state estimation and control design steps are carried out directly on the original DPS by using infinite-dimensional control theories, and then spatial approximation or discretization is performed in the numerical simulation stage for realization purposes. The notable advantage of this approach is that it eliminates the need for spatial discretization of the PDEs in the design stage, which directly treats the original DPS while designing estimators and controllers. Along this line, a novel MPC was developed in the late lumping manner for regular linear DPS, containing stable regular systems and exponentially stabilizable systems [38]. An MHE was proposed to tackle the challenge of constrained output estimation for discrete-time PDE models while considering system and measurement disturbances [117]. The proposed designs in [38, 117] were mainly verified via scalar PDEs, and not for the systems of PDEs representing pipeline networks, and the parameter estimation was not investigated in [117].

In addition to this, when applying MPC and MHE design to a distributed parameter pipeline system, several challenges arise. Firstly, the model under consider-

ation is characterized by a set of first-order hyperbolic PDEs that are not spectral, thereby indicating the absence of slow-fast dynamic separation. Secondly, in industrial applications, parameters such as pipe friction are often not accurately known, and unmeasurable states further complicate the task of state and parameter estimation, necessitating careful consideration during the design of the estimator. Thirdly, to track the desired output and stabilize the system around the corresponding steady state, one needs to first find the steady state by solving a static equation and utilize it in an MPC scheme [118], while the potential challenge is that a feasible solution may not always exist.

Motivated by the preceding discussions, to meet the various operational demands in the pipeline industry, this chapter aims to develop discrete-time tracking MPC for a distributed parameter pipeline system with branched topology by using the first principle model and MHE design for the purpose of state and parameter estimation. The controller and estimator designs are based on the late lumping method, which avoids spatially discretizing the PDEs so that the infinite-dimensional nature of the original pipeline system is preserved. A preliminary study was previously conducted in [119], focusing on output tracking for a single pipe through the design of a two-layer model predictive controller (consisting of a trajectory planner and tracking MPC). However, in this work, we extend the scope to address a more complex and commonly encountered type of pipeline network by incorporating state/parameter estimation into the design of a novel tracking MPC. The main contributions of this chapter are summarized as follows:

1). A branched pipeline network modelled by six nonlinear coupled first-order hyperbolic PDEs with a boundary input is proposed and investigated. The Cayley-Tustin method is employed to establish the corresponding discrete-time infinite-dimensional model, which preserves the continuous-time system properties without requiring spatial approximation or order reduction [14]. Along this line, one can obtain the analytical solution for the distributed parameter pipeline systems.

2). The MHE design of a discrete-time distributed parameter pipeline system is proposed to realize the state estimation (of pressure and flow velocity) and constrained parameter estimation (of friction coefficient) based on the available plant or input information and measurement that are corrupted with bounded disturbances.

3). The single-layer tracking MPC scheme is proposed for discrete-time distributed parameter pipeline network systems to enable specific operations while maintaining physical flow constraints, by extending the recently published contribution [120] on tracking MPC design for finite-dimensional systems to that of infinite-dimensional systems.

4). Finally, the effectiveness of the proposed designs is verified via case studies. Sensitivity studies are further provided to show the robustness of the proposed designs.

This chapter is organized as follows. In Section 3.2, the description of the mathematical model of a pipeline network is introduced, and the linearized model is derived based on specific space-varying equilibrium profiles for the system. The discrete-time infinite-dimensional realization is realized for the resulting model using the Cayley-Tustin approach. In Section 3.3, the tracking MPC scheme and the state and parameters estimation are proposed. The validation results are shown to demonstrate the estimator and controller performance in Section 3.4. Finally, Section 3.5 provides the conclusions.

3.2 Mathematical Model

In this section, the isothermal Euler equations in the form of first-order coupled nonlinear hyperbolic PDEs are introduced for modelling the flow dynamics of a single liquid pipeline. Based on these, we establish the dynamic model for a branching pipeline network. Using the Cayley–Tustin transform, we further develop an infinite-dimensional discrete-time pipeline model with a closed-form solution, which will be used for MPC and MHE designs in Section 3.3.

3.2.1 Single pipeline dynamics

In this study, the following assumptions are considered [119]: (1) The transported flow is a one-dimensional single-phase liquid flow, where mass flux, density, and pressure are only functions of time and axial position; (2) each pipe is a rigid buried pipe, and any change in cross-sectional area along the liquid stream can be considered negligible; (3) small variations in density represent the presence of local compressibility. (4)

the transported flow is assumed to be viscous and isothermal, implying that any temperature changes resulting from pressure variations and friction effects can be disregarded.

The fluid flow dynamics can be mathematically described by a set of coupled nonlinear first-order hyperbolic PDEs [1][119]:

$$\begin{aligned}
&\frac{\partial \rho}{\partial t} + v\frac{\partial \rho}{\partial \zeta} + \rho\frac{\partial v}{\partial \zeta} = 0 \\
&\rho\frac{\partial v}{\partial t} + \rho v\frac{\partial v}{\partial \zeta} + \frac{\partial p}{\partial \zeta} + \rho g\sin(\alpha) + \rho\frac{\lambda v|v|}{2D} = 0 \\
&\frac{\partial p}{\partial t} + v\frac{\partial p}{\partial \zeta} + a^2\rho\frac{\partial v}{\partial \zeta} = 0
\end{aligned} \tag{3.1}$$

with the boundary conditions:

$$\rho(l,t) = \rho_l(t), v(0,t) = u(t), p(l,t) = p_l(t) \tag{3.2}$$

for $(\zeta, t) \in (0, L) \times (0, \infty)$. In (3.1), the state variables are represented by v (flow velocity), p (flow pressure) and ρ (flow density). The term $g\sin(\alpha)$ represents the ζ-component of the original gravity acceleration, where g denotes the gravity acceleration and α denotes the inclination angle. The parameter a represents the propagation velocity of sound within the fluid, λ denotes a dimensionless friction coefficient, and D refers to the pipe diameter. System (3.1) can be derived from the well-known water hammer equations [121], which are relatively straightforward mathematical models that make assumptions of isentropic flow. For buried pipelines, temperature differences between a pipe segment and the ground can be neglected in practice. Along this line, one can approximately model the fluid flow dynamics as an isothermal process without invoking the energy conservation law. A similar formulation of the gas pipeline flow system can be found in [122] that mass flow rate and pressure are regarded as system states.

The process of determining steady states for each state involves equating the temporal derivative terms to zero in (3.1), leading to the following expressions:

$$\begin{aligned}
&v_{ss}\frac{d\rho_{ss}}{d\zeta} + \rho_{ss}\frac{dv_{ss}}{d\zeta} = 0 \\
&\rho_{ss}v_{ss}\frac{dv_{ss}}{d\zeta} + \frac{dp_{ss}}{d\zeta} + \rho_{ss}g\sin\alpha + \rho_{ss}\frac{\lambda v_{ss}|v_{ss}|}{2D} = 0 \\
&v_{ss}\frac{dp_{ss}}{d\zeta} + a^2\rho_{ss}\frac{dv_{ss}}{d\zeta} = 0
\end{aligned} \tag{3.3}$$

Linearization can be achieved by utilizing the derived steady state profiles and introducing new state variables $\bar{v}(\zeta,t) = v(\zeta,t) - v_{ss}(\zeta)$, $\bar{p}(\zeta,t) = p(\zeta,t) - p_{ss}(\zeta)$ and $\bar{\rho}(\zeta,t) = \rho(\zeta,t) - \rho_{ss}(\zeta)$. By considering $\bar{p} = a^2\bar{\rho}$ (since $a^2 = dp/d\rho$), the system can be reduced to the following two-state pipeline model:

$$\frac{\partial}{\partial t}\begin{bmatrix}\bar{p}(\zeta,t)\\ \bar{v}(\zeta,t)\end{bmatrix} + A\frac{\partial}{\partial \zeta}\begin{bmatrix}\bar{p}(\zeta,t)\\ \bar{v}(\zeta,t)\end{bmatrix} + B\begin{bmatrix}\bar{p}(\zeta,t)\\ \bar{v}(\zeta,t)\end{bmatrix} = 0 \tag{3.4}$$

where

$$\begin{aligned} A &= \begin{bmatrix}0 & N\\ G & 0\end{bmatrix}, N = a^2\rho_{ss}, G = \frac{1}{\rho_{ss}}\\ B &= \begin{bmatrix}0 & 0\\ Q & F\end{bmatrix}, Q = \frac{g\sin\alpha}{a^2\rho_{ss}} + \frac{\lambda v_{ss}^2}{2Da^2\rho_{ss}}, F = \frac{\lambda v_{ss}}{D}\end{aligned} \tag{3.5}$$

The corresponding boundary conditions are specified as:

$$\bar{p}(L,t) = 0, \bar{v}(0,t) = u(t) \tag{3.6}$$

By performing basic algebraic manipulations, the state space representation of the boundary control system (BCS) is obtained as follows:

$$\begin{aligned} \frac{\partial x(\zeta,t)}{\partial t} &= \bar{\mathcal{A}}x(\zeta,t), \bar{\mathcal{B}}x(\zeta,t) = u(t)\\ y_c(t) &= C_c x(\zeta,t), y_m(t) = C_m x(\zeta,t)\end{aligned} \tag{3.7}$$

where $x(\zeta,t) = [\bar{p}(\zeta,t); \bar{v}(\zeta,t)]$ and $x(\cdot,t) \in \mathcal{X}$ with $\mathcal{X} = L^2((0,L)^2, R)$ defined to be a separable Hilbert space. The input, controlled and measured outputs of the system are represented by $u(t) \in L^2_{loc}([0,\infty), U)$, $y_c(t), y_m(t) \in L^2_{loc}([0,\infty), Y)$, respectively, where U and Y are finite-dimensional. The continuous-time operators are represented by the following notations:

$$\begin{aligned} \bar{\mathcal{A}} &= -\begin{bmatrix}0 & N\frac{\partial}{\partial\zeta}\\ G\frac{\partial}{\partial\zeta} + Q & F\end{bmatrix}\\ \bar{\mathcal{B}} &= [0, \int_0^L \delta(\eta)(\cdot)d\eta]\\ C_c &= [\int_0^L \delta(\eta - \eta_c)(\cdot)d\eta, 0]\\ C_m &= [\int_0^L \delta(\eta - \eta_m)(\cdot)d\eta, 0]\end{aligned} \tag{3.8}$$

where δ represents the Dirac delta function, and η_c and η_m are the arbitrary point of interest along the pipeline axial direction. This indicates that the input of the system

is the velocity of the fluid entering the system from the upstream direction, controlled through boundary actuation. The flow pressure at the point η_c is designated as the controlled output, while the measured output is taken as the pressure at η_m. The domain of $\bar{\mathcal{A}}$ is $\mathcal{D}(\bar{\mathcal{A}}) = \{\phi(\zeta) = [\phi_1(\zeta); \phi_2(\zeta)] \in \mathcal{X} | \phi(\zeta)$ is absolutely continuous, $\frac{d\phi}{d\zeta} \in L_2(0, L)$, and $\phi_1(L) = 0\}$.

However, the inclusion of $u(t)$ at the boundary in equation (3.7) leads to an inhomogeneous boundary condition. In order to obtain homogeneous boundary conditions and simplify the process of designing the controller, an abstract linear state-space model is formulated as follows:

$$\begin{aligned} \frac{\partial x(\zeta,t)}{\partial t} &= \mathcal{A}x(\zeta,t) + \mathcal{B}u(t) \\ y_c(t) = C_c x(\zeta,t), y_m(t) &= C_m x(\zeta,t) \end{aligned} \tag{3.9}$$

where $\mathcal{A}$ takes the same expression as $\bar{\mathcal{A}}$, but with a different domain as: $\mathcal{D}(\mathcal{A}) = \{\phi(\zeta) = [\phi_1(\zeta); \phi_2(\zeta)] \in \mathcal{X} | \phi(\zeta)$ is absolutely continuous, $\frac{d\phi}{d\zeta} \in L_2(0, L)$, and $\phi_1(L) = 0, \phi_2(0) = 0\}$. After calculating the following inner product formula ([123], Remark 10.1.6), one can determine the expression of operator $\mathcal{B}$:

$$\left\langle \bar{\mathcal{A}}x, \psi \right\rangle = \langle x, \mathcal{A}^*\psi \rangle + \left\langle \bar{\mathcal{B}}x, \mathcal{B}^*\psi \right\rangle \tag{3.10}$$

where the adjoint operator can be found through solving the inner product formula $\langle \mathcal{A}\phi, \psi \rangle = \langle \phi, \mathcal{A}^*\psi \rangle$, which has the expression as:

$$\mathcal{A}^* = \begin{bmatrix} 0 & G\frac{\partial}{\partial\zeta} - Q \\ N\frac{\partial}{\partial\zeta} & -F \end{bmatrix} \tag{3.11}$$

with the associated domain defined as: $\mathcal{D}(\mathcal{A}^*) = \{\psi(\zeta) = [\psi_1(\zeta); \psi_2(\zeta)] \in \mathcal{X} | \psi(\zeta)$ is absolutely continuous, $\frac{d\psi}{d\zeta} \in L_2(0, L)$, and $\psi_1(L) = 0, \psi_2(0) = 0\}$. Therefore, (3.10) leads to (3.12) by substituting operators $\bar{\mathcal{A}}$ and $\mathcal{A}^*$:

$$\left\langle \bar{\mathcal{B}}x, \mathcal{B}^*\psi \right\rangle = Nu(t)\psi_1(0) \tag{3.12}$$

Finally, the operator $\mathcal{B}$ has the expression as $\mathcal{B} = [N\delta(\zeta); 0]$.

3.2.2 Dynamics of liquid flow for a network

In this section, a general branching pipeline networks is considered as shown in Fig. 3.1. The pipeline system is assumed to have three interconnected pipe segments, with

pipe 1 branching out into two separate pipes that supply two consumer communities after being connected to a pump station. In this architecture, the velocity of pumped flow is considered as the boundary actuation at the upstream of pipe 1. Fig. 3.1 also illustrates the coordinate systems corresponding to the pipes. This means that the pressure in the end of pipe 1 is identical to those in the beginning of pipe 2 and 3, and the sum of flows at the branching point are equal to zero [111]. The state variables at the opposite end of the pipes $(v_1(0,t); v_2(l_2,t), v_3(l_3,t))$ are governed by the discharged flow from the pump station and consumer flows. Mathematically, the boundary conditions are expressed as follows:

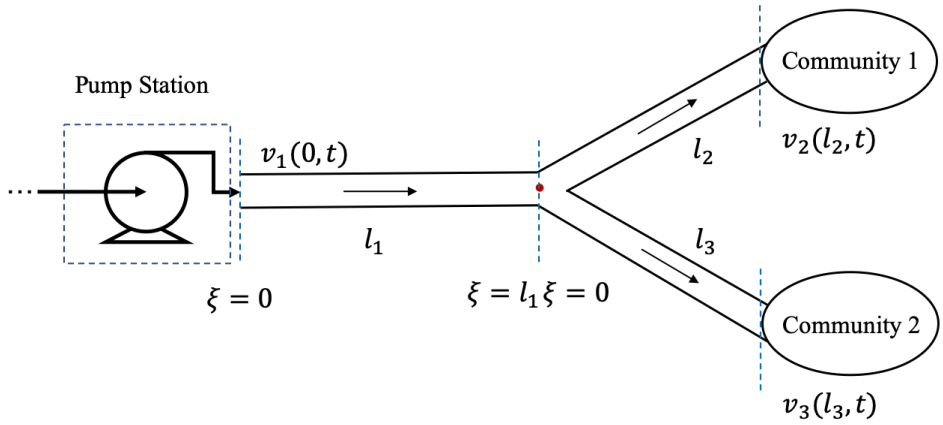

Figure 3.1: Sketch of the branching pipeline system under consideration.

$$\begin{aligned} &v_1(0,t) = u(t), v_2(l_2,t) = v_2(t), v_3(l_3,t) = v_3(t), \\ &p_1(l_1,t) = p_2(0,t) = p_3(0,t), v_1(l_1,t) = v_2(0,t) + v_3(0,t) \end{aligned} \tag{3.13}$$

$v_2(t)$ and $v_3(t)$ are the given flows to consumers that may vary with time. The initial conditions for the three pipes are specified as $p_i(\zeta,0) = p_i(\zeta), v_i(\zeta,0) = v_i(\zeta), \zeta \in [0,l_i], i = 1,2,3$. In addition, we assume that pressure and flow are measured at the other end of the branching point, namely $p_m(t) = [p_1(0,t), p_2(l_2,t), p_3(l_3,t)]$ are measured. Along this line, three pipeline segments can be modelled as a cascaded PDE system. In this work, we aim to control the flow or pressure at any location within the pipeline network via manipulating the inlet flow of pipe 1. It is worth noting that measurements are not available at the branching point.

Based on the continuity and momentum balance laws, the dynamics of the overall

pipe flow are mathematically described in the continuous-time setting as follows [109]:

$$\begin{aligned}\frac{\partial x^e(\zeta,t)}{\partial t} &= \mathcal{A}^e x^e(\zeta,t) + \mathcal{B}^e u^e(t)\\ y_c^e(t) &= C_c^e x^e(\zeta,t)\\ y_m^e(t) &= C_m^e x^e(\zeta,t)\end{aligned} \tag{3.14}$$

where the extended state $x^e(\zeta,t) = [x^{(1)}(\zeta,t); x^{(2)}(\zeta,t); x^{(3)}(\zeta,t)]$ and the input $u^e(t) = [u(t), 0, 0]$. The superscript (i) denotes the number of the ith pipe segment. The representation of extended operators is shown below:

$$\begin{aligned}\mathcal{A}^e &= \text{bdiag}[\mathcal{A}^{(1)}, \mathcal{A}^{(2)}, \mathcal{A}^{(3)}]\\ \mathcal{B}^e &= [\mathcal{B}; \mathbf{0}; \mathbf{0}]\\ C_c^e &= [\mathbf{0}, \mathbf{0}, C_c]\\ C_m^e &= \text{bdiag}[C_m^{(1)}, C_m^{(2)}, C_m^{(3)}]\end{aligned} \tag{3.15}$$

where

$$\begin{aligned}\mathcal{A}^{(i)} &= -\begin{bmatrix} 0 & N\frac{\partial}{\partial\zeta} \\ G\frac{\partial}{\partial\zeta} + Q^{(i)} & F^{(i)} \end{bmatrix}, i = 1,2,3\\ C_m^{(i)} &= [\int_0^L \delta(\eta - \eta_{mi})(\cdot)d\eta, 0], i = 1,2,3\end{aligned} \tag{3.16}$$

and $\mathcal{D}(\mathcal{A}^e) = \{\phi(\zeta) = [\phi_1(\zeta); \phi_2(\zeta); ...; \phi_6(\zeta)] \in L_2(0,L)^6 | \phi(\zeta)$ is abs. cont., and $\phi_2(0) = 0, \phi_4(l_2) = 0, \phi_6(l_3) = 0, \phi_1(l_1) = \phi_3(0) = \phi_5(0), \phi_2(l_1) = \phi_4(0) + \phi_6(0)\}$. In equation (3.15), $\mathbf{0}$ denotes the vector of two zero elements. Considering the difficulties in addressing unbounded operators and handling constraints, we will convert the continuous-time model into a discrete-time one to facilitate the MPC/MHE design.

3.2.3 Model time discretization

In this section, we discretize the linearized continuous-time model (3.14) by employing a time discretization scheme. More specifically, we apply the Cayley-Tustin time discretization framework [14] since this transformation leads to a discrete-time infinite-dimensional model and important system properties (stability, input-output mapping) stay invariant, which provides essential theoretical guarantees when applying discrete-time designs back to the original continuous-time systems [100, 124, 125].

Given a time discretization parameter $h > 0$, one can apply the Cayley-Tustin time discretization to the continuous-time pipeline model (3.14) as follows:

$$\begin{aligned}
\frac{x^e((k+1)h) - x^e(kh)}{h} &\approx \mathcal{A}^e \frac{x^e((k+1)h) + x^e(kh)}{2} + \mathcal{B}^e u^e(kh) \\
y_c^e(kh) &\approx C_c^e \frac{x^e((k+1)h) + x^e(kh)}{2} \\
y_m^e(kh) &\approx C_m^e \frac{x^e((k+1)h) + x^e(kh)}{2}
\end{aligned} \tag{3.17}$$

The continuous-time input signal can be linked to the discrete-time counterpart via: $\frac{u^e(kh)}{\sqrt{h}} = \frac{1}{h}\int_{kh}^{(k+1)h} u^e(t)dt$. As reported in [14], the difference between continuous- and discrete-time inputs $\|\frac{u^e(kh)}{\sqrt{h}} - u^e(t)\|$ converges to zero as $h \to 0$. In a similar way, one can obtain the discrete-time outputs from their continuous-time counterparts. Along this line, the discrete-time distributed parameter pipeline system is formulated as:

$$\begin{aligned}
x_{k+1} &= \mathcal{A}_d x_k + \mathcal{B}_d u_k \\
y_{ck} &= C_{cd} x_k + \mathcal{D}_{cd} u_k \\
y_{mk} &= C_{md} x_k + \mathcal{D}_{md} u_k
\end{aligned} \tag{3.18}$$

where one denotes discrete-time spatial operators $\mathcal{A}_d$, $\mathcal{B}_d$, C_{cd}, $\mathcal{D}_{cd}$, C_{md}, $\mathcal{D}_{md}$ as follows:

$$\begin{bmatrix} \mathcal{A}_d & \mathcal{B}_d \\ C_{cd} & \mathcal{D}_{cd} \\ C_{md} & \mathcal{D}_{md} \end{bmatrix} = \begin{bmatrix} -I(\cdot) + 2\gamma\mathcal{R}(\gamma,\mathcal{A}) & \sqrt{2\gamma}\mathcal{R}(\gamma,\mathcal{A})\mathcal{B} \\ \sqrt{2\gamma}C_c\mathcal{R}(\gamma,\mathcal{A}) & \mathcal{G}_c(\gamma) \\ \sqrt{2\gamma}C_m\mathcal{R}(\gamma,\mathcal{A}) & \mathcal{G}_m(\gamma) \end{bmatrix} \tag{3.19}$$

where $\gamma = 2/h$. $\mathcal{R}(\gamma,\mathcal{A})$ denotes the resolvent operator $\mathcal{R}(\gamma,\mathcal{A}) = (\gamma I - \mathcal{A})^{-1}$ with s evaluated at γ. $\mathcal{G}_c(\gamma)$ and $\mathcal{G}_m(\gamma)$ are transfer functions from input to controlled output $y_c(t)$ and measured output $y_m(t)$, respectively. For simplicity, superscript e in x, u, y and all discrete operators in (3.18) and (3.19).

3.2.4 Resolvent operator

To fully establish the discrete-time model (3.18), it is crucial to find the resolvent operator based on its continuous-time equivalent. This can be done by performing the Laplace transformation and considering the zero input condition. This results in a solution in the frequency domain for the distributed parameter pipeline system, expressed as follows:

$$x^e(\zeta,s) = e^{M\zeta}x^e(0,s) + \int_0^\zeta e^{M(\zeta-\eta)}P(\zeta,s)x^e(\eta,0)d\eta \tag{3.20}$$

where

$$M = \text{bdiag}[W^{(1)}, W^{(2)}, W^{(3)}], e^{M\zeta} = \text{bdiag}[e^{W^{(1)}\zeta}, e^{W^{(2)}\zeta}, e^{W^{(3)}\zeta}]$$

$$W^{(i)} = \begin{bmatrix} -\frac{Q^{(i)}}{G} & -\frac{(F^{(i)}+s)}{G} \\ -\frac{s}{N} & 0 \end{bmatrix}, e^{W^{(i)}\zeta} = \begin{bmatrix} M_{11}^{(i)}(\zeta, s) & M_{12}^{(i)}(\zeta, s) \\ M_{21}^{(i)}(\zeta, s) & M_{22}^{(i)}(\zeta, s) \end{bmatrix}, i = 1, 2, 3$$

$$P(\zeta, s) = A^{-1} = \begin{bmatrix} 0 & P_{12}(\zeta, s) \\ P_{21}(\zeta, s) & 0 \end{bmatrix}$$

Through further mathematical transformations, the state evolution matrix is derived with closed-form analytical expressions, given by:

$$M_{11}^{(i)}(\zeta, s) = e^{-\frac{Q^{(i)}\zeta}{2G}}(\cosh(\frac{H}{2G\sqrt{N}}\zeta) - \frac{Q^{(i)}\sqrt{N}}{H}\sinh(\frac{H}{2G\sqrt{N}}\zeta))$$

$$M_{12}^{(i)}(\zeta, s) = e^{-\frac{Q^{(i)}\zeta}{2G}}(-\frac{2\sqrt{N}(F^{(i)} + s)}{H})\sinh(\frac{H}{2G\sqrt{N}}\zeta))$$

$$M_{21}^{(i)}(\zeta, s) = e^{-\frac{Q^{(i)}\zeta}{2G}}(-\frac{2Gs}{\sqrt{N}H})\sinh(\frac{H}{2G\sqrt{N}}\zeta))$$

$$M_{22}^{(i)}(\zeta, s) = e^{-\frac{Q^{(i)}\zeta}{2G}}(\cosh(\frac{H}{2G\sqrt{N}}\zeta) + \frac{Q^{(i)}\sqrt{N}}{H}\sinh(\frac{H}{2G\sqrt{N}}\zeta))$$

where

$$H = \sqrt{NQ^{(i)^2} + 4Gs^2 + 4FGs},\ i = 1, 2, 3$$

By evaluating the frequency-domain solution (3.20) at the boundary conditions $x_2(0, s) = 0, x_1(l_1, s) = x_3(0, s) = x_5(0, s), x_2(l_1, s) = x_4(0, s) + x_6(0, s), x_4(l_2, s) = 0, x_6(l_2, s) = 0$, one can solve for $x_1(0, s)$, $x_2(0, s)$, $x_4(0, s)$, $x_6(0, s)$ and then determine the final form of the resolvent operator:

$$x_e(\zeta, s) = \mathcal{R}(s, \mathcal{A}^e)x_e(\zeta, 0) \tag{3.21}$$

where $\mathcal{R}(s, \mathcal{A}^e) = [\mathcal{R}_{ij}(s, \mathcal{A}^e)]_{6\times6}$, with $i, j = 1, 2, ..., 6$. The analytic expressions of the extended resolvent operator is shown in Appendix A.3. Therefore, one can determine the discrete-time model (3.18) of the liquid pipeline by substituting the obtained resolvent operator into (3.19).

3.3 Controller and Estimator Design

In this section, a tracking MPC scheme is introduced for the pipeline network to steer the controlled output to a desired set-point in an infinite-dimensional discrete-time setting. Due to the absence of sensors distributed throughout the entire pipeline network, non-measurable states and uncertain parameters are estimated using MHE.

3.3.1 MHE formulation

In industrial applications, it is often necessary to reconstruct unmeasured states using a limited number of measurements. In comparison to other estimation techniques, MHE enables the simultaneous estimation of both states and parameters, incorporating recent measurements and accommodating constraints in a single problem formulation [126][127]. Based on the MHE designs for lumped parameter systems [57][58] [128] [129], this section proposes an MHE for a discrete-time pipeline system (3.18) that accounts for constraints, with the objective of determining the optimal possible estimation of the state evolution and parameters by utilizing current and past input and output information [55].

To model the actual fluid flow dynamics in a better way, a state disturbance term ω defined in finite-dimensional Hilbert spaces W is introduced to (3.18), which is equipped with a spatial operator G. Measurement disturbances in the output y_m in (3.18) are considered and expressed by v, which is defined in finite-dimensional Hilbert spaces Y. It is worth noting that the considered process and measurement disturbance are added in the continuous-time model, and both are norm bounded and distributed with zero means. Along a similar procedure as Section 3.2.3 (3.18), we further obtain the following discrete-time model:

$$\begin{aligned} x_{k+1} &= \mathcal{A}_d x_k + \mathcal{B}_d u_k + G_d \omega_k \\ y_{mk} &= C_{md} x_k + \mathcal{D}_{md} u_k + v_k \end{aligned} \tag{3.22}$$

where the discrete operator G_d have a similar expression as $\mathcal{B}_d$ in (3.19), that is $G_d = \sqrt{2\gamma}\mathcal{R}(\gamma, \mathcal{A})G$. For simplicity, we denote $v_k = G_{md} + \bar{v}_k$ (G_{md} is the transfer function from ω to y_m). In (3.22), the controlled output is not taken into account in this estimation problem.

When it comes to industrial applications, parameters such as pipe friction (i.e., λ in (3.1)) are often not accurately known due to various factors, e.g., surface roughness, and fluid parameters, making it difficult to model accurately. Therefore, estimating the friction coefficient λ is crucial for pipeline modelling.

Based on the preceding model description, one can formulate the MHE problem. More specifically, at any stage $k = N_e, N_e + 1, ...$, the optimization objective is to find estimates of system states $x_{k-N_e}, ..., x_k$ and parameter λ using measurements

$\{y_j\}_{j=k-N_e}^{j=k}$, $\{u_j\}_{j=k-N_e}^{j=k}$ and a prediction $\bar{x}_{k-N_e}$ of the state x_{k-N_e}. $\hat{x}_{k-N_e|k}, ..., \hat{x}_{k|k}$ are introduced to denote the estimates of $x_{k-N_e}, ..., x_k$ at stage k respectively. Therefore, at stage k, the optimal estimation of the state and parameter is obtained by solving the following optimization problem:

$$\min_{\hat{x}_{k-N_e|k}, \hat{\lambda}_{k-N_e|k}} J_k(\hat{x}_{k-N_e|k}; \hat{\lambda}_{k-N_e|k}) \tag{3.23}$$

where $J_k(\hat{x}_{k-N_e|k}; \hat{\lambda}_{k-N_e|k})$ is defined as follows:

$$\begin{aligned} &\langle \begin{bmatrix} \hat{x}_{k-N_e|k} - \bar{x}_{k-N_e} \\ \hat{\lambda}_{k-N_e|k} - \bar{\lambda}_{k-N_e} \end{bmatrix}, \mu \begin{bmatrix} \hat{x}_{k-N_e|k} - \bar{x}_{k-N_e} \\ \hat{\lambda}_{k-N_e|k} - \bar{\lambda}_{k-N_e} \end{bmatrix} \rangle \\ &+ \sum_{j=k-N_e}^{k} \langle y_{mj} - C_d(\hat{\lambda}_j)\hat{x}_{j|k} - \mathcal{D}_d(\hat{\lambda}_j)u_j, y_{mj} - C_d(\hat{\lambda}_j)\hat{x}_{j|k} - \mathcal{D}_d(\hat{\lambda}_j)u_j \rangle \end{aligned} \tag{3.24}$$

where $\langle \cdot \rangle$ is the inner product. N_e denotes the estimation horizon and $\mu \geq 0$ is utilized to adjust the trade-off between the two components of the cost. The first component in the cost function (3.24), is the weighted term, penalizing the distance of the current estimated state from its prediction. The second term in (3.24) represents the prediction error, which is calculated based on the recent measurements.

The optimization problem (3.23) should respect the state equality constraints:

$$\hat{x}_{j+1|k} = \mathcal{A}_d(\hat{\lambda}_j)\hat{x}_{j|k} + \mathcal{B}_d(\hat{\lambda}_j)u_j, j = k - N_e, ..., k - 1 \tag{3.25}$$

and the following parameter constraints:

$$\hat{\lambda}_j \in [\lambda_{\min}, \lambda_{\max}] \tag{3.26}$$

The prediction is determined using the state space model (3.22) with the assumption that $\omega_k = 0$ based on the estimate $\hat{x}_{k-N_e|k-1}$. Then, the prediction is computed as

$$\bar{x}_{k-N_e+1} = \mathcal{A}_d(\hat{\lambda}_{k-N_e|k})\hat{x}_{k-N_e|k} + \mathcal{B}_d(\hat{\lambda}_{k-N_e|k})u_{k-N_e} \tag{3.27}$$

for $k = N_e+1, N_e+2, ...$ Considering that the infinite-dimensional estimate $\hat{x}_{k-N_e|k}$ may not be feasible in practice, an auxiliary disturbance is introduced as $G_w\hat{\omega}_{k-N_e-1|k} = \hat{x}_{k-N_e|k} - \bar{x}_{k-N_e}$ [117]. Therefore, the minimization problem is converted to:

$$\begin{aligned} J_k(\hat{\omega}_{k-N_e-1|k}; \hat{\lambda}_{k-N_e|k}) &= \langle \begin{bmatrix} G_w\hat{\omega}_{k-N_e-1|k} \\ \hat{\lambda}_{k-N_e|k} - \bar{\lambda}_{k-N_e} \end{bmatrix}, \mu \begin{bmatrix} G_w\hat{\omega}_{k-N_e-1|k} \\ \hat{\lambda}_{k-N_e|k} - \bar{\lambda}_{k-N_e} \end{bmatrix} \rangle \\ &+ \sum_{j=k-N_e}^{k} \langle y_{mj} - C_d(\hat{\lambda}_j)\hat{x}_{j|k} - \mathcal{D}_d(\hat{\lambda}_j)u_j, y_{mj} - C_d(\hat{\lambda}_j)\hat{x}_{j|k} - \mathcal{D}_d(\hat{\lambda}_j)u_j \rangle \end{aligned} \tag{3.28}$$

Then, at any stage $k = N_e + 1, N_e + 2, ...,$ by solving the optimization problem (3.28), and an optimal trajectory of the system state $\{\hat{x}_{k-N_e|k}, \cdots, \hat{x}_{k|k}\}$ and parameter $\{\hat{\lambda}_{k-N_e|k}, \cdots, \hat{\lambda}_{k|k}\}$ are obtained. From the solution, the current optimal estimate of the current state and parameter are denoted as $\hat{x}_k \leftarrow \hat{x}_{k|k}$ and $\hat{\lambda}_k \leftarrow \hat{\lambda}_{k|k}$, respectively. At the next sampling instance, $k+1$, the estimation window is shifted one step ahead, and one can obtain the state estimate $\hat{x}_{k+1}$ and parameter estimate $\hat{\lambda}_{k+1}$.

3.3.2 Tracking MPC formulation

In this chapter, the focus is on investigating whether the considered pipeline network can be manipulated to achieve a desired pressure or flow within a specified timeframe, aiming to meet a given demand. While there are various objective functions for optimizing oil and gas transportation, this study specifically addresses the goal of reaching desired set-points efficiently [130].

To track a desired output, we aim to formulate a tracking-type objective function. The synthesis is based on the infinite-dimensional discrete-time state-space model (3.18). Specifically, the proposed MPC integrates trajectory planning and tracking by formulating them as a unified optimization problem. The decision variables in this problem include a planned reachable trajectory, characterized by its desired state, along with the corresponding sequence of inputs and future control inputs [131]. The optimization problem aims to minimize the following cost function:

$$V_N(x^s, u^s, y_c^s, U_k) = V_t(x^s, u^s, y_c^s, U_k) + V_P(x^s, u^s, y_c^s) \tag{3.29}$$

which includes a tracking cost term and a penalty term that accounts for the deviation between the desired equilibrium and the target set-point:

$$V_t(x^s, u^s, y_c^s, U_k) = \sum_{j=0}^{N_c-1} \langle (y_{c,k+j|k} - y^s), Q_c(y_{c,k+j|k} - y^s) \rangle \tag{3.30a}$$
$$+ \langle (u_{k+j|k} - u^s), R_c(u_{k+j|k} - u^s) \rangle + \langle (x_{k+N_c-1|k} - x^s), \bar{Q}_c(x_{k+N_c-1|k} - x^s) \rangle$$
$$V_P(x^s, u^s, y_c^s) = \sum_{j=0}^{T-1} \left\| y_c^s(j) - y^r(j) \right\|_S^2 \tag{3.30b}$$

where N_c is the prediction horizon and $N_c \leq T$. Q_c and R_c are symmetric positive semidefinite operators, while S is a symmetric positive definite spatial operator. The

spatial operator $\bar{Q}_c$ is specifically utilized to penalize the terminal state which is essential for ensuring the stability of the model. The superscripts 's' and 'r' represent the desired equilibrium and the expected output signal, respectively. In this formulation, $U_k := \{u_{k+1|k}, \cdots, u_{k+N_c|k}\}$ is the input sequence to be optimized. In (3.30a), the term V_t penalizes the deviation of the open-loop predicted trajectory from the planned reachable reference within the prediction horizon N_c. In (3.30b), the term V_P is designed to penalize the deviation between the planned reachable trajectory and the reference to be tracked predicted over a single period T [120].

Therefore, for the given current estimated state $\hat{x}_k$ at time k, the following optimal control problem is constructed:

$$\min_{x^s, u^s, U_k} \; V_N(x^s, u^s, U_k) \tag{3.31a}$$

$$\text{s.t.} \;\; x_{k+j+1|k} = \mathcal{A}_d(\hat{\lambda}_k) x_{k+j|k} + \mathcal{B}_d(\hat{\lambda}_k) u_{k+j|k} \tag{3.31b}$$

$$y_{c,k+j|k} = \mathcal{C}_d(\hat{\lambda}_k) x_{k+j|k} + \mathcal{D}_d(\hat{\lambda}_k) u_{k+j|k} \tag{3.31c}$$

$$x_{k|k} = \hat{x}_k \tag{3.31d}$$

$$u_{k+j|k} \in [u_{\min}, u_{\max}] \tag{3.31e}$$

$$x^s = \mathcal{A}_d(\hat{\lambda}_k) x^s + \mathcal{B}_d(\hat{\lambda}_k) u^s \tag{3.31f}$$

$$y_c^s = \mathcal{C}_d(\hat{\lambda}_k) x^s + \mathcal{D}_d(\hat{\lambda}_k) u^s \tag{3.31g}$$

The optimal solution to this optimization problem is indicated by (x^{s*}, u^{s*}, U_k^*). Constraints (3.31b)-(3.31d) specify the predicted trajectories of the system starting from the currently estimated state $\hat{x}_k$ derived from the estimator (3.28). Constraint (3.31e) denotes the input constraints. Constraints (3.31f)-(3.31g) define the planned desired steady state prediction.

In order to determine $\bar{Q}_c$ in the objective function, one needs to solve the following discrete-time Lyapunov equation:

$$\mathcal{A}_d^* \bar{Q}_c \mathcal{A}_d - \bar{Q}_c = -\mathcal{C}_d^* Q_c \mathcal{C}_d \tag{3.32}$$

or equivalently, by solving the continuous-time Lyapunov equation:

$$\mathcal{A}^* \bar{Q}_c + \bar{Q}_c \mathcal{A} = -\mathcal{C}^* Q_c \mathcal{C} \tag{3.33}$$

on the dual space of $\mathcal{X}_{-1}$. It worth noting that the operator $\bar{Q}_c$ is the unique positive self-adjoint solution of (3.32) and (3.33) if $\mathcal{A}$ is strongly stable [100]. The adjoint

operator can be determined using the formula $\langle \mathcal{A}\psi, \phi \rangle = \langle \psi, \mathcal{A}^* \phi \rangle$:

$$\mathcal{A}^* = \text{bdiag}[\mathcal{A}^{(1)^*}, \mathcal{A}^{(2)^*}, \mathcal{A}^{(3)^*}] \tag{3.34}$$

with the same domain of $\mathcal{A}^e$, where

$$\mathcal{A}^{(i)^*} = \begin{bmatrix} 0 & G\frac{\partial}{\partial \zeta} - Q_i \\ N\frac{\partial}{\partial \zeta} & -F_i \end{bmatrix}, i = 1, 2, 3 \tag{3.35}$$

By multiplying both sides of equation (3.33) with a spatial function $X(\zeta)$, and substituting the expressions of operator $\mathcal{A}$ and $\mathcal{A}^*$, one can finally obtain $\bar{Q}_c$ using numerical integration.

3.3.3 Implementation strategy

In the following, we propose a scheme and an algorithm for iteratively running the proposed MHE and MPC. Fig. 3.2 depicts the block diagram of the comprehensive control strategy.

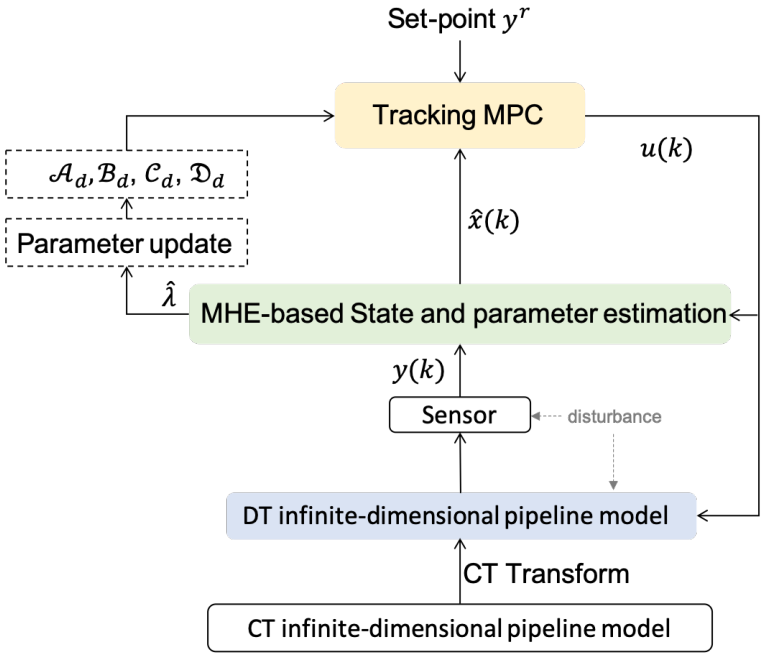

Figure 3.2: Block diagram of the overall control strategy.

By following the above workflow chart, the linearized continuous-time infinite-dimensional pipeline model is discretized in time into a discrete-time counterpart

using Cayley-Tustin approach as in Section 3.2.3. Considering the presence of measurement and plant disturbances, we deploy MHE for state and parameter estimation. The MHE receives the process measurements continuously and provides the estimated states and parameters based on the input $u(k)$. In this case, only one value from the sequence is retained [132], specifically, the last instance in the sequence. The discrete-time operators obtain the estimated parameter $\hat{\lambda}$ to realize the parameter update. The tracking MPC obtains the estimated state and updated discrete-time operators, and predicts the future progression of the system across the entire prediction horizon for the given set-points. The first input $u(k)$ from the optimal input trajectory, derived from solving the optimization problem, is applied to the plant for implementation.

The aforementioned implementation strategy of the proposed tracking MPC and MHE algorithm is summarized in Table 3.1.

Table 3.1: Implementation algorithm of the proposed MHE and MPC

Implementation Algorithm of the Proposed MHE and MPC
Initialize:
1) Specify the scalar weight μ and horizons N_e in (3.28);
2) Specify the prediction horizons N_c, the positive definite function Q_c, R_c and determine $\bar{Q}$ in (3.31);
At time k:
3) Collect measurements $\{y_j\}_{j=k-N_e}^{j=k}$, $\{u_j\}_{j=k-N_e}^{j=k}$ and obtain prior estimate $\hat{x}_{k-N_e\|k-N_e-1}$;
4) Solve (3.28) for $\hat{\omega}_{k-N_e-1\|k}$ and $\hat{\lambda}_{k-N_e\|k}$ subject to constraint (3.25-3.27);
5) Obtain $\{\hat{x}_{j\|k}\}_{j=k-N_e}^{j=k}$ and $\{\hat{\lambda}_{j\|k}\}_{j=k-N_e}^{j=k}$using optimal estimate $\hat{\omega}_{k-N_e-1\|k}$ from step 4);
6) Update $\mathcal{R}(s,\mathcal{A}^e)$ in (3.21) and discrete-time operators based on $\hat{\lambda}_{k\|k}$;
7) Solve (3.31) for $\{U_j\}_{j=k}^{j=k+N_c}$ with updated operators and $\hat{x}_{k\|k}$ and $\hat{\lambda}_{k\|k}$;
8) Implement the optimal control action $u^*_{k+1\|k}$ to the discrete-time plant;
9) Repeat steps 3)-9) with $k \leftarrow k+1$;

3.4 Simulation Results

In this section, the considered branching pipeline network is used to verify the effectiveness of the proposed MHE and tracking MPC designs. First, the estimation performance of the proposed MHE is tested with different horizon lengths and disturbance levels. Then, the control performance of the tracking MPC is investigated

via sensitivity analysis. Finally, by implementing the MHE and MPC recursively, the results are provided for the considered branching pipeline network.

The pipeline parameters are given in Table 3.2, and the equilibrium profiles are shown in Fig. 3.3 for each pipe segment by using (3.3). The pipeline system is transformed into a discrete-time one by performing the Cayley-Tustin approach, where all the discrete-time operators have analytical expressions. For all the simulation cases, the time discretization interval is selected as h = 8s. The obtained integral operators are computed utilizing the trapezoidal rule with spatial discretization interval $\Delta\zeta = 0.01$ for numerical realization. The following initial conditions are considered $x_1(\zeta,0) = 0.79\zeta, x_2(\zeta,0) = 0.01\zeta, x_3(\zeta,0) = 7890 + 13.15\zeta, x_4(\zeta,0) = 51 - 0.0051\zeta, x_5(\zeta,0) = 7890 + 14.15\zeta, x_6(\zeta,0) = 51 - 0.0051\zeta$. The constraints on λ are $\lambda_{\min} = 0.002$ and $\lambda_{\max} = 0.5$, and constraints on u are $u_{\min} = 0.9$ and $u_{\max} = 5.6$ for all the simulation. The proposed MHE and MPC framework are implemented in MATLAB (MathWorks R2019a) and the MATLAB built-in *fmincon* function is used to solve the optimization problem in each iteration.

Table 3.2: Notations and values of parameters [1]

Description	Notation	Value
Pipeline length	L_i, $i = 1,2,3$	10,000 m
Pipeline diameter	D_i, $i = 1,2,3$	0.2065 m
Inclination angle	$[\alpha_1, \alpha_2, \alpha_3]$	[-0.00256,0.00456, 0.00156]
Speed of sound	a	1059 m/s
Gravity acceleration	g	9.81 m/s^2

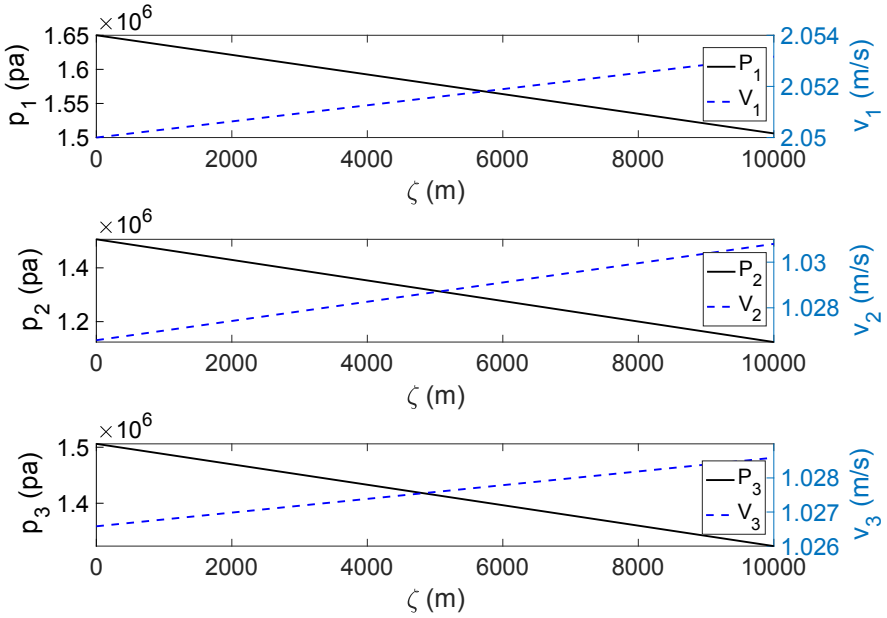

Figure 3.3: Steady states of pressure (black solid line) and flow velocity (blue dashed line) for pipe 1, 2, 3 (top to bottom), respectively.

3.4.1 Performance of proposed MHE

The performance of the state and parameter estimation by solving the problem defined in (3.28) are analyzed in this section. In this case, we consider constraints on the process and measurement noise, $\omega_k \in [-r_w, r_w]$ and $v_k \in [-r_v, r_v]$. The priori estimate of x_0 at the initial step is taken as zero. To quantify the estimation performance, we consider the Normalized Root Mean Square Error (NRMSE) to evaluate the output estimation error:

$$\text{RMSE} = \frac{1}{S}\sum_{s=1}^{S}\sqrt{\sum_{k=1}^{T}\frac{\left\|e_{k,s}\right\|^2}{T}},\ \text{NRMSE} = \frac{\text{RMSE}}{\bar{y}} \tag{3.36}$$

where $e_{k,s}$ denotes the output estimation error at time k in the s-th simulation run. S and T are the number of simulation runs and simulation horizon. $\bar{y}$ is the mean value of the measurements. In this case, the values of S and T are taken as 400 and 200, respectively. We investigate the influence of different estimation horizon, disturbance levels and value of μ on the estimation performance of proposed MHE, as shown from Table 3.3 to 3.6.

.

Table 3.3: Estimation performance (NRMSE, $\times 10^{-4}$) of y_{m1} for different N_e, r_w,r_v and μ

N_e	r_w	r_v	μ				
			0.1	0.01	0.001	0.0001	0
5	0.4	0.4	5.9238	4.4226	4.4422	4.4568	6.2809
	0.04	0.04	5.2431	4.2173	4.2481	4.2430	5.8457
10	0.4	0.4	3.1700	3.1743	3.1742	3.1681	3.1741
	0.04	0.04	3.1899	3.1882	3.1880	3.1880	3.1880
15	0.4	0.4	2.7840	2.7833	2.7832	2.7832	2.7832
	0.04	0.04	2.6524	2.6519	2.6519	2.6519	2.6519

Table 3.4: Estimation performance (NRMSE, $\times 10^{-4}$) of y_{m2} for different N_e, r_w,r_v and μ

N_e	r_w	r_v	μ				
			0.1	0.01	0.001	0.0001	0
5	0.4	0.4	4.1664	4.1635	4.1634	4.1655	4.2634
	0.04	0.04	4.0516	4.0507	4.0507	4.0507	4.0612
10	0.4	0.4	3.6110	3.7890	3.6129	3.6128	3.6042
	0.04	0.04	3.5728	3.7422	3.5689	3.5691	3.5689
15	0.4	0.4	3.2816	3.2813	3.2812	3.2812	3.2812
	0.04	0.04	3.1234	3.1231	3.1231	3.1231	3.1231

Table 3.5: Estimation performance (NRMSE, $\times 10^{-4}$) of y_{m3} for different N_e, r_w,r_v and μ

N_e	r_w	r_v	μ				
			0.1	0.01	0.001	0.0001	0
5	0.4	0.4	3.4256	3.4249	3.4247	3.4239	3.4247
	0.04	0.04	3.3805	3.3990	3.3988	3.3988	3.4214
10	0.4	0.4	2.9451	2.9247	2.9415	2.9415	2.9358
	0.04	0.04	2.8760	2.8609	2.8703	2.8704	2.8702
15	0.4	0.4	2.9113	2.9107	2.9106	2.9106	2.9106
	0.04	0.04	2.8343	2.8339	2.8338	2.8338	2.8338

Table 3.6: Parameter estimation performance (RMSE) for different N_e, r_w,r_v and μ

N_e	r_w	r_v	μ				
			0.1	0.01	0.001	0.0001	0
5	0.4	0.4	0.0980	0.1148	0.0834	0.0833	0.1095
	0.04	0.04	0.0771	0.1174	0.0745	0.0777	0.0745
10	0.4	0.4	0.0449	0.0377	0.0377	0.0450	0.0377
	0.04	0.04	0.0259	0.0260	0.0260	0.0260	0.0260
15	0.4	0.4	0.0277	0.0277	0.0277	0.0277	0.0277
	0.04	0.04	0.0185	0.0185	0.0185	0.0185	0.0185

Tables 3.3 - 3.5 present the estimation performances (in terms of NRMSE) for the three measured outputs with different values for parameters N_e and r_w, r_v and μ. The performance is dependent on both N_e and μ. For μ ranging from 0.1 to 0, the MHE performances are quite similar. The performance is strongly affected by N_e. Specifically, the larger N_e is, the better estimation performance becomes. For the performance of parameter estimation (Table 3.6), in general, the estimation errors (RMSE) decrease with larger of estimation horizon and smaller disturbance level. With the fixed estimation horizon length N_e, r_w and r_v, the estimation results are improved by applying smaller μ. Fig. 3.4 illustrates the parameter estimates for all the cases. We observe that the error is relatively large even in scenarios with low-level disturbances, but this error is influenced by the choice of the estimation horizon. With a larger estimation horizon, the estimated friction coefficient $\hat{\lambda}$ is closer to the true value.

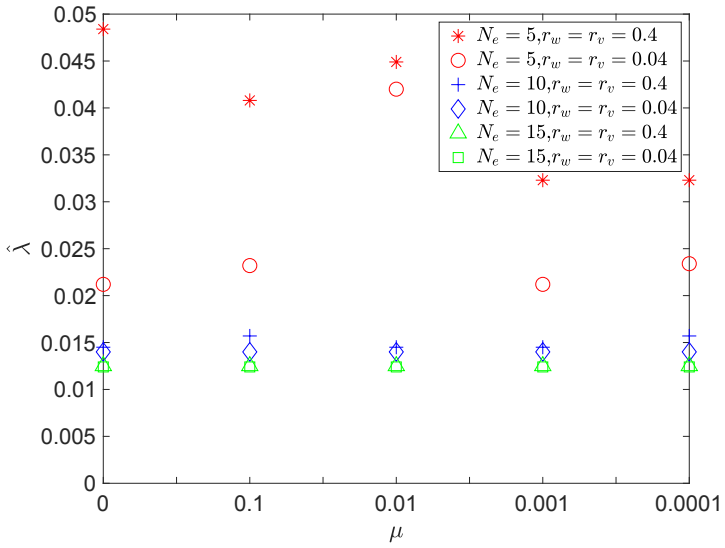

Figure 3.4: Parameter estimates for different N_e and r_w, r_v. The λ_{true} for each pipeline is 0.011.

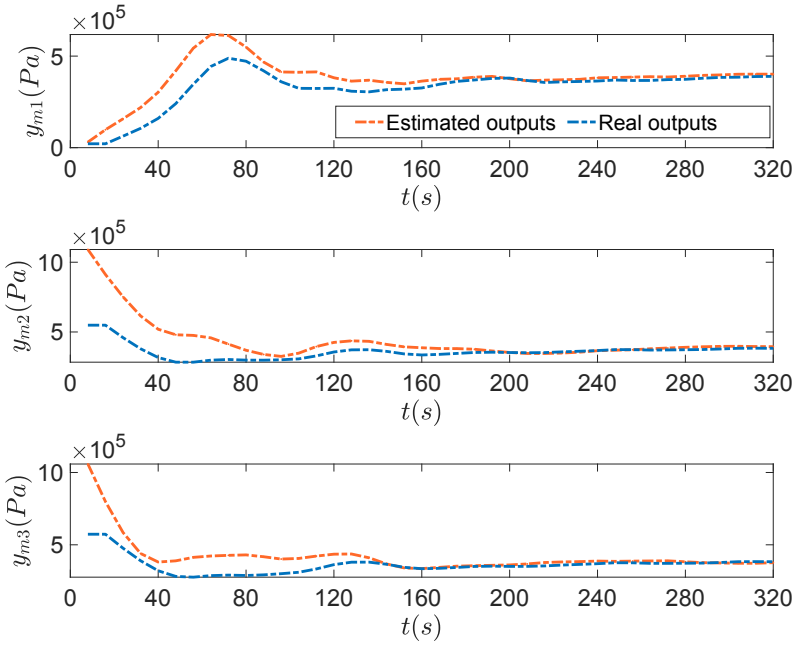

Figure 3.5: Trajectories of estimated outputs (red dashed line) and real outputs (blue dashed line).

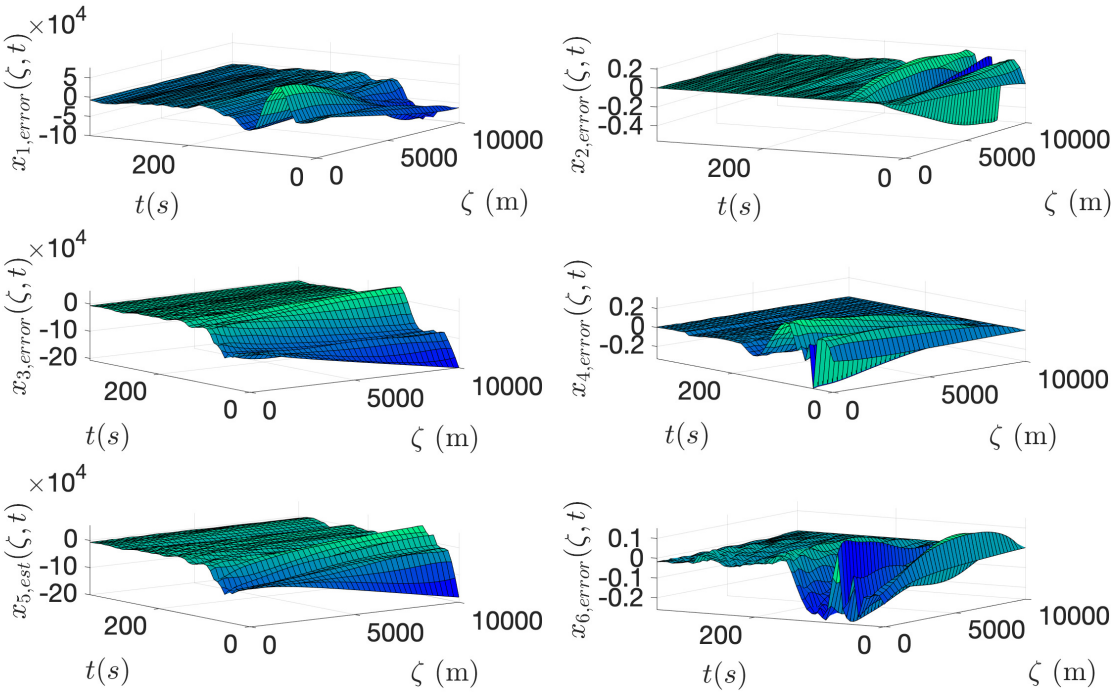

Figure 3.6: Profiles of state estimation error.

Fig. 3.5 presents a comparison between the estimated outputs, disturbed outputs and the real outputs. It is evident from the graph that the intrinsic dynamics of the pipeline model are stable, as the open-loop outputs tend to steady states. The estimation error profiles for each state are illustrated in Fig. 3.6. Despite some initial oscillations, the error profiles gradually converge to zero, indicating that the estimation process is accurate and reliable. This is a crucial aspect for the pipeline system, as accurate estimations are essential for maintaining stable operation. Overall, the results presented in this section demonstrate the effectiveness and reliability of the proposed MHE for the pipeline model.

3.4.2 Performance of proposed tracking MPC

In this section, the proposed tracking MPC is implemented to the pipeline system, and the closed-loop performance is analyzed. The location $\eta_c = 7250m$ in the third pipe is chosen, and the set-point is selected as $y^r = 1.3408 \times 10^6$. The control and prediction horizons are both set to 45 steps in this case.

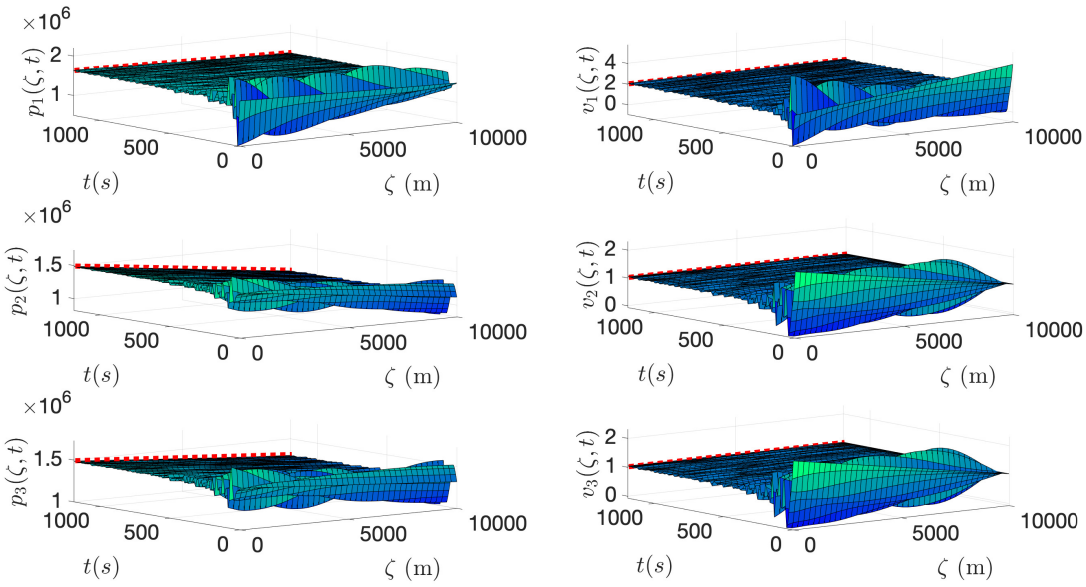

Figure 3.7: Profiles of closed-loop states under MPC and the desired equilibrium states for the set-point are denoted by red dashed line.

The results depicted in Figs. 3.7 - 3.9 provide insights into the performance of the MPC on the closed-loop pipeline system. After implementing the MPC control law into the pipeline model, the resulting closed-loop state profiles are shown in Fig. 3.7. The results clearly demonstrate the stabilization of the closed-loop system, given that the states in each pipe are able to track their desired steady states with faster convergence rates. This is also supported by the output profiles depicted in Fig. 3.8, which show that the controlled output under the MPC law converges to the considered set-point. The corresponding manipulated input is illustrated in Fig. 3.9.

Table 3.7: Performance comparison of tracking MPC with different cost weights

Q_c	R_c	S		
		1	10	100
1	1	2.8717	0.3511	0.2232
	5	4.6151	0.3127	0.1712
5	1	1.0470	1.0470	1.0470
	5	1.0470	1.0470	1.0470

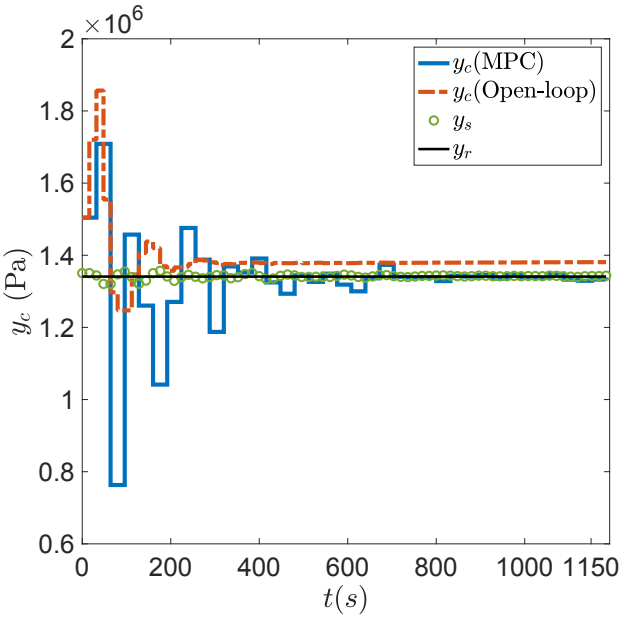

Figure 3.8: Trajectories of y_c for the closed-loop system (blue solid line), the open-loop output (red dashed line), the trajectory planner (green circled line) and the target reference (black solid line).

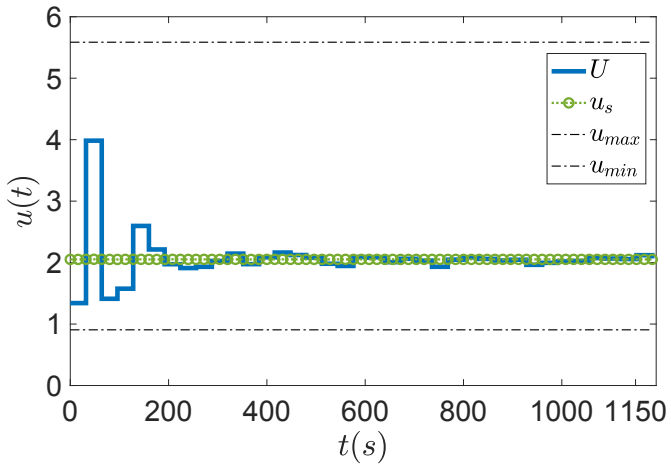

Figure 3.9: Trajectories of input for the closed-loop system (blue solid line), the desired input (green circled line) and constraints (black dashed line).

Furthermore, the performance comparison of the tracking MPC with different cost weights (Q_c and R_c) and parameter S is investigated. To reduce the influence of transient dynamics, the normalized mean absolute error calculated over time range $[800, 1150]$ is used for performance evaluation. As illustrated in Table 3.7, it is evident that by using the tracking MPC, the tracking error is small and stays within a

reasonable range (0.1712 to 4.6151) under these conditions considered. Specifically, when selecting the weights as $Q_c = 1$, $R_c = 5$ and $S = 100$ for MPC implementation, the normalized mean absolute error is minimized, which corresponds to the case discussed in Section 3.4.3.

3.4.3 Performance of combined MHE and tracking MPC

Instead of using full information of system states and the actual parameter value, the estimated states and parameter obtained from MHE are utilized in MPC. The combined control and state and parameter estimation approach proposed in Section 3.3 is implemented into the branching pipeline model. In this case, we also test a case of controlling the flow velocity at $\eta_c = 7250m$ in the third pipe, but instead of one set-point, two set-points are considered, i.e., $y^r = \begin{cases} 1.3337 \times 10^6, t < 800s \\ 1.4137 \times 10^6, \text{otherwise} \end{cases}$. We have chosen for an estimation horizon of 15 sampling periods and prediction horizons of 45 sampling periods. For initializing the implementation algorithm shown in Table 3.1, we take $Q_c = 1, R_c = 5, S = 100$ and $\mu = 0.001$.

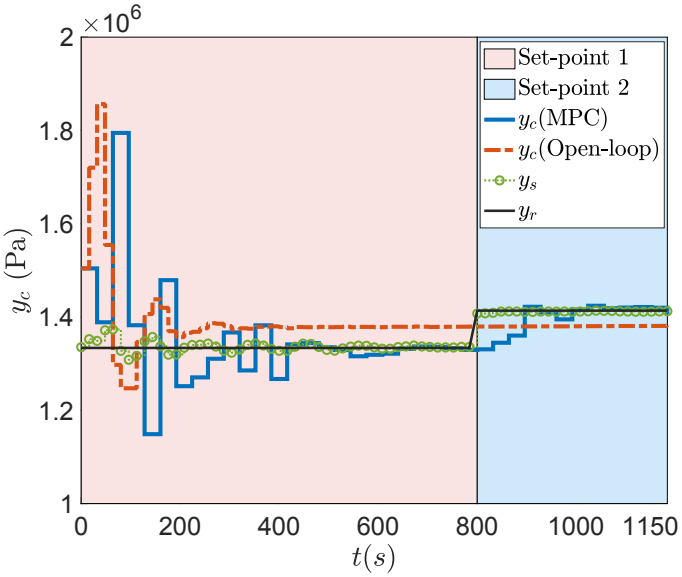

Figure 3.10: Trajectories of y_c for the closed-loop system (blue solid line), the open-loop output (red dashed line), the trajectory planner (green circled line) and the target reference (black solid line); Each set-point tracking is marked with a different color.

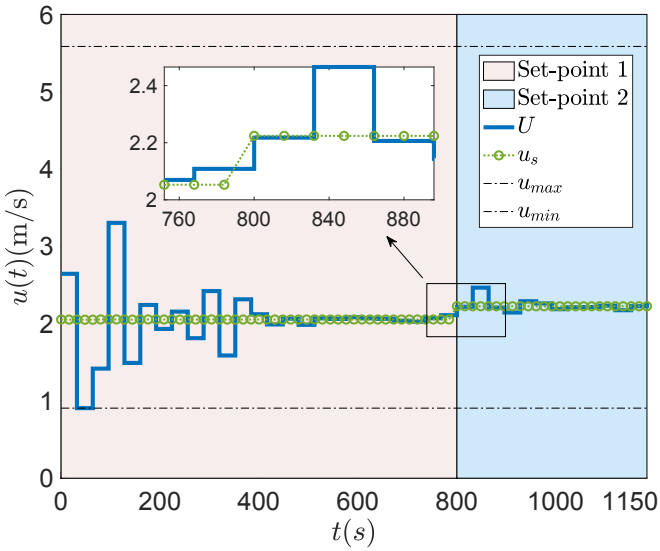

Figure 3.11: Trajectories of input for the closed-loop system (blue solid line), the desired input (green circled line) and constraints (black dashed line).

Fig. 3.10 shows the trajectories of closed-loop output y_c (MPC) (blue solid line), the open-loop output y_c (red dashed line), the trajectory planner y_s (green circled line) and the target reference y_r (black solid line). The trajectory planner gradually converges to the given set-points around 500s, after that, a small deviation can be observed between the trajectory of the planner and the set-points. Additionally, the closed-loop output trajectory y_c converges to the planner trajectory y_s in a similar manner. When there is a sudden change in the set-point, the system is able to converge to the new trajectory of the planner within 100s. The corresponding input actions are illustrated in Fig. 3.11, where the green circled line denotes the desired input, and the solid blue line denotes the desired input to track the considered set-points. It is worth noting that the control actions satisfy the considered constraints, and control effort is necessary to achieve output tracking of the first set-point in the first half of the time horizon. While less control action is required to track the second set-point after that. Fig. 3.12 illustrates the state evolution profiles of the branched pipeline system under the control of the MPC scheme. Figures in the first column are the pressure and flow velocity of pipe 1, second column denotes those of pipe 2, and third column denotes those of pipe 3. The closed-loop states demonstrate the ability to converge towards the target steady state profiles, where the red dashed line

denotes the steady state profile corresponding the first set-point, and the blue dashed line denotes the steady state profile corresponding the second set-point. The overall performance of the combined MHE-MPC strategy is remarkable as the controlled pressure are kept close to the reference values.

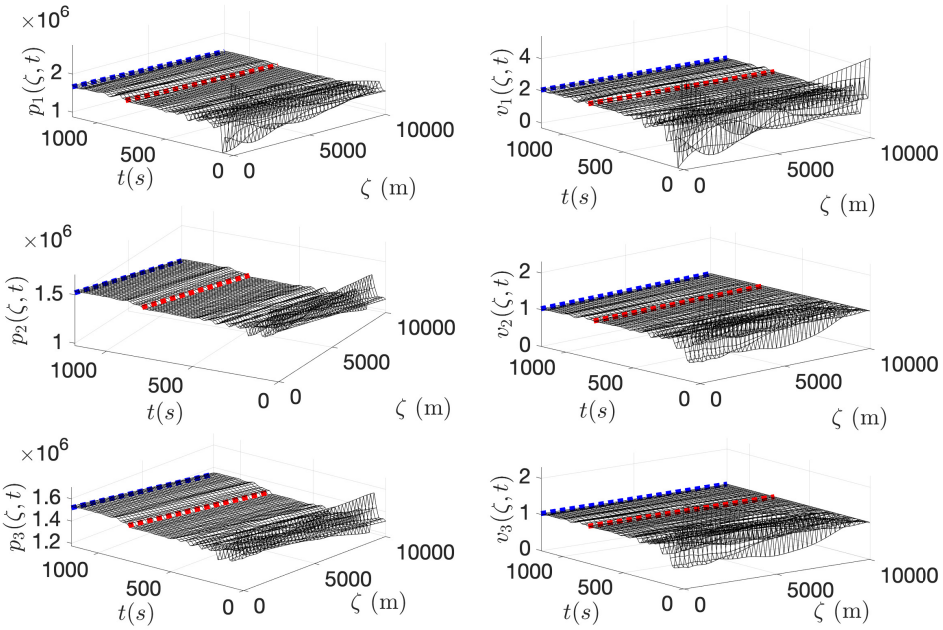

Figure 3.12: The closed-loop state profiles, the desired equilibrium state for set-point 1 (red dashed line) and the desired equilibrium state for set-point 2 (blue dashed line).

3.5 Conclusions

In this chapter, a receding horizon control and estimation framework has been proposed and implemented for distributed parameter pipeline systems. The branched pipeline network was modelled by six linearized first-order coupled hyperbolic PDEs with boundary actuation. The Cayley-Tustin time discretization approach was applied to convert the continuous-time linearized pipeline systems into a discrete-time infinite-dimensional model while preserving important system properties. To meet flow regulation within pipeline systems and handle physical constraints on inputs and outputs, a novel tracking MPC was designed. Furthermore, the MHE was applied in jointly estimating the spatial-temporal states and unknown parameters. Finally, the applicability and robustness of the proposed MPC and MHE designs were demonstrated via numerical examples.

Chapter 4

Dynamic Modelling and Model Predictive Control of a Continuous Pulp Digester

4.1 Introduction

The pulp and paper industry has a profound influence on the economy of the world, which produces pulp, paper, paperboard, and various cellulose-based products. Even though electronic media and paperless communication have been widely expanded, the global pulp and paper market is growing steadily at a rate of over 1% per year [133, 134]. For instance, the global consumption of paper and board amounted to an estimated 399 million metric tons in 2020. It is expected that demand will increase steadily over the next decade, reaching approximately 461 million metric tons in 2030 [135]. The vast majority of increasing demand mainly comes from the following categories of products [136]: personal hygiene paper products, food packaging products, corrugated packaging materials, and paper-based medicinal materials (shown in Figure 4.1), which are closely related to the growing e-commerce business and awareness of safety and hygiene, especially under the pandemic situation of COVID-19. Advanced process control and state-of-the-art process optimization techniques would provide enormous opportunities for maximized efficiency and optimized energy usage to satisfy the steadily growing need.

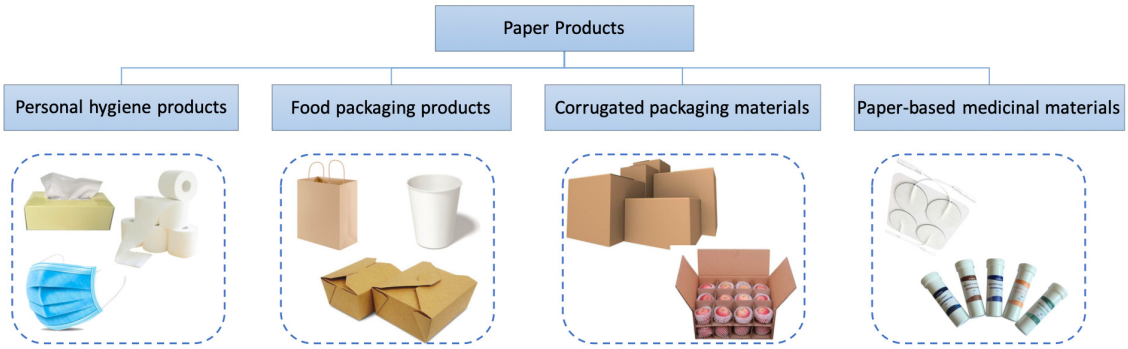

Figure 4.1: The categories of paper products

The pulp and paper mills aim to convert wood chips into pulp, the raw material for different types of products. In general, a pulping process can be classified into mechanical pulping, chemical pulping, and thermomechanical pulping according to the fundamental mechanism of separating wood fibers [137]. More than two-thirds of globally produced pulp comes from Kraft pulping which belongs to the chemical pulping process [138]. In the Kraft pulping process, the conversion of wood chips into pulp mainly takes place in a pressured vertical cylindrical reactor known as the pulp digester, which operates in a batch manner or as a continuous process. Due to lower space requirements and lower energy costs, continuous pulp digesters are predominantly used in industrial applications [134]. As illustrated in Figure 4.2, the typical continuous digesters consist of three basic zones: an impregnation zone, a cook zone, and a wash zone. White liquor and pre-steamed wood chips are introduced at the top of the digester into the impregnation zone where the liquor penetrates the wet chips. After that, the two streams flow downwards into the cook zone where the most delignification reactions occur. Then, the spent liquor is withdrawn from the digester at extraction screens. At the same time, the cooked pulp moves downwards to the wash zone where the chips are washed by the counter-current flow of cold wash liquor. The cooked pulp is then removed from the bottom of the digester. In particular, the cooking degree is evaluated by the Kappa number, which denotes the residual lignin content of the pulp.

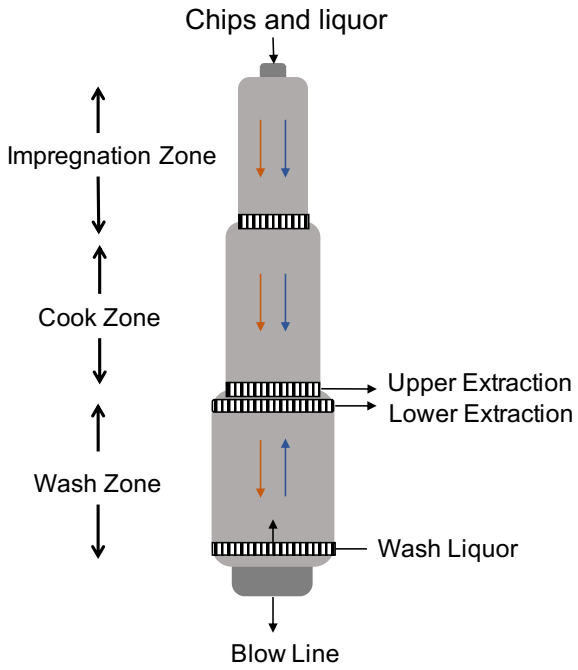

Figure 4.2: Simplified scheme of a continuous pulp digester [3]

Due to the complex nature of the delignification process, numerous mathematical models for the pulp digesters have been proposed over the last few decades. Three widely used dynamic models are known as the Purdue, Gustafson, and Andersson models, which have similar conceptual bases and assumptions [139, 140, 141]. These kinetic models show the effect of a change of temperature on the reaction rate constants for different wood components according to the Arrhenius expression [134]. The main differences are the numbers of wood components, the assumption of consecutive or parallel reactions, and the assumption about how the delignification reaction takes place along the digester length. Among them, the most commonly used model is the extended Purdue model, which is followed and further developed by other researchers [3, 142, 143].

When it comes to the controller design for the pulp digesters, a wide variety of control methods, such as reduced dimension control, robust control, and generic algorithms have been investigated [144, 7]. Since one of the main objectives of the pulp digester is to produce pulp with specific properties with minimum chemical and energy inputs, the digester is usually operated in a constrained setting[145]. In this

case, model predictive control (MPC) as a widely deployed methodology in different types of processes is capable of handling such requirements. Michaelsen et al. [146] developed a model predictive controller for a Kamyr digester using a real-time mechanistic model compensated by an optimal state estimator and the performance demonstrated to be superior when compared with proportional-integral (PI) control in offline simulations. Lee and Datta [147] designed a model predictive control system coupled with an extended Kalman filter for a batch-type pulp digester. Along the same line of work, Wisnewski and Doyle [148] analyzed the performance of linear MPC and nonlinear MPC for set-point tracking and unmeasured disturbance rejection. Alexandridis and Sarimveis [149] employed an adaptive MPC based on a radial basis function ANN model for Kappa number control of continuous pulp digesters. H.-K. Choi and J. S.-I. Kwon [150, 151, 152, 153] developed a class of MPC for continuous pulp digester and batch pulp digester based on the proposed multi-scale model. However, even though the aforementioned works have made a valuable contribution toward the modelling and controller design for the pulp digester, there still some aspects which did not receive much attention and/or accurate consideration. First of all, most of the works depend on the approximation of the PDE into a large-scale ordinary differential equation (ODE), which is generally prone to approximation error and is difficult to capture the spatial kinetics properties within the digester. In addition, these approaches need to perform the spatial discretization in an early lumping manner, which dramatically increases the complexity of the calculations and might induce numerical instability and/or alter the fundamental control theoretical properties, such as controllability, observability, and stabilizability [8, 19]. Secondly, grade transitions have increased significance in pulping mills, which is necessitated by optimal production scheduling and planning policies. Hundreds of grade transitions are required every year for pulp digesters, which is even more frequent when the market demand increases [143, 152]. The targets of operational variables are considerably different to meet various market demands, the shift operations, therefore, need to be taken into account when the controller is developed and its realization. Thirdly, the co-current flow and counter-current flow in the digester need to be considered in accurate manner, mainly due to the fact that the main control manipulation is performed in the top part of the digester, while the controlled variable is physically

measured at the outlet of the digester [134].

Motivated by the aforementioned issues, this chapter considers a bilinear transformation of a continuous infinite-dimensional system to a discrete one by the application of the Cayley-Tustin time discretization approach, in which the physical characteristics (energy) and theoretical properties of considered systems are preserved [14]. In addition, the finite-dimensional MPC setting is extended to the distributed parameter pulp digester system to realize constant target tracking and achieve optimal grade transitions. The cascade zones (cook zone and wash zone) of the digester are considered as an extended distributed parameter system, which is described by the system of 10 transport-reaction hyperbolic PDEs.

In this chapter, the claimed novelty is the extension of linear MPC designs for the finite-dimensional system to the infinite-dimensional one to realize constant set-points tracking. Particularly, the pulp digester system described by a set of coupled nonlinear hyperbolic PDEs is considered, which can capture the spatiotemporal evolution of wood chips and wash liquor. In addition, the linearized continuous-time model is transformed to a linear discrete-time infinite-dimensional model, and the fundamental continuous-time properties (including stability, controllability and observability) are preserved under the Cayley–Tustin transformation. Moreover, a discrete-time observer for the system of hyperbolic PDEs is proposed, accounting for the available output measurement and the system states reconstruction. Finally, the controller design provides optimal asymptotic stabilization and target tracking realization of the system with the inclusion of output and input constraints.

The chapter is organized as follows: we initially present a dynamic model to describe the delignification process in the continuous pulp digester. Then, the developed model is linearized and discretized in time by utilizing the Cayley-Tustin approach. Lastly, we propose a Luenberger observer-based model predictive controller for the discrete model to realize the target tracking. The simulation results demonstrate the performance of the proposed controller design.

4.2 Problem Formulation

In this section, the mathematical model of the pulp digester process is introduced. In particular, the equilibrium profiles are calculated to proceed with the linearization of the original nonlinear system. For the sake of simplicity, an infinite-dimensional representation is given to illustrate the linearized system. Finally, a discrete-time model is obtained utilizing the Cayley-Tustin discretization framework.

4.2.1 Model description

The main section of a continuous pulp digester can be divided into the co-current zone and counter-current zone, which are also referred to as cook zone and wash zone respectively, as shown in Figure 4.3. Each zone can be modelled by a set of nonlinear coupled PDEs, which are derived from the first principle. The models of cook zone and wash zone are similar, but different flow direction of the liquor. Generally, each volume in the digester contains three phases, solid phase, entrapped liquor phase, and free liquor phase. In particular, the combination of solid phase and entrapped liquor phase is further referred to as the wood chip phase, and the details of the conceptual model of the mass in the digester are shown in Figure 4.4. The wood chips are often assumed to consist of five components, and the entrapped liquor and free liquor contain four same components. For more details of the model, one can see the references [3, 154].

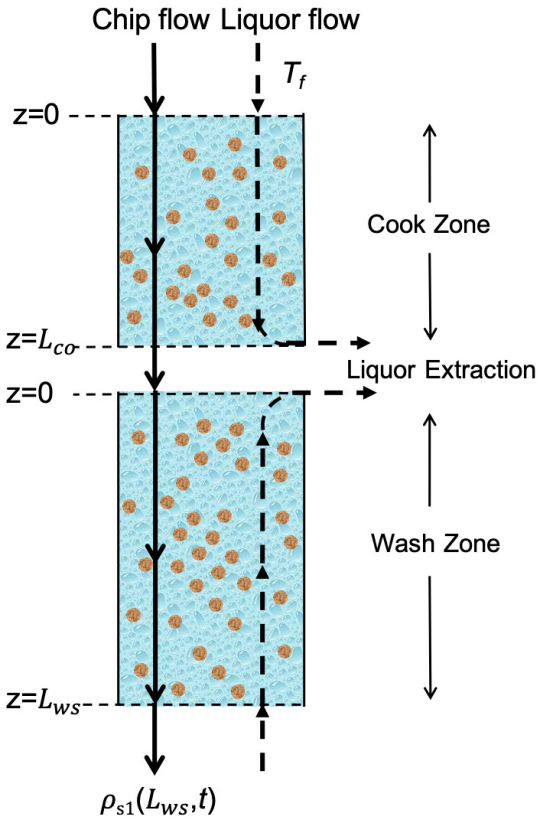

Figure 4.3: The cook zone and wash zone in a digester

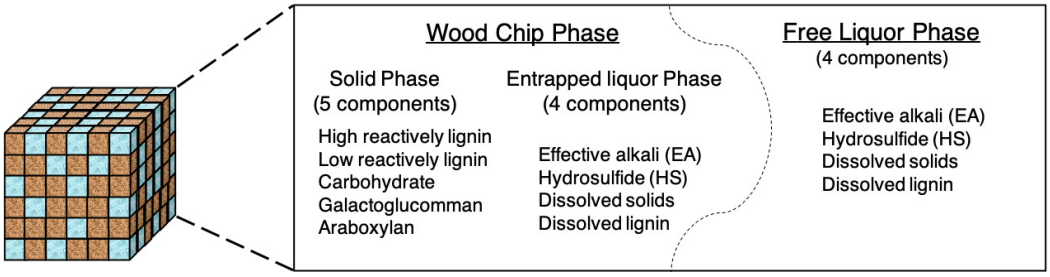

Figure 4.4: The conceptual model of the mass in a digester

Based on the model proposed by Michelsen [154], the following assumptions are considered to obtain a simple model which describes some dominant dynamics of the process. Wood chips are assumed to be of equal size and to have a constant volume during cooking. The volume flows of wood chips and free liquor are assumed to be equal at all space positions, and the chip compaction profile is assumed to be stationary, expressed as a piecewise linear function of position. The cross-sectional area

is assumed to be constant in the digester. For simplicity, the degradation of carbohydrates is assumed to follow a lignin reduction linearly and the concentrations of dissolved solids in the entrapped liquor and free liquor can be omitted [154, 155, 156]. There is a linear approximation relationship between the lignin and carbohydrate in solid phase, $\rho_{carb} = 0.36 + 0.84\rho_{lig}$, as a result, the lignin and carbohydrate need not necessarily be regarded as being two states of the system [154]. In addition, according to Gustafson et al. [140], the carbohydrate reaction rate in the bulk delignification period is proportional to the lignin reaction rate as $R_{carb} = 0.47R_{lig}$.

Hence, from control and monitoring point of view, the following variables are important, which are considered as the states of the model:

$\rho_s(z,t)$: concentration of lignin of solid phase (%)

$\rho_e(z,t)$: concentration of alkali of entrapped liquor phase (g/l)

$\rho_f(z,t)$: concentration of alkali of free liquor phase (g/l)

$T_c(z,t)$: temperature of wood chip phase (K)

$T_f(z,t)$: temperature of free liquor phase (K)

Based on the abovementioned assumption, the mathematical models of cook zone and wash zone can be simplified to the following equations:

$$
\begin{aligned}
0 \le z \le L_{co} \begin{cases}
\frac{\partial \rho_s^{\mathcal{C}}(z,t)}{\partial t} = -v_c \frac{\partial \rho_s^{\mathcal{C}}(z,t)}{\partial z} - R_s^{\mathcal{C}} \\
\frac{\partial \rho_e^{\mathcal{C}}(z,t)}{\partial t} = -v_c \frac{\partial \rho_e^{\mathcal{C}}(z,t)}{\partial z} + \frac{D_{EA}^{\mathcal{C}}}{\varepsilon_c}(\rho_f^{\mathcal{C}}(z,t) - \rho_e^{\mathcal{C}}(z,t)) - \rho_{ODW}(b_1 + 0.47b_2)R_s^{\mathcal{C}} \\
\frac{\partial \rho_f^{\mathcal{C}}(z,t)}{\partial t} = -v_f \frac{\partial \rho_f^{\mathcal{C}}(z,t)}{\partial z} - \frac{D_{EA}^{\mathcal{C}}}{\varepsilon_f}(\rho_f^{\mathcal{C}}(z,t) - \rho_e^{\mathcal{C}}(z,t)) \\
\frac{\partial T_c^{\mathcal{C}}(z,t)}{\partial t} = -v_c \frac{\partial T_c^{\mathcal{C}}(z,t)}{\partial z} + \left[1.47\rho_c \Delta H_R R_s^{\mathcal{C}} + U(T_f^{\mathcal{C}}(z,t) - T_c^{\mathcal{C}}(z,t))\right]/C_{pe} \\
\frac{\partial T_f^{\mathcal{C}}(z,t)}{\partial t} = -v_f \frac{\partial T_f^{\mathcal{C}}(z,t)}{\partial z} - U(T_f^{\mathcal{C}}(z,t) - T_c^{\mathcal{C}}(z,t))/C_{pf} + b(z)u(t)
\end{cases} \\
0 \le z \le L_{ws} \begin{cases}
\frac{\partial \rho_s^{\mathcal{W}}(z,t)}{\partial t} = -v_c \frac{\partial \rho_s^{\mathcal{W}}(z,t)}{\partial z} - R_s^{\mathcal{W}} \\
\frac{\partial \rho_e^{\mathcal{W}}(z,t)}{\partial t} = -v_c \frac{\partial \rho_e^{\mathcal{W}}(z,t)}{\partial z} + \frac{D_{EA}^{\mathcal{W}}}{\varepsilon_c}(\rho_f^{\mathcal{W}}(z,t) - \rho_e^{\mathcal{W}}(z,t)) - \rho_{ODW}(b_1 + 0.47b_2)R_s^{\mathcal{W}} \\
\frac{\partial \rho_f^{\mathcal{W}}(z,t)}{\partial t} = v_f \frac{\partial \rho_f^{\mathcal{W}}(z,t)}{\partial z} - \frac{D_{EA}^{\mathcal{W}}}{\varepsilon_f}(\rho_f^{\mathcal{W}}(z,t) - \rho_e^{\mathcal{W}}(z,t)) \\
\frac{\partial T_c^{\mathcal{W}}(z,t)}{\partial t} = -v_c \frac{\partial T_c^{\mathcal{W}}(z,t)}{\partial z} + \left[1.47\rho_c \Delta H_R R_s^{\mathcal{W}} + U(T_f^{\mathcal{W}}(z,t) - T_c^{\mathcal{W}}(z,t))\right]/C_{pe} \\
\frac{\partial T_f^{\mathcal{W}}(z,t)}{\partial t} = v_f \frac{\partial T_f^{\mathcal{W}}(z,t)}{\partial z} - U(T_f^{\mathcal{W}}(z,t) - T_c^{\mathcal{W}}(z,t))/C_{pf}
\end{cases}
\end{aligned}
\tag{4.1}
$$

where the superscript $\mathcal{C}$ and $\mathcal{W}$ indicate the cook zone and wash zone, respectively. $R_s^{\mathcal{C}}$ and $R_s^{\mathcal{W}}$ are the rate of consumption of mass of solid per chip volume in cook zone and wash zone, describing by the Arrhenius coefficients, $R_s^{\mathcal{C}} = A_1 e^{-\frac{E_1}{T_c^{\mathcal{C}}}} \rho_e^{\mathcal{C}}(\rho_s^{\mathcal{C}} -$

ρ_s^0), $R_s^{\mathcal{W}} = A_1 e^{-\frac{E_1}{T_c^{\mathcal{W}}}} \rho_e^{\mathcal{W}} (\rho_s^{\mathcal{W}} - \rho_s^0)$. ρ_s^0 denotes the non-reactive lignin in wood. The mass diffusion rate D_{EA} usually take the form, $D_{EA}^{\mathcal{C}} = 0.16\sqrt{T_c^{\mathcal{C}}} e^{\frac{-2452.4}{T_c^{\mathcal{C}}}} (-2.0\rho_s^{\mathcal{C}} + 0.13(\frac{\rho_e^{\mathcal{C}}}{32.0})^{0.55} + 0.58)$ and $D_{EA}^{\mathcal{W}} = 0.16\sqrt{T_c^{\mathcal{W}}} e^{\frac{-2452.4}{T_c^{\mathcal{W}}}} (-2.0\rho_s^{\mathcal{W}} + 0.13(\frac{\rho_e^{\mathcal{W}}}{32.0})^{0.55} + 0.58)$. ε_c is the chip compaction, which increases from the entry through the cook zone, reaching a maximum at the main extraction, $\varepsilon_c(z) = \varepsilon_{10} + \varepsilon_{11} z$, and $\varepsilon_f(z) = 1 - \varepsilon_c(z)$. U denotes the heat-transfer coefficient, and the heat capacities of the entrapped and free liquor phases (C_{pe} and C_{pf}) are determined by the mixing rules based on weighted averages [142]. In this case, the input is the temperature of free liquor and the distribution is described by the actuation distribution function $b(z) = 1_{[z_a - \varepsilon, z_a + \varepsilon]}$. The controlled output is defined as the concentration of lignin of solid phase at the outlet in wash zone, and the measurements of each state at the outlet are assumed available which are taken as the measured outputs. Under the beforementioned assumptions, the Kappa number can be approximated as a nonlinear relation with the concentration of lignin of solid phase, where $Kappa(z,t) = (653.4\rho_s^{\mathcal{C}}(z,t))/(1.84\rho_s^{\mathcal{C}}(z,t) + 0.36)$.

The boundary conditions for the cook zone are given at $z = 0$ (see Figure 4.3):

$$\rho_s^{\mathcal{C}}(0,t) = \rho_{s_0}, \rho_e^{\mathcal{C}}(0,t) = \rho_{e_0}, \rho_f^{\mathcal{C}}(0,t) = \rho_{f_0}, T_c^{\mathcal{C}}(0,t) = T_{c0}, T_f^{\mathcal{C}}(0,t) = T_{f0} \tag{4.2}$$

and for the wash zone at $z = 0$ and $z = L_{ws}$:

$$\begin{aligned} &\rho_s^{\mathcal{W}}(0,t) = \rho_s^{\mathcal{C}}(L_{co},t), \rho_e^{\mathcal{W}}(0,t) = \rho_e^{\mathcal{C}}(L_{co},t), \rho_f^{\mathcal{W}}(L_{ws},t) = \rho_{f_0}, \\ &T_c^{\mathcal{W}}(0,t) = T_c^{\mathcal{C}}(L_{co},t), T_f^{wash}(L_{ws},t) = T_{f0} \end{aligned} \tag{4.3}$$

4.2.2 Model linearization

In order to reduce the mathematical complexity of the nonlinear process model, we make the linearization around the system equilibrium point or spatially nonuniform steady-state by setting the time derivative terms to be zero. The steady-states are solved numerically using the finite difference method. As a result, the corresponding steady-states profiles are illustrated in Figure 4.5. Additionally, we assume that L_{co} and L_{ws} are the same, which denote as L for notation simplicity, and introduce the following notations to define the local dynamics from the states of the cook zone to

the states of the wash zone:

$$\begin{aligned} x^{(C)}(z,t) &= [\rho_s^{\mathcal{C}}(z,t); \rho_e^{\mathcal{C}}(z,t); \rho_f^{\mathcal{C}}(z,t); T_c^{\mathcal{C}}(z,t); T_f^{\mathcal{C}}(z,t)] \\ x^{(\mathcal{W})}(z,t) &= [\rho_s^{\mathcal{W}}(z,t); \rho_e^{\mathcal{W}}(z,t); \rho_f^{\mathcal{W}}(z,t); T_c^{\mathcal{W}}(z,t); T_f^{\mathcal{W}}(z,t)] \end{aligned} \tag{4.4}$$

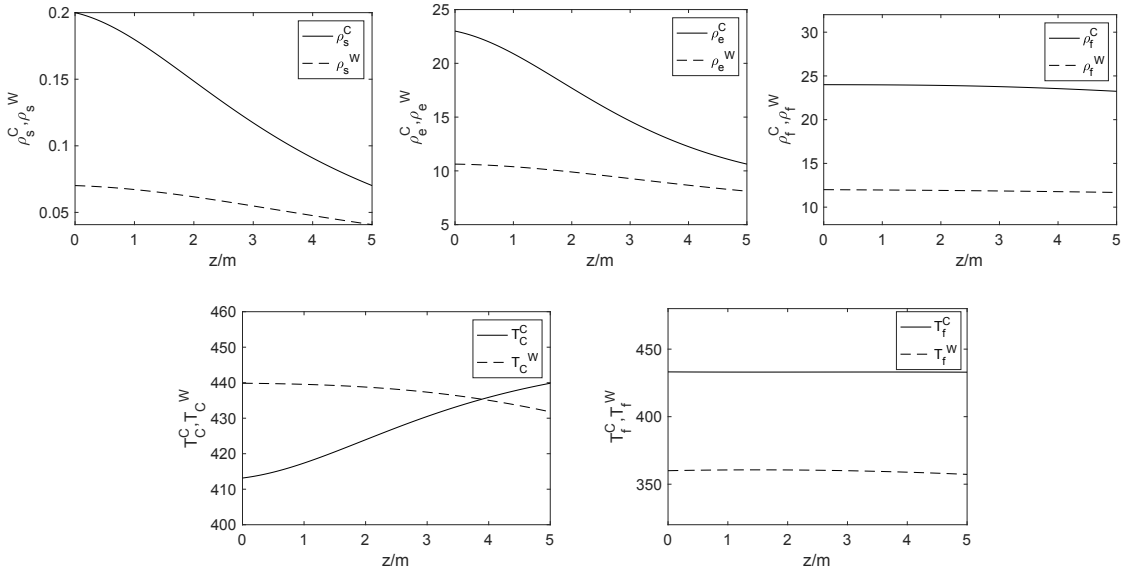

Figure 4.5: Steady-state profiles of the digester (The solid lines denote the steady-states of the components in cook zone; the dash lines denote the steady-states of the corresponding components in wash zone.)

The above nonlinear model Equation (4.1) can be linearized applying the Taylor series expansion. The linearized model is then obtained as:

$$\begin{aligned} \dot{x}^{(C)}(z,t) &= \mathcal{A}_1 x^{(C)}(z,t) + \mathcal{B}_1 u(t) \\ \dot{x}^{(\mathcal{W})}(z,t) &= \mathcal{A}_2 x^{(\mathcal{W})}(z,t) \\ y_c(t) &= C_2 x^{(\mathcal{W})}(z,t) \\ y_m(t) &= \begin{bmatrix} C_{m1} x^{(C)}(z,t) \\ C_{m2} x^{(\mathcal{W})}(z,t) \end{bmatrix} \end{aligned} \tag{4.5}$$

where $z_1 \in [0, L]$ and $z_2 \in [0, L]$. The operator $\mathcal{A}_1(\cdot) = (V_1 \frac{\partial}{\partial z} + \psi_1(z))(\cdot)$ and $\mathcal{A}_2(\cdot)$ $= (V_2 \frac{\partial}{\partial z} + \psi_2(z))(\cdot)$, where

$$V_1 = \text{diag}\{-v_c, -v_c, -v_f, -v_c, -v_f\}, V_2 = \text{diag}\{-v_c, -v_c, v_f, -v_c, v_f\}$$

and

$$\psi_1(z)=\begin{bmatrix} J_{11}(z) & J_{12}(z) & 0 & J_{14}(z) & 0 \\ J_{21}(z) & J_{22}(z) & J_{23}(z) & J_{24}(z) & 0 \\ J_{31}(z) & J_{32}(z) & J_{33}(z) & J_{34}(z) & 0 \\ J_{41}(z) & J_{42}(z) & 0 & J_{44}(z) & J_{45}(z) \\ 0 & 0 & J_{53}(z) & J_{54}(z) & J_{55}(z) \end{bmatrix}, \psi_2(z)=\begin{bmatrix} \bar{J}_{11}(z) & \bar{J}_{12}(z) & 0 & \bar{J}_{14}(z) & 0 \\ \bar{J}_{21}(z) & \bar{J}_{22}(z) & \bar{J}_{23}(z) & \bar{J}_{24}(z) & 0 \\ \bar{J}_{31}(z) & \bar{J}_{32}(z) & \bar{J}_{33}(z) & \bar{J}_{34}(z) & 0 \\ \bar{J}_{41}(z) & \bar{J}_{42}(z) & 0 & \bar{J}_{44}(z) & \bar{J}_{45}(z) \\ 0 & 0 & \bar{J}_{53}(z) & \bar{J}_{54}(z) & \bar{J}_{55}(z) \end{bmatrix}$$

where the $J_{i,j}(z)$ and $\bar{J}_{i,j}(z)(i,j=1,2,...,5)$ are the nonlinear term evaluated at steady-state by ignoring the 2nd order and higher order terms, such as $J_{1,1}=-A_1\rho_{e,ss}e^{-\frac{E_1}{T_{c,ss}}}$, $J_{1,2}=A_1(\rho_{s1}^0-\rho_{s1,ss})e^{-\frac{E_1}{T_{c,ss}}}$. The input operator $\mathcal{B}_1$ is defined as a bounded operator $\mathcal{B}_1$ =[0; 0; 0; 0; $b(z)$] and $b(z)=\frac{1}{2\bar{z}_L}1_{[z_L-\bar{z}_L,z_L+\bar{z}_L]}(z)$. The controlled output operator $\mathcal{C}_2$ is determined as $\mathcal{C}_2(\cdot)=\text{diag}\{\int_0^L\delta(z-L)(\cdot)d\eta$,0,0,0,0$\}$, and the measured output operators are defined as $\mathcal{C}_{m1}$=diag$\{\int_0^L\delta(z-L)(\cdot)d\eta,\int_0^L\delta(z-L)(\cdot)d\eta,\int_0^L\delta(z-L)(\cdot)d\eta,\int_0^L\delta(z-L)(\cdot)d\eta,\int_0^L\delta(z-L)(\cdot)d\eta\}$ and $\mathcal{C}_{m2}=\text{diag}\{\int_0^L\delta(z-L)(\cdot)d\eta,\int_0^L\delta(z-L)(\cdot)d\eta,\int_0^L\delta(z-L)(\cdot)d\eta,\int_0^L\delta(z)(\cdot)d\eta,\int_0^L\delta(z-L)(\cdot)d\eta\}$, respectively.

In this form, the domains of operator $\mathcal{A}_1$ and $\mathcal{A}_2$ are $\mathcal{D}(\mathcal{A}_1)=\{[\phi_1(z);\phi_2(z);\phi_3(z);\phi_4(z);\phi_5(z)]\in L_2(0,L)^5|\phi_i(z)$ are abs. cont., and $\phi_i(0)=0,i=1,2,...,5\}$, and $\mathcal{D}(\mathcal{A}_2)=\{[\phi_6(z);\phi_7(z);\phi_8(z);\phi_9(z);\phi_{10}(z)]\in L_2(0,L)^5|\phi_j(z)$ are abs. cont.,$j=6,7,...,10$ and $\phi_j(L)=0,j=8,10\}$, respectively.

Mathematically, the dynamics of the above cascade system (cook zone and wash zone) can be described by the following extended system:

$$\begin{aligned} \dot{x}(z,t) &= \mathcal{A}x(z,t)+\mathcal{B}u(t) \\ y_c(t) &= \mathcal{C}_c x(z,t) \\ y_m(t) &= \mathcal{C}_m x(z,t) \end{aligned} \tag{4.6}$$

with boundary conditions given below:

$$\begin{aligned} &x_1(0,t)=0,x_2(0,t)=0,x_3(0,t)=0,x_4(0,t)=0,x_5(0,t)=0 \\ &x_6(0,t)=x_1(L,t),x_7(0,t)=x_2(L,t),x_8(L,t)=0,x_9(0,t)=x_4(L,t),x_{10}(L,t)=0 \end{aligned} \tag{4.7}$$

where the extended state $x(z,t)=[x^{(C)}(z,t);x^{(W)}(z,t)]$ and the corresponding extended operators are given as follows:

$$\begin{aligned} \mathcal{A}(\cdot)&=V\frac{\partial}{\partial z}(\cdot)+\psi(z)(\cdot),V=\text{bdiag}\{V_1,V_2\},\psi(z)=\text{bdiag}\{\psi_1,\psi_2\} \\ \mathcal{B}&=[\mathcal{B}_1;\mathbf{0}],\mathcal{C}_c=[\mathbf{0},\mathcal{C}_2],\mathcal{C}_m=\text{bdiag}\{\mathcal{C}_{m1},\mathcal{C}_{m2}\} \end{aligned} \tag{4.8}$$

The state $x(z,t)\in\mathcal{X}$, with $\mathcal{X}=L^2((0,L),\mathbb{R}^{10})$ being defined as a real separable Hilbert space with inner product $\langle\cdot,\cdot\rangle$. The input $u(t)\in L^2_{loc}([0,\infty),\mathcal{U})$ and output

$y(t) \in L^2_{loc}([0,\infty),\mathcal{Y})$, where $\mathcal{U}$ and $\mathcal{Y}$ are real separable Hilbert spaces. Based on the coupling conditions Equation (4.3), we have the domain of $\mathcal{A}$, which is $\mathcal{D}(\mathcal{A}) = \mathcal{D}(\mathcal{A}_1) \bigoplus \mathcal{D}(\mathcal{A}_2) = \{[\phi_1;\phi_2;...;\phi_5] \in L_2(0,L)^5, [\phi_6;\phi_7;...;\phi_{10}] \in L_2(0,L)^5 | [\phi_1;\phi_2;...;\phi_5] \in \mathcal{D}(\mathcal{A}_1), [\phi_6;\phi_7;...;\phi_{10}] \in \mathcal{D}(\mathcal{A}_2)$, and $\phi_1(L) = \phi_6(0), \phi_2(L) = \phi_7(0), \phi_4(L) = \phi_9(0)\}$ [32]. The adjoint operator $\mathcal{A}^*$ is easily found using the inner product formula, $\langle \mathcal{A}\varphi_i, \phi_i \rangle = \langle \varphi_i, \mathcal{A}^*\phi_i \rangle, i = 1,2,...,10$, and is:

$$\mathcal{A}^*(\cdot) = -V\frac{\partial(\cdot)}{\partial z} + \psi^*(z)(\cdot) \tag{4.9}$$

with its domain defined as $\mathcal{D}(\mathcal{A}^*) = \{[\phi_1;\phi_2;...;\phi_5] \in L_2(0,L)^5, [\phi_6;\phi_7;...;\phi_{10}] \in L_2(0,L)^5$, $\phi_i(z)$ is absolutely continuous, $\frac{d\phi_i}{dz} \in L_2(0,L)$, with $i = 1,2,...,10$, and $\phi_j(L) = 0, j = 3,5,6,7,9, \phi_m(0) = 0, m = 8,10, \phi_1(L) = \frac{v_6}{v_1}\phi_6(0), \phi_2(L) = \frac{v_7}{v_2}\phi_7(0), \phi_4(L) = \frac{v_9}{v_4}\phi_9(0)\}$.

4.3 Model Discretization

In this section, the Cayley-Tustin discretization framework is considered and applied to the linearized digester system without any spatial approximation induced. By the use of Cayley–Tustin transformation, a discrete-time state-space model for describing the extended digester system is established and realized by determining the resolvent operator, which is amenable to the discrete observer and controller designs. Meanwhile, the essential properties of the continuous-time system stay invariant under this transformation, such as conservative (energy preserving) [157], stability [158], observability [52, 100], controllability.

4.3.1 Cayley-Tustin time discretization framework

The above linear system in Equation (4.6) is considered. For a given time discretization $h > 0$, and for $j \geq 1$ the Cayley-Tustin discretization is given by:

$$\begin{aligned} \frac{x(jh) - x((j-1)h)}{h} &\approx \mathcal{A}\frac{x(jh) + x((j-1)h)}{2} + \mathcal{B}u(jh) \\ y_c(jh) &\approx C_c\frac{x(jh) + x((j-1)h)}{2} \\ y_m(jh) &\approx C_m\frac{x(jh) + x((j-1)h)}{2} \end{aligned} \tag{4.10}$$

with $x(0) = x_0$, where the spatial dependence of x is omitted for brevity. Then, let $\frac{u_j^{(h)}}{\sqrt{h}}$ be an approximation of $u(jh)$ by the mean value within a given sampling time,

$\frac{u_j^{(h)}}{\sqrt{h}} = \frac{1}{h}\int_{(j-1)h}^{jh} u(t)dt$. It has been shown in [14] that $\frac{u_j^{(h)}}{\sqrt{h}}$ converges to $u(jh)$ as $h \to 0$ in several different ways, similar for $Y(jh)$. Further, rewriting Equation (4.10) gives the discrete time dynamics Equation (4.11). It is frequently called Tustin discretization in the engineering literature, which is proposed in 1940s by Tustin and referred as Tustin transform in digital and sample-data control literature [19].

$$\begin{aligned} \frac{x_j - x_{j-1}}{h} &\approx \mathcal{A}\frac{x_j + x_{j-1}}{2} + \mathcal{B}\frac{u_j}{\sqrt{h}} \\ \frac{y_{cj}}{\sqrt{h}} &\approx C_c\frac{x_j + x_{j-1}}{2} \\ \frac{y_{mj}}{\sqrt{h}} &\approx C_m\frac{x_j + x_{j-1}}{2} \end{aligned} \tag{4.11}$$

Through some basic computations, the following infinite-dimensional discrete-time state space model is obtained:

$$\begin{aligned} x_j &= \mathcal{A}_d x_{j-1} + \mathcal{B}_d u_j \\ y_{cj} &= C_{cd} x_{j-1} + \mathcal{D}_{cd} u_j \\ y_{mj} &= C_{md} x_{j-1} + \mathcal{D}_{md} u_j \end{aligned} \tag{4.12}$$

where $\mathcal{A}_d$, $\mathcal{B}_d$, C_d, $\mathcal{D}_d$, C_{cd} and C_{md} are the discrete-time spatial operators and we denote:

$$\begin{pmatrix} \mathcal{A}_d & \mathcal{B}_d \\ C_{cd} & \mathcal{D}_{cd} \\ C_{md} & \mathcal{D}_{md} \end{pmatrix} = \begin{pmatrix} -I + 2\delta\mathcal{R}(z,\delta) & \sqrt{2\delta}\mathcal{R}(z,\delta)\mathcal{B} \\ \sqrt{2\delta}C_c\mathcal{R}(z,\delta) & \mathcal{G}_c(\delta) \\ \sqrt{2\delta}C_m\mathcal{R}(z,\delta) & \mathcal{G}_m(\delta) \end{pmatrix} \tag{4.13}$$

where $\delta = 2/h$ and the resolvent is $\mathcal{R}(z,\delta) = (\delta - \mathcal{A})^{-1}$. Clearly, one must satisfy $\delta \in \rho(\mathcal{A})$ so that the resolvent operator is well-defined. In particular, $\mathcal{G}_c(\delta)$ denotes the transfer function from input to controlled output $\mathcal{G}_c(\delta) = C_c(\delta - \mathcal{A})^{-1}\mathcal{B}$, and $\mathcal{G}_m(\delta)$ denotes the transfer function from input to measured outputs $\mathcal{G}_m(\delta) = C_m(\delta - \mathcal{A})^{-1}\mathcal{B}$. The unbounded operators $\mathcal{A}$ of the continuous-time system are mapped into bounded operators $\mathcal{A}_d$ in the discrete-time counterpart through Cayley transform, which describe by the resolvent operator with $\mathcal{A}_d(\cdot) = [\delta - \mathcal{A}]^{-1}[\delta + \mathcal{A}](\cdot) = -I(\cdot) + 2\delta[\delta - \mathcal{A}]^{-1}(\cdot) = -I(\cdot) + 2\delta\mathcal{R}(\delta,\mathcal{A})(\cdot)$. In addition, it has been demonstrated that the controllability and stability are invariant under this transformation [14].

4.3.2 Resolvent operator

The resolvent operator can be obtained by utilizing the Laplace transform. Under the zero input condition, we can have the following expression,

$$\frac{\partial x(z,s)}{\partial z} = V^{-1}(sI-\psi)x(z,s) - V^{-1}x(z,0) \tag{4.14}$$

where ψ is taken as the average of $\psi(z)$. By solving the above ODE, one obtains:

$$x(z,s) = e^{\{V^{-1}(sI-\psi)z\}}x(0,s) - \int_0^z e^{\{V^{-1}(sI-\psi)(z-\eta)\}}V^{-1}x(\eta,0)d\eta \tag{4.15}$$

Since ψ is the block diagonal matrix and V is already in diagonal form, the matrix F is finally a block diagonal matrix, denoted as follows:

$$F = V^{-1}(sI-\psi) = \begin{bmatrix} [F_1]_{5\times5} & \mathbf{0}_{5\times5} \\ \mathbf{0}_{5\times5} & [F_2]_{5\times5} \end{bmatrix} \tag{4.16}$$

Then $e^{Fz} = \text{diag}(e^{F_1 z}, e^{F_2 z})$ and we denote $[M_{ij}(z,s)]_{10\times10} = e^{Fz}$ for simplicity.

In order to obtain the unknown boundary conditions, one needs to evaluate the boundary conditions in Equation (4.7) as follows:

(1) At $z = 0$, one can plug $x_1(0,t) = 0, x_2(0,t) = 0, x_3(0,t) = 0, x_4(0,t) = 0, x_5(0,t) = 0$ into Equation (4.15) which leads to $M_{ij}(0,s) = 0, i = 1,2,...5, j = 6,7,...10$.

(2) At $z = L$, one can firstly substitute $x_6(0,s) = x_1(L,t), x_7(0,s) = x_2(L,t), x_9(0,s) = x_4(L,t)$ into Equation (4.15) which yields

$$\begin{aligned} x_6(0,s) &= -\sum_{k=1}^{10}\int_0^L M_{1k}(L-\eta,s)V_{vkk}x_k(\eta,0)d\eta \\ x_7(0,s) &= -\sum_{k=1}^{10}\int_0^L M_{2k}(L-\eta,s)V_{vkk}x_k(\eta,0)d\eta \\ x_9(0,s) &= -\sum_{k=1}^{10}\int_0^L M_{4k}(L-\eta,s)V_{vkk}x_k(\eta,0)d\eta \end{aligned} \tag{4.17}$$

where V_v denotes V^{-1}. Then, substituting the boundary conditions $x_8(L,s) = 0$, $x_{10}(L,s) = 0$, one can have

$$\begin{aligned} &\begin{bmatrix} M_{88} & M_{810} \\ M_{108} & M_{1010} \end{bmatrix}\begin{bmatrix} x_8(0,s) \\ x_{10}(0,s) \end{bmatrix} \\ &= \begin{bmatrix} \sum_{k=1}^{10}\int_0^L M_{8k}(L-\eta,s)V_{vkk}x_k(\eta,0)d\eta - M_{86}x_6(0,s) - M_{87}x_7(0,s) - M_{89}x_9(0,s) \\ \sum_{k=1}^{10}\int_0^L M_{10k}(L-\eta,s)V_{vkk}x_k(\eta,0)d\eta - M_{106}x_6(0,s) - M_{107}x_7(0,s) - M_{109}x_9(0,s) \end{bmatrix} \end{aligned} \tag{4.18}$$

By substituting $x_6(0,s)$, $x_7(0,s)$, $x_9(0,s)$ and solving the above equations, we can obtain the expressions of $x_8(0,s)$ and $x_{10}(0,s)$ as follows,

$$\begin{aligned}
x_8(0,s) =& G_{11}(\sum_{k=1}^{10}\int_0^L M_{8k}(L-\eta,s)V_{vkk}x_k(\eta,0)d\eta) \\
&+ G_{12}(\sum_{k=1}^{10}\int_0^L M_{10k}(L-\eta,s)V_{vkk}x_k(\eta,0)d\eta) \\
&+ (G_{11}M_{86}+G_{12}M_{106})\sum_{k=1}^{10}\int_0^L M_{1k}(L-\eta,s)V_{vkk}x_k(\eta,0)d\eta \\
&+ (G_{11}M_{87}+G_{12}M_{107})\sum_{k=1}^{10}\int_0^L M_{2k}(L-\eta,s)V_{vkk}x_k(\eta,0)d\eta \\
&+ (G_{11}M_{89}+G_{12}M_{109})\sum_{k=1}^{10}\int_0^L M_{4k}(L-\eta,s)V_{vkk}x_k(\eta,0)d\eta
\end{aligned} \tag{4.19}$$

$$\begin{aligned}
x_{10}(0,s) =& G_{21}(\sum_{k=1}^{10}\int_0^L M_{8k}(L-\eta,s)V_{vkk}x_k(\eta,0)d\eta) \\
&+ G_{22}(\sum_{k=1}^{10}\int_0^L M_{10k}(L-\eta,s)V_{vkk}x_k(\eta,0)d\eta) \\
&+ (G_{21}M_{86}+G_{22}M_{106})\sum_{k=1}^{10}\int_0^L M_{1k}(L-\eta,s)V_{vkk}x_k(\eta,0)d\eta \\
&+ (G_{21}M_{87}+G_{22}M_{107})\sum_{k=1}^{10}\int_0^L M_{2k}(L-\eta,s)V_{vkk}x_k(\eta,0)d\eta \\
&+ (G_{21}M_{89}+G_{22}M_{109})\sum_{k=1}^{10}\int_0^L M_{4k}(L-\eta,s)V_{vkk}x_k(\eta,0)d\eta
\end{aligned} \tag{4.20}$$

where

$$G = \begin{bmatrix} M_{88} & M_{810} \\ M_{108} & M_{1010} \end{bmatrix}^{-1} \tag{4.21}$$

Therefore, the resolvent operator is determined as following form by substituting the boundary conditions (Equation (4.7)):

$$x(z,s) = [\mathcal{R}_{ij}(z,s)]_{10\times 10}x(\eta,0) \tag{4.22}$$

where

$$\mathcal{R}_{ij} = \begin{cases} \mathcal{R}c_{ij}, i \in [1,5], j \in [1,10] \\ \mathcal{R}w_{ij}, i \in [6,10], j \in [1,10] \end{cases} \tag{4.23}$$

where

$$\mathcal{R}c_{ij} = -\int_0^z M_{ij}(z-\eta,s)V_{vjj}(\cdot)d\eta, i \in [1,5], j \in [1,10] \tag{4.24}$$

$$\begin{aligned}
\mathcal{R}w_{ij} &= (M_{i8}(z,s)G_{11} + M_{i10}(z,s)G_{21})\int_0^L M_{8j}(L-\eta,s)V_{vjj}(\cdot)d\eta \\
&+ (M_{i8}(z,s)G_{12} + M_{i10}(z,s)G_{22})\int_0^L M_{10j}(L-\eta,s)V_{vjj}(\cdot)d\eta \\
&+ (M_{i8}(z,s)G_{11}M_{86}(L,s) + M_{i8}(z,s)G_{12}M_{106}(L,s) + M_{i10}(z,s)G_{21}M_{86}(L,s) \\
&+ M_{i10}(z,s)G_{22}M_{106}(L,s) - M_{i6}(z,s))\int_0^L M_{1j}(L-\eta,s)V_{vjj}(\cdot)d\eta \\
&+ (M_{i8}(z,s)G_{11}M_{87}(L,s) + M_{i8}(z,s)G_{12}M_{107}(L,s) + M_{i10}(z,s)G_{21}M_{87}(L,s) \\
&+ M_{i10}(z,s)G_{22}M_{107}(L,s) \\
&- M_{i7}(z,s))\int_0^L M_{2j}(L-\eta,s)V_{vjj}(\cdot)d\eta + (M_{i8}(z,s)G_{11}M_{89}(L,s) + M_{i8}(z,s)G_{12}M_{109}(L,s) \\
&+ M_{i10}(z,s)G_{21}M_{89}(L,s) + M_{i10}(z,s)G_{22}M_{109}(L,s) - M_{i9}(z,s))\int_0^L M_{4j}(L-\eta,s)V_{vjj}(\cdot)d\eta \\
&- \int_0^z M_{ij}(z-\eta,s)V_{vjj}(\cdot)d\eta, i \in [6,10], j \in [1,10]
\end{aligned}$$

The discrete-time operators in Equation (4.13) can be solved by straightforwardly substituting the above resolvent operators. Afterwards, the discrete-time linear model is obtained:

$$\begin{aligned}
x(z,k) &= \mathcal{A}_d x(z,k-1) + \mathcal{B}_d u(k) \\
y_c(k) &= \mathcal{C}_{cd} x(z,k-1) + \mathcal{D}_{cd} u(k) \\
y_m(k) &= \mathcal{C}_{md} x(z,k-1) + \mathcal{D}_{md} u(k)
\end{aligned} \tag{4.25}$$

with the boundary conditions (Equation (4.7)).

4.4 Observer-Based MPC Design

An observer-based model predictive controller is designed for the discrete-time pulp digester system. In particular, a discrete Luenberger observer is designed first to reconstruct the states based on the available real-time measurements. The Luenberger observer is one of the practical and easy-to-realize observer, which is further considered in a discrete setting controller realization. The constrained optimal controller design for the finite-dimensional system theory is extended and deployed for

the infinite-dimensional digester system. The overall closed-loop operation of the digester process is schematically presented in Figure 4.6.

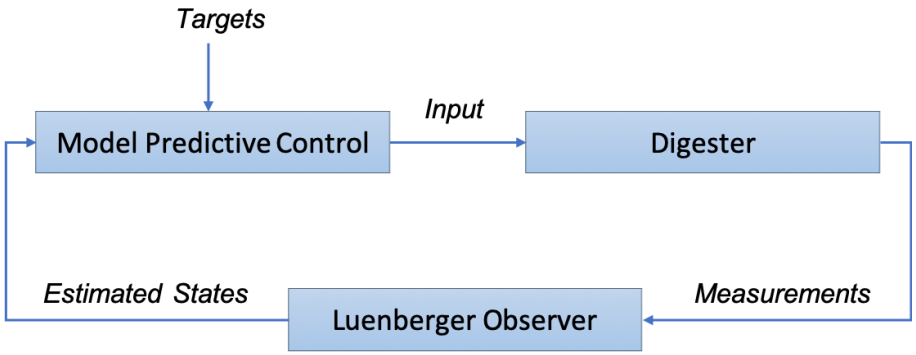

Figure 4.6: The proposed closed-loop operation framework

4.4.1 Discrete Luenberger observer design

Firstly, let us recall the linearized discrete-time model:

$$\begin{aligned} x(z,k) &= \mathcal{A}_d x(z,k-1) + \mathcal{B}_d u(k) \\ y_m(k) &= C_{md} x(z,k-1) + \mathcal{D}_{md} u(k) \end{aligned} \tag{4.26}$$

The discrete Luenberger observer is presented by the following standard form:

$$\begin{aligned} \hat{x}(\zeta,k) &= \mathcal{A}_d \hat{x}(\zeta,k-1) + \mathcal{B}_d u(k) + L_d(y_m(k) - \hat{y}_m(k)) \\ \hat{y}_m(k) &= C_{md} \hat{x}(\zeta,k-1) + \mathcal{D}_{md} u(k) \end{aligned} \tag{4.27}$$

where the reconstructed state $\hat{x}(\zeta,k)$ is defined as a copy of the system dynamics and L_d is the discrete observer gain to be designed. Stability of the observer implies that the state estimation error, $e_k = x(\zeta,k) - \hat{x}(\zeta,k)$, converges to zero within a certain time. The error dynamic equation is shown as follows:

$$e_k = (\mathcal{A}_d - L_d C_d) e_{k-1} = \tilde{\mathcal{A}}_d e_{k-1} \tag{4.28}$$

To guarantee the operator $\tilde{\mathcal{A}}_d$ in the state estimation error dynamics given by Equation (4.28) is stable, the design objective is to determine the appropriate spatially varying gain L_d. By Curtain and Zwart [52], it can be shown that the operator $\tilde{\mathcal{A}}_d$ is power stable if and only if there exists a non-negative self-adjoint operator Q_d such that

$$\tilde{\mathcal{A}}_d Q_d \tilde{\mathcal{A}}_d^* - Q_d = -M_d, \text{on } \mathcal{X} \tag{4.29}$$

where M_d is a positive definite design parameter.

Then, let us assume that the pair $(\mathcal{A}, C)$ is exponential detectable, then if there exists a nonnegative self-adjoint operator Q_d which is the solution of the following operator Riccati equation [53, 159]:

$$\mathcal{A}_d Q_d \mathcal{A}_d^* - Q_d - L_d(P + 2I)L_d^* + M_d = 0, \text{on } \mathcal{X} \tag{4.30}$$

where

$$L_d = T(P + I)^{-1}, T = \mathcal{A}_d Q_d C_d^*, P = C_d Q_d C_d^*$$

The observer gain $L_d = \mathcal{A}_d Q_d C_d^* (C_d Q C_d^* + I)^{-1}$ is a strongly stabilizing gain which guarantees the power stability of $\tilde{\mathcal{A}}_d = \mathcal{A}_d - L_d C_d$. To solve the algebraic Riccati Equation (4.30), one can utilize the numerical iteration methods, such as Newton-Kleinman iteration method [160], and the detailed procedures were provided [159].

4.4.2 MPC design for target tracking

The ultimate objective of a pulp and paper mill is to ensure the specified quality of the end products while meeting the production targets and minimizing the operational costs. As a result, frequent grade transition is required for pulp digesters, accounting for the blow-line pulp variation subject to various demands on certain paper products. In other words, the desired product quality needs to change in the middle of the operation, i.e., the shift operations. To realize it, the MPC is developed for the infinite-dimensional setting, emerging from the finite-dimensional linear time-invariant systems, see Rawlings et al. [18].

In this case, we consider that the system output is required to track a nonzero target vector, y_t, then state and input vectors, x_t and u_t, are required which bring the system to y_t at steady-state [104, 161, 162]. The state and input target can be computed by solving the following quadratic program.

$$\begin{aligned} &\min_{x_t, u_t} (u_t - \bar{u})^T R_t (u_t - \bar{u}) \\ &\text{s.t.} \quad \begin{bmatrix} I - A_d & -B_d \\ C_d & D_d \end{bmatrix} \begin{bmatrix} x_t \\ u_t \end{bmatrix} = \begin{bmatrix} 0 \\ y_t \end{bmatrix} \\ &\qquad u_{\min} \le u_t \le u_{\max} \\ &\qquad y_{\min} \le y_t \le y_{\max} \end{aligned} \tag{4.31}$$

In this quadratic program, $\bar{u}$ is the set point for the manipulated variables and R_t, is symmetric positive definite. Notice that, often, the input set point is not specified and it can be assumed zero in order to use [163]. The equality constraints guarantee a steady-state solution and offset free tracking of the target vector [104]. u_{min}, u_{max}, y_{min}, y_{max} are the input and output constraints, respectively.

Then, the the following quadratic objective function is used for the regulator to track a nonzero target vector.

$$\begin{aligned}
\min_{u^N} \sum_{j=0}^{N-1} & \langle (y_{k+j|k} - y_t), Q(y_{k+j|k} - y_t) \rangle + \langle (u_{k+j|k} - u_t), R(u_{k+j|k} - u_t) \rangle \\
& + \langle (x_{k+N-1|k} - x_t), \bar{Q}(x_{k+N-1|k} - x_t) \rangle \\
\text{s.t. } & \text{Lunberger observer, Equation (4.27)} \\
& u_{\min} \leq u_{k+j|k} \leq u_{\max} \\
& y_{\min} \leq y_{k+j|k} \leq y_{\max}
\end{aligned} \tag{4.32}$$

where N is the prediction horizon, and Q, R are symmetric positive semidefinite and symmetric positive definite spatial operator, respectively. $\bar{Q}$ is the spatial operator to penalize the terminal state which depends on the stability of the given model. The target vector x_t, and u_t are computed from the quadratic program in Equation (4.31). $y_{k+j|k}$ and $u_{k+j|k}$ represent the output and input variables at future time $k+j$ predicted at current time k, and the term $\Delta u_{k+j|k}$ denotes the change of an input vector at time $k+j$ as $\Delta u_{k+j|k} = u_{k+j|k} - u_{k+j-1|k}$. The vector u^N includes the control sequence $\{u_{k|k}, u_{k+1|k}, u_{k+2|k}, ..., u_{k+N-1|k}\}$ and the first element $u_{k|k}$ will be injected to the plant as the future control action.

As discussed by H. Kwakernaak and R. Sivan [161], using the targets computed from Equation (4.31), we define a shifted input $\tilde{u}_k = u_k - u_t$, a shifted state $\tilde{x}_k = \hat{x}_k - x_t$, and a shifted output $\tilde{y}_k = \hat{y}_k - y_t$ to reduce the problem to the standard form. The corresponding constraints can be translated to constraints on $\tilde{u}$ and $\tilde{y}$.

Thus the regulator optimization problem Equation (4.32) becomes:

$$\begin{aligned}
&\min_{u^N} \sum_{j=0}^{N-1} \langle \tilde{y}_{k+j|k}, Q\tilde{y}_{k+j|k}\rangle + \langle \tilde{u}_{k+j|k}, R\tilde{u}_{k+j|k}\rangle + \langle \tilde{x}_{k+j|k}, \bar{Q}\tilde{x}_{k+j|k}\rangle \\
&\text{s.t.} \quad \tilde{x}_{k+j|k} = \mathcal{A}_d \tilde{x}_{k+j-1|k} + \mathcal{B}_d \tilde{u}_{k+j|k} \\
&\qquad \tilde{y}_{k+j|k} = \mathcal{C}_d \tilde{x}_{k+j-1|k} + \mathcal{D}_d \tilde{u}_{k+j|k} \\
&\qquad u_{\min} - u_{t|k} \le \tilde{u}_{k+j|k} \le u_{\max} - u_{t|k} \\
&\qquad y_{\min} - y_{t|k} \le \tilde{y}_{k+j|k} \le y_{\max} - y_{t|k}
\end{aligned} \tag{4.33}$$

According to the nature of transport reaction systems, the operator $\bar{Q}$ can be determined from the positive self-adjoint solution of the following discrete-time Lyapunov equation:

$$\mathcal{A}_d^* \bar{Q} \mathcal{A}_d - \bar{Q} = -\mathcal{C}_d^* Q \mathcal{C}_d \tag{4.34}$$

or equivalently the continuous-time Lyapunov equation [100]:

$$\mathcal{A}^* \bar{Q} + \bar{Q}\mathcal{A} = -\mathcal{C}^* Q \mathcal{C} \tag{4.35}$$

In addition, the operator $\bar{Q}$ is the unique positive self-adjoint solution of the Lyapunov equations (Equation (4.34) and (4.35)) [38, 105].

Before further manipulate the objective function (Equation (4.33)), we introduce the following notations: $Y_k = \{y_{k+n}\}_{n=1}^N \in \mathcal{Y}^N$ and $U_k = \{u_{k+n}\}_{n=1}^N \in \mathcal{U}^N$. As a result, the straightforward algebraic manipulation of the objective function presented in Equation (4.33) leads to the following quadratic programming optimization problem:

$$\begin{aligned}
&\min_{U_k} \langle U_k, HU_k\rangle + 2\langle U_k, F\tilde{x}_k\rangle + \langle \tilde{x}_k, \bar{Q}\tilde{x}_k\rangle \\
&\text{s.t.} \quad U_{\min} \le U_k \le U_{\max} \\
&\qquad Y_{\min} \le GU_k + S\tilde{x}_k \le Y_{\max}
\end{aligned} \tag{4.36}$$

where $H \in \mathcal{L}(\mathcal{U}^N)$ is positive and self-adjoint, which is given by:

$$h_{i,j} = \begin{cases} \mathcal{D}_d^* Q \mathcal{D}_d + \mathcal{B}_d^* \bar{Q} \mathcal{B}_d + R & \text{for } i = j \\ \mathcal{D}_d^* Q \mathcal{C}_d \mathcal{A}_d^{i-j-1} \mathcal{B}_d + \mathcal{B}_d^* \bar{Q} \mathcal{A}_d^{i-j} \mathcal{B}_d & \text{for } i > j \\ h_{j,i}^* & \text{for } i < j \end{cases} \tag{4.37}$$

and F is given by $F = \{\mathcal{D}_d^* Q \mathcal{C}_d \mathcal{A}_d^{k-1} + \mathcal{B}_d^* \bar{Q} \mathcal{A}_d^k\}_{k=1}^{N-1}$. The mateix G is a lower triangular given by

$$g_{i,j} = \begin{cases} \mathcal{D}_d & \text{for } i = j \\ \mathcal{C}_d \mathcal{A}_d^{i-j-1} \mathcal{B}_d & \text{for } i > j \\ 0 & \text{for } i < j \end{cases}$$

and $S = \{C_d \mathcal{A}_d^{k-1}\}_{k=1}^{N}$.

The inner products in the objective function given in Equation (4.36) are vector products as U is the finite-dimensional input space, and therefore we have a finite dimensional quadratic optimization problem:

$$\begin{aligned} &\min_{U_k} U_k^T H U_k + 2U_k^T F \tilde{x}_k \\ &\text{s.t.} \quad \begin{bmatrix} I \\ -I \\ G \\ -G \end{bmatrix} U_k \leq \begin{bmatrix} U_{\max} \\ -U_{\min} \\ Y_{\max} - S\tilde{x}_k \\ -Y_{\min} + S\tilde{x}_k \end{bmatrix} \end{aligned} \tag{4.38}$$

Here we neglect the term $\langle \tilde{x}_k, \bar{Q}\tilde{x}_k \rangle$ as $\tilde{x}_k$ is the initial condition for step $k+1$ and cannot be affected by the control input. Thus, the optimal input trajectory (U_k) can be obtained as the solution of the feasible quadratic optimization problem (Equation (4.38)) converges to zero.

4.5 Numerical Simulations

In this section, the closed-loop performance of the proposed MPC framework is demonstrated. The temperature of free liquor flowing into the cook zone is selected as the manipulated input variable and the concentration of lignin is selected as the controlled output variable. In this case, we consider the target tracking of the output by using the proposed MPC. The resulting constrained optimization problem is quadratic programming problem which is solved using the MATLAB subroutine QuadProg. Both the control and prediction horizons are chosen to be 50 sampling periods. The sampling time is set to be 10 min and the internal spatial discretization is taken as 0.05 m.

The type of wood entering the digester was assumed to be softwood and the parameters that characterize this type of wood are shown in Table 4.1. A similar study for hardwood species can be realized based on the listed parameters in Table 4.1. For the initial conditions of the dynamic system, we consider $x_1(z,0) = 0.067z, x_2(z,0) = 0.1646z, x_3(z,0) = 0.2377z, x_4(z,0) = 1.7073z, x_5(z,0) = 0.8661z, x_6(z,0) = 0.0336 + 2.87 \times 10^{-4}z, x_7(z,0) = 0.8232 + 0.0095z, x_8(z,0) = 0.0012z, x_9(z,0) = 8.5363 + 0.1767z$, and $x_{10}(z,0) = -0.086z$. It is worth noting that the initial conditions of the states in the linearized model need to be taken sufficiently small, such that the designed

control law for the linearized model can be applied to the original nonlinear PDE model around the steady states of interest. In addition, $\varepsilon = 0.05$ is chosen for the input operator. The selected parameter values for MPC implementation are listed in Table 4.2 .

Table 4.1: Notations and values of parameters

Process parameters and notations	Values of hardwood	Values of softwood	Ref.
Entering wood-chip flow rate $\dot{V}_c$	1.3964 m^3/min	1.3964 m^3/min	[128]
Entering white-liquor flow rate $\dot{V}_f$	2.3497 m^3/min	2.3497 m^3/min	[128]
Digester cross sectional area A	21 m^2	21 m^2	[159]
Non-reactive lignin in wood ρ_s^0	0	0	[128]
Preexponential factor of lignin reactions A_1	0.3954 $m^3/kg{\cdot}min$	0.2809 $m^3/kg{\cdot}min$	[128]
Activation energy for lignin E_1	38 $kJ/mol \cdot K$	38 $kJ/mol \cdot K$	[159]
Stoichiometric coefficient for lignin reactions b_1	0.21	0.166	[128]
Stoichiometric coefficient for carbohydrates reactions b_2	0.49	0.395	[128]
Heat capacities of the wood C_{ps}	1.47 $kJ/kg \cdot K$	1.47 $kJ/kg \cdot K$	[159]
Heat capacities of the liquor C_{pl}	4.19 $kJ/kg \cdot K$	4.19 $kJ/kg \cdot K$	[159]
Heat of reaction ΔH_R	-581 kJ/kg	-581 kJ/kg	[159]
Water density ρ_w	1000 kg/m^3	1000 kg/m^3	[159]

Table 4.2: Parameters for the MPC design

Descriptions	Notations	Values
Sampling time	h	10 min
Prediction horizon	N	50
Input weight	R	0.5
Output weight	Q	0.5
Input constraints	$[u_{min}, u_{max}]$	$[400K, 445K]$
Controlled output constraints	$[y_{min}, y_{max}]$	$[4\%, 17\%]$

As illustrated in Figure 4.7, the open-loop states converge to their corresponding steady-states rapidly which indicates the original plant is intrinsically stable. The figures in the left column represent the evolution of the states in the cook zone, and the right column denotes the evolution of the states in the wash zone. Figures 4.7(a) and 4.7(f) show how the concentration of lignin decreases smoothly down toward the end of the cooking zone where the reactions are stopped (or quenched) by displacement

of the hot liquor with dilute wash liquor from below. Hence, no significant decrease occurs in the wash zone. The concentration of alkali of entrapped liquor phase in the feed flow to the cook zone is about 23 g/l (as shown in Figure 4.7(b)) and then is consumed giving a decreasing profile down toward the extraction. At the bottom of the wash zone, the concentration of alkali of entrapped liquor phase is about 8 g/l (as shown in Figure 4.7(g)). A similar trend occurs for the alkali of the free liquor phase, as shown in Figures 4.7(c) and 4.7(h). Figures 4.7(d) and 4.7(e) show the temperature profiles for the two phases (wood chip phase and free liquor phase) at cook zone, and the temperature profiles of them at wash zone are shown in Figures 4.7(i) and 4.7(j). The temperature of wood chips rises due to the exothermic reactions and is also affected by the high temperature of the circulation liquor. Below the extraction screens, in the wash zone, the chips are rapidly cooled down by the wash water which has a temperature of 360K at the inlet in the bottom.

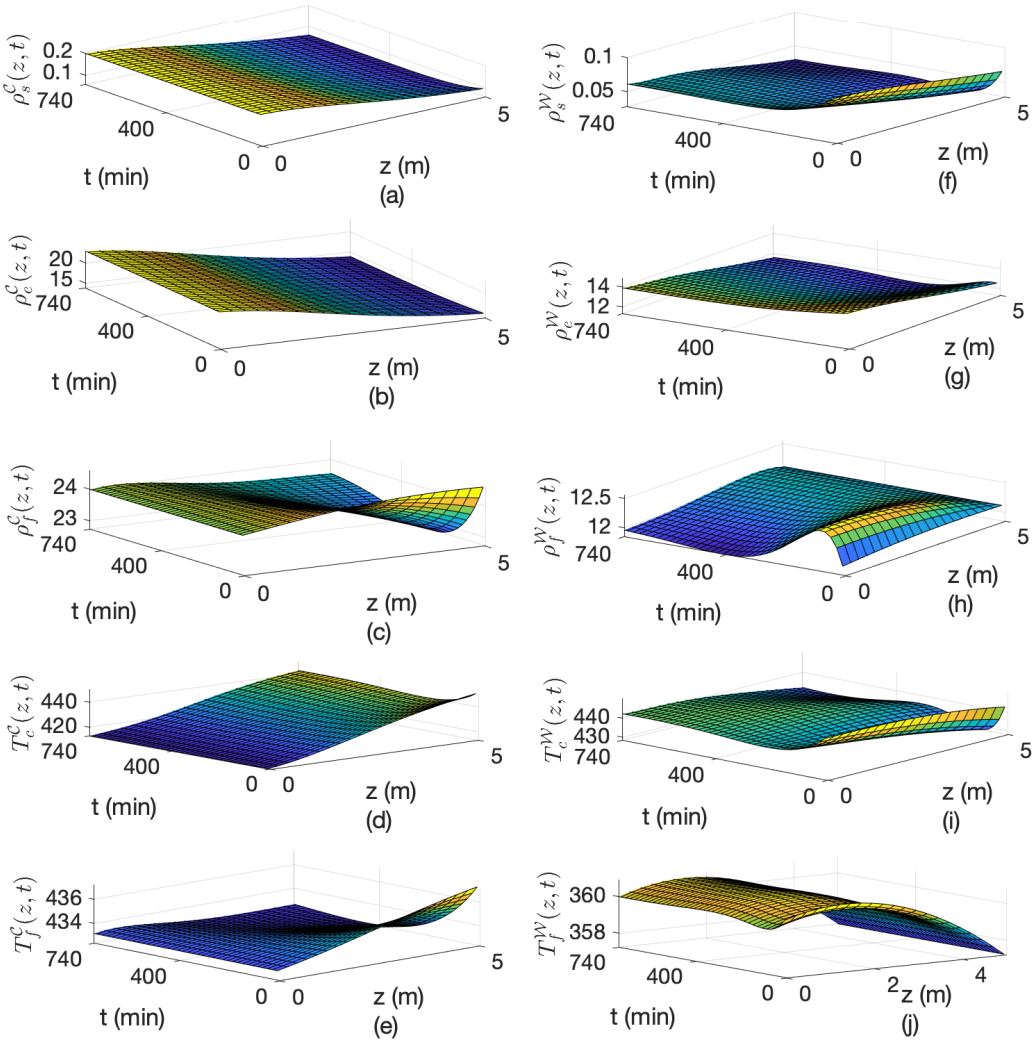

Figure 4.7: The open-loop state profiles of the digester

By implementing the proposed MPC frameworks, we aim to steer the system to the desired targets without violating the physical constraints of actuators and sensors. In this case, we consider the shifted output targets, which are chosen as $y_{t1} = 0.15$ and $y_{t2} = 0.05$, respectively. First of all, the steady-state target x_t and input vector u_t are computed from the quadratic program Equation (4.31). Then, based on the operator Riccati Equation (4.30), we determine Q_d in the discrete-time observer design. The estimate state $\hat{x}$ from the Luenberger observer is then utilized for the MPC design. Finally, the optimal input trajectory is computed by solving the above optimization problem outlined in Equation (4.38) with a receding horizon prediction formulation.

The state evolutions of the closed-loop system under the MPC law are obtained and shown in Figure 4.8. Comparing with the open-loop state profiles, the closed-loop system is able to track the target steady-states when the grade shift happens (t = 370 min). In addition, three pairs of states in cook zone and wash zone are successfully connected through the extend system (Equation (4.6)), such as, $\rho_s^{\mathcal{C}}(z,t)$ and $\rho_s^{\mathcal{W}}(z,t)$; $\rho_e^{\mathcal{C}}(z,t)$ and $\rho_e^{\mathcal{W}}(z,t)$; $T_c^{\mathcal{C}}(z,t)$ and $T_c^{\mathcal{W}}(z,t)$.

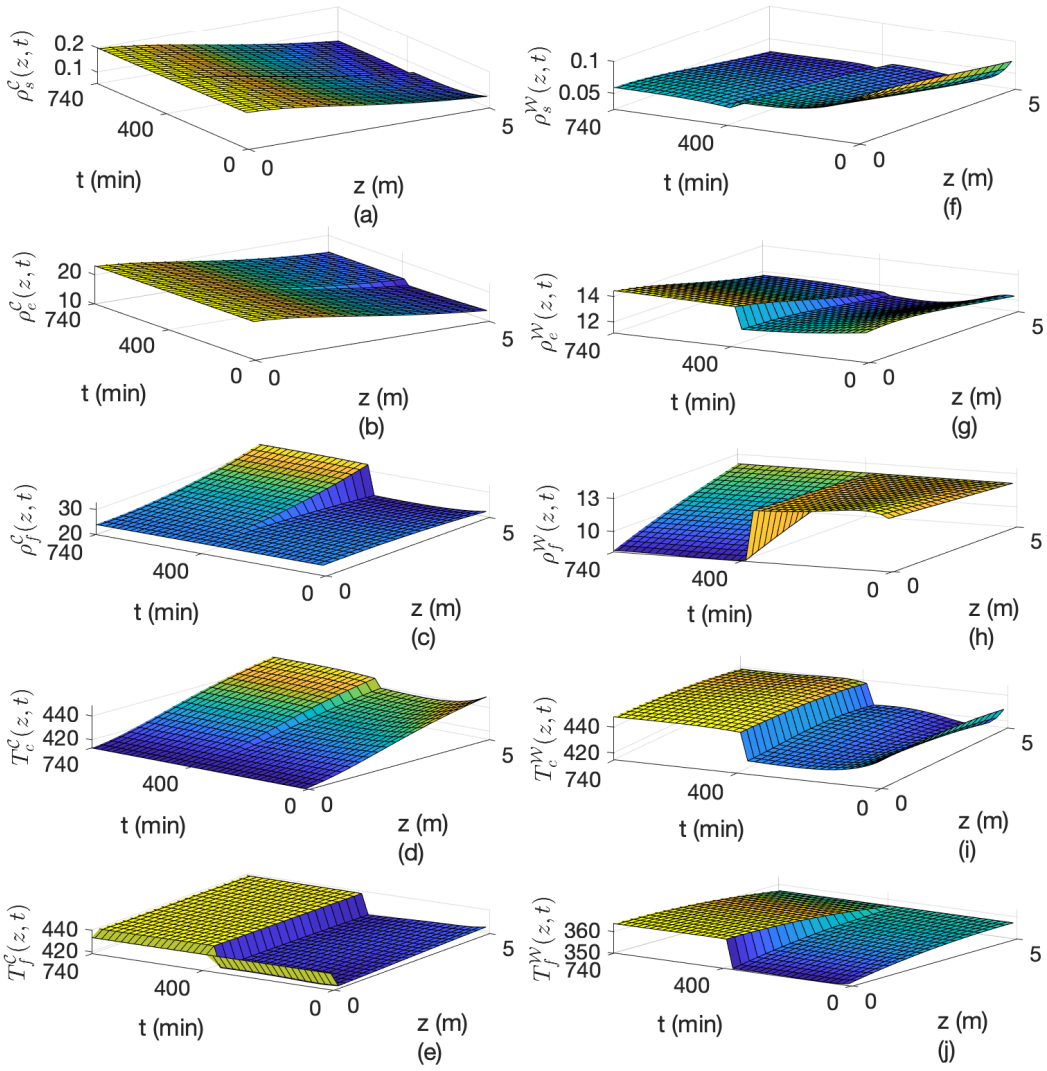

Figure 4.8: The state profiles of the digester under closed-loop operation

The open-loop output profile and the close-loop profile under the observer-based MPC law are shown in Figure 4.9 (a). Without implementing the controller, the con-

centration of lignin converges to its steady-state, while violating the given constraints of the system. In the closed-loop system, the concentration of lignin is able to track the targets or desired values and satisfies the requirements of the constraint simultaneously. As the targets are switched, the output can also achieve target tracking across the original steady-state. Specifically, the target tracking above the steady-state is realized in the first period, $t \in [0, 370]$, where $y_{t1} = 0.15$ is considered. Similarly, the target tracking below the steady-state is realized in the second period (i.t.,$t \in (370, 740]$) when $y_{t2} = 0.05$ is taken into account. Typically, this results in higher yield, thus lowering the operating cost significantly [134]. The free-liquor temperature profile, computed by the proposed model-based MPC system at each sampling time, is presented in Figure 4.9 (b). The input trajectory corresponds to the output variables, that is, in the first 370 minutes, the optimal input variables fluctuate between 410-415 and converge to 413K when the output goes to track target 1. In the last 370 minutes, the corresponding input rises and stabilizes at 441K when target 1 switches to target 2. In these two stages of tracking, the input variables are constrained within the given bounds of actuators. There are some over-shooting phenomena while tracking the set-points, which might be caused by the instantaneous jump in the set-points. Avoiding such overshoot can be achieved in different ways, including tuning the controller to be less aggressive, utilizing relatively small initial conditions, or reformulating the problem into the form of a time-dependent, sufficiently smooth trajectory [164].

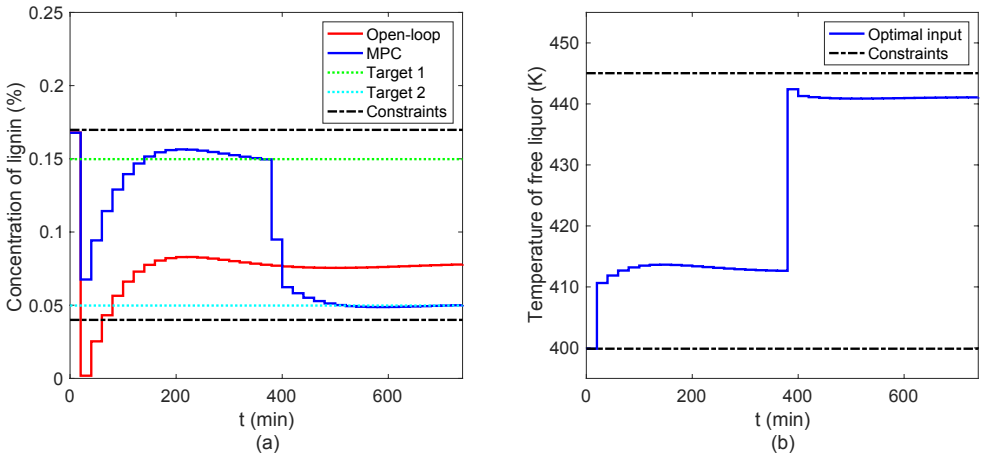

Figure 4.9: (a) The concentration profile of lignin (b) The optimal manipulated input trajectory under closed-loop operation

In order to further investigate the performance of the proposed MPC design, a truly unknown disturbance is considered, which potentially causes the temperature of free liquor needed for degradation reaction drops (rises) below (above) the temperature needed for degradation reaction. In addition, it is assumed that the addition of disturbance does not affect the feasibility of input and output constraints. Specifically, we consider the input disturbance $d(t) = 20\ \sin(0.6t)$ is injected to the system, causing the sinusoidal trend on the open-loop state profiles. As shown in Figure 4.10 (a), it is apparent that the open-loop output responses oscillate due to input disturbance injection. In this case, the proposed MPC controller is able to simultaneously realize disturbance rejection and target tracking in a short time, and satisfies the given constraints. The corresponding manipulated input is shown in Figure 4.10 (b). It can be clearly seen that the proposed MPC achieves a good control performance under the consideration of input disturbance.

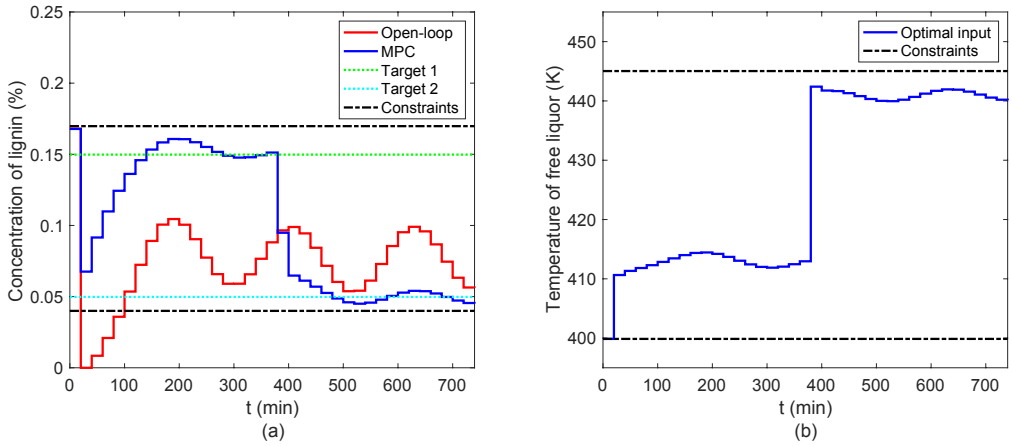

Figure 4.10: (a) The concentration profile of lignin considering the disturbance (b) The optimal manipulated input trajectory considering the disturbance under closed-loop operation

Figure 4.11 shows the open-loop spatio-temporal profile of the Kappa number in the cook zone and wash zone. A significant decrease in Kappa number can be observed in the cook zone ($0 \leq z \leq 5$) as the temperature of free liquor increases. After the chips enter the counter-current wash zone ($5 \leq z \leq 10$), the Kappa number drops unobvious since the temperature of wash liquor cools down in this area. Blow-line Kappa number transients during the two grade transitions are depicted in Figure

4.12. The proposed controller is able to further regulate the blow-line Kappa number with no disturbance and under disturbance by manipulating the temperature of free liquor entering the cook zone. The simulation studies demonstrate that the extended system is able to describe the dynamics of the original cascade system which contains a co-current zone and a counter-current zone. Furthermore, it is possible to realize the optimal control of the output in the wash zone through the operation of the input in the cook zone. The effectiveness can be demonstrated from the proposed MPC design.

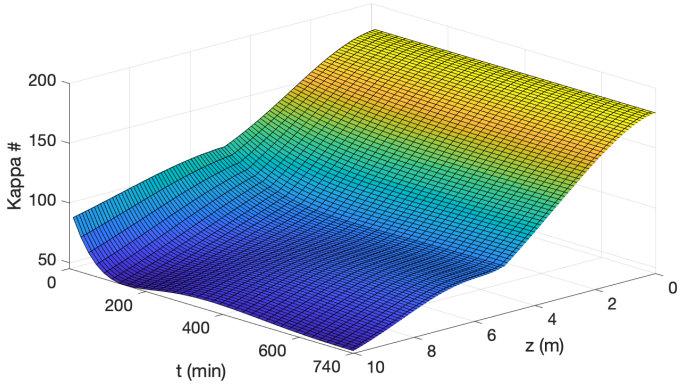

Figure 4.11: The open-loop spatio-temporal profile of the Kappa number

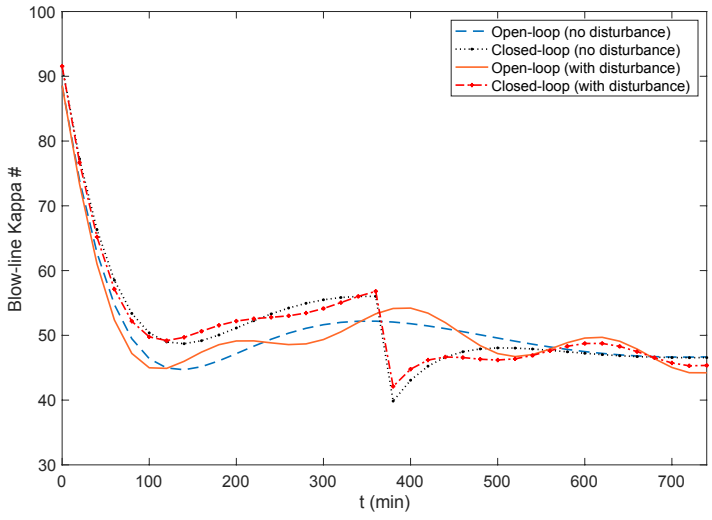

Figure 4.12: Blow-line Kappa number transients for grade change transitions

4.6 Conclusions

In this chapter, dynamic modelling and model predictive control design of a continuous pulp digester described by ten linearized first-order coupled hyperbolic equations was developed. The connected cook zone and wash zone of the digester were modelled as a cascade PDE system. By using Cayley–Tustin transformation, the linearized continuous-time infinite-dimensional model was transformed into a discrete-time infinite-dimensional model without spatial discretization and model reduction which preserves the input-output stability of the system. A Luenberger observer was designed to realize the state estimation of the system and the discrete-time Riccati equation was used to calculate the observer gain. The model predictive controller was formulated on that basis to realize target tracking and account for input and output constraints when it comes to the shift operations of the digester. The closed-loop simulation results have demonstrated that the controlled variables were able to reach to the target values and satisfy the actuators' constraints simultaneously.

Chapter 5

Sensor Location Selection for Continuous Pulp Digesters with Delayed Measurements

5.1 Introduction

The continuous pulp digester has been predominantly utilized to convert the wood chips into pulp in industrial applications when it comes to the pulping process operation [4]. The typical continuous pulp digester is a complex heterogeneous reactor, consisting of several zones in which the white liquor reacts with wood chips to remove lignin and subsequently free wood fibers [134]. As illustrated in Figure 5.1, the wood chips and white liquor are added to the impregnation zone where wood chips are soaked by the cooking liquor via penetration and diffusion mechanism. After that, the temperature of the chip mixture is rapidly increased through the external heat exchangers, and the mixture then enters the cooking zone where the most delignification reactions occur at an elevated temperature. The spent liquor is withdrawn from the digester at extraction screens. At the same time, the cooked pulp moves downwards to the wash zone where the chips are washed and cooled down by the counter-current flow of wash liquor. Finally, the delignification reaction is stopped and the cooked pulp is removed from the bottom of the digester. For the entire pulping process, the temperature of operation plays a key role as the temperature of wood chips and free liquor will have a significant influence on the pulp quality. More specifically, the concentration of lignin in the wood chip phase, the concentration of effective alkali (EA) alkali, and hydrosulfide (HS) in entrapped and free liquor phase

will be affected through the coupled relationship of temperature including the rate of the consumption of mass and mass diffusion rate with temperature. In particular, the cooking zone temperature is the most important, because it has a large influence upon the pulp quality for cooking degree (viz., kappa number) and pulp viscosity.

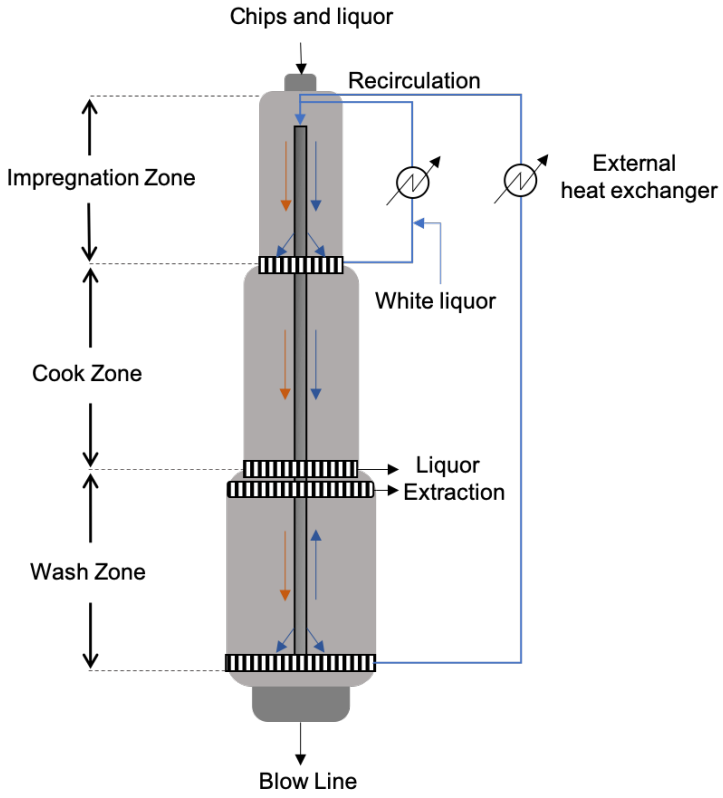

Figure 5.1: Simplified scheme of a continuous pulp digester [4]

Due to the industrial importance the considerable effort has been made in the past few decades to model the delignification process of continuous pulp digesters based on the reaction and diffusion dynamics, and chip-bed compaction. Three widely used dynamic models are known as the Purdue model [139], Gustafson model [140], and Andersson model [141], which have been the bases for the further development of digester models [3, 142, 143, 165, 166, 150, 167, 151]. When it comes to the controller design for the continuous pulp digester, one of the main objectives is to produce pulps that achieve specific quality according to different wood species while respecting distinctive operating conditions. To this end, great efforts have been made to meet various objectives based on the various control methods, such as model predictive

control (MPC), adaptive control, dynamic matrix control (DMC), reduced dimension control (RDC), and genetic algorithms (GA) et.al [152, 147, 144, 153, 168, 7, 149].

The state information or the process knowledge is essential for such controllers and/or regulators design. However, the full state information is not often available due to the special features of the continuous digester, physical constraints of sensor installation, and/or the prohibitive expense of implementing spatially-distributed sensors. In addition, some important process variables are sampled infrequently and there are long time delays associated with their measurement. Due to this, the state estimation for the pulp digester attracts a lot of attention in both academia and industry. Along this line, the extended Kalman filter was proposed to construct the true states of a batch pulp digester using online measurements of various liquor characteristics, which shows a good convergence property, even when the state errors and disturbances are undermodeled [147]. The optimal state estimation was realized utilizing the subspace identification techniques and Kalman filter for a continuous digester [169]. The partial least squares methodology was utilized to generate the dynamic model based on input-output data collected from an industrial continuous digester [170]. A multi-rate extended Kalman filter was applied to obtain state estimates that converge to the true plant states in presence of parametric mismatches, unmeasured disturbances and large errors in the initial state estimates [171]. However, even though the aforementioned works have made valuable contributions toward the estimator design for the pulp digester, there are still some aspects which did not receive much attention and consideration. On the one hand, the spatial discretization of partial differential equation (PDE) in the estimator design stage dramatically increases the complexity of the calculations in estimator design and might induce numerical instability and/or alter the fundamental control theoretical properties (controllability, observability, stability). On the other hand, the delayed measurement need to be considered because of the possible low sampling rate of the continuous pulp digester.

The accuracy of the estimation depends not only on the type of estimator but also on the location of the sensors, especially for distributed parameter systems (DPS). The sensor placement problem has been considered by many researchers in the area of chemical process control, and a number of different performance criteria for sensor placement have been taken into account. One of the earliest approaches is to maxi-

mize the observability through a choice of the sensor locations to improve the degree of complete observability for the deterministic state reconstruction problem [61, 62]. For the system with stochastic disturbances, unmeasured states can be estimated with the Kalman filter, and the optimal selection of measurements can be determined by minimizing the average variance of the state estimates [63] or the steady-state error variance [64]. There are also some other criteria to evaluate the performance of sensor locations including detection of load disturbances and location for optimal control [61]. These approaches have mature applications on the lumped parameter systems which are described by ordinary differential equations (ODEs), and have been gradually extended and applied to the DPS in recent years. For example, the modal observability and controllability measures was utilized to determine optimal sensor and actuator locations of parabolic PDEs [65]. The optimal area for sensing or actuation in advective PDEs was determined by maximizing the support of the observability or controllability Gramian, respectively [66]. It was demonstrated that the nuclear norm of the solution to the operator Riccati equation is the steady-state minimum error variance of an estimate for DPS [67]. The placement of a single sensor and/or a single actuator in advection-diffusion equations with proportional feedback control was addressed [68]. Most of the previous contributions of the sensor selection for DPS mainly consider the spectral systems described by parabolic PDEs, which can be addressed by means of model reduction techniques also known in estimation and control theory as the early lumping approach. However, for non-spectral systems (e.g., first order hyperbolic PDEs), where the slow-fast dynamic separation does not hold there are less contributions in the literature. Hence, in this chapter, the sensor placement for the typical transport-reaction system described by the hyperbolic PDE systems are investigated to motivate and emphasize the issues associated with transport-reaction system setting.

Motivated by the aforementioned issues, this chapter considers the discrete-time state estimation and sensor placement for stochastic model of continuous pulp digester with delayed boundary/point-wise measurements. The temperature dynamics of a continuous pulp digester is studied, and it is described by coupled PDE-ODE with measurement delay. The Cayley-Tustin time discretization approach is utilized to obtain the discrete-time model with analytical expression that is easier to im-

plement in practical applications. The delayed measurements are expressed by an additional hyperbolic PDE, and treated as the new states of the extended model. The unbounded boundary/ point-wise measurement is considered and can be transformed to a bounded one using Cayley-Tustin approach. The discrete-time Kalman filter is designed with the stochastic discrete-time digester system to realize the state estimation, and the sensor location selection for the temperature measurements is investigated by minimizing the steady-state error variance of the estimated states.

This chapter is organized as follows: In Section 5.2, a dynamic model that describes the temperature system of the cook zone of continuous digester is introduced. The model is discretized in time by utilizing Cayley-Tustin approach. Based on the discrete-time model, the discrete Kalman Filter is designed and the optimal location for the temperature sensors is investigated in Section 5.3. In Section 5.4, the performance of the estimator is examined on a number of examples. In Section 5.5, concluding remarks are made.

5.2 Model Formulation for Pulp Digester

In this section, we introduce the simplified temperature model formulation of a continuous pulp digester. In order to formulate the state-space model, the original model with measurement delay is equivalently transformed to a standard state-space model by introducing the transport PDE. Based on this model, the discrete-time infinite-dimensional model is obtained utilizing the Cayley-Tustin transform framework. A schematic diagram of the model formulation is illustrated in Figure 5.2.

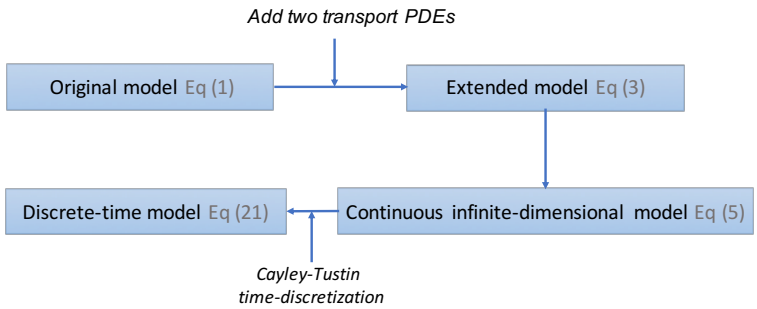

Figure 5.2: Block diagram of the model formulation

5.2.1 Model formulation

Considering that the most of delignification reaction occurs in the cooking zone of a digester [143], we focus on analysis of this zone which can be seen as a vertical tubular reactor of co-current flow in two phases. In addition, the existence of delay in the measurements or sensors is considered, which may be due to slow sampling rate, missing measurement issues, the indirect laboratory analytical test of these measurements, etc. A specified process schematic is shown in Figure 5.3. The top position of this process is denoted as $z = 0$, and the liquor extraction at the bottom position is denoted as $z = L$. The pre-prenetrated wood chips and free liquor are introduced at the top of the cook zone and the liquor is heated to reaction temperatures achieved by liquor circulation through the cook heater. Therefore, the temperature of heated liquor at the top of the cook zone is selected as the manipulated variable which can be adjusted using the external heater.

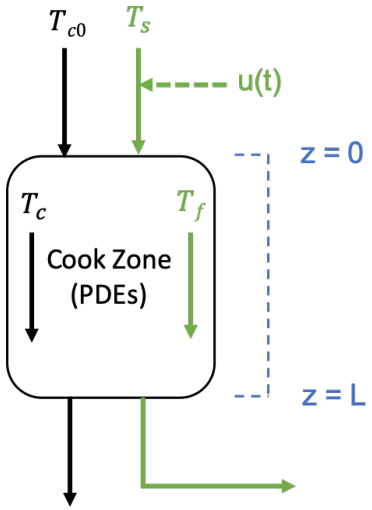

Figure 5.3: The scheme of cook zone in a pulp digester

The following assumptions are considered. The dynamic variations of chip porosity, the mass variations of solid and liquor, and the variation in external volume flow rate are neglected. The heat released by the exothermic reactions and energy transfer due to diffusion of components between the entrapped liquor phase and free liquor phase can be ignored. Considering the most important components in the chemical reactions taken place in the digester, only lignin in solid phase and effective alkali in

liquor phase are taken into account in the reaction rate equations. A further simplification is made by considering only temperature behaviour as neglecting the heat due the reaction makes the temperature variables independent of the concentration variables. A temperature model is derived from the conservation laws to describe the co-current flow in two phases, the liquid phase and the solid phase in the digester, which has been successfully applied to a continuous paper pulp digester at the M-real pulp mill in Husum, Sweden [172].

In the ensuing model, the temperature variables are functions of both vertical position z and time t. $T_f(z,t)$ denotes the temperature of free liquor phase, and $T_c(z,t)$ denotes the temperature of chip phase. $T_s(t)$ denotes the free liquor temperature in the steam zone. Based on the aforementioned description, the mathematical model of the temperature behaviour in the cook zone of digester can be modelled by the following set of equations:

$$\frac{\partial T_c}{\partial t} = -\frac{V_c}{A\varepsilon_c}\frac{\partial T_c}{\partial z} + U(T_f - T_c)/C_{pe} \tag{5.1a}$$

$$\frac{\partial T_f}{\partial t} = -\frac{V_f}{A\varepsilon_f}\frac{\partial T_f}{\partial z} - U(T_f - T_c)/C_{pf} \tag{5.1b}$$

$$\frac{dT_s}{dt} = [-\frac{v_{f,s}}{h_s - h_l} - \frac{k_{lz} - k_{lw}}{C_{pf}\rho_f}]T_s + [\frac{v_{f,s}}{h_s - h_l} + \frac{k_{lz}}{C_{pf}\rho_f}]u + \frac{k_{lw}T_a}{C_{pf}\rho_f} \tag{5.1c}$$

$$y_m(t) = \begin{bmatrix} T_c(l_{m1}, t - \tau_1) \\ T_f(l_{m2}, t - \tau_2) \end{bmatrix} \tag{5.1d}$$

The boundary conditions are given by:

$$T_c(0,t) = T_{c0}; T_f(0,t) = T_s(t). \tag{5.2}$$

where V_c and V_f denote the volume of chip and free liquor respectively, and A is the digester cross sectional area. ε_c is the chip compaction, which increases from the entry through the cook zone, reaching a maximum at the main extraction, $\varepsilon_c(z) = \varepsilon_{10} + \varepsilon_{11}z$, and $\varepsilon_f(z) = 1 - \varepsilon_c(z)$. U denotes the heat-transfer coefficient and relates the rate of energy transfer due to conduction between the wood chips and the free liquor per degree temperature difference per volume of chip [142]. The mixing rules based on weighted averages are utilized to determine heat capacities of the entrapped and free liquor phases, namely, C_{pe} and C_{pf}, which can be further obtained from the heat capacities of the wood C_{ps} and the liquor C_{pl} [173]. $v_{f,s}$ denotes the steam

velocity, and h_s and h_l are the height of steam and liquor level, respectively The sensible heat transfer can be written equivalently as $k_{lz}(T_s - u)$, and the heat transfer through the digester shell is $k_{lw}(T_s - T_a)$ where T_a is the ambient temperature. The system input $u(t)$ denotes the steam temperature or the inlet temperature of free liquor at the top of cook zone. The measured output $y_m(t)$ contains the temperature measurement of wood chip and free liquor. Particularly, the time delays (τ_1, τ_2) denote the measurement delays or sensor delays at the bottom of the cook zone. The parameters l_{m1} and l_{m2} represent the sensor locations to measure the temperature of wood chip and free liquor, respectively.

5.2.2 State-space model formulation

In order to formulate the state-space model, the time delay can be firstly "removed" at a cost of adding a transport PDE into the plant. Replacing the terms $T_c(l_{m1}, t-\tau_1)$ and $T_f(l_{m2}, t-\tau_2)$ by two transport equations with velocity $\mu_1 := \frac{l_{m1}}{\tau_1}$ and $\mu_2 := \frac{l_{m2}}{\tau_2}$ (e.g.[174, 175]), the original system (Equation (5.1)) is equivalently expressed as:

$$\frac{\partial T_c}{\partial t} = -\frac{V_c}{A\varepsilon_c}\frac{\partial T_c}{\partial z} + U(T_f - T_c)/C_{pe} \tag{5.3a}$$

$$\frac{\partial T_f}{\partial t} = -\frac{V_f}{A\varepsilon_f}\frac{\partial T_f}{\partial z} - U(T_f - T_c)/C_{pf} \tag{5.3b}$$

$$\frac{\partial T_w}{\partial t} = -\mu_1\frac{\partial T_w}{\partial z} \tag{5.3c}$$

$$\frac{\partial T_v}{\partial t} = -\mu_2\frac{\partial T_v}{\partial z} \tag{5.3d}$$

$$\frac{dT_s}{dt} = [-\frac{v_{f,s}}{h_s - h_l} - \frac{k_{lz} - k_{lw}}{C_{pf}\rho_f}]T_s + [\frac{v_{f,s}}{h_s - h_l} + \frac{k_{lz}}{C_{pf}\rho_f}]u + \frac{k_{lw}T_a}{C_{pf}\rho_f} \tag{5.3e}$$

$$y_m(t) = \begin{bmatrix} T_w(l_{m1}, t) \\ T_v(l_{m2}, t) \end{bmatrix} \tag{5.3f}$$

The corresponding boundary conditions for this configuration are:

$$\begin{aligned} T_c(0,t) = T_{c0}; T_f(0,t) = T_s(t). \\ T_w(0,t) = T_c(l_{m1}, t); T_v(0,t) = T_f(l_{m2}, t) \end{aligned} \tag{5.4}$$

Then, the original state is extended with these new state, resulting in $x(z,t) = [T_c(z,t), T_f(z,t), T_w(z,t), T_v(z,t), T_s(t)]^T =: [x_1(z,t), x_2(z,t), x_3(z,t), x_4(z,t), x_5(t)]^T \in \mathcal{X} \bigoplus \mathbb{R}$ is considered, where $\mathcal{X}$ is a real Hilbert spaces $L_2(0,l)^4$ with the inner product $\langle \cdot, \cdot \rangle$, and $\mathbb{R}$ denotes a real space. The input $u(t) \in L^2_{loc}([0,\infty), \mathcal{U})$ and output

$y(t) \in L^2_{loc}([0,\infty), \mathcal{Y})$, where $\mathcal{U}$ and $\mathcal{Y}$ are real separable Hilbert spaces. The extended infinite-dimensional continuous-time state-space model can be further formulated as:

$$\dot{x}(z,t) = \mathcal{A}x(z,t) + \mathcal{B}u(t) \tag{5.5a}$$

$$y(t) = \mathcal{C}x(z,t) \tag{5.5b}$$

In this form, one can define the system operator $\mathcal{A}(\cdot) = V\frac{\partial(\cdot)}{\partial z} + \psi(z)(\cdot)$ on its domain

$$\mathcal{A}(\cdot) = \begin{bmatrix} -v_c\frac{\partial(\cdot)}{\partial z} + J_{11}(\cdot) & J_{12}(\cdot) & 0 & 0 & 0 \\ J_{21}(\cdot) & -v_f\frac{\partial(\cdot)}{\partial z} + J_{22}(\cdot) & 0 & 0 & 0 \\ 0 & 0 & -\mu_1\frac{\partial(\cdot)}{\partial z} & 0 & 0 \\ 0 & 0 & 0 & -\mu_2\frac{\partial(\cdot)}{\partial z} & 0 \\ 0 & 0 & 0 & 0 & m_1 \end{bmatrix} \tag{5.6}$$

$$\mathcal{D}(\mathcal{A}) = \left\{ \begin{array}{c} \phi_i(z) \in L_2(0,l)^4, x_5 \in \mathbb{R}: \\ \phi_i(z) \text{ is abs. cont.}, \frac{d\phi_i}{dz} \in L_2(0,l), \text{ with } i = 1,2,3,4, \\ \phi_1(0) = 0, \phi_2(0) = x_5, \phi_3(0) = \phi_1(l_{m1}), \phi_4(0) = \phi_2(l_{m2}) \end{array} \right\} \tag{5.7}$$

where $v_c = \frac{V_c}{A\varepsilon_c}, v_f = \frac{V_f}{A\varepsilon_f}$, $J_{11} = -U/C_{pe}$, $J_{12} = U/C_{pe}$, $J_{21} = U/C_{pf}$, $J_{22} = -U/C_{pf}$, $m_1 = [-\frac{v_{f,s}}{h_s - h_l} - \frac{k_{lz} - k_{lw}}{C_{pf}\rho_f}]$, $m_3 = \frac{k_{lw}T_a}{C_{pf}\rho_f}$. The input operator $\mathcal{B}$ is defined as a bounded operator $\mathcal{B} = [\mathbf{0}; \mathbf{0}; \mathbf{0}; \mathbf{0}; m_2]$, and $m_2 = [\frac{v_{f,s}}{h_s - h_l} + \frac{k_{lz}}{C_{pf}\rho_f}]$. The operator $\mathcal{C}$ is determined as $\mathcal{C}(\cdot) = diag[\mathbf{0}, \mathbf{0}, \int_0^l \delta(z - l_{m1})(\cdot)d\eta, \int_0^l \delta(z - l_{m2})(\cdot)d\eta, \mathbf{0}]$ because the sensors used for measurement are located in l_{m1} and l_{m2}, respectively.

In this infinite-dimensional state-space model, there is the uncertainty of operator $\mathcal{C}$ because the sensor locations l_{m1} and l_{m2} need to be determined. Likewise, this also leads to the unknowns of μ_1 and μ_2, which in turn leads to the uncertainty of operator $\mathcal{A}$.

5.2.3 Model time-discretization

Based on the continuous-time infinite-dimensional system, we introduce the Cayley-Tustin discretization framework to transform the continuous system to the discrete-time one. Let us consider the above linear system in Equation (5.5) and a given a time discretization $h > 0$, and for $j \geq 1$ the Cayley-Tustin discretization is given by

$$\frac{x(jh) - x((j-1)h)}{h} \approx \mathcal{A}\frac{x(jh) + x((j-1)h)}{2} + \mathcal{B}u(jh) \tag{5.8a}$$

$$y(jh) \approx \mathcal{C}\frac{x(jh) + x((j-1)h)}{2} \tag{5.8b}$$

with $x(0) = x_0$, where we omit the spatial dependence of x for brevity. Then let $\frac{u_j^{(h)}}{\sqrt{h}}$ be an approximation of $u(jh)$ by the mean value within a given sampling time, $\frac{u_j^{(h)}}{\sqrt{h}} = \frac{1}{h}\int_{(j-1)h}^{jh} u(t)dt$. It has been shown in [14] that $\frac{u_j^{(h)}}{\sqrt{h}}$ converges to $u(jh)$ as $h \to 0$ in several different ways, similar for $Y(jh)$. Further, rewriting Equation (5.8) gives the discrete time dynamics Equation (5.9). It is frequently called Tustin discretization in the engineering literature, which is discovered in 1940s by Tustin and referred as Tustin transform in digital and sample-data control literature [19].

$$\frac{x_j^{(h)} - x_{j-1}^{(h)}}{h} \approx \mathcal{A}\frac{x_j^{(h)} + x_{j-1}^{(h)}}{2} + \mathcal{B}\frac{u_j^{(h)}}{\sqrt{h}}, x_0^{(h)} = X_0 \tag{5.9a}$$

$$\frac{y_j^{(h)}}{\sqrt{h}} \approx C\frac{x_j^{(h)} + x_{j-1}^{(h)}}{2} \tag{5.9b}$$

Through some basic computations, the following infinite-dimensional discrete-time state space model is obtained:

$$x_j^{(h)} = \mathcal{A}_d x_{j-1}^{(h)} + \mathcal{B}_d u_j^{(h)} \tag{5.10a}$$

$$y_j^{(h)} = C_d x_{j-1}^{(h)} + \mathcal{D}_d u_j^{(h)} \tag{5.10b}$$

where $\mathcal{A}_d$, $\mathcal{B}_d$, C_d, $\mathcal{D}_d$ are the discrete-time spatial operators and we denote:

$$\begin{pmatrix} \mathcal{A}_d & \mathcal{B}_d \\ C_d & \mathcal{D}_d \end{pmatrix} = \begin{pmatrix} [\delta - \mathcal{A}]^{-1}[\delta - \mathcal{A}] & \sqrt{2\delta}[\delta - \mathcal{A}]^{-1}\mathcal{B} \\ \sqrt{2\delta}C[\delta - \mathcal{A}]^{-1} & C[\delta - \mathcal{A}]^{-1}\mathcal{B} \end{pmatrix} \tag{5.11}$$

where $\delta = 2/h$ and the resolvent is $\mathcal{R}(\delta, \mathcal{A}) = (\delta I - \mathcal{A})^{-1}$. Clearly, one must satisfy $\delta \in \rho(\mathcal{A})$ so that the resolvent operator is well-defined. In particular, $C(\delta - \mathcal{A})^{-1}\mathcal{B}$ denotes the transfer function of the continuous model (5.5). The unbounded operators $\mathcal{A}$ of the continuous-time system are mapped into bounded operators $\mathcal{A}_d$ in the discrete-time counterpart through Cayley transform. In addition, it has been demonstrated that the controllability and stability are invariant under this transformation. The continuous state evolutional operator $\mathcal{A}$ is discretized in time and $\mathcal{A}_d$ can be described by the resolvent operator as follows:

$$\begin{aligned} \mathcal{A}_d(\cdot) &= [\delta I - \mathcal{A}]^{-1}[\delta I + \mathcal{A}](\cdot) \\ &= -I(\cdot) + 2\delta[\delta I - \mathcal{A}]^{-1}(\cdot) \\ &= -I(\cdot) + 2\delta\mathcal{R}(\delta, \mathcal{A})(\cdot) \end{aligned} \tag{5.12}$$

where I is an identity operator.

5.2.4 Resolvent operator

From the previous section, one can find the resolvent operator $\mathcal{R}(\delta, \mathcal{A}) = (\delta I - \mathcal{A})^{-1}$ of the system operator $\mathcal{A}$, and then the discrete operators $(\mathcal{A}_d, \mathcal{B}_d, \mathcal{C}_d, \mathcal{D}_d)$ can be easily realized. Recalling the continuous-time system model (5.5), the resolvent operator can be obtained by taking Laplace transform. Under the zero input condition, we can have the following expression:

$$\frac{\partial x_1(z,s)}{\partial z} = \frac{s + J_{11}}{v_c} x_1(z,s) + \frac{J_{12}}{v_c} x_2(z,s) + \frac{1}{v_c} x_1(z,0) \tag{5.13a}$$

$$\frac{\partial x_2(z,s)}{\partial z} = \frac{s + J_{22}}{v_f} x_2(z,s) + \frac{J_{21}}{v_f} x_1(z,s) + \frac{1}{v_f} x_2(z,0) \tag{5.13b}$$

$$\frac{\partial x_3(z,s)}{\partial z} = -\frac{s}{\mu_1} x_3(z,s) + \frac{1}{\mu_1} x_3(z,0) \tag{5.13c}$$

$$\frac{\partial x_4(z,s)}{\partial z} = -\frac{s}{\mu_2} x_4(z,s) + \frac{1}{\mu_2} x_4(z,0) \tag{5.13d}$$

$$x_b(s) = \frac{1}{s - m_1} x_b(0) \tag{5.13e}$$

By solving the above ODE, a frequency-domain solution of the distributed digester system is finally obtained as follows:

$$\begin{bmatrix} x_1(z,s) \\ x_2(z,s) \end{bmatrix} = e^{Mz} \begin{bmatrix} x_1(0,s) \\ x_2(0,s) \end{bmatrix} - \int_0^z e^{M(z-\eta)} V_0^{-1} \begin{bmatrix} x_1(\eta,0) \\ x_2(\eta,0) \end{bmatrix} d\eta \tag{5.14a}$$

$$x_3(z,s) = e^{-\frac{s}{\mu_1} z} x_3(0,s) + \int_0^z e^{-\frac{s}{\mu_1}(z-\eta)} \frac{1}{\mu_1} x_3(\eta,0) d\eta \tag{5.14b}$$

$$x_4(z,s) = e^{-\frac{s}{\mu_2} z} x_4(0,s) + \int_0^z e^{-\frac{s}{\mu_2}(z-\eta)} \frac{1}{\mu_2} x_4(\eta,0) d\eta \tag{5.14c}$$

where

$$V_0 = \begin{bmatrix} -v_c & 0 \\ 0 & -v_f \end{bmatrix}, B_0 = \begin{bmatrix} s - J_{11} & -J_{12} \\ -J_{21} & s - J_{22} \end{bmatrix}, M = V_0^{-1} B_0 \tag{5.15}$$

For simplicity, one can introduce the following notations in order to determine the resolvent operator:

$$e^{Mz} = \begin{bmatrix} M_{11}(z,s) & M_{12}(z,s) \\ M_{21}(z,s) & M_{22}(z,s) \end{bmatrix} \tag{5.16}$$

After further manipulations, the closed-form analytical solutions of the state evolution matrix can be arranged as follows:

$$\begin{cases} M_{11}(z,s) = e^{\frac{Gz}{2v_c v_f}} \left[\frac{K}{F} \sinh(\frac{Fz}{2v_c v_f}) + \cosh(\frac{Fz}{2v_c v_f}) \right] \\ M_{12}(z,s) = \frac{2J_{12}v_f}{F} e^{\frac{Gz}{2v_c v_f}} \sinh(\frac{Fz}{2v_c v_f}) \\ M_{21}(z,s) = \frac{2J_{21}v_c}{F} e^{\frac{Gz}{2v_c v_f}} \sinh(\frac{Fz}{2v_c v_f}) \\ M_{22}(z,s) = e^{\frac{Gz}{2v_c v_f}} \left[-\frac{K}{F} \sinh(\frac{Fz}{2v_c v_f}) + \cosh(\frac{Fz}{2v_c v_f}) \right] \end{cases} \tag{5.17}$$

where F, G, K are denoted as:

$$F = \sqrt{(J_{11}-s)^2 v_f^2 + 2v_c v_f (2J_{12}J_{21} + (J_{11}-s)(s-J_{22})) + (J_{22}-s)^2 v_c^2}$$

$$G = J_{11}v_f + J_{22}v_c - s(v_c + v_f)$$

$$K = J_{11}v_f - J_{22}v_c + s(v_f - v_c)$$

Therefore, with the boundary conditions given by $x_3(0,s) = x_1(l_{m1},s)$ and $x_4(0,s) = x_4(l_{m2},s)$, $x_3(z,s)$ and $x_4(z,s)$ can be obtained. The resolvent operator can be expressed as follows:

$$x(z,s) = \mathcal{R}(s,\mathcal{A})x(\eta,0) \tag{5.18}$$

where

$$\mathcal{R}(s,\mathcal{A}) = \begin{bmatrix} \mathcal{R}_{11} & \mathcal{R}_{12} & 0 & 0 & \mathcal{R}_{15} \\ \mathcal{R}_{21} & \mathcal{R}_{22} & 0 & 0 & \mathcal{R}_{25} \\ \mathcal{R}_{31} & \mathcal{R}_{32} & \mathcal{R}_{33} & 0 & \mathcal{R}_{35} \\ \mathcal{R}_{41} & \mathcal{R}_{42} & 0 & \mathcal{R}_{44} & \mathcal{R}_{45} \\ 0 & 0 & 0 & 0 & \mathcal{R}_{55} \end{bmatrix} \tag{5.19}$$

where

$$\begin{cases} \mathcal{R}_{i1}(\cdot) = \int_0^z \frac{1}{v_c} M_{i1}(z-\eta,s)(\cdot)d\eta, i = 1,2 \\ \mathcal{R}_{i2}(\cdot) = \int_0^z \frac{1}{v_f} M_{i2}(z-\eta,s)(\cdot)d\eta, i = 1,2 \\ \mathcal{R}_{i5}(\cdot) = \frac{M_{i2}(z,s)}{s-m_1}(\cdot), i = 1,2 \\ \mathcal{R}_{31}(\cdot) = e^{-\frac{s}{\mu_1}z} \int_0^{l_{m1}} \frac{1}{v_c} M_{11}(l_{m1}-\eta,s)(\cdot)d\eta \\ \mathcal{R}_{32}(\cdot) = e^{-\frac{s}{\mu_1}z} \int_0^{l_{m1}} \frac{1}{v_f} M_{12}(l_{m1}-\eta,s)(\cdot)d\eta \\ \mathcal{R}_{33}(\cdot) = \int_0^z e^{-\frac{s}{\mu_1}(z-\eta)} \frac{1}{\mu_1}(\cdot)d\eta \\ \mathcal{R}_{35}(\cdot) = e^{-\frac{s}{\mu_1}z} \frac{M_{12}(l_{m1},s)}{s-m_1}(\cdot) \\ \mathcal{R}_{41}(\cdot) = e^{-\frac{s}{\mu_2}z} \int_0^{l_{m2}} \frac{1}{v_c} M_{21}(l_{m2}-\eta,s)(\cdot)d\eta \\ \mathcal{R}_{42}(\cdot) = e^{-\frac{s}{\mu_2}z} \int_0^{l_{m2}} \frac{1}{v_f} M_{22}(l_{m2}-\eta,s)(\cdot)d\eta \\ \mathcal{R}_{44}(\cdot) = \int_0^z e^{-\frac{s}{\mu_2}(z-\eta)} \frac{1}{\mu_2}(\cdot)d\eta \\ \mathcal{R}_{45}(\cdot) = e^{-\frac{s}{\mu_2}z} \frac{M_{22}(l_{m2},s)}{s-m_1}(\cdot) \\ \mathcal{R}_{55}(\cdot) = \frac{1}{s-m_1}(\cdot) \end{cases} \tag{5.20}$$

Now, the discrete-time operators in Equation (5.11) can be solved by straightforwardly substituting the above resolvent operators. Afterwards, the discrete-time linear model is obtained:

$$x(z,k) = \mathcal{A}_d x(z,k-1) + \mathcal{B}_d u(k) \tag{5.21a}$$

$$y(k) = \mathcal{C}_d x(z,k-1) + \mathcal{D}_d u(k) \tag{5.21b}$$

with the boundary conditions Equation (5.4). It is worth noting that the uncertainty of the sensor location l_{m1} and l_{m2} will lead to the uncertainty of the resolvent operator and then further effects on the operators $\mathcal{A}_d$, $\mathcal{B}_d$, $\mathcal{C}_d$ and $\mathcal{D}_d$.

5.3 State Estimation and Sensor Placement for the Stochastic System

5.3.1 Discrete stochastic model formulation

In order to account for the process and measurement noise of the digester, the Kalman filter is developed as an one-step ahead predictor. In this case, one can introduce the bounded operators G_w accounting for spatial influence of state noise ω_k at each time instance. By assuming that there is no prior knowledge of the noise source, the discrete-time digester system with addictive disturbances/noises is considered in the following form:

$$x_k = \mathcal{A}_d x_{k-1} + \mathcal{B}_d u_k + G_w \omega_k \tag{5.22a}$$

$$y_k = \mathcal{C}_d x_{k-1} + \mathcal{D}_d u_k + v_k \tag{5.22b}$$

where ω_k denotes process noise, which is the zero mean multivariate normal distribution with covariance Q_k given as $\omega_k \sim \mathcal{N}(0, Q_k)$, $E[\omega_k \omega_j^T] = Q_k \delta_{k,j}$, and $\delta_{k,j}$ is the Dirac delta function, i.e., $\delta_{k,j} = 1$ if $k = j$ and $\delta_{k,j} = 0$ otherwise, while v_k represents measurement noise at time step k of having zero mean Gaussian white noise with covariance R_k denoted as $v_k \sim \mathcal{N}(0, R_k)$, $E[v_k v_j^T] = R_k \delta_{k,j}$, and $E[v_k \omega_j^T] = 0$. Furthermore, we consider independent process noise and measurement noise. In order to guarantee the consistency in the time instants of the discrete digester system and the standard discrete Kalman filter structure in finite-dimensional setting, one can

express y_k by the state x_k instead of x_{k-1} in Equation (5.21) and Equation (5.22), which yields the following:

$$x_k = \mathcal{A}_d x_{k-1} + \mathcal{B}_d u_k + G_w \omega_k \tag{5.23a}$$

$$y_k = \bar{C}_d x_k + \bar{\mathcal{D}}_d u_k + v_k \tag{5.23b}$$

where the associated discrete-time spatial operators are denoted as follows [53]:

$$\begin{pmatrix} \mathcal{A}_d & \mathcal{B}_d & G_w \\ \bar{C}_d & \bar{\mathcal{D}}_d & - \end{pmatrix} = \begin{pmatrix} -I + 2\delta\mathcal{R}(z,\delta) & \sqrt{2\delta}\mathcal{R}(z,\delta)\mathcal{B} & \sqrt{2\delta}\mathcal{R}(z,\delta)G \\ -\sqrt{2\delta}C\mathcal{R}(z,-\delta) & \mathcal{G}(-\delta) & - \end{pmatrix} \tag{5.24}$$

5.3.2 Discrete kalman filter design

In this section, a classical discrete-time Kalman filter is designed for the well-defined stochastic discrete-time digester system (5.22). Kalman filter is often realized in two steps, including a prediction step and an updating step, also referred as a priori estimation step and a posteriori estimation step [176]. Firstly, the following notations are introduced.

$$\begin{aligned} \hat{x}_k^- &= E[x_k \mid y_1, y_2, ..., y_{k-1}] = \text{a priori estimate} \\ \hat{x}_k^+ &= E[x_k \mid y_1, y_2, ..., y_k] = \text{a posteriori estimate} \end{aligned} \tag{5.25}$$

In addition, we use the term P_k to denote the covariance of the estimation error. P_k^- denotes the covariance of the estimation error of $\hat{x}_k^-$, $P_k^- = E[(x_k - \hat{x}_k^-)(x_k - \hat{x}_k^-)^*]$, and P_k^+ denotes the covariance of the estimation error of $\hat{x}_k^+$, $P_k^+ = E[(x_k - \hat{x}_k^+)(x_k - \hat{x}_k^+)^*]$.

We begin the estimation process with the guess of initial conditions which are described as below:

$$\begin{cases} \hat{x}_0^+ = E(x_0) = \hat{x}_0 \\ P_0^+ = E[(x_0 - \hat{x}_0^+)(x_0 - \hat{x}_0^+)^*] = Q_0 \end{cases} \tag{5.26}$$

Then, one has the following prior estimation or prediction step, with measurement up to time $k-1$:

$$\begin{cases} P_k^- = \mathcal{A}_d P_{k-1}^+ \mathcal{A}_d^* + G_w Q_{k-1} G_w^* = \mathcal{A}_d (\mathcal{A}_d P_{k-1}^+)^* + G_w Q_{k-1} G_w^* \\ \hat{x}_k^- = \mathcal{A}_d \hat{x}_{k-1}^+ + \mathcal{B}_d u_k \end{cases} \tag{5.27}$$

The posterior estimation or update step is given as follows, by using additional output measurement y_k at time instance k:

$$\begin{cases} K_k = P_k^- \bar{C}_d^* (\bar{C}_d P_k^- \bar{C}_d^* + R_k)^{-1} = (\bar{C}_d P_k^-)^* [\bar{C}_d (\bar{C}_d P_k^-)^* + R_k]^{-1} \\ P_k^+ = (I - K_k \bar{C}_d) P_k^- (I - K_k \bar{C}_d)^* + K_k R_k K_k^* \\ \quad = I P_k^- I^* - K_k \bar{C}_d P_k^- I^* - I P_k^- \bar{C}_d^* K_k^* + K_k \bar{C}_d P_k^- \bar{C}_d^* K_k^* + K_k R_k K_k^* \\ \quad = I P_k^- I^* - K_k \bar{C}_d P_k^- I^* - I (\bar{C}_d P_k^-)^* K_k^* + K_k \bar{C}_d (\bar{C}_d P_k^-)^* K_k^* + K_k R_k K_k^* \\ \hat{x}_k^+ = \hat{x}_k^- + K_k (y_k - \bar{C}_d \hat{x}_k^- - \bar{\mathcal{D}}_d u_k) \end{cases} \tag{5.28}$$

The basic configuration extends the design algorithm of a standard discrete-time finite-dimensional Kalman filter [176]. Compared to the general matrix forms of state space representation in finite-dimensional systems, the discrete spatial operators $(\mathcal{A}_d, \mathcal{B}_d, \bar{\mathcal{C}}_d, \bar{\mathcal{D}}_d, G_w)$ need to be treated carefully as they are induced by Cayley-Tustin time discretization. In addition, the covariances P_k^- and P_k^+ are two-dimensional and self-adjoint with spatial characteristics.

5.3.3 Optimal sensor location

The basic idea of optimal sensor selection is to select the sensor locations among a given finite location set, which provides information about the dynamic system. To realize this goal, the optimal sensor selection can be formulated as an optimization problem, aiming to minimize a given objective function related to the dynamic characteristics of the system. As we mentioned earlier, most of the previous contributions in terms of the sensor selection for DPS mainly consider the spectral systems, with less attention on the non-spectral systems. Thus, the optimal sensor selection is investigated for the continuous pulp digester described by the first-order hyperbolic PDEs to determine the appropriate sensor location from a set of candidate locations of the temperature sensors. Meanwhile, in order to compare the selection results of sensor location based on different criteria, a general model of plug flow reactor which is described as first order hyperbolic PDE system is investigated in this chapter.

A simple model of the plug flow reactor with constant transport velocity v and spatial function ψ associated with linearized kinetics of the chemical reaction along the reactor can be described by the following equations:

$$x_t(z,t) = -v\frac{\partial x(z,t)}{\partial z} + \psi(z)x(z,t) + b(z)u(t) \tag{5.29a}$$

$$y(t) = \mathcal{C}x(z,t) \tag{5.29b}$$

$$x(0,t) = 0, x(z,0) = x_0 \tag{5.29c}$$

where $x(\cdot,t) \in L_2((0,1),\mathbb{R})$ is the system state. The actuation distribution function $b(z)$ is assumed spatially uniform, which accounts for the uniform cooling with the jacket fluid flow. The point measurement is specified with the operator $\mathcal{C}$, which depends on the sensor location l_m, and it can be denoted as $\mathcal{C}(f(z)) = \int_0^l \delta(z - l_m)f(z)d\eta$. One can further define the spatial linear operator $\mathcal{A}(\cdot) = -v\frac{\partial(\cdot)}{\partial z} + \psi(z)(\cdot)$

with a domain $\mathcal{D}(\mathcal{A}) = \{\phi(z) \in L_2(0,1) | \phi(z)$ is abs. cont., $\frac{d\phi}{dz} \in L_2(0,1), \phi(0) = 0\}$, where abs.cont. denotes that ϕ is absolutely continuous.

Considering the system without state and measurement disturbances, and the observability gramian can be evaluated in sensor's potential position by solving the Lyapunov equation. In this case, the observability gramian is well-defined as $L_c\psi = \lim_{\tau\to\infty} \int_0^\tau \mathcal{T}(t)^* C^* C \mathcal{T}(t)\psi dt$, where $\mathcal{A}$ generates a C_0 semigroup $\mathcal{T}(t)$. Then, if $\mathcal{T}(t)$ is strongly stable, L_c is the unique solution of the continuous-time observation Lyapunov equation $\mathcal{A}^* L_c\varphi + L_c\mathcal{A}\varphi = -C^*C\varphi, \varphi \in \mathcal{D}(\mathcal{A})$, where φ is a spatial function [100]. In order to obtain L_c, the adjoint operator $\mathcal{A}^*$ needs to be found using the inner product formula, $\langle \mathcal{A}\varphi, \phi\rangle = \langle \varphi, \mathcal{A}^*\phi\rangle$, and is $\mathcal{A}^*(\cdot) = -v\frac{\partial(\cdot)}{\partial\zeta} + \psi^*(z)(\cdot)$ with a domain $\mathcal{D}(\mathcal{A}^*) = \{\phi(z) \in L_2(0,1) | \phi(z)$ is abs. cont., $\frac{d\phi}{dz} \in L_2(0,1), \phi(1) = 0\}$. The observability gramian can be obtained further by substituting operators $\mathcal{A}$ and $\mathcal{A}^*$ into the above Lyapunov equation and rearrange as:

$$\frac{\partial L_c}{\partial z} = -\frac{2\psi}{v} L_c - \frac{1}{v} C^* C, L_c \in \mathcal{D}(\mathcal{A}^*) \tag{5.30}$$

Then, the trace norm (nuclear norm) of the observability is utilized to quantify observability for different sensor location, which has been found to be one of the most meaningful measures of observability because it takes the observability of entire system into account [177]. However, when the system is corrupted by disturbances, if the point of maximum observability still the best locations from the viewpoint of estimation error. We introduce the following algorithm to handle such situation.

The objective is to minimize the steady-state error variance of the estimated states, which is in the nuclear norm [67]. The value of steady-state error variance is dependent on the measurement operator C, and hence on the number of sensors, as well as on the sensor noise covariance R_k. Thus, minimizing the steady-state error variance is a reasonable design goal when it comes to the sensor location selection. The sensor locations are defined as the discrete optimization variables and the constraints are typically the given sensor number.

$$\min_{\vartheta\in\Omega^n} \ \|P_{ss}(\vartheta)\|_1 \tag{5.31a}$$

$$\text{s.t.} \ \ g(\vartheta) = n, \tag{5.31b}$$

$$\vartheta^{lb} \le \vartheta \le \vartheta^{ub}, \tag{5.31c}$$

$$\vartheta \in \mathbb{Z}^{+}. \tag{5.31d}$$

where $\vartheta = \{\theta_1, \theta_2, ..., \theta_n\}$ represents the sensor locations defined by a set of integers, $\|P_{ss}(\vartheta)\|_1$ is the nuclear norm of steady-state error variance, $g(\vartheta)$ denotes the total number of sensor locations, n is the given sensor number, ϑ^{lb} and ϑ^{ub} are the lower and upper bounds of ϑ, respectively, and $\mathbb{Z}^{+}$ denotes the set of positive integers. The minimum solution of Equation (5.31) is then the optimal sensor configuration as follows:

$$\vartheta^{*} = arg \min_{\vartheta \in \Omega^n} \ \|P_{ss}(\vartheta)\|_1 \tag{5.32a}$$

$$\text{s.t.} \ \ g(\vartheta) = n, \tag{5.32b}$$

$$\vartheta^{lb} \leq \vartheta \leq \vartheta^{ub}, \tag{5.32c}$$

$$\vartheta \in \mathbb{Z}^{+}. \tag{5.32d}$$

Problem (5.32) can be solved by the following procedure.

1) determine the feasible sensor location set $\mathbf{\Omega}^n$

2) For every sensor configuration $\vartheta \in \mathbf{\Omega}^n$, solve the problem (5.32).

3) The optimal sensor location of the considered system is obtained as ϑ^{*}.

For the considered pulp digester, the possible sensor locations are assumed distributed in the range [0,5] and shown in Table 5.1. In the simulation section, the optimal locations of measurement sensors will be discussed further based on the proposed selection procedure.

Table 5.1: Locations considered for each sensor

Temperature locations of wood chips/l_{m1}	Temperature locations of free liquor/l_{m2}
0.2, 1, 2, 3, 4, 5	0.2, 1, 2, 3, 4, 5

5.4 Simulation Results

In this section, we provide numerical examples associated with the discrete-time Kalman filter design and sensor location selection. First, the developed infinite-dimensional discrete-time Kalman filter for the digester system is simulated and the corresponding results are discussed in detail. Two cases are further considered, including the spatially distributed process noise and the spatially centered process noise.

Then, the general case of first-order hyperbolic PDE discussed in Section 5.3.3 is revisited to demonstrate the performance of the proposed filter and compare the results of sensor location by using different criteria, including maximum observability and minimum variance estimation. The numerical simulation is further investigated to determine the optimal sensor placement, which might provide guidance for sensor location selection and efficient monitoring of digester systems in practice.

5.4.1 Performance of state estimation for pulp digester

The values of all system parameters and for simulations are listed in Table 5.2. For the initial conditions of the dynamic system, we consider $x_1(z,0) = 0.18\sin(0.4\pi z), x_2(z,0) = 0.87\sin(0.4\pi z)$. As for the Cayley-Tustin time discretization, we choose $h = 2s$ at the time discretization interval. The spatial discretization interval is taken as $\Delta z = 0.05$. The time delays (τ_1, τ_2) are considered as $(30, 30)$, which has been demonstrated with a full-scale digester [172]. Firstly, the open-loop temperature perturbations of cook zone are simulated in Figure 5.4 with the activated control action $u(t) = 4\sin(0.05t)$. It is apparent that the behavior of the state evolution profile follows the periodic wave trend induced by the given input.

Table 5.2: Notation and values of parameters [2]

Process parameters	Notations	Numerical Values
Volumetric flow rate of chip	V_c	$0.0267\ m^3/min$
Volumetric flow rate of free liquor	V_f	$0.09\ m^3/min$
Digester cross sectional area	A	$21\ m^2$
Interphase heat-transfer coefficient	U	$827\ kJ/min \cdot K \cdot m^3$
Heat capacities of the wood	C_{ps}	$1.47\ kJ/kg \cdot K$
Heat capacities of the liquor	C_{pl}	$4.19\ kJ/kg \cdot K$

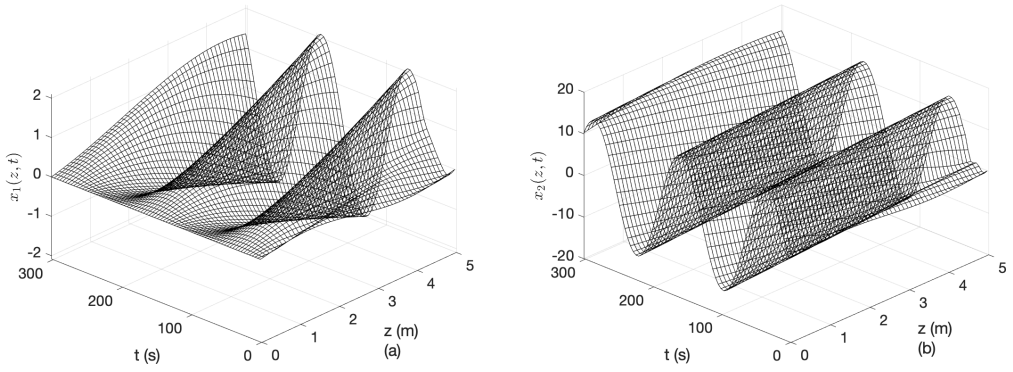

Figure 5.4: Perturbations of open-loop state profiles

Performance of Discrete Kalman Filter

The developed discrete-time Kalman filter configuration is applied to the stochastic linear infinite-dimensional discrete-time digester system (5.23), and the performance is analyzed. In addition, the sensor location is first considered at the bottom of cook zone, that means $l_{m1} = l_{m2} = l$. Based on that, two different disturbances are considered: spatially distributed and centered disturbance. In both cases, the plant and measurement noises, we take $\omega_k \sim \mathcal{N}(0, Q_k)$, $E[\omega_k \omega_j^T] = Q_k \delta_{k,j}$, $v_k \sim \mathcal{N}(0, R_k)$, $E[v_k v_j^T] = R_k \delta_{k,j}$, $E[v_k \omega_j^T] = 0$ with $Q_k = 0.005$ and $R_k = diag(1, 2)$. The estimated initial conditions are $\hat{x}_1(z, 0) = 0.16sin(0.4\pi z)$ and $\hat{x}_2(z, 0) = 0.8sin(0.4\pi z)$.

Case 1: Spatially distributed process noise

In this case, the spatially distributed noise is considered first for the description of the noise on the state distribution in the spatial domain, which is defined as $g(z) = 1 + 30sech(100(z - 0.1))$. The operator is defined as $G(z) = [\mathbf{1}, \mathbf{1}, \mathbf{1}, \mathbf{1}, \mathbf{1}]^T$, which means the process noise exists the whole process.

Profiles of the state with noise and the estimated state are presented in Figure 5.5 and Figure 5.6. Compared with Figure 5.4, it can be seen that there are some noisy oscillations in the two states induced by the process noise and measurement noise, and the developed Kalman filter is capable of reconstructing the entire spatiotemporal state profile and reducing noises present in the process and measurement simultaneously. Moreover, in Figure 5.7, the filtering performance of outputs is presented, including the temperature of wood chips and free liquor, respectively. The filtered

output of interest matches perfectly with the one in the noise-free system, largely eliminating the noises involved in the stochastic digester system. The measurement error and the estimation error are utilized to evaluate the estimation accuracy of the designed Kalman filter, as shown in Figure 5.8. It is clear that the designed filter can reduce the estimation error to an acceptable range despite the large measurement error.

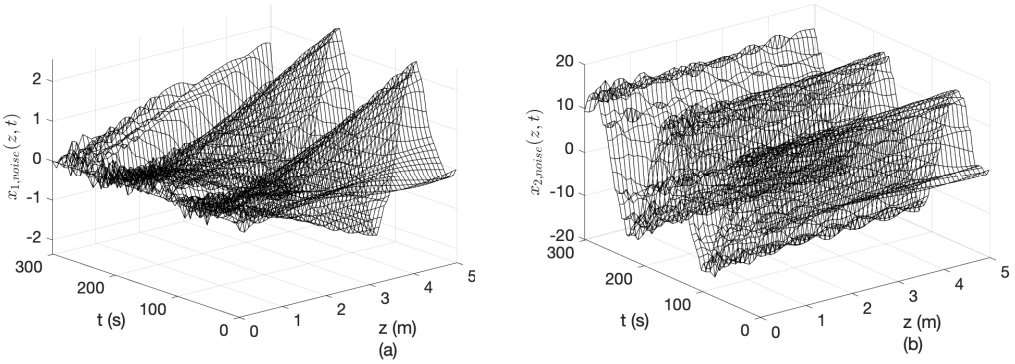

Figure 5.5: Profile of the states with noise

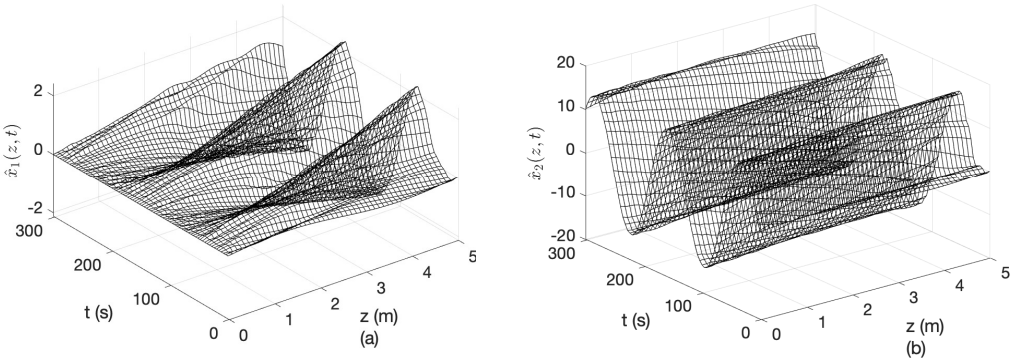

Figure 5.6: Profile of the estimated states

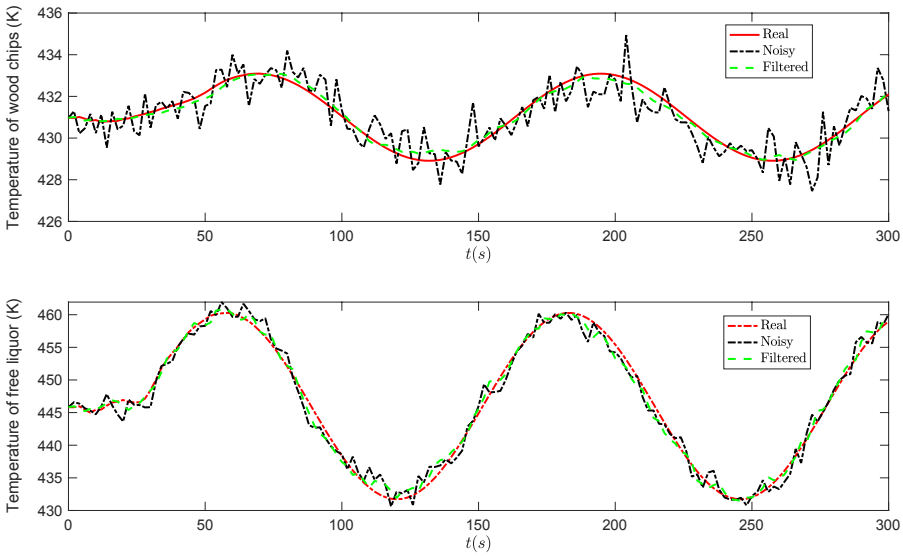

Figure 5.7: Filtering performance of outputs

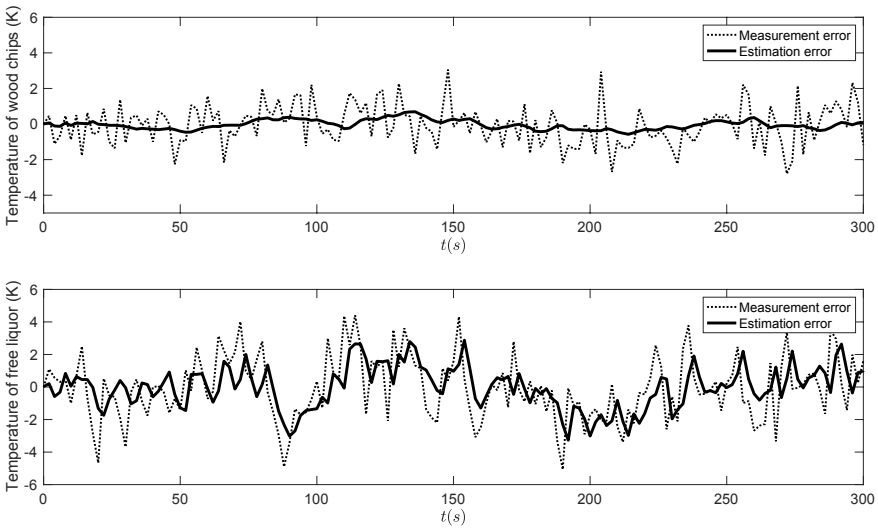

Figure 5.8: The measurement error and estimation error for case 1

Case 2: Spatially centered process noise

In this case, the spatially centered process noise is considered and we assume the noise only appears in the temperature of wood chips. The centered disturbance illustrated as function $g(z) = 20sech(100(z - 0.2))$, and the operator is defined as

$G(z) = [g(z), \mathbf{0}, g(z), \mathbf{0}, \mathbf{0}]^T$. Different from case 1, we assume that the process noise appears when measuring the temperature of the wood chips.

Figure 5.9 shows the state profiles with noise and the estimated state using the designed Kalman filter. It is apparent that the temperature profile of wood chips is quite noisy in Figure 5.9 (a), while after applying the developed discrete-time Kalman filter, one can directly see that the noise has been filtered out, and the original state evolution is revealed as shown in Figure 5.9 (b). Although the temperature of wood chips and free liquor is coupled, in this case, the temperature of free liquor is relatively less affected by noise, therefore the profile of the estimated state for x_2 is not provided. By comparing the filtered state evolution with the original one (Figure 5.4), the effectiveness of the proposed discrete Kalman filter can be verified. From the comparison of outputs in Figure 5.10, one can notice that the measured output profiles in the two figures are quite noisy, as shown in the black dashed lines, and the proposed Kalman filter can smooth out the noises in outputs and make the filtered output converge to real output profiles, as shown in green dashed lines and red solid lines, respectively.

To quantity the estimation performance of the proposed Kalman filter, the measurement error and the estimation error are calculated based on the actual outputs, as shown in Figure 5.11. The measurement error is defined as the difference between the measurement and the actual output, and the estimation error denotes the difference between the filtered output using the Kalman filter and the actual output. The measurement errors of both outputs are relatively random and large. After applying the Kalman filter, the estimated temperature of wood chips is close to the real one as the estimation error is smooth and relatively small. Although the measurement error is largest when the time lag is around $55s$, the Kalman filter can also achieve relatively better estimation. As for the temperature of free liquor, the estimation performance is much better since the estimation error converges to zero within $60s$ which might be caused by the spatially localized noise only appearing in the temperature of wood chips or x_1.

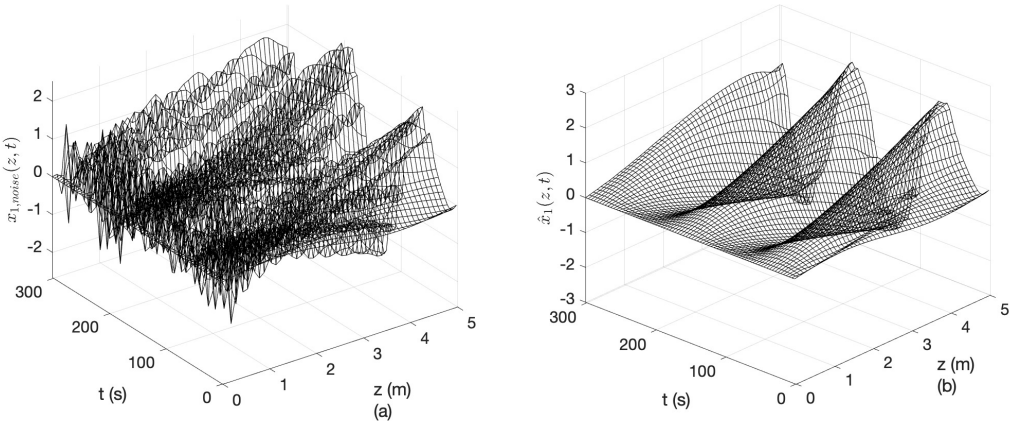

Figure 5.9: Profiles of the state with noise and the estimated states

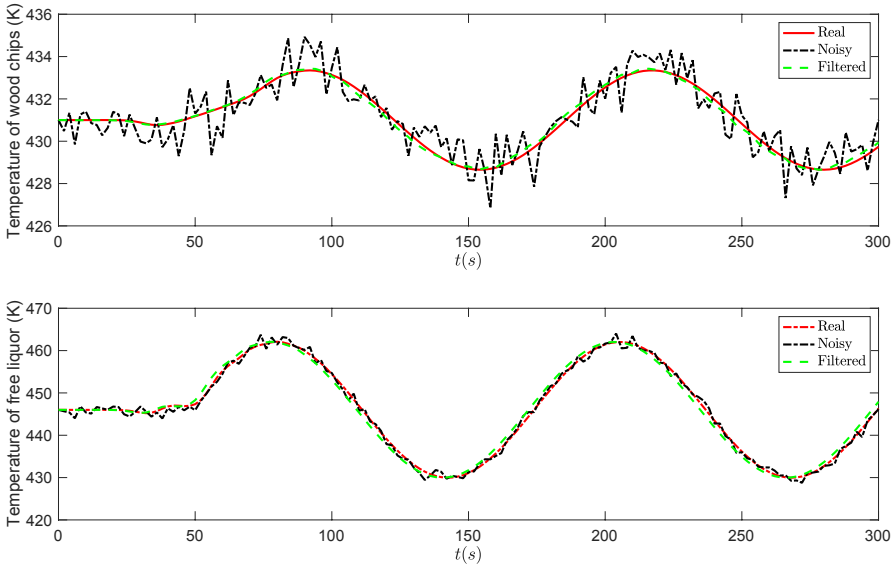

Figure 5.10: Filtering performance of outputs

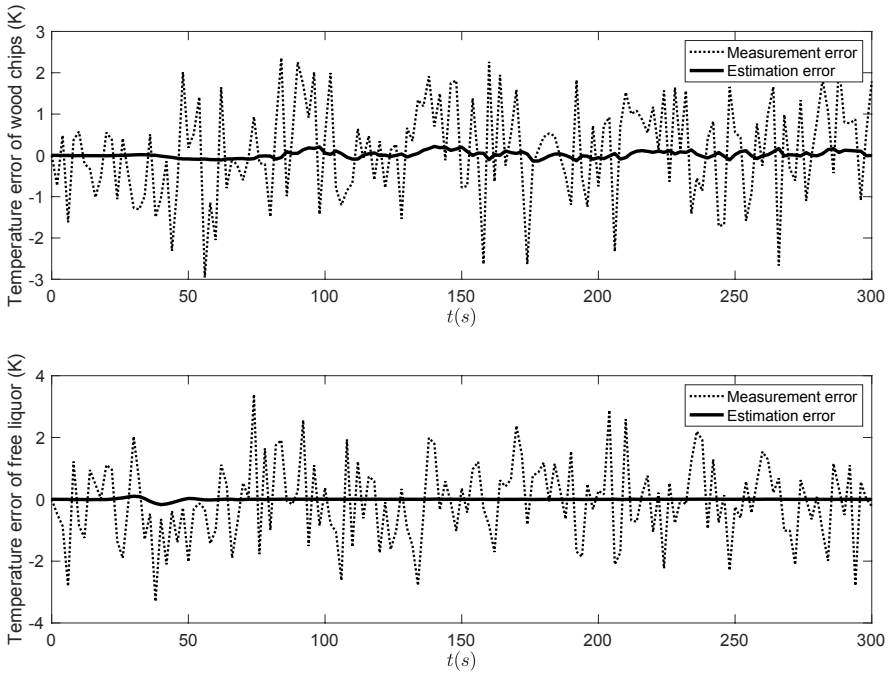

Figure 5.11: The measurement error and estimation error for case 2

5.4.2 Determination of optimal sensor placement

Sensor location selection for the first order hyperbolic PDE

In this section, the proposed Kalman filter design and sensor selection are applied to the scalar hyperbolic system presented in Section 5.3.3. The discrete-time linear hyperbolic PDE system corresponding to Equation (5.29) is obtained by applying Cayley-Tustin transformation and is given in the following form:

$$x(z,k) = \mathcal{A}_d x(z,k-1) + \mathcal{B}_d u(k) + \omega(k), x(z,0) = x_0 \tag{5.33a}$$

$$y(k) = \mathcal{C}_d x(z,k) + \mathcal{D}_d u(k) + v(k) \tag{5.33b}$$

where

$$\begin{cases} \mathcal{A}_d(\cdot) = [\delta I - \mathcal{A}]^{-1}[\delta I + \mathcal{A}](\cdot) \\ \qquad = -I(\cdot) + 2\delta \left[\int_0^z \frac{1}{\nu}(\cdot) e^{-\frac{1}{\nu}(\psi-\delta)\eta} d\eta\right] e^{\frac{1}{\nu}(\psi-\delta)z} \\ \mathcal{B}_d = \sqrt{2\delta}[\delta I - \mathcal{A}]^{-1}\mathcal{B}(z) \\ \quad = \sqrt{2\delta}\left[\int_0^z \frac{1}{\nu}\mathcal{B}(\eta) e^{-\frac{1}{\nu}(\psi-\delta)\eta} d\eta\right] e^{\frac{1}{\nu}(\psi-\delta)z} \\ C_d(\cdot) = -\sqrt{2\delta}C[-\delta I - \mathcal{A}]^{-1}(\cdot) \\ \qquad = -\sqrt{2\delta}\left[\int_0^{l_m} \frac{1}{\nu}(\cdot) e^{-\frac{1}{\nu}(\psi+\delta)\eta} d\eta\right] e^{\frac{1}{\nu}(\psi+\delta)l_m} \\ \mathcal{D}_d = C[-\delta I - \mathcal{A}]^{-1}\mathcal{B} + \mathcal{D} \\ \quad = \left[\int_0^{l_m} \frac{1}{\nu}\mathcal{B}(\eta) e^{-\frac{1}{\nu}(\psi+\delta)\eta} d\eta\right] e^{\frac{1}{\nu}(\psi+\delta)l_m} \end{cases} \tag{5.34}$$

The simulation result of the Kalman filter design given Equations (5.26)-(5.28) for the discrete scalar hyperbolic PDE system is shown in Figure 5.12. In this case, the spatial parameter in the operator A is chosen to be $\psi = 0.5$, while the input operator $B(0 < z < 1) = 1$ represents spatially uniform realized heat transfer across the reactor shell. The time varying input is considered as $u(k) = 3sin(2\pi k)$, the potential position of the sensor location l_m is considered as $[0.05, 0.1, 0.2, 0.3, 0.4, 0.5, 0.6, 0.7, 0.8, 0.9, 1]$. The initial conditions are taken as $x_0 = 5sin(2\pi z)$ and $\hat{x}_0 = 3sin(4\pi z)$. The process noise and measurement noise are considered as $\omega_k \sim \mathcal{N}(0, Q_k)$ with $Q_k = 0.05$, and $v_k \sim \mathcal{N}(0, R_k)$ with $R_k = 0.1$.

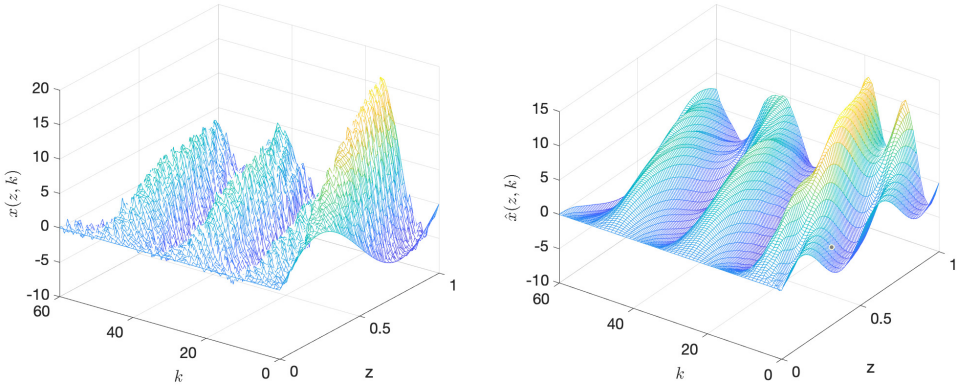

Figure 5.12: Profiles of the state with noise and the estimated state

Figure 5.13 illustrates the relationship between the trace norm of the observability and the single sensor's location along with the spatial position. The steady-state of the trace norm of estimation error covariance subject to the location of the sensor is also shown in Figure 5.13. As it is expected, the trace norm of observability gramian

increases as the sensor moves towards the end of the reactor and reaches a maximum at the last point in space. This confirms the application-based and practical reasoning that sensor placement at the end of the tubular reactor is the best choice. However, the trace norm of estimation covariance shows roughly a quadratic relationship with the sensor location and reaches the minimum point at 0.7. The results indicate that for the scalar hyperbolic PDE, maximizing observability does not generally guarantee the minimum variance estimation. In the other words, it also implies that the maximum observability is not the best criteria for the sensor location from minimizing estimation error viewpoint.

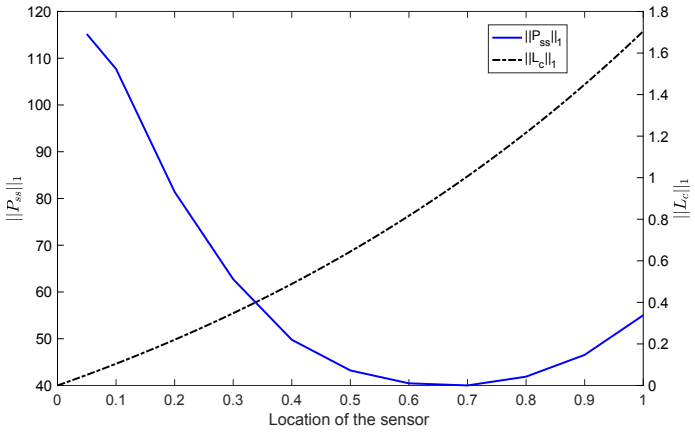

Figure 5.13: Comparison of the trace of steady-state estimation error covariance and trace of observability versus the spatial location of the sensor

Sensor location selection for the pulp digester

We performed several simulation runs to evaluate the performance of the proposed method for computing optimal locations of measurement sensors. Each sensor has 6 possible locations distributed in the range $[0, 5]$ as already shown in Table 5.1.

Based on the algorithm shown in Section 5.3, we compute the optimal sensor locations by minimizing the proposed cost function. By solving Equation (5.32), the optimal sensor locations can be determined. In this case, the optimal sensor locations were found at $\vartheta^* = [1, 3]$, where the minimum cost was 181.5726. Figure 5.14 shows the distribution of the $\|P_{ss}\|_1$, and it can be seen that $\|P_{ss}\|_1$ is relatively large when the temperature sensor of free liquor is located close to the upper boundary (i.e., l_{m2}

is small and close to 0). When the sensor is located far from the upper boundary, the value of trace becomes smaller and not much different from each other. The minimum value appears when the temperature sensor of free liquor is located at $3m$. Even though the variation of trace norm of different temperature sensor locations is not changed much, the H-factor value will change sensitively because the cooking temperature has an exponential relationship with it. The H-factor is an important pulping variable that combines cooking temperature and time into a single variable that indicates the extent of reaction [178].

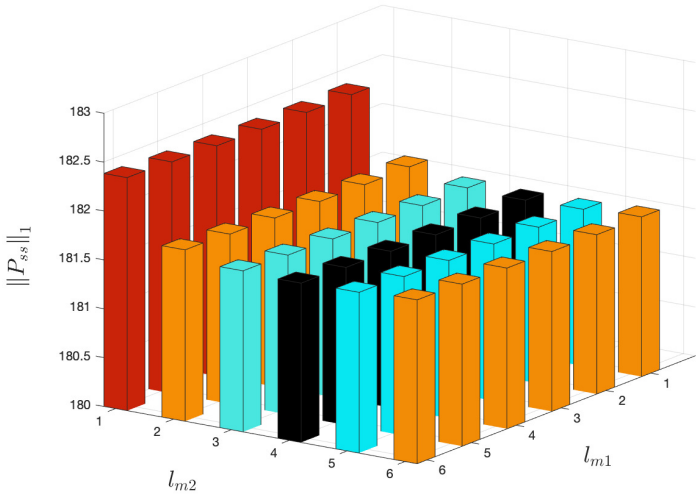

Figure 5.14: The trace norm values of different sensor locations under the consideration of given sensors location

This framework offers a planning and implementation view of distributed sensor locations in which a possible number of sensors and placement. First, the sensor location selection for the tubular reactor or pulp digester is not straightforward, which indicates that it is not recommended to select the sensor position at the very end based on intuition, especially in the presence of process noise. This result has been demonstrated through two examples in this work, which is consistent with the results proposed in the reference [67, 179]. Secondly, the locations corresponding to maximum observability are not always the best from the viewpoint of estimation error, especially when the system is noisy in most practical applications. Thirdly, the optimal sensor locations are recommended at $3m$ for the temperature sensors of free liquor and wood

chips based on the considered model, parameters, noise information, and candidate sensor locations. When it comes to the industrial application, engineers can apply this framework to determine the appropriate sensor location from a set of candidate locations of the temperature sensors based on the information of the sensor type and the noise source conditions. As a result, based on the selected sensor location, the control module can be integrated to control the cooking zone temperature to stabilize pulp quality and/or maximize the production rate with more accuracy. However, when the feasible sensor location set has relatively large candidates, the computational cost will also increase by using the proposed method. The computation issue will be addressed in future work.

5.5 Conclusions

In this chapter, the state estimation and sensor placement for the stochastic continuous pulp digester with measurement delay were investigated from the monitoring point of view. The temperature system of a continuous pulp digester was modeled by two coupled hyperbolic partial differential equations and an ordinary differential equation, and there exists the measurement delay at the considered outputs. In order to realize discrete implementation, the Cayley-Tustin transform was utilized to map the continuous-time system to the discrete-time model representation without spatial discretization and model reduction which preserves the input-output stability of the plant. The discrete-time infinite-dimensional Kalman filter was applied to estimate the system states using the process measurements. The selection of sensor location was then addressed based on the estimator design and investigated by minimizing the variance of estimate error. The effectiveness and feasibility of the proposed Kalman filter were verified by a set of simulations, and this framework offers a planning and implementation view of distributed sensor locations in which a possible number of sensors and placement.

Chapter 6

A Robust Model Predictive Control Strategy for Multi-Model Infinite-Dimensional Transport-Reaction Systems

6.1 Introduction

MPC is one of the techniques of optimal control, and also known as the open-loop optimal feedback control as the open-loop optimal control computation is repeated with the feedback update [180]. Over the past decades, MPC has become one of the dominant methods of chemical process control in terms of successful industrial applications. However, the above conventional MPC may lead to the predicted behavior is not identical to actual behavior in the presence of uncertainty. The uncertainty can arise in many different ways, such as the model of the system is inaccurate, the system may exist unknown disturbance, or the state of the system may not be perfectly known. A typical consideration is a linear time-invariant system with uncertainties in the feedback loop [162]. A multi-plant description also be introduced when model uncertainty in parameterized by a finite list of possible plants[181]. The polytopic uncertainty was further defined when the real system within the convex hull defined by the list of possible plants [162]. Also, the uncertainty was considered when the unknown disturbance occurs which is bounded in some norm.

Therefore, the robust control strategies need to be considered which concern that the systems are uncertain in some sense. A robust controller indicates that it is able

to guarantee the closed-loop stability for different operating conditions of the process. Previous studies, including a survey by Qin and Badgwell [17], have highlighted the significance of robust stability in industrial MPC applications, with current approaches relying on extensive closed-loop simulations prior to implementation and detuning during commissioning. Researchers such as Zafiriou and Marchal have explored the contraction properties of MPC to establish necessary and sufficient conditions for robust stability, particularly with input and output constraints [182, 183]. Badgwell has developed robust stability conditions specifically for single-input, single-output finite impulse response plants [181]. Broadly, the existing literature on robustness in MPC can be grouped into the following general categories.

The first category is to realize robust stability by solving a min-max optimization problem that is minimize a control objective function with the worst possible scenario. Different min-max control algorithms were proposed for open-loop stable systems with time-invariant and time-varying parameter uncertainties [180]. A robust MPC algorithm was presented for stable linear systems with continuous uncertainty by adding cost contracting constraints that prevent the sequence of optimal controller costs from increasing for the true plant [184]. A min-max robust MPC was proposed to handle the output tracking case where the plant steady state is unknown [185]. However, one of the drawbacks of the min-max approaches is the obtained control performance is very conservative due to the condition of stability guarantee. Other drawback is the computational intensity since the resulted optimization problems are very expensive to solve on-line. Therefore, from the process industry application point of view, this control method might become infeasible when it comes to the practical implementation.

The second category is the state-contracting based method. Khotare et al. [162]. Zheng [186] and Michalska and Mayne [187] have described ways of including the state constraints that impart robustness to MPC algorithms. A robust MPC strategy was proposed for the polytopic uncertain models based on an infinite-horizon linear quadratic regulator (LQR), and further extended to the constrained case by involving the linear matrix inequality (LMI) constraints [162]. Zheng [186] imposes a state contraction constraint that requires the largest possible terminal state to be smaller than the initial state at the end of some user specified horizon. Mayne and Michalska

[187] were able to robustly stabilize nonlinear processes by using a terminal state constraint that ensures the process eventually enters a region in input space that is equivalent to the unconstrained problem. Although the stability can be guaranteed for stable, unstable systems with some classes of model uncertainty, it results a quite conservative control law since the control actions are obtained from a fixed state-feedback gain through the infinite prediction horizon. Additionally, it may cause infeasibility due to the hard state contraction constraints.

The third category is the one based on the cost-contraction formulation, proposed in the seminal work of Badgwell [181]. This method has been specifically developed for regulating the operation of open-loop stable systems with multi-plant uncertainty. Its stability is achieved through the incorporation of constraints into the control optimization problem, which prevents the controller cost functions from increasing at consecutive sampling steps [188]. In the case of systems with unmeasured disturbances and the same type of model uncertainty, Odloak extended the aforementioned method to address output tracking [185, 48]. The resulting MPC controller is offset-free, as it utilizes a state-space model based on the incremental form of the system inputs, eliminating the need for an intermediate layer in the control structure to compute a feasible steady state, as proposed in Kassmann, Badgwell, and Hawkins [189].

Compared to the aforementioned contributions on RMPC for finite-dimensional systems, relevant studies on the RMPC design for infinite-dimensional systems have attracted less attention. Nevertheless, the underlying fact is that the majority of transport-reaction processes described by PDE models exhibit uncertainty, i.e., unknown or partially known time-varying process parameters like reaction rate. Presence of uncertain variables and unmodeled dynamics, if not taken into account in the controller design, may lead to poor performance of the controller or even to closed-loop instability. Considering that, a robust nonlinear MPC for nonlinear convection-diffusion-reaction systems was proposed, utilizing a set of reduced order approximations of the plant reconstructed on-line through projection methods on proper orthogonal decomposition (POD) basis functions [49]. A robust model predictive control methodology was designed to a chemical fixed-bed reactor described by a polytopic family of linearized hyperbolic partial differential equations (PDEs), which was initially transformed into the set of ODEs by the method of characteristics [190]. A

tube-based model predictive control scheme for an active vibration damping control of stacker cranes was proposed [191]. However, most of these contributions are based on continuous-time infinite-dimensional models or continuous-time finite-dimensional models after applying some forms of model reductions. Hence, the design of RMPC schemes with the guarantee of stability remains an open field for DPS, mostly when the infinite-dimensional model shall be considered in the problem formulation.

Motivated by these considerations, it is intended in this chapter the development of a robustly stabilizing MPC strategy for distributed parameter transport-reaction systems, which properly accommodates the plant uncertainty. Specifically, we consider the model uncertainty arises when some parameters of system are not exactly known, but lied in a set which can be characterized in some quantitative way. The main objective of is to develop a robust MPC synthesis that allows explicit incorporation of the model uncertainty description into the problem formulation.

The major features of the proposed algorithm are summarized as follows:

1) The model uncertainty under the DPS setting incorporated into the controller formulation is one based upon the multi-model infinite-dimensional setting.

2) The stabilizing MPC algorithm developed by [38] for infinite-dimensional models is extended to the robust case concerning the multi-plant model uncertainty.

3) The robustness is guaranteed by restricting the future behavior of the controller cost function for each plant in the uncertainty description.

4) Properties of systems under the proposed RMPC are discussed, including algorithm feasibility, and closed-loop convergence of the infinite-dimensional system.

The rest of this chapter is organized into 6 sections: Section 6.2 formulates the multi-model infinite-dimensional model. Section 6.3 presents the proposed RMPC synthesis. Section 6.4 analyzes closed-loop properties and finally, typical hyperbolic/parabolic PDE examples are provided in Section 6.5.

6.2 Multi-Model Description

Transport-reaction processes represent the core of relevant first principle based models in chemical engineering practice. The prominent feature of transport-reaction systems is that their models belong to the class of distributed parameter systems (DPS), which

are given by partial differential and/or delay equations.

6.2.1 Continuous-time infinite-dimensional model

The uncertainty in the dynamics of the system is assumed to be of the multi-plant type where the true dynamics is unknown but belongs to a finite set of possible dynamics. In this case, one can consider a finite set of p models $\theta = (\mathcal{A}_\theta, \mathcal{B}_\theta, \mathcal{C}_\theta)$ defined as $\Omega := \{\theta_1, \cdots, \theta_p\}$ and denote each individual plant in the set as $\theta_i = (\mathcal{A}_i, \mathcal{B}_i, \mathcal{C}_i)$.

Typical linear infinite-dimensional continuous-time transport-reaction systems can be extended to a multi-model formulation and described by the following general form as:

$$\begin{aligned} \dot{x}(\zeta,t) &= \mathcal{A}_\theta x(\zeta,t) + \mathcal{B}_\theta u(t), \quad x(\zeta,0) = x_0 \\ y(t) &= \mathcal{C}_\theta x(\zeta,t) \end{aligned} \tag{6.1}$$

where spatial state is $x(\zeta,t) \in L_2((0,l),\mathcal{X})$, where $\mathcal{X}$ is being defined as separable Hilbert space. The input is $u(t) \in L_2^{loc}([0,\infty),U)$ and the U is real Hilbert space, $y(t) \in L_2^{loc}([0,\infty),Y)$ and Y is real Hilbert space. $\mathcal{A}_\theta : \mathcal{D}(\mathcal{A}_\theta) \subset \mathcal{X} \mapsto \mathcal{X}$ is an infinitesimal generator of a C_0-semigroup $\mathbb{T}_{\mathcal{A}_\theta}(t)$ on $\mathcal{X}$. The operators $\mathcal{B}_\theta \in \mathcal{L}(U,\mathcal{X})$, and $\mathcal{C}_\theta \in \mathcal{L}(\mathcal{X},Y)$ are assumed to be bounded operators.

Let us assume that we have selected a model from the set Ω that most likely represent the plant in its actual operation point, referred to as the nominal model $\theta_n \in \Omega$. We also assume that the true plant model is θ_t such that $\theta_t \in \Omega$, although we do not know which model of set Ω is the true one.

Assumption 1. Each plant θ_i is stable or exponentially stabilizable. Moreover, it is assumed that the state of the real plant is prefect measurable.

6.2.2 Discrete-time infinite-dimensional model

Based on the continuous-time infinite-dimensional model Eq. (6.1), we introduce the Cayley-Tustin discretization framework to transform the continuous system to the discrete one. For a given time discretization interval $h > 0$ on $t \in ((k-1)h, kh)$, and

for $k \geq 1$ the Cayley-Tustin discretization is given by:

$$\begin{aligned} \frac{x(kh) - x((k-1)h)}{h} &\approx \mathcal{A}_\theta \frac{x(kh) + x((k-1)h)}{2} + \mathcal{B}_\theta u(kh) \\ y(kh) &\approx \mathcal{C}_\theta \frac{x(kh) + x((k-1)h)}{2} \end{aligned} \tag{6.2}$$

This discretization framework follows an implicit mid-point integration rule, and is a symmetric and symplectic integration scheme leading to a structure- and energy-preserving time discretization. The discrete input is given by the mean value sampling as $\frac{u(kh)}{\sqrt{h}} = \frac{1}{h}\int_{(k-1)h}^{kh} u(t)dt$ [117] . It has been shown in [14] that $\frac{u(kh)}{\sqrt{h}}$ converges to $u(t)$ as $h \longrightarrow 0$, and similar expressions hold for y_k. Through some basic computations, the following infinite-dimensional discrete-time multi-model for system (6.1) is obtained:

$$\begin{aligned} x_k &= \mathcal{A}_d(\theta)x_{k-1} + \mathcal{B}_d(\theta)u_k \\ y_k &= \mathcal{C}_d(\theta)x_{k-1} + \mathcal{D}_d(\theta)u_k \end{aligned} \tag{6.3}$$

where one denotes $\mathcal{A}_d(\theta)$, $\mathcal{B}_d(\theta)$, $\mathcal{C}_d(\theta)$, $\mathcal{D}_d(\theta)$ are the discrete-time spatial operators with the expressions as follows:

$$\begin{bmatrix} \mathcal{A}_d(\theta) & \mathcal{B}_d(\theta) \\ \mathcal{C}_d(\theta) & \mathcal{D}_d(\theta) \end{bmatrix} = \begin{bmatrix} -I(\cdot) + 2\sigma\mathcal{R}(\sigma,\theta) & \sqrt{2\sigma}\mathcal{R}(\sigma,\theta)\mathcal{B}_\theta \\ \sqrt{2\sigma}\mathcal{C}_\theta\mathcal{R}(\sigma,\theta) & \mathcal{G}_\theta(\sigma) \end{bmatrix} \tag{6.4}$$

where $\sigma = 2/h$ and $\mathcal{R}(\sigma,\theta)$ represents the resolvent operator $\mathcal{R}(\sigma,\theta) = (\sigma I - \mathcal{A}_\theta)^{-1}$ with s evaluated at σ. $\mathcal{G}_\theta(\sigma)$ denotes the transfer function from the input $u(t)$ to the controlled output $y(t)$ evaluated at σ. In Eqs. (6.3) and (6.4), we ease the h for notational simplicity.

An important concept is that most physically realizable dynamical systems do not typically include a feedthrough operator, which represents the instantaneous transfer of a signal from the input to the output. The mapping between continuous and discrete infinite-dimensional systems is referred as the Cayley-Tustin discretization method. Another significant property of this discretization method is that it does not alter the nature of the transformed system. Specifically, the conventional application of forward in time Euler discretization may potentially convert a stable continuous system into an unstable discrete system, whereas backward in time Euler discretization may transform an unstable system into a discrete, stable one.

6.3 RMPC Design

As presented in [38], at a given sampling time k, the cost function of a conventional MPC controller (which require the θ to be completely deterministic) for the infinite-dimensional system is given by:

$$J(u^N) = \sum_{j=0}^{\infty} \langle y_{k+j|k}, Q y_{k+j|k} \rangle + \langle u_{k+j|k}, R u_{k+j|k} \rangle \tag{6.5}$$

where Q and R are positive self-adjoint weights on the outputs $y_{k+j|k}$ and inputs $u_{k+j|k}$, respectively. Here it is assumed for simplicity that U and Y are (finite-dimensional) real-valued spaces.

The infinite-horizon objective function can be cast into a finite-horizon objective function under certain assumptions on the inputs beyond the control horizon. Furthermore, a penalty term needs to be added to the objective function to account for the inputs and outputs beyond the horizon.

$$J(u^N) = \sum_{j=0}^{N-1} \langle y_{k+j|k}, Q y_{k+j|k} \rangle + \langle u_{k+j|k}, R u_{k+j|k} \rangle + \langle x_{k+N-1|k}, \bar{Q} x_{k+N-1|k} \rangle \tag{6.6}$$

In the following, the conventional MPC is extended to the robust case where the multi-plant infinite-dimensional representation Eq.(6.3) is adopted. In this way, the robust MPC finds the optimal input u^N that minimize the nominal model cost function with given Q and R:

$$J(u^N, \theta_n) = \min_{u^N} \sum_{j=0}^{N-1} \langle y_{\theta_n,k+j|k}, Q y_{\theta_n,k+j|k} \rangle + \langle u_{k+j|k}, R u_{k+j|k} \rangle + \langle x_{\theta_n,k+N-1|k}, \bar{Q}_{(\theta_n)} x_{\theta_n,k+N-1|k} \rangle \tag{6.7a}$$

$$\text{s.t.} \quad x_{\theta_i,k+j} = \mathcal{A}_d(\theta_i) x_{\theta_i,k+j-1} + \mathcal{B}_d(\theta_i) u_{k+j}, \theta_i \in \Omega \tag{6.7b}$$

$$y_{\theta_i,k+j} = C_d(\theta_i) x_{\theta_i,k+j-1} + \mathcal{D}_d(\theta_i) u_{k+j}, \theta_i \in \Omega \tag{6.7c}$$

$$J(u^N, \theta_i) \leq J(\hat{u}^N, \theta_i), \theta_i \in \Omega \tag{6.7d}$$

$$u_{\min} \leq u_{k+j} \leq u_{\max} \tag{6.7e}$$

$$y_{\min} \leq y_{\theta_i,k+j} \leq y_{\max}, \theta_i \in \Omega \tag{6.7f}$$

$$x_{\theta_i,-1} = x_{\theta_t}, \theta_i \in \Omega \tag{6.7g}$$

where $u^N = \{u_{k+0|k}\ u_{k+1|k} \cdots u_{k+N-1|k}\}$, which is denoted as U_k. In Eq. (6.7d), $\hat{u}^N$ is referred to as the shifted control sequence at time k, which is obtained based on

a solution to the same problem at time $k-1$, also denoted as $\hat{U}_k$. It is a sequence made by shifting one step ahead the optimal sequence U^*_{k-1} and adding in the tail the admissible equilibrium input at time $k-1$. In this case, $\hat{U}_k$ is given by:

$$\begin{aligned} \hat{U}_k &= PU^*_{k-1} \\ P &= \begin{bmatrix} 0 & I & \cdots & 0 & 0 \\ \vdots & \ddots & \ddots & & \vdots \\ \vdots & & \ddots & \ddots & \vdots \\ 0 & \cdots & \cdots & 0 & I \\ 0 & \cdots & \cdots & 0 & 0 \end{bmatrix} \end{aligned} \tag{6.8}$$

In the robust MPC formulation, Eqs. (6.7b) and (6.7c) are the state-space models in the set $\mathbf{\Omega}$ with the initial condition Eq. (6.7g). Eqs. (6.7e) and (6.7f) denote the input and output constraints, respectively. Eq. (6.7d) is the robustness constraint for $i = 1, \cdots, p$, which ensures that the optimal plant cost does not exceed the feasible plant cost at each time step k. Alternatively, it requires the cost function values for each plant in the set $\mathbf{\Omega}$ do not exceed the cost values computed using the current measured state and the shifted input sequence. Although the objective function of the controller is based on the nominal model, the robustness constraints are imposed on all the elements models of $\mathbf{\Omega}$ thus assuring the robustness of the controller. In the ensuring section, we will demonstrate the feasibility of the shifted control sequence $\hat{U}_k$ at each time step k.

Remark: In the robustness constraint, $\bar{Q}_{(\theta_i)}$ is considered to account for all the possible plants in the set, which can be obtained from the positive self-adjoint solution of the discrete-time Lyapunov equation:

$$\mathcal{A}^*_d(\theta_i)\bar{Q}_{(\theta_i)}\mathcal{A}_d(\theta_i) - \bar{Q}_{(\theta_i)} = -\mathcal{C}^*_d(\theta_i)Q\mathcal{C}_d(\theta_i), i = 1, \cdots, p \tag{6.9}$$

or equivalently the continuous-time Lyapunov equation:

$$\mathcal{A}^*(\theta_i)\bar{Q}_{(\theta_i)} + \bar{Q}_{(\theta_i)}\mathcal{A}(\theta_i) = -\mathcal{C}^*(\theta_i)Q\mathcal{C}(\theta_i), i = 1, \cdots, p \tag{6.10}$$

on the dual space of X_{-1}.

Remark: At each sampling time k, the feasible plant cost (right hand side of Eq. 6.7d) is constant, and the optimal plant cost (left hand side of Eq. 6.7d) is a strictly convex function of the input U_k. The objective function in Eq. 6.7 is also convex,

which means that the RMPC algorithm is a convex program and there exist a unique optimal input U_k^*.

Remark: In the proposed RMPC framework, the current state is assumed to be known. When it comes to the real application, a state observer can be adopted in the controller, such as Luenberger observer, Kalman filter.

The given objective function and robustness constraint in Eq. 6.7 are quadratic and the remaining constraints are linear, therefore the proposed RMPC consists of a convex quadratically constrained quadratic program (QCQP), which can be written as:

$$\begin{aligned}
&\min_{U_k} \; U_k^T H_{\theta_n} U_k + 2U_k^T F_{\theta_n} x_{\theta_n,k} \\
&\text{s.t.} \;\; U_k^T H_{\theta_i} U_k + 2U_k^T F_{\theta_i} x_{\theta_i,k} \le \hat{U}_k^T H_{\theta_i} \hat{U}_k + 2\hat{U}_k^T F_{\theta_i} x_{\theta_i,k}, i = 1, \cdots p \\
&\qquad \begin{bmatrix} I \\ -I \\ G \\ -G \end{bmatrix} U_k \le \begin{bmatrix} U_{\max} \\ -U_{\min} \\ Y_{\max} - Sx_k \\ -Y_{\min} + Sx_k \end{bmatrix}
\end{aligned} \tag{6.11}$$

where $H_{\theta_i} \in \mathcal{L}(\mathcal{U}^N)$ is positive and self-adjoint, which is given by:

$$h_{m,n} = \begin{cases} \mathcal{D}_d^*(\theta_i) Q \mathcal{D}_d(\theta_i) + \mathcal{B}_d^*(\theta_i) \bar{Q} \mathcal{B}_d(\theta_i) + R & \text{for } m = n \\ \mathcal{D}_d^*(\theta_i) Q \mathcal{C}_d(\theta_i) \mathcal{A}_d^{m-n-1}(\theta_i) \mathcal{B}_d(\theta_i) + \mathcal{B}_d^*(\theta_i) \bar{Q} \mathcal{A}_d^{m-n}(\theta_i) \mathcal{B}_d(\theta_i) & \text{for } m > n \\ h_{n,m}^* & \text{for } m < n \end{cases} \tag{6.12}$$

and F_{θ_i} is given by

$$F_{\theta_i} = \{\mathcal{D}_d(\theta_i)^* Q \mathcal{C}_d(\theta_i) \mathcal{A}_d^{k-1}(\theta_i) + \mathcal{B}_d^*(\theta_i) \bar{Q} \mathcal{A}_d^k(\theta_i)\}_{k=1}^{N-1} \tag{6.13}$$

The matrix H_{θ_n} and F_{θ_n} in the cost function can be obtained by substituting the discrete operators $(\mathcal{A}_d(\theta_n), \mathcal{B}_d(\theta_n), \mathcal{C}_d(\theta_n), \mathcal{D}_d(\theta_n))$ of the nominal model into the expression of Eqs. 6.12 and 6.13.

The input and output constraints can be written in the form of linear inequality in Eq. 6.11. The matrix G is a lower triangular given by

$$g_{m,n} = \begin{cases} \mathcal{D}_d(\theta_i) & \text{for } m = n \\ \mathcal{C}_d(\theta_i) \mathcal{A}_d^{m-n-1}(\theta_i) \mathcal{B}_d(\theta_i) & \text{for } m > n \\ 0 & \text{for } m < n \end{cases}$$

and $S = \{\mathcal{C}_d(\theta_i) \mathcal{A}_d^{k-1}(\theta_i)\}_{k=1}^{N}$.

For the implementation, the obtained QCQP can be solved via nonlinear programming, or be further cast as the following second-order cone program (SOCP),

which, in turn, can be expressed as a semi-definite program (SDP) by writing constraints as a linear matrix inequality (LMI), which can be solved via SOCP or SDP solver. In this work, the interior point method [192] via fmincon function is utilized for implementation, which is one of the powerful general purpose solver.

$$
\begin{aligned}
&\min_{U_k,T} \; 2U_k^T F_{\theta_n} x_{\theta_n,k} + T \\
&\text{s.t.} \quad \left\| \begin{bmatrix} 2H_{\theta_n}^{\frac{1}{2}} U_k \\ T-1 \end{bmatrix} \right\|_2 \leqslant T+1 \\
&\quad \left\| \begin{bmatrix} 2H_{\theta_i}^{\frac{1}{2}} U_k \\ \hat{U}_k^T H_{\theta_i} \hat{U}_k + 2\hat{U}_k^T F_{\theta_i} x_{\theta_i,k} - 2U_k^T F_{\theta_i} x_{\theta_i,k} - 1 \end{bmatrix} \right\|_2 \leqslant \hat{U}_k^T H_{\theta_i} \hat{U}_k + 2\hat{U}_k^T F_{\theta_i} x_{\theta_i,k} \\
&\quad - 2U_k^T F_{\theta_i} x_{\theta_i,k} + 1, i = 1, \cdots p \\
&\quad \begin{bmatrix} I \\ -I \\ G \\ -G \end{bmatrix} U_k \leq \begin{bmatrix} U_{\max} \\ -U_{\min} \\ Y_{\max} - Sx_k \\ -Y_{\min} + Sx_k \end{bmatrix}
\end{aligned}
\tag{6.14}
$$

6.4 Properties of Systems Under RMPC

In this section, properties of systems under RMPC are discussed. Convergence to the equilibrium is proven by the monotonically decreasing of the optimal cost function.

Proposition 1. *If the proposed RMPC is feasible at time step k, the shifted control sequence $\hat{U}_{k+1}$ is the feasible solution at sampling time $k+1$.*

Proof. The optimal solution at time step k is $U_k^* = \{u_{k+0|k}^* \; u_{k+1|k}^* \cdots u_{k+N-1|k}^*\}$, and the corresponding optimal state trajectory is denoted as $X_k^* = \{x_{k+0|k}^* \; x_{k+1|k}^* \cdots x_{k+N-1|k}^*\}$, and the corresponding optimal output trajectory is $Y_k^* = \{y_{k+0|k}^* \; y_{k+1|k}^* \cdots y_{k+N-1|k}^*\}$.

The shifted control sequence at time step $k+1$ used in the robustness constraint Eq. (6.7d) is $\hat{U}_{k+1} = \{u_{k+1|k}^* \cdots u_{k+N-1|k}^* \; 0\}$. Since $(u_{k+n|k}^*)_{n=1}^{N-1} \in \mathcal{U}$, the input constraints is satisfied for $\hat{U}_{k+1}$. Similarly, the output constraints is satisfied for the corresponding shifted output trajectory $(y_{k+n|k}^*)_{n=1}^{N-1} \in \mathcal{Y}$. As no model perturbation is considered, by substituting the shifted control sequence into the discrete-time true plant model $\theta_t = [\mathcal{A}_{d_t} \; \mathcal{B}_{d_t} \; \mathcal{C}_{d_t} \; \mathcal{D}_{d_t}]$, the corresponding shifted state trajectory can be written as $\hat{X}_{k+1} = \{x_{k+1|k}^* \cdots x_{k+N-1|k}^* \; \mathcal{A}_d x_{k+N-1|k}^*\}$, and the corresponding shifted output trajectory is $\hat{Y}_{k+1}^* = \{y_{k+1|k}^* \cdots y_{k+N-1|k}^* \; \mathcal{C}_d x_{k+N-1|k}^*\} \in \mathcal{Y}$. Hence, the input and output constraints satisfaction is guaranteed.

We check the feasibility of the robustness constraint. If $J(U_{k+1},\theta_i)-J(\hat{U}_{k+1},\theta_i)\leq 0$, then $\hat{U}_{k+1}$ is a feasible solution. By using Lyapunov equation,

$$
\begin{aligned}
&J(\hat{U}_{k+1},\theta_i)\\
=&\sum_{j=0}^{N-2}\langle y^*_{k+j+1|k},Qy^*_{k+j+1|k}\rangle+\langle u^*_{k+j+1|k},Ru^*_{k+j+1|k}\rangle+\langle C_dx^*_{k+N-1|k},QC_dx^*_{k+N-1|k}\rangle\\
&+\langle \mathcal{A}_dx^*_{k+N-1|k},\bar{Q}\mathcal{A}_dx^*_{k+N-1|k}\rangle\\
=&\sum_{j=0}^{N-1}\langle y^*_{k+j|k},Qy^*_{k+j|k}\rangle+\langle u^*_{k+j|k},Ru^*_{k+j|k}\rangle+\langle x^*_{k+N-1|k},\bar{Q}x^*_{k+N-1|k}\rangle-\langle y_{k|k},Qy_{k|k}\rangle\\
&-\langle u_{k|k},Ru_{k|k}\rangle\\
=&J(U^*_k,\theta_i)-\langle y_{k|k},Qy_{k|k}\rangle-\langle u_{k|k},Ru_{k|k}\rangle
\end{aligned}
$$

As a result of Q and R are positive definite, we have $J(U_{k+1},\theta_i)-J(\hat{U}_{k+1},\theta_i)\leq 0$. Finally, it can be concluded that $\hat{U}_{k+1}$ is a feasible solution at time $k+1$. □

The following theorem shows that the control algorithm produced by the solution of Eq. 6.7 provides convergence of the true plant/system output to the origin.

Theorem 1. *The optimal plant cost $\bar{J}_k$ is monotonically decreasing along the predicted trajectory, and $\bar{J}^*_{k+1}-\bar{J}^*_k\leq-\langle y_{k|k},Qy_{k|k}\rangle-\langle u_{k|k},Ru_{k|k}\rangle$, and as a consequence, will converge to zero.*

Proof. Let us assume that we have found the optimal solution at the initial time step $k=0$, denoted as $U^*_0=\{u^*_{0|0}\ u^*_{1|0}\cdots u^*_{N-1|0}\}$. The corresponding optimal state trajectory and optimal output trajectory are denoted as $X^*_0=\{x^*_{0|0}\ x^*_{1|0}\cdots x^*_{N-1|0}\}$ and $Y^*_0=\{y^*_{0|0}\ y^*_{1|0}\cdots y^*_{N-1|0k}\}$, respectively.

At time step $k=0$, the optimal plant cost is given by

$$\bar{J}^*_0=\sum_{j=0}^{N-1}\langle y^*_{j|0},Qy^*_{j|0}\rangle+\langle u^*_{j|0},Ru^*_{j|0}\rangle+\langle x^*_{N-1|0},\bar{Q}x^*_{N-1|0}\rangle \tag{6.15}$$

Assume that the first optimal input $u^*_{0|0}$ is injected into the plant. The feasible input is taken as $\hat{U}_1=\{u^*_{1|0}\cdots u^*_{N-1|0}\ 0\}$, and the shifted state trajectory and output trajectory are written as $\hat{X}_1=\{x^*_{1|0}\cdots x^*_{N-1|0}\ \mathcal{A}_dx^*_{N-1|0}\}$, $\hat{Y}_0=\{y^*_{1|0}\cdots y^*_{N-1|0k}\ C_dx^*_{N-1|0}\}$,

respectively. The feasible plant cost at time step $k = 1$ can be written as

$$\begin{aligned}\hat{\bar{J}}_1 &= \sum_{j=1}^{N-1} \langle y^*_{j|0}, Q y^*_{j|0}\rangle + \langle u^*_{j|0}, R u^*_{j|0}\rangle + \langle C_d x^*_{N-1|0}, Q C_d x^*_{N-1|0}\rangle + \langle \mathcal{A}_d x^*_{N-1|0}, \bar{Q}\mathcal{A}_d x^*_{N-1|0}\rangle \\ &= \sum_{j=0}^{N-1} \langle y^*_{j|0}, Q y^*_{j|0}\rangle + \langle u^*_{j|0}, R u^*_{j|0}\rangle + \langle C_d x^*_{N-1|0}, Q C_d x^*_{N-1|0}\rangle + \langle \mathcal{A}_d x^*_{N-1|0}, \bar{Q}\mathcal{A}_d x^*_{N-1|0}\rangle \\ &\quad - \langle y_{0|0}, Q y_{0|0}\rangle - \langle u_{0|0}, R u_{0|0}\rangle\end{aligned} \tag{6.16}$$

Because for arbitrary $x \in D(A)$, it satisfy Lyapunov equation. Subtract 6.15 from 6.16 to obtain

$$\begin{aligned}\hat{\bar{J}}_1 - \bar{J}^*_0 &= \langle C_d x^*_{N-1|0}, Q C_d x^*_{N-1|0}\rangle + \langle \mathcal{A}_d x^*_{N-1|0}, \bar{Q}\mathcal{A}_d x^*_{N-1|0}\rangle - \langle x^*_{N-1|0}, \bar{Q} x^*_{N-1|0}\rangle \\ &\quad - \langle y_{0|0}, Q y_{0|0}\rangle - \langle u_{0|0}, R u_{0|0}\rangle \\ &= -\langle y_{0|0}, Q y_{0|0}\rangle - \langle u_{0|0}, R u_{0|0}\rangle\end{aligned} \tag{6.17}$$

Then we assume that the optimal solution is found at time $k = 1$. We know that the plant lies in the family $\mathbf{\Omega}$, so the robustness constraint must be satisfied for the actual plant at time $k = 1$. This implies that the optimal plant cost cannot exceed the feasible plant cost:

$$\bar{J}^*_1 - \hat{\bar{J}}_1 \leq 0 \tag{6.18}$$

Combine Eq. 6.17 with Eq. 6.18 to obtain

$$\bar{J}^*_1 - \bar{J}^*_0 \leq -\langle y_{0|0}, Q y_{0|0}\rangle - \langle u_{0|0}, R u_{0|0}\rangle \tag{6.19}$$

The same argument can be repeated for all the time steps to show that

$$\bar{J}^*_{k+1} - \bar{J}^*_k \leq -\langle y_{k|k}, Q y_{k|k}\rangle - \langle u_{k|k}, R u_{k|k}\rangle \tag{6.20}$$

As a result of Q and R are positive definite, the right hand side of Eq. 6.20 approaches zero and we have $\bar{J}^*_{k+1} \leq \bar{J}^*_k$. This shows that the optimal plant cost is monotonically decreasing along the predicted trajectory. Since the plant cost have zero lower bound, the left hand side of Eq. 6.20 converges to zero as $k \to \infty$. The input and output will converge to the origin as $k \to \infty$. □

6.5 Simulation Results

The purpose of this section is to apply the proposed control schemes and to evaluate their performances through simulation of a hyperbolic system and parabolic system respectively. The nominally stabilizing MPC [38], is implemented for performance comparison with the proposed RMPC. The parameter values in the simulation are adopted from the publication [106].

6.5.1 RMPC for hyperbolic system

In this section, we are interested in the construction of a discrete model for the convection dominated system, i.e., plug flow reactor. The Cayley-Tustin approach is applied to convert the first order hyperbolic PDE from a continuous to a discrete state space setting.

Considering the continuous model given by Eq. 6.1, which is the linear infinite-dimensional system model on the Hilbert space $L_2(0,1)$, the spatial operators are defined as follows:

$$\mathcal{A}_\theta(\cdot) = -v_\theta \frac{\partial(\cdot)}{\partial \zeta} + \psi_\theta(\zeta)(\cdot), \mathcal{B} = b(\zeta), \mathcal{C}(\cdot) = \int_0^l \delta(\zeta - l)(\cdot)\eta, \mathcal{D} = 0 \tag{6.21}$$

The spatial linear operator $\mathcal{A}_\theta(\cdot)$ with a domain $\mathcal{D}(\mathcal{A}_\theta) = \{\phi_\theta(\zeta) \in L_2(0,1) | \phi_\theta(\zeta)$ is abs. cont., $\frac{d\phi_\theta}{d\zeta} \in L_2(0,1), \phi_\theta(0) = 0\}$, where abs.cont. denotes that ϕ_θ is absolutely continuous. The output is taken as the state at the exit of the reactor, and one assume that the continuous model does not contain a feedthrough term. The discrete-time model can be obtained by applying Cayley-Tustin transformation presented in Section 6.2.2. The resolvent operator is obtained for the scalar hyperbolic system can be calculated through Laplace transform and expressed as follows:

$$\begin{aligned} \mathcal{R}(z,\delta)(\cdot) &= (\delta - \mathcal{A}_\theta)^{-1}(\cdot) \\ &= \left[\int_0^\zeta \frac{1}{v_\theta}(\cdot) e^{-\frac{1}{v_\theta}\int_0^\eta (\psi_\theta(\phi) - \delta) d\phi} d\eta \right] e^{\frac{1}{v_\theta}\int_0^\zeta (\psi_\theta(\phi) - \delta) d\phi} \end{aligned} \tag{6.22}$$

Substituting the resolvent operator into the expression of discrete time operators Eq.

6.4, one can obtain the discrete time model of Eq. 6.3.

$$\begin{aligned}
\mathcal{A}_d(\theta)(\cdot) &= [\delta I - \mathcal{A}_\theta]^{-1}[\delta I + \mathcal{A}_\theta](\cdot) \\
&= -I(\cdot) + 2\delta \left[\int_0^\zeta \frac{1}{v_\theta}(\cdot) e^{-\frac{1}{v_\theta}\int_0^\eta (\psi_\theta - \delta)d\phi} d\eta \right] e^{\frac{1}{v_\theta}\int_0^\zeta (\psi_\theta - \delta)d\phi} \\
\mathcal{B}_d(\theta) &= \sqrt{2\delta}[\delta I - \mathcal{A}_\theta]^{-1}\mathcal{B}(\zeta) \\
&= \sqrt{2\delta} \left[\int_0^\zeta \frac{1}{v_\theta}\mathcal{B}(\eta) e^{-\frac{1}{v_\theta}\int_0^\eta (\psi_\theta - \delta)d\phi} d\eta \right] e^{\frac{1}{v_\theta}\int_0^\zeta (\psi_\theta - \delta)d\phi} \\
\mathcal{C}_d(\theta)(\cdot) &= \sqrt{2\delta}\mathcal{C}[\delta I - \mathcal{A}_\theta]^{-1}(\cdot) \\
&= \sqrt{2\delta} \left[\int_0^l \frac{1}{v_\theta}(\cdot) e^{-\frac{1}{v_\theta}\int_0^\eta (\psi_\theta - \delta)d\phi} d\eta \right] e^{\frac{1}{v_\theta}\int_0^l (\psi_\theta - \delta)d\phi} \\
\mathcal{D}_d(\theta) &= \mathcal{C}[\delta I - \mathcal{A}_\theta]^{-1}\mathcal{B} + \mathcal{D} \\
&= \left[\int_0^l \frac{1}{v_\theta}\mathcal{B}(\eta) e^{-\frac{1}{v_\theta}\int_0^\eta (\psi_\theta - \delta)d\phi} d\eta \right] e^{\frac{1}{v_\theta}\int_0^l (\psi_\theta - \delta)d\phi}
\end{aligned} \tag{6.23}$$

To demonstrate successful application of the robust model predictive controller, the discretization time $h = 0.05$ is chosen, which implies that the $\delta = 40$, and $d\zeta = 0.01$ is chosen for numerical integration. A uniform state weight function in the Lyapunov function is chosen as $Q(\zeta) = 5$, and constant spatial function $B = 2$ and $R = 10$. The initial condition is $x_0 = 1 - cos(2\pi\zeta)$ and MPC horizon is 15. The constraints for the input and output are given as $-0.3 \leq y \leq 0.65$ and $-0.35 \leq u \leq 0.05$.

Before proceeding with the analysis of the properties of the proposed robust MPC, its use will be justified for this specific system through a performance comparison with the corresponding nominally stabilizing MPC when there is a model uncertainty. To this end, four linear models will comprise the set, including $v = 1, \phi = 0.5$ (model 1), $v = 5, \phi = 2$ (model 2), $v = 1.5, \phi = 0.5$ (model 3), $v = 0.8, \phi = 0.5$ (model 4). Here, the nominal model used in both MPC controllers is represented by model 2 and model 1 is assumed to represent the true process.

The resulting output and input responses are shown in Figs. 6.1. In this case, there is a clear superiority of the robust MPC over the nominal MPC, showing that the latter cannot satisfy the given output constraints when the controller considers model 2 to forecast the dynamic behavior of the controlled outputs. The state with RMPC is shown in Figure 6.2. Then, one can conclude that, although the nominal MPC provides nominal stability, there is no guarantee that stability will be preserved in the presence of a realistic model uncertainty.

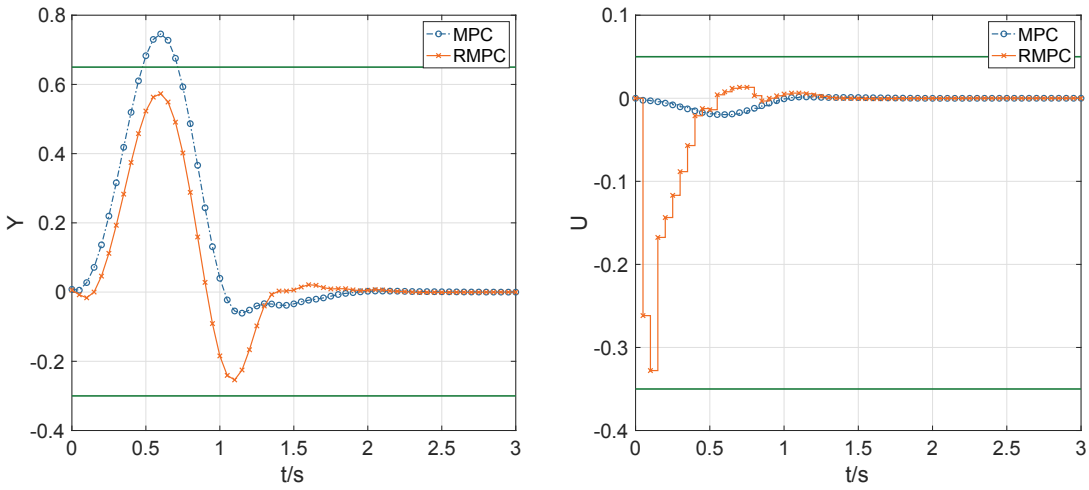

Figure 6.1: Comparison between the profile of a closed-loop system under the implementation of the nominal MPC and RMPC.

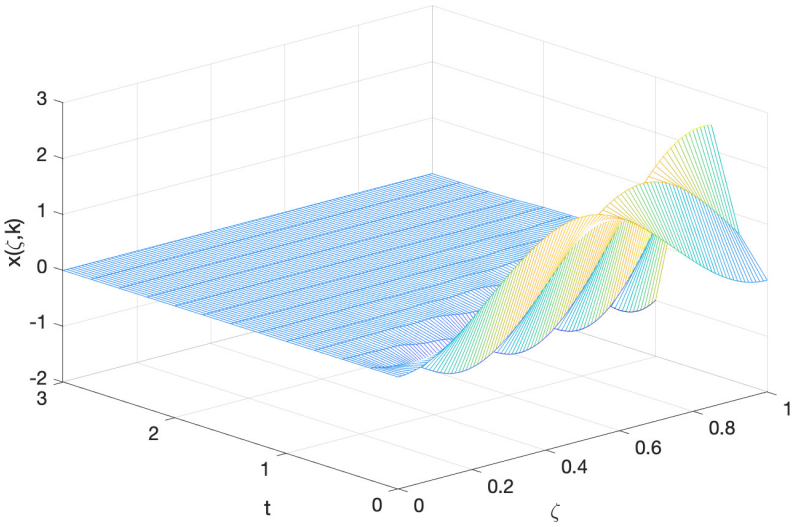

Figure 6.2: State profile evolution under the proposed RMPC.

6.5.2 RMPC for parabolic system

In this section, the diffusion dominated model of an axial dispersion reactor is considered, which is described by the parabolic PDE with Dirichlet boundary condition.

Similarly, it leads to the linear infinite-dimensional system model on the Hilbert

space $L_2(0,1)$, the spatial operators are defined as follows:

$$\mathcal{A}_\theta(\cdot) = v_\theta \frac{\partial^2(\cdot)}{\partial \zeta^2} + \psi_\theta(\zeta)(\cdot), \mathcal{B} = b(\zeta), C(\cdot) = \int_0^l \delta(\zeta - \zeta_0)(\cdot)\eta, \mathcal{D} = 0 \tag{6.24}$$

The spatial linear operator $\mathcal{A}_\theta(\cdot)$ with a domain $\mathcal{D}(\mathcal{A}_\theta) = \{\phi_\theta(\zeta) \in L_2(0,1) | \phi_\theta(\zeta)$ is abs. cont., $\frac{d\phi_\theta}{d\zeta} \in L_2(0,1), \frac{d^2\phi_\theta}{d\zeta^2} \in L_2(0,1), \phi_\theta(0) = 0 = \phi_\theta(1)\}$. The output is the state of the PDE at a point within the domain, i.e., at $\zeta = \zeta_0$. The operator $\mathcal{A}$ has eigenvalues $\lambda_n = -v_\theta n^2\pi^2 + \psi_\theta$ which determine stability of the system and associated eigenvectors $\phi_n(\zeta) = \sqrt{2}sin(n\pi\zeta), n \geq 1$. In the case when $\psi_\theta \leq v_\theta(n\pi)^2$, which implies that the $\lambda \leq 0$, the parabolic system with the Dirichlet boundary condition is always stable.

By performing Cayley-Tustin approach, one can obtain the resolvent operator, which is:

$$\begin{aligned}
\mathcal{R}(z,\delta)(\cdot) &= (\delta - \mathcal{A}_\theta)^{-1}(\cdot) \\
&= \frac{1}{\sqrt{s-\psi_\theta}} \frac{sinh(\sqrt{s-\psi_\theta}\zeta)}{sinh(\sqrt{s-\psi_\theta})} \int_0^1 (\cdot) sinh[\sqrt{s-\psi_\theta}(1-\eta)]d\eta \\
&- \int_0^\zeta \frac{1}{\sqrt{s-\psi_\theta}} (\cdot) sinh[\sqrt{s-\psi_\theta}(\zeta-\eta)]d\eta
\end{aligned} \tag{6.25}$$

With the described system resolvent operator, one can directly obtain the discrete time operators as follows:

$$\begin{aligned}
\mathcal{A}_d(\theta)(\cdot) &= [\delta I - \mathcal{A}_\theta]^{-1}[\delta I + \mathcal{A}_\theta](\cdot) \\
&= -I(\cdot) + 2\delta[\frac{1}{\sqrt{s-\psi_\theta}} \frac{sinh(\sqrt{s-\psi_\theta}\zeta)}{sinh(\sqrt{s-\psi_\theta})} \int_0^1 (\cdot) sinh[\sqrt{s-\psi_\theta}(1-\eta)]d\eta \\
&\quad - \int_0^\zeta \frac{1}{\sqrt{s-\psi_\theta}} (\cdot) sinh[\sqrt{s-\psi_\theta}(\zeta-\eta)]d\eta] \\
\mathcal{B}_d(\theta) &= \sqrt{2\delta}[\delta I - \mathcal{A}_\theta]^{-1}\mathcal{B}(\zeta) \\
&= \sqrt{2\delta}[\frac{1}{\sqrt{s-\psi_\theta}} \frac{sinh(\sqrt{s-\psi_\theta}\zeta)}{sinh(\sqrt{s-\psi_\theta})} \int_0^1 B sinh[\sqrt{s-\psi_\theta}(1-\eta)]d\eta \\
&\quad - \int_0^\zeta \frac{1}{\sqrt{s-\psi_\theta}} B sinh[\sqrt{s-\psi_\theta}(\zeta-\eta)]d\eta]
\end{aligned} \tag{6.26}$$

$$
\begin{aligned}
C_d(\theta)(\cdot) &= \sqrt{2\delta}C[\delta I - \mathcal{A}_\theta]^{-1}(\cdot) \\
&= \sqrt{2\delta}[\frac{1}{\sqrt{s-\psi_\theta}}\frac{sinh(\sqrt{s-\psi_\theta}\zeta)}{sinh(\sqrt{s-\psi_\theta})}\int_0^1(\cdot)sinh[\sqrt{s-\psi_\theta}(1-\eta)]d\eta \\
&\quad - \int_0^{\zeta_0}\frac{1}{\sqrt{s-\psi_\theta}}(\cdot)sinh[\sqrt{s-\psi_\theta}(\zeta_0-\eta)]d\eta] \\
\mathcal{D}_d(\theta) &= C[\delta I - \mathcal{A}_\theta]^{-1}\mathcal{B} + \mathcal{D} \\
&= \frac{1}{\sqrt{s-\psi_\theta}}\frac{sinh(\sqrt{s-\psi_\theta}\zeta)}{sinh(\sqrt{s-\psi_\theta})}\int_0^1 Bsinh[\sqrt{s-\psi_\theta}(1-\eta)]d\eta \\
&\quad - \int_0^{\zeta_0}\frac{1}{\sqrt{s-\psi_\theta}}Bsinh[\sqrt{s-\psi_\theta}(\zeta_0-\eta)]d\eta
\end{aligned}
\tag{6.27}
$$

In simulation, the actuation distribution function is given as $\mathcal{B} = 1$, $Q = 5$ and $R = 0.01$. Initial condition is assumed as $x_0 = -(\zeta - 0.5)^2 + 0.5^2$, and $h = 0.05$ with MPC horizon 5. The value of the terminal penalty is calculated by accounting for 5 eigenmodes, which is $n = m = 5$. The constraints on the input and the output are given as $0 \leq y \leq 0.3$ and $-0.16 \leq u \leq 0$. Four linear models comprise the set, including $\nu = 0.1, \psi = 8$ (model 1), $\nu = 1, \psi = 0.8$ (model 2), $\nu = 3, \psi = 3$ (model 3), $\nu = 0.5, \psi = 1$ (model 4). Here, the nominal model used in both MPC controllers is represented by model 2 and model 1 is assumed to represent the true process.

Figure 6.3 displays the dynamic behavior of the controlled outputs and manipulated inputs under the implementation of the nominal MPC and RMPC, respectively. It is apparent that the nominal MPC fails to stabilize the output at the origin, and over time, the closed-loop trajectory exhibits a slight divergence. In contrast, the RMPC is capable to steer the output to the origin with a fast converge rate even under uncertainty. The evolution of state profile of the closed-loop parabolic PDE system with the Dirichlet boundary condition is shown in Figure 6.4.

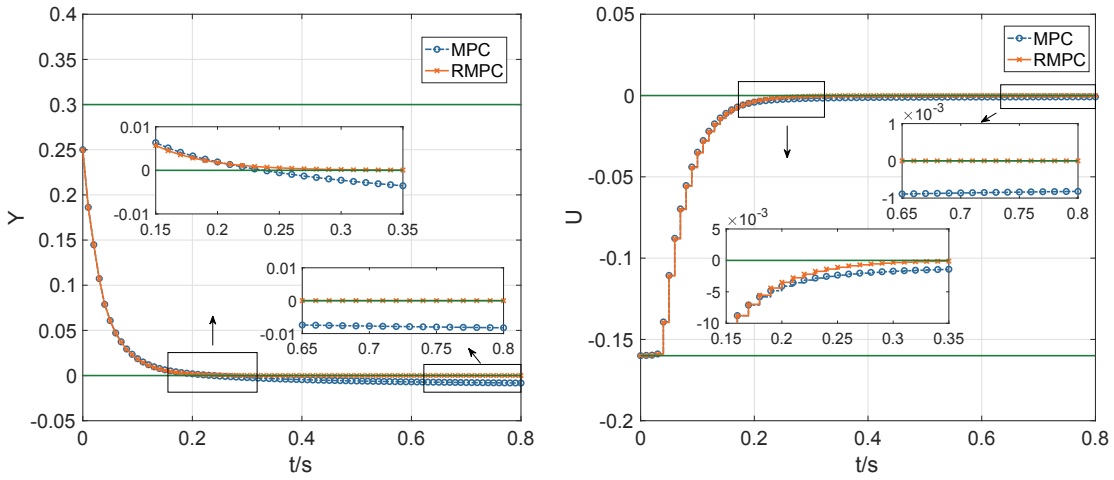

Figure 6.3: Comparison between the profile of a closed-loop system under the implementation of the nominal MPC and RMPC.

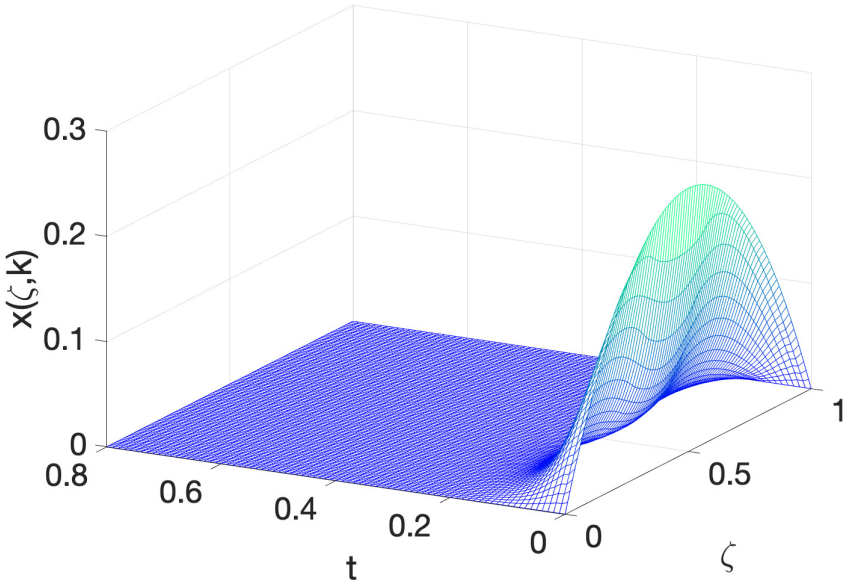

Figure 6.4: State profile evolution under the proposed RMPC.

6.6 Conclusions

In this chapter, a robust model predictive control synthesis was proposed, for constrained multi-model transport-reaction systems described by hyperbolic PDEs and parabolic PDEs. The optimization and control were carried out in the infinite spatial setting derived from accurate Cayley-Tustin transformation. The proposed algorithm

was based on restricting the future behavior of the controller cost function for each plant in the uncertainty description, and the properties of systems under the proposed RMPC were further discussed. The effectiveness was demonstrated through numerical simulation. The performance of the proposed method will be tested on large-scale DPS in future work, for example, to guarantee stabilization when there are some switching operations, such as the feedstock grade transition from hardwood to softwood.

Chapter 7

Conclusions and Future Work

7.1 Conclusions

This thesis investigates model predictive control and monitoring for large-scale distributed parameter chemical and petrochemical processes, taking into account physical constraints, varying operating demands, measurement noises/disturbances, and multi-plant uncertainty.

In Chapter 2, this thesis developed a MPC algorithms for a jacket tubular reactor as the distributed parameter system, considering the input and state constraints. The plant was described by a set of nonlinear coupled hyperbolic PDEs considering a simple reversible exothermic reaction taking place in the reactor. In particular, a spatially varying jacket temperature was considered instead of a constant one. After applying linearization around a given equilibrium operating point of interest, a linearized PDE model was obtained for modeling tubular reactor dynamics. For model time-discretization, the Cayley-Tustin transform was utilized to map the continuous-time system to the discrete-time model representation without spatial discretization and model reduction, which preserves the input-output stability of the plant. Model predictive controllers were formulated on that basis to realize model stabilization and account for the input and output constraints. For state estimation, an observer-based MPC realization was proposed and realized by solving the corresponding operator Riccati equation, which was utilized in the construction of Luenberger observer gains. Finally, two numerical examples were provided to demonstrate the feasibility of the proposed MPC design.

In Chapter 3, this thesis proposed a receding horizon control and estimation frame-

work and implemented for distributed parameter pipeline systems. The branched pipeline network was modelled by six linearized first-order coupled hyperbolic PDEs with boundary actuation. The Cayley-Tustin time discretization approach was applied to obtain the discrete-time infinite-dimensional model. To meet flow regulation within pipeline systems and handle physical constraints on inputs and outputs, a novel tracking MPC was designed. Furthermore, the MHE was applied in simultaneously estimating the spatial-temporal states and unknown parameters. Finally, the applicability and robustness of the proposed MPC and MHE designs were demonstrated via numerical examples.

In Chapter 4, this thesis developed the dynamic modeling and MPC design of a continuous pulp digester described by 10 linearized first-order coupled hyperbolic equations. The connected cook zone and wash zone of the digester were modeled as a cascade PDE system. Similarly, the Cayley–Tustin method was applied to obtain the discrete-time infinite-dimensional model. A Luenberger observer was designed to realize the state estimation of the system. The model predictive controller was formulated on that basis to realize target-tracking and account for input and output constraints during shift operations of the digester. The closed-loop simulation results demonstrated that the controlled variables were able to reach to the target values and satisfy the actuators' constraints simultaneously.

Chapter 5 investigated the state estimation and sensor placement for the stochastic continuous pulp digester with measurement delay were investigated from the monitoring point of view. In this case, we focused on the analysis of the temperature system of a continuous pulp digester which was modeled by two coupled hyperbolic partial differential equations and an ODE, and there exists the measurement delay at the considered outputs. In order to realize discrete implementation, the Cayley–Tustin transform was utilized. The discrete-time infinite-dimensional Kalman filter was applied to estimate the system states using the process measurements. The selection of sensor location was then addressed based on the estimator design and investigated by minimizing the variance of estimate error. The effectiveness and feasibility of the proposed Kalman filter were verified by a set of simulations, and this framework offers a planning and implementation view of distributed sensor locations in which a possible number of sensors and placement.

When it comes to industrial applications, the conventional MPC may lead to the predicted behavior is not identical to actual behavior in the presence of uncertainty. Motivated by this consideration, Chapter 6 explored the robust MPC strategy for distributed parameter transport-reaction systems, which properly accommodates the plant uncertainty. The model uncertainty under the DPS setting incorporated into the controller formulation was one based upon the multi-model infinite-dimensional setting. The proposed algorithm was based on restricting the future behavior of the controller cost function for each plant in the uncertainty description, and the properties of systems under the proposed RMPC were further discussed. The effectiveness was demonstrated in hyperbolic PDEs and parabolic PDEs through numerical simulation.

7.2 Future work

This thesis developed advanced and robust model predictive control and monitoring realizations for large-scale distributed parameter systems which are modelled from chemical and petrochemical processes. Nevertheless, there are still some open questions regarding this subject, and a number of them are briefly mentioned here.

Firstly, investigating the recirculation operation through external heat exchange in modeling the continuous pulp digester can provide a more precise understanding of the dynamics of each component during the cooking process. Additionally, studying pipeline systems that incorporate pumps or valves, monitoring multiple batches, and detecting and locating leaks would be meaningful for practical applications.

Secondly, exploring the development of robust MPC for linear parameter-varying infinite-dimensional systems, as well as systems with delays are definitely within the scope of future research. In addition, the implementation of robust MPC for complex systems is generally limited by the optimization problem, which is time-consuming and computationally expensive. The development of a novel efficient method to solve the RMPC optimization problem can be explored.

Thirdly, the exploration of sensor placement for DPS is still ongoing, and there is a need for a computationally efficient and reliable algorithm that can effectively select sensor locations from a wide range of candidate positions and determine the optimal number of sensors.

Bibliography

[1] Junyao Xie, Xiaodong Xu, and Stevan Dubljevic. Long range pipeline leak detection and localization using discrete observer and support vector machine. *AIChE Journal*, 65(7):e16532, 2019.

[2] Lu Zhang, Junyao Xie, and Stevan Dubljevic. Dynamic modeling and model predictive control of a continuous pulp digester. *AIChE Journal*, 68(3):e17534, 2022.

[3] Finn A Michelsen and Bjarne A Foss. A comprehensive mechanistic model of a continuous Kamyr digester. *Applied Mathematical Modelling*, 20(7):523–533, 1996.

[4] Moksadur Rahman, Anders Avelin, and Konstantinos Kyprianidis. An approach for feedforward model predictive control of continuous pulp digesters. *Processes*, 7(9):602, 2019.

[5] Weiguo Xie, Ioannis Bonis, and Constantinos Theodoropoulos. Data-driven model reduction-based nonlinear MPC for large-scale distributed parameter systems. *Journal of Process Control*, 35:50–58, 2015.

[6] Ole Morten Aamo. Leak detection, size estimation and localization in pipe flows. *IEEE Transactions on Automatic Control*, 61(1):246–251, 2015.

[7] Limei Ding, Andreas Johansson, and Thomas Gustafsson. Application of reduced models for robust control and state estimation of a distributed parameter system. *Journal of Process Control*, 19(3):539–549, 2009.

[8] W Harmon Ray. *Advanced Process Control*. McGraw- Hill, New York, 1981.

[9] Lanny D Schmidt. *The engineering of chemical reactions*. Oxford university press New York, 2005.

[10] Gilbert F Froment, Kenneth B Bischoff, and Juray De Wilde. *Chemical reactor analysis and design*, volume 2. Wiley New York, 1990.

[11] Thang Van Pham, Didier Georges, and Gildas Besançon. Predictive control with guaranteed stability for water hammer equations. *IEEE Transactions on Automatic Control*, 59(2):465–470, 2013.

[12] Junyao Xie. *Estimation, soft sensing and servo-control of linear distributed and lumped parameter systems*. PhD thesis, University of Alberta, 2021.

[13] Ville Havu and Jarmo Malinen. Laplace and Cayley transforms - an approximation point of view. In *Proceedings of the 44th IEEE Conference on Decision and Control*, pages 5971–5976. IEEE, 2005.

[14] Ville Havu and Jarmo Malinen. The Cayley transform as a time discretization scheme. *Numerical Functional Analysis and Optimization*, 28(7-8):825–851, 2007.

[15] David Q Mayne, James B Rawlings, Christopher V Rao, and Pierre OM Scokaert. Constrained model predictive control: Stability and optimality. *Automatica*, 36(6):789–814, 2000.

[16] James B Rawlings. Tutorial overview of model predictive control. *IEEE Control Systems Magazine*, 20(3):38–52, 2000.

[17] S Joe Qin and Thomas A Badgwell. A survey of industrial model predictive control technology. *Control Engineering Practice*, 11(7):733–764, 2003.

[18] James Blake Rawlings, David Q Mayne, and Moritz Diehl. *Model predictive control: theory, computation, and design*, volume 2. Nob Hill Publishing Madison, WI, 2017.

[19] Gene F Franklin, J David Powell, Michael L Workman, et al. *Digital control of dynamic systems*, volume 3. Addison-wesley Menlo Park, CA, 1998.

[20] Karl J Åström and Björn Wittenmark. *Computer-controlled systems: theory and design*. Courier Corporation, 2013.

[21] Claes Johnson. *Numerical solution of partial differential equations by the finite element method*. Courier Corporation, 2012.

[22] A Baaiu, F Couenne, Laurent Lefevre, Y Le Gorrec, and M Tayakout. Structure-preserving infinite dimensional model reduction: Application to adsorption processes. *Journal of Process Control*, 19(3):394–404, 2009.

[23] Redha Moulla, Laurent Lefevre, and Bernhard Maschke. Pseudo-spectral methods for the spatial symplectic reduction of open systems of conservation laws. *Journal of Computational Physics*, 231(4):1272–1292, 2012.

[24] Ngoc Minh Trang Vu, Laurent Lefevre, Rémy Nouailletas, and Sylvain Brémond. Symplectic spatial integration schemes for systems of balance equations. *Journal of Process Control*, 51:1–17, 2017.

[25] Panagiotis D Christofides and J Chow. Nonlinear and robust control of PDE systems: Methods and applications to transport-reaction processes. *Appl. Mech. Rev.*, 55(2):B29–B30, 2002.

[26] Ruth F Curtain and Anthony J Pritchard. *Infinite dimensional linear systems theory*. Springer, 1978.

[27] George Weiss and Hans Zwart. An example in linear quadratic optimal control. *Systems & Control Letters*, 33(5):339–349, 1998.

[28] Kirsten A Morris. *Controller Design for Distributed Parameter Systems*. Springer, 2020.

[29] Christopher I. Byrnes, István G Laukó, David S Gilliam, and Victor I Shubov. Output regulation for linear distributed parameter systems. *IEEE Transactions on Automatic Control*, 45(12):2236–2252, 2000.

[30] Vivek Natarajan, David S Gilliam, and George Weiss. The state feedback regulator problem for regular linear systems. *IEEE Transactions on Automatic Control*, 59(10):2708–2723, 2014.

[31] Junyao Xie, Charles Robert Koch, and Stevan Dubljevic. Discrete output regulator design for linear distributed parameter systems. *International Journal of Control*, 95(3):603–619, 2022.

[32] Junyao Xie, Charles Robert Koch, and Stevan Dubljevic. Discrete-time model-based output regulation of fluid flow systems. *European Journal of Control*, 57:1–13, 2021.

[33] Antonios Armaou and Panagiotis D Christofides. Robust control of parabolic PDE systems with time-dependent spatial domains. *Automatica*, 37(1):61–69, 2001.

[34] Yury V Orlov. *Discontinuous systems: Lyapunov analysis and robust synthesis under uncertainty conditions*. Springer Science & Business Media, 2008.

[35] Nael H El-Farra, Antonios Armaou, and Panagiotis D Christofides. Analysis and control of parabolic PDE systems with input constraints. *Automatica*, 39(4):715–725, 2003.

[36] Qingqing Xu and Stevan Dubljevic. Linear model predictive control for transport-reaction processes. *AIChE Journal*, 63(7):2644–2659, 2017.

[37] Stevan Dubljevic, Nael H El-Farra, Prashant Mhaskar, and Panagiotis D Christofides. Predictive control of parabolic PDEs with state and control constraints. *International Journal of Robust and Nonlinear Control: IFAC-Affiliated Journal*, 16(16):749–772, 2006.

[38] Stevan Dubljevic and Jukka-Pekka Humaloja. Model predictive control for regular linear systems. *Automatica*, 119:109066, 2020.

[39] Andrey Smyshlyaev and Miroslav Krstic. *Adaptive control of parabolic PDEs*. Princeton University Press, 2010.

[40] Henrik Anfinsen and Ole Morten Aamo. *Adaptive control of hyperbolic PDEs*. Springer, 2019.

[41] Rudolf Emil Kalman et al. Contributions to the theory of optimal control. *Bol. Soc. Mat. Mexicana*, 5(2):102–119, 1960.

[42] Rudolph Emil Kalman. A new approach to linear filtering and prediction problems. *Journal of Basic Engineering*, 82(1):35–45, 1960.

[43] Eduardo F Camacho and Carlos Bordons Alba. *Model predictive control*. Springer science & business media, 2013.

[44] Jacques Richalet, André Rault, JL Testud, and J Papon. Model predictive heuristic control. *Automatica*, 14(5):413–428, 1978.

[45] Stevan Dubljevic and Panagiotis D Christofides. Predictive control of parabolic PDEs with boundary control actuation. *Chemical Engineering Science*, 61(18):6239–6248, 2006.

[46] Stevan Dubljevic and Panagiotis D Christofides. Predictive output feedback control of parabolic partial differential equations (PDEs). *Industrial & Engineering Chemistry Research*, 45(25):8421–8429, 2006.

[47] Zhi Q Zheng and Manfred Morari. Robust stability of constrained model predictive control. In *1993 American Control Conference*, pages 379–383. IEEE, 1993.

[48] Márcio AF Martins and Darci Odloak. A robustly stabilizing model predictive control strategy of stable and unstable processes. *Automatica*, 67:132–143, 2016.

[49] Míriam R García, Carlos Vilas, Lino O Santos, and Antonio A Alonso. A robust multi-model predictive controller for distributed parameter systems. *Journal of Process Control*, 22(1):60–71, 2012.

[50] David G Luenberger. Observing the state of a linear system. *IEEE Transactions on Military Electronics*, 8(2):74–80, 1964.

[51] David Luenberger. An introduction to observers. *IEEE Transactions on Automatic Control*, 16(6):596–602, 1971.

[52] Ruth F Curtain and Hans Zwart. *An introduction to infinite-dimensional linear systems theory*, volume 21. Springer Science & Business Media, 2012.

[53] Junyao Xie, Qingqing Xu, Dong Ni, and Stevan Dubljevic. Observer and filter design for linear transport-reaction systems. *European Journal of Control*, 49:26–43, 2019.

[54] Jarinah Mohd Ali, N Ha Hoang, Mohamed Azlan Hussain, and Denis Dochain. Review and classification of recent observers applied in chemical process systems. *Computers & Chemical Engineering*, 76:27–41, 2015.

[55] Matthew J Tenny, James B Rawlings, and Stephen J Wright. Closed-loop behavior of nonlinear model predictive control. *AIChE Journal*, 50(9):2142–2154, 2004.

[56] Christopher V Rao, James B Rawlings, and Jay H Lee. Constrained linear state estimation—a moving horizon approach. *Automatica*, 37(10):1619–1628, 2001.

[57] Angelo Alessandri, Marco Baglietto, and Giorgio Battistelli. Receding-horizon estimation for discrete-time linear systems. *IEEE Transactions on Automatic Control*, 48(3):473–478, 2003.

[58] Angelo Alessandri and Moath Awawdeh. Moving-horizon estimation with guaranteed robustness for discrete-time linear systems and measurements subject to outliers. *Automatica*, 67:85–93, 2016.

[59] Jordan Jalving and Victor M Zavala. An optimization-based state estimation framework for large-scale natural gas networks. *Industrial & Engineering Chemistry Research*, 57(17):5966–5979, 2018.

[60] Kaarthik Sundar and Anatoly Zlotnik. State and parameter estimation for natural gas pipeline networks using transient state data. *IEEE Transactions on Control Systems Technology*, 27(5):2110–2124, 2018.

[61] Th J Harris, JF Macgregor, and JD Wright. Optimal sensor location with an application to a packed bed tubular reactor. *AIChE Journal*, 26(6):910–916, 1980.

[62] PC Müller and HI Weber. Analysis and optimization of certain qualities of controllability and observability for linear dynamical systems. *Automatica*, 8(3):237–246, 1972.

[63] Lewis Meier, John Peschon, and Robert Dressler. Optimal control of measurement subsystems. *IEEE Transactions on Automatic Control*, 12(5):528–536, 1967.

[64] Harold Joseph Kushner. *Introduction to stochastic control*. Holt, Rinehart and Winston New York, 1971.

[65] Marc Van De Wal and Bram De Jager. A review of methods for input/output selection. *Automatica*, 37(4):487–510, 2001.

[66] Umesh Vaidya, Rajeev Rajaram, and Sambarta Dasgupta. Actuator and sensor placement in linear advection PDE. In *2011 50th IEEE Conference on Decision and Control and European Control Conference*, pages 5395–5400. IEEE, 2011.

[67] Minxin Zhang and Kirsten Morris. Sensor choice for minimum error variance estimation. *IEEE Transactions on Automatic Control*, 63(2):315–330, 2017.

[68] Daniel WM Veldman, Rob HB Fey, Hans J Zwart, Marc MJ van de Wal, Joris DBJ van den Boom, and Hendrik Nijmeijer. Sensor and actuator placement for proportional feedback control in advection-diffusion equations. *IEEE Control Systems Letters*, 4(1):193–198, 2019.

[69] Dieter Armbruster, Simone Göttlich, and Michael Herty. A scalar conservation law with discontinuous flux for supply chains with finite buffers. *SIAM Journal on Applied Mathematics*, 71(4):1070–1087, 2011.

[70] JM Douglas and DWT Rippin. Unsteady state process operation. *Chemical Engineering Science*, 21(4):305–315, 1966.

[71] DWT Rippin. Recycle reactor as a model of incomplete mixing. *Industrial & Engineering Chemistry Fundamentals*, 6(4):488–492, 1967.

[72] JM Douglas and NY Gaitonde. Analytical estimates of performance of chemical oscillators. *Industrial & Engineering Chemistry Fundamentals*, 6(2):265–276, 1967.

[73] Joseph Sang-Il Kwon, Michael Nayhouse, Gerassimos Orkoulas, and Panagiotis D Christofides. Crystal shape and size control using a plug flow crystallization configuration. *Chemical Engineering Science*, 119:30–39, 2014.

[74] Ilyasse Aksikas, Joseph J Winkin, and Denis Dochain. Optimal LQ-feedback regulation of a nonisothermal plug flow reactor model by spectral factorization. *IEEE Transactions on Automatic Control*, 52(7):1179–1193, 2007.

[75] Ilyasse Aksikas, Joseph J Winkin, and Denis Dochain. Asymptotic stability of infinite-dimensional semilinear systems: Application to a nonisothermal reactor. *Systems & Control Letters*, 56(2):122–132, 2007.

[76] Liu Liu, Biao Huang, and Stevan Dubljevic. Model predictive control of axial dispersion chemical reactor. *Journal of Process Control*, 24(11):1671–1690, 2014.

[77] Anna Vasičkaninová, Monika Bakošová, Juraj Oravec, and Alajos Mészáros. Model predictive control of a tubular chemical reactor. In *2019 22nd International Conference on Process Control (PC19)*, pages 228–233. IEEE, 2019.

[78] Diogo Rodrigues, Julien Billeter, and Dominique Bonvin. Semi-analytical solutions for tubular chemical reactors. *Chemical Engineering Science*, 172:239–249, 2017.

[79] Hong Qian and Daniel A Beard. Thermodynamics of stoichiometric biochemical networks in living systems far from equilibrium. *Biophysical Chemistry*, 114(2-3):213–220, 2005.

[80] Yaşar Demirel. Modeling of thermodynamically coupled reaction-transport systems. *Chemical Engineering Journal*, 139(1):106–117, 2008.

[81] Denis Constales, Gregory S Yablonsky, Dagmar R D'hooge, Joris W Thybaut, and Guy B Marin. *Advanced data analysis and modelling in chemical engineering*. Elsevier, 2016.

[82] MM Denn. Optimal linear control of distributed systems. *Industrial & Engineering Chemistry Fundamentals*, 7(3):410–413, 1968.

[83] LB Koppel, Y-P Shih, and DR Coughanowr. Optimal feedback control of a class of distributed-parameter systems with space-independent controls. *Industrial & Engineering Chemistry Fundamentals*, 7(2):286–295, 1968.

[84] Dejan M Bošković and Miroslav Krstić. Backstepping control of chemical tubular reactors. *Computers & chemical engineering*, 26(7-8):1077–1085, 2002.

[85] Andrey Smyshlyaev and Miroslav Krstic. Backstepping observers for a class of parabolic PDEs. *Systems & Control Letters*, 54(7):613–625, 2005.

[86] Ilyasse Aksikas, Joseph J Winkin, and Denis Dochain. Optimal LQ-feedback control for a class of first-order hyperbolic distributed parameter systems. *ESAIM: Control, Optimisation and Calculus of Variations*, 14(4):897–908, 2008.

[87] Leily Mohammadi, Ilyasse Aksikas, Stevan Dubljevic, and J Fraser Forbes. Optimal boundary control of coupled parabolic PDE–ODE systems using infinite-dimensional representation. *Journal of Process Control*, 33:102–111, 2015.

[88] David WT Rippin. Simulation of single-and multiproduct batch chemical plants for optimal design and operation. *Computers & Chemical Engineering*, 7(3):137–156, 1983.

[89] Kai Sundmacher and Zhiwen Qi. Conceptual design aspects of reactive distillation processes for ideal binary mixtures. *Chemical Engineering and Processing: Process Intensification*, 42(3):191–200, 2003.

[90] Christos Georgakis. A model-free methodology for the optimization of batch processes: Design of dynamic experiments. *IFAC Proceedings Volumes*, 42(11):536–541, 2009.

[91] JL Testud, J Richalet, A Rault, and J Papon. Model predictive heuristic control: Applications to industial processes. *Automatica*, 14(5):413–428, 1978.

[92] Huilan Shang, J Fraser Forbes, and Martin Guay. Model predictive control for quasilinear hyperbolic distributed parameter systems. *Industrial & Engineering Chemistry Research*, 43(9):2140–2149, 2004.

[93] A Senthil Kumar and Zainal Ahmad. Model predictive control (MPC) and its current issues in chemical engineering. *Chemical Engineering Communications*, 199(4):472–511, 2012.

[94] Alejandro Marquez, Jairo José Espinosa Oviedo, and Darci Odloak. Model reduction using proper orthogonal decomposition and predictive control of distributed reactor system. *Journal of Control Science and Engineering*, 2013, 2013.

[95] Liangfeng Lao, Matthew Ellis, and Panagiotis D Christofides. Economic model predictive control of transport-reaction processes. *Industrial & Engineering Chemistry Research*, 53(18):7382–7396, 2014.

[96] Preet Joy, Kristina Rossow, Falco Jung, Hans-Ulrich Moritz, Werner Pauer, Alexander Mitsos, and Adel Mhamdi. Model-based control of continuous emulsion co-polymerization in a lab-scale tubular reactor. *Journal of Process Control*, 75:59–76, 2019.

[97] Victor M Zavala and Lorenz T Biegler. Optimization-based strategies for the operation of low-density polyethylene tubular reactors: nonlinear model predictive control. *Computers & Chemical Engineering*, 33(10):1735–1746, 2009.

[98] Pascal Dufour, Youssoufi Touré, Denise Blanc, and Pierre Laurent. On nonlinear distributed parameter model predictive control strategy: on-line calculation time reduction and application to an experimental drying process. *Computers & Chemical Engineering*, 27(11):1533–1542, 2003.

[99] Ioannis Bonis, Weiguo Xie, and Constantinos Theodoropoulos. A linear model predictive control algorithm for nonlinear large-scale distributed parameter systems. *AIChE Journal*, 58(3):801–811, 2012.

[100] Ruth F Curtain and Job Oostveen. Bilinear transformations between discrete- and continuous-time infinite-dimensional linear systems. In *Proceedings of the International Symposium MMAR'97, Miedzyzdroje, Poland*, pages 861–870, 1997.

[101] DR Hahn, LT Fan, and CL Hwang. Optimal startup control of a jacketed tubular reactor. *AIChE Journal*, 17(6):1394–1401, 1971.

[102] Ulises Badillo-Hernandez, Jesus Alvarez, and Luis Alvarez-Icaza. Efficient modeling of the nonlinear dynamics of tubular heterogeneous reactors. *Computers & Chemical Engineering*, 123:389–406, 2019.

[103] Ilyasse Aksikas. *Analysis and LQ-optimal control of infinite-dimensional semilinear systems: Application to a plug flow reactor*. PhD thesis, UCL, 2005.

[104] Kenneth R Muske and James B Rawlings. Model predictive control with linear models. *AIChE Journal*, 39(2):262–287, 1993.

[105] Marius Tucsnak and George Weiss. *Observation and control for operator semigroups*. Springer Science & Business Media, 2009.

[106] Qingqing Xu and Stevan Dubljevic. Model predictive control of solar thermal system with borehole seasonal storage. *Computers & Chemical Engineering*, 101:59–72, 2017.

[107] Kenneth R Muske. *Linear model predictive control of chemical processes*. PhD thesis, University of Texas at Austin, 1995.

[108] ARD Thorley and CH Tiley. Unsteady and transient flow of compressible fluids in pipelines—a review of theoretical and some experimental studies. *International Journal of Heat and Fluid Flow*, 8(1):3–15, 1987.

[109] Junyao Xie and Stevan Dubljevic. Discrete-time modeling and output regulation of gas pipeline networks. *Journal of Process Control*, 98:30–40, 2021.

[110] Henrik Anfinsen and Ole Morten Aamo. Disturbance rejection in the interior domain of linear 2×2 hyperbolic systems. *IEEE Transactions on Automatic Control*, 60(1):186–191, 2014.

[111] Henrik Anfinsen and Ole Morten Aamo. Leak detection, size estimation and localization in branched pipe flows. *Automatica*, 140:110213, 2022.

[112] Ajit Gopalakrishnan and Lorenz T Biegler. Economic nonlinear model predictive control for periodic optimal operation of gas pipeline networks. *Computers & Chemical Engineering*, 52:90–99, 2013.

[113] Kai Liu, Lorenz T Biegler, Bingjian Zhang, and Qinglin Chen. Dynamic optimization of natural gas pipeline networks with demand and composition uncertainty. *Chemical Engineering Science*, 215:115449, 2020.

[114] Jan-Frederik Mennemann, Lukas Marko, Jakob Schmidt, Wolfgang Kemmetmüller, and Andreas Kugi. Nonlinear model predictive control of a variable-speed pumped-storage power plant. *IEEE Transactions on Control Systems Technology*, 29(2):645–660, 2019.

[115] Nai-Yuan Chiang and Victor M Zavala. Large-scale optimal control of interconnected natural gas and electrical transmission systems. *Applied Energy*, 168:226–235, 2016.

[116] Kirsten Morris and W Levine. Control of systems governed by partial differential equations. *The Control Theory Handbook*, 2010.

[117] Junyao Xie, Jukka-Pekka Humaloja, Charles Robert Koch, and Stevan Dubljevic. Constrained receding horizon output estimation of linear distributed parameter systems. *IEEE Transactions on Automatic Control*, 2022.

[118] Jukka-Pekka Humaloja and Stevan Dubljevic. Setpoint tracking of exponentially stable linear hyperbolic systems using model predictive control. In *2022 American Control Conference (ACC)*, pages 3476–3481. IEEE, 2022.

[119] Lu Zhang and Stevan Dubljevic. Target tracking by model predictive control design for a pipeline system. In *2022 American Control Conference (ACC)*, pages 5368–5373. IEEE, 2022.

[120] Julian Berberich, Johannes Köhler, Matthias A Müller, and Frank Allgöwer. Linear tracking MPC for nonlinear systems—part i: The model-based case. *IEEE Transactions on Automatic Control*, 67(9):4390–4405, 2022.

[121] Sašo Blažič, Drago Matko, and Gerhard Geiger. Simple model of a multi-batch driven pipeline. *Mathematics and Computers in Simulation*, 64(6):617–630, 2004.

[122] H Prashanth Reddy, Shankar Narasimhan, S Murty Bhallamudi, and Saikot Bairagi. Leak detection in gas pipeline networks using an efficient state estimator. part-i: Theory and simulations. *Computers & Chemical Engineering*, 35(4):651–661, 2011.

[123] Marius Tucsnak and George Weiss. *Observation and control for operator semigroups*. Springer Science & Business Media, 2009.

[124] Ernst Hairer, Marlis Hochbruck, Arieh Iserles, and Christian Lubich. Geometric numerical integration. *Oberwolfach Reports*, 3(1):805–882, 2006.

[125] Jarmo Malinen, Olof Staffans, and George Weiss. When is a linear system conservative? *Quarterly of Applied Mathematics*, 64(1):61–91, 2006.

[126] Kenneth R Muske, James B Rawlings, and Jay H Lee. Receding horizon recursive state estimation. In *1993 American Control Conference*, pages 900–904. IEEE, 1993.

[127] Christopher V Rao, James B Rawlings, and David Q Mayne. Constrained state estimation for nonlinear discrete-time systems: Stability and moving horizon approximations. *IEEE Transactions on Automatic Control*, 48(2):246–258, 2003.

[128] Peter Kühl, Moritz Diehl, Tom Kraus, Johannes P Schlöder, and Hans Georg Bock. A real-time algorithm for moving horizon state and parameter estimation. *Computers & Chemical Engineering*, 35(1):71–83, 2011.

[129] Dan Sui, Le Feng, and Morten Hovd. Robust output feedback model predictive control for linear systems via moving horizon estimation. In *2008 American Control Conference*, pages 453–458. IEEE, 2008.

[130] Martin Gugat, Günter Leugering, Alexander Martin, Martin Schmidt, Mathias Sirvent, and David Wintergerst. MIP-based instantaneous control of mixed-integer PDE-constrained gas transport problems. *Computational Optimization and Applications*, 70:267–294, 2018.

[131] Florian D Brunner, Matthias A Müller, and Frank Allgöwer. Enhancing output-feedback MPC with set-valued moving horizon estimation. *IEEE Transactions on Automatic Control*, 63(9):2976–2986, 2018.

[132] Fatemeh Karimi Pour, Pablo Segovia, Lucien Etienne, and Eric Duviella. An mhe-based MPC strategy for simultaneous energy generation maximization and water level management in inland waterways. *IFAC-PapersOnLine*, 55(33):20–26, 2022.

[133] Pratima Bajpai. *Biermann's Handbook of Pulp and Paper: Volume 1: Raw Material and Pulp Making*. Elsevier, 2018.

[134] Moksadur Rahman, Anders Avelin, and Konstantinos Kyprianidis. A review on the modeling, control and diagnostics of continuous pulp digesters. *Processes*, 8(10):1231, 2020.

[135] M. Garside Publisher. Paper Industry - Statistics & Facts. `https://www.statista.com/statistics/1089078/demand-paper-globally-until-2030/`, 2021.

[136] Kun Liu, Hui Wang, Huayu Liu, Shuanxi Nie, Haishun Du, and Chuanling Si. Covid-19: Challenges and perspectives for the pulp and paper industry worldwide. *BioResources*, 15(3):4638–4641, 2020.

[137] Hyun-Kyu Choi and Joseph Sang-Il Kwon. Modeling and control of cell wall thickness in batch delignification. *Computers & Chemical Engineering*, 128:512–523, 2019.

[138] Pablo Domínguez de María. *Industrial biorenewables: a practical viewpoint*. John Wiley & Sons, 2016.

[139] C Smith. Studies of the mathematical modelling, simulation, and control of the operation of a Kamyr continuous digester for the kraft process. *Purdue University: West Lafayette, Indiana, USA*, 1974.

[140] Richard R Gustafson, Charles A Sleicher, William T McKean, and Bruce A Finlayson. Theoretical model of the kraft pulping process. *Industrial & Engineering Chemistry Process Design and Development*, 22(1):87–96, 1983.

[141] Niclas Andersson. *Modelling of kraft cooking kinetics using near infrared spectroscopy*. PhD thesis, Karlstad University Studies, 2003.

[142] Philip A Wisnewski, Francis J Doyle III, and Ferhan Kayihan. Fundamental continuous-pulp-digester model for simulation and control. *AIChE journal*, 43(12):3175–3192, 1997.

[143] Sharad Bhartiya, Pascal Dufour, and Francis J Doyle III. Fundamental thermal-hydraulic pulp digester model with grade transition. *AIChE journal*, 49(2):411–425, 2003.

[144] Tracy Clarke-Pringle and John F MacGregor. Reduced dimension control of dynamic systems. *Industrial & Engineering Chemistry Research*, 39(8):2970–2980, 2000.

[145] Mehmet Mercangoz and Francis J Doyle. Model-based control in the pulp and paper industry. *IEEE Control Systems Magazine*, 26(4):30–39, 2006.

[146] R Michaelsen, T Christensen, GG Lunde, and K Johansson. Model predictive control of a continuous Kamyr digester. *Pulp and Paper Canada*, 95:146–146, 1994.

[147] Jay H Lee and AK Datta. Nonlinear inferential control of pulp digesters. *AIChE journal*, 40(1):50–64, 1994.

[148] Philip A Wisnewski and Francis J Doyle III. A reduced model approach to estimation and control of a Kamyr digester. *Computers & Chemical Engineering*, 20:S1053–S1058, 1996.

[149] Alex Alexandridis and Haralambos Sarimveis. Nonlinear adaptive model predictive control based on self-correcting neural network models. *AIChE Journal*, 51(9):2495–2506, 2005.

[150] Hyun-Kyu Choi and Joseph Sang-Il Kwon. Multiscale modeling and control of kappa number and porosity in a batch-type pulp digester. *AIChE Journal*, 65(6):e16589, 2019.

[151] Hyun-Kyu Choi and Joseph Sang-Il Kwon. Multiscale modeling and multiobjective control of wood fiber morphology in batch pulp digester. *AIChE Journal*, 66(7):e16972, 2020.

[152] Hyun-Kyu Choi, Sang Hwan Son, and Joseph Sang-Il Kwon. Inferential model predictive control of continuous pulping under grade transition. *Industrial & Engineering Chemistry Research*, 60(9):3699–3710, 2021.

[153] Sang Hwan Son, Hyun-Kyu Choi, and Joseph Sang-Il Kwon. Application of offset-free koopman-based model predictive control to a batch pulp digester. *AIChE Journal*, 2021.

[154] Finn Are Michelsen. *A dynamic mechanistic model and model-based analysis of a continuous Kamyr digester*. Citeseer, 1995.

[155] J Funkquist. Grey-box identification of a continuous digester—a distributed-parameter process. *Control Engineering Practice*, 5(7):919–930, 1997.

[156] Limei Ding, Thomas Gustafsson, and Andreas Johansson. Physical model parameter estimation of a nonlinear process. In *2006 IEEE Conference on Computer Aided Control System Design, 2006 IEEE International Conference on Control Applications, 2006 IEEE International Symposium on Intelligent Control*, pages 2933–2938. IEEE, 2006.

[157] Jarmo Malinen, Olof Staffans, and George Weiss. When is a linear system conservative? *Quarterly of Applied Mathematics*, 64(1):61–91, 2006.

[158] Olof Staffans. *Well-posed linear systems*, volume 103. Cambridge University Press, 2005.

[159] Junyao Xie, Charles Robert Koch, and Stevan Dubljevic. Discrete output regulator design for linear distributed parameter systems. *International Journal of Control*, pages 1–17, 2020.

[160] David Kleinman. Stabilizing a discrete, constant, linear system with application to iterative methods for solving the riccati equation. *IEEE Transactions on Automatic Control*, 19(3):252–254, 1974.

[161] Huibert Kwakernaak and Raphael Sivan. *Linear optimal control systems*, volume 1. Wiley-interscience New York, 1972.

[162] Mayuresh V Kothare, Venkataramanan Balakrishnan, and Manfred Morari. Robust constrained model predictive control using linear matrix inequalities. *Automatica*, 32(10):1361–1379, 1996.

[163] Gabriele Pannocchia and James B Rawlings. Disturbance models for offset-free model-predictive control. *AIChE journal*, 49(2):426–437, 2003.

[164] Sasa V Rakovic and William S Levine. *Handbook of model predictive control*. Springer, 2018.

[165] Juyeong Jung, Hyun-Kyu Choi, Sang Hwan Son, Joseph Sang-Il Kwon, and Jay H Lee. Multiscale modeling of fiber deformation: Application to a batch pulp digester for model predictive control of fiber strength. *Computers & Chemical Engineering*, 158:107640, 2022.

[166] Moksadur Rahman, Erik Dahlquist, and Konstantinos Kyprianidis. Modelling and diagnostics of process faults in continuous pulp digesters. *Computers & Chemical Engineering*, 157:107589, 2022.

[167] Sang Hwan Son, Hyun-Kyu Choi, and Joseph Sang-Il Kwon. Multiscale modeling and control of pulp digester under fiber-to-fiber heterogeneity. *Computers & Chemical Engineering*, 143:107117, 2020.

[168] Sang Hwan Son, Hyun-Kyu Choi, Jiyoung Moon, and Joseph Sang-Il Kwon. Hybrid koopman model predictive control of nonlinear systems using multiple edmd models: An application to a batch pulp digester with feed fluctuation. *Control Engineering Practice*, 118:104956, 2022.

[169] Francis J Doyle III and Ferhan Kayihan. Reaction profile control of the continuous pulp digester. *Chemical Engineering Science*, 54(13-14):2679–2688, 1999.

[170] Alex Alexandridis, Haralambos Sarimveis, and George Bafas. Modeling and control of continuous digesters using the pls methodology. *Chemical Engineering Communications*, 191(10):1271–1284, 2004.

[171] Nitin Padhiyar, Akhil Gupta, Abhishek Gautam, Sharad Bhartiya, Francis J Doyle III, Sachi Dash, and Sujit Gaikwad. Nonlinear inferential multi-rate control of kappa number at multiple locations in a continuous pulp digester. *Journal of Process Control*, 16(10):1037–1053, 2006.

[172] Limei Ding, Thomas Gustafsson, and Andreas Johansson. Model parameter estimation of simplified linear models for a continuous paper pulp digester. *Journal of Process Control*, 17(2):115–127, 2007.

[173] K Pougatch, M Salcudean, and I Gartshore. A numerical model of the reacting multiphase flow in a pulp digester. *Applied Mathematical Modelling*, 30(2):209–230, 2006.

[174] Miroslav Krstic and Andrey Smyshlyaev. Backstepping boundary control for first-order hyperbolic PDEs and application to systems with actuator and sensor delays. *Systems & Control Letters*, 57(9):750–758, 2008.

[175] Hideki Sano. Stability analysis of heat exchangers with delayed boundary feedback. *Automatica*, 127:109540, 2021.

[176] Dan Simon. *Optimal state estimation: Kalman, H infinity, and nonlinear approaches*. John Wiley & Sons, 2006.

[177] Abhay K Singh and Juergen Hahn. Sensor location for stable nonlinear dynamic systems: Multiple sensor case. *Industrial & Engineering Chemistry Research*, 45(10):3615–3623, 2006.

[178] Yoshitatsu Mori, Ryuuzaburou Sueda, and Satoru Takeuchi. Pulp cooking control and wood species change control for a Kamyr continuous digester. In *SICE 2003 Annual Conference (IEEE Cat. No. 03TH8734)*, volume 1, pages 397–402. IEEE, 2003.

[179] Ivan FY Tello, Alain Vande Wouwer, and Daniel Coutinho. Early lumping observer design and sensor placement for transport-reaction systems. *Journal of Process Control*, 112:12–20, 2022.

[180] Jay H Lee and Zhenghong Yu. Worst-case formulations of model predictive control for systems with bounded parameters. *Automatica*, 33(5):763–781, 1997.

[181] Thomas A Badgwell. Robust model predictive control of stable linear systems. *International Journal of Control*, 68(4):797–818, 1997.

[182] Evanghelos Zafiriou. Robust model predictive control of processes with hard constraints. *Computers & Chemical Engineering*, 14(4-5):359–371, 1990.

[183] Evanghelos Zafiriou and Andre L Marchal. Stability of SISO quadratic dynamic matrix control with hard output constraints. *AIChE Journal*, 37(10):1550–1560, 1991.

[184] Sameer Ralhan and Thomas A Badgwell. Robust control of stable linear systems with continuous uncertainty. *Computers & Chemical Engineering*, 24(11):2533–2544, 2000.

[185] Darci Odloak. Extended robust model predictive control. *AIChE Journal*, 50(8):1824–1836, 2004.

[186] Zhi Qiang Alex Zheng. *Robust control of systems subject to constraints*. PhD thesis, California Institute of Technology, 1995.

[187] Hannah Michalska and David Q Mayne. Robust receding horizon control of constrained nonlinear systems. *IEEE Transactions on Automatic Control*, 38(11):1623–1633, 1993.

[188] James B Rawlings and Kenneth R Muske. The stability of constrained receding horizon control. *IEEE Transactions on Automatic Control*, 38(10):1512–1516, 1993.

[189] Dean E Kassmann, Thomas A Badgwell, and Robert B Hawkins. Robust steady-state target calculation for model predictive control. *AIChE Journal*, 46(5):1007–1024, 2000.

[190] L Mohammadi, S Dubljevic, and JF Forbes. Robust characteristic-based MPC of a fixed-bed reactor. In *Proceedings of the 2010 American Control Conference*, pages 4421–4426. IEEE, 2010.

[191] Jawad Ismail and Steven Liu. Tube-based robust model predictive control for a distributed parameter system modeled as a polytopic lpv (extended version). *arXiv preprint arXiv:2003.05962*, 2020.

[192] Miguel Sousa Lobo, Lieven Vandenberghe, Stephen Boyd, and Hervé Lebret. Applications of second-order cone programming. *Linear algebra and its applications*, 284(1-3):193–228, 1998.

Appendix

A.1 The derivations of $\mathcal{A}^*$ and $\mathcal{C}^*$

In system linearization, we need to determine the $\mathcal{A}^*$ and $\mathcal{C}^*$ beforehand based on the linearized continuous-time model in order to construct the model predictive controller. In this section, the derivations of $\mathcal{A}^*$ and $\mathcal{C}^*$are provided as following.

Let us recall the operator $\mathcal{A}(\cdot) = V\frac{\partial(\cdot)}{\partial\zeta} + A(\zeta)(\cdot)$ which on its domain

$$\begin{aligned}\mathcal{D}(\mathcal{A}) =&\{\psi_i(\zeta) \in L_2(0,1) | \psi_i(\zeta) \text{ is absolutely continuous, } \frac{d\psi_i}{d\zeta} \in L_2(0,1), \text{ with } i = 1,2,\\ &3,4, \text{ and } \psi_1(0) = 0, \psi_2(0) = 0, \psi_3(0) = 0, \psi_4(1) = 0\}\end{aligned} \tag{7.1}$$

It is easy to find the adjoint operator $\mathcal{A}^*$ using the inner product formula, $\langle \mathcal{A}\varphi_i, \phi_i\rangle = \langle \varphi_i, \mathcal{A}^*\phi_i\rangle$, as follows:

$$\begin{aligned}
&\langle \mathcal{A}\varphi_i, \phi_i\rangle \\
&= \langle (V\frac{\partial(\cdot)}{\partial\zeta} + A(\zeta)(\cdot))\varphi_i, \phi_i\rangle \\
&= \int_0^L (V\frac{\partial\varphi_i}{\partial\zeta} + A(\zeta)\varphi_i)\phi_i^* d\zeta \\
&= V\int_0^L \frac{\partial\varphi_i}{\partial\zeta}\phi_i^* d\zeta + \int_0^L A(\zeta)\varphi_i\phi_i^* d\zeta \\
&= V((\phi_i^*\varphi_i)|_0^L - \int_0^L \varphi_i\frac{\partial\phi_i^*}{\partial\zeta}d\zeta) + \langle A(\zeta)\varphi_i, \phi_i\rangle \\
&= V(\phi_1^*(L)\varphi_1(L) + \phi_2^*(L)\varphi_2(L) + \phi_3^*(L)\varphi_3(L) - \phi_4^*(0)\varphi_4(0)) + \langle \varphi_i, (-V\frac{\partial(\cdot)}{\partial\zeta}\phi_i)\rangle + \langle \varphi_i, A^*(\zeta)\phi_i\rangle \\
&= V(\phi_1^*(L)\varphi_1(L) + \phi_2^*(L)\varphi_2(L) + \phi_3^*(L)\varphi_3(L) - \phi_4^*(0)\varphi_4(0)) + \langle \varphi_i, (-V\frac{\partial(\cdot)}{\partial\zeta}\phi_i + A^*(\zeta))\phi_i\rangle
\end{aligned}$$

Therefore, one can obtain the follows

$$\mathcal{A}^*(\cdot) = -V\frac{\partial(\cdot)}{\partial\zeta} + A^*(\zeta)(\cdot) \tag{7.2}$$

which is defined by its domain

$$\mathcal{D}(\mathcal{A}^*) =\{\phi_i(\zeta) \in L_2(0,1), \phi_i(\zeta) \text{ is absolutely continuous, } \frac{d\phi_i}{d\zeta} \in L_2(0,1), \text{ with } i = 1,2,$$

$$3,4, \text{ and } \phi_1(1)=0, \phi_2(1)=0, \phi_3(1)=0, \phi_4(0)=0\} \tag{7.3}$$

Similarly, one can obtain the expression of the adjoint operator $\mathcal{C}^*$ of $\mathcal{C}$, where

$$\mathcal{C}(\cdot)=\text{diag}\{\int_0^L(\cdot)\delta(\zeta-L)d\zeta, \int_0^L(\cdot)\delta(\zeta-L)d\zeta, \int_0^L(\cdot)\delta(\zeta-L)d\zeta, \int_0^L(\cdot)\delta(\zeta)d\zeta\}$$

The derivations of $\mathcal{C}^*$ is given as follows:

$$\begin{aligned}
&\langle \mathcal{C}\varphi_i, \phi_i\rangle \\
&= \langle \begin{bmatrix} \int_0^L \varphi_1\delta(\zeta-L)d\zeta & 0 & 0 & 0 \\ 0 & \int_0^L \varphi_2\delta(\zeta-L)d\zeta & 0 & 0 \\ 0 & 0 & \int_0^L \varphi_3\delta(\zeta-L)d\zeta & 0 \\ 0 & 0 & 0 & \int_0^L \varphi_4\delta(\zeta-L)d\zeta \end{bmatrix}, \begin{bmatrix}\phi_1\\ \phi_2\\ \phi_3\\ \phi_4\end{bmatrix}\rangle \\
&= \begin{bmatrix} \int_0^L[\int_0^L \varphi_1(\zeta)\delta(\zeta-L)]d\zeta]\phi_1^*(\eta)d\eta & 0 \\ 0 & \int_0^L[\int_0^L \varphi_2(\zeta)\delta(\zeta-L)]d\zeta]\phi_2^*(\eta)d\eta \\ 0 & 0 \\ 0 & 0 \end{bmatrix} \\
&\qquad \begin{matrix} 0 & 0 \\ 0 & 0 \\ \int_0^L[\int_0^L \varphi_3(\zeta)\delta(\zeta-L)]d\zeta]\phi_3^*(\eta)d\eta & 0 \\ 0 & \int_0^L[\int_0^L \varphi_4(\zeta)\delta(\zeta)]d\zeta]\phi_4^*(\eta)d\eta \end{matrix} \\
&= \begin{bmatrix} \int_0^L \varphi_1(\zeta)[\delta(\zeta-L)][\int_0^L \phi_1^*(\eta)d\eta]d\zeta & 0 \\ 0 & \int_0^L \varphi_2(\zeta)[\delta(\zeta-L)][\int_0^L \phi_2^*(\eta)d\eta]d\zeta \\ 0 & 0 \\ 0 & 0 \end{bmatrix} \\
&\qquad \begin{matrix} 0 & 0 \\ 0 & 0 \\ \int_0^L \varphi_3(\zeta)[\delta(\zeta-L)][\int_0^L \phi_3^*(\eta)d\eta]d\zeta & 0 \\ 0 & \int_0^L \varphi_4(\zeta)[\delta(\zeta)][\int_0^L \phi_4^*(\eta)d\eta]d\zeta \end{matrix} \\
&= \langle \varphi_i, \mathcal{C}^*\phi_i\rangle
\end{aligned}$$

Thus,

$$\mathcal{C}^*(\cdot)=\text{diag}\{\delta(\zeta-L)\int_0^L(\cdot)d\eta, \delta(\zeta-L)\int_0^L(\cdot)d\eta, \delta(\zeta-L)\int_0^L(\cdot)d\eta, \delta(\zeta)\int_0^L(\cdot)d\eta\} \tag{7.4}$$

A.2 Link between discrete Lyapunov equation and continuous Lyapunov equation under the Cayley-Tustin time discretization frame

In the Section of Observer-based MPC in Chapter 2, it proposed that the solution Q_d can be find by solving the Discrete Lyapunov equation. However, the solution is

not straightforward in calculation, and therefore we need to solve the corresponding continuous Lyapunov equation in oder to get a stabilizing observer gain. Hence, we provide the demonstration of the link between discrete Lyapunov equation and continuous Lyapunov equation under the Cayley-Tustin time discretization frame.

$$\langle X, [\tilde{\mathcal{A}}_d^* Q_d \tilde{\mathcal{A}}_d - Q_d]X\rangle = -\langle X, [\tilde{C}_d^* N \tilde{C}_d]X\rangle \tag{7.5}$$

where $\tilde{\mathcal{A}}_d = -I(\cdot) + 2\delta[\delta I - \mathcal{A}_c]^{-1}, \tilde{C}_d = \sqrt{2\delta}C[\delta - \mathcal{A}_c]^{-1}$.

Let us substitute $\tilde{\mathcal{A}}_d$ and $\tilde{C}_d$, we have

$$\tilde{\mathcal{A}}_d^* Q_d \tilde{\mathcal{A}}_d - Q_d = -C_d^* N C_d$$
$$\{-[\delta I - \mathcal{A}_c]^* + 2\delta I\} Q_d \{-[\delta I - \mathcal{A}_c] + 2\delta I\} - [\delta I - \mathcal{A}_c]^* Q_d [\delta I - \mathcal{A}_c] = -2\delta C^* N C$$
$$[\delta I + \mathcal{A}_c^*] Q_d [\delta I + \mathcal{A}_c] - [\delta I - \mathcal{A}_c]^* Q_d [\delta I - \mathcal{A}_c] = -2\delta C^* N C$$
$$2\delta Q_d \mathcal{A}_c + 2\delta \mathcal{A}_c{}^* Q_d = -2\delta C^* N C$$
$$\mathcal{A}_c{}^* Q_d + Q_d \mathcal{A}_c = -C^* N C$$

where clearly becomes operator Lyapunov equation.

A.3 Resolvent operator in Eq. (3.21)

The resolvent operator in Eq.(3.21) is shown as below:

$$\mathcal{R}(s, \mathcal{A}^e) = [\mathcal{R}_{ij}(s, \mathcal{A}^e)]_{6\times 6} \tag{7.6}$$

where

$$\mathcal{R}_{i1}(s, \mathcal{A}^e)(\cdot) = \varepsilon_{i1}^{(1)}(\zeta, s)(\cdot) + M_{i1}\varrho_1, i = 1, 2$$
$$\mathcal{R}_{i2}(s, \mathcal{A}^e)(\cdot) = \varepsilon_{i2}^{(1)}(\zeta, s)(\cdot) + M_{i1}\varrho_2, i = 1, 2$$
$$\mathcal{R}_{i3}(s, \mathcal{A}^e)(\cdot) = M_{i1}^{(1)}(\zeta, s)(-cef_2 \frac{\varepsilon_{21}^{(2)}(l_2, s)}{M_{22}^{(2)}(l_2, s)})(\cdot), i = 1, 2$$
$$\mathcal{R}_{i4}(s, \mathcal{A}^e)(\cdot) = M_{i1}^{(1)}(\zeta, s)(-cef_2 \frac{\varepsilon_{22}^{(2)}(l_2, s)}{M_{22}^{(2)}(l_2, s)})(\cdot), i = 1, 2$$
$$\mathcal{R}_{i5}(s, \mathcal{A}^e)(\cdot) = M_{i1}^{(1)}(\zeta, s)(-cef_2 \frac{\varepsilon_{21}^{(3)}(l_3, s)}{M_{22}^{(2)}(l_2, s)})(\cdot), i = 1, 2$$
$$\mathcal{R}_{i6}(s, \mathcal{A}^e)(\cdot) = M_{i1}^{(1)}(\zeta, s)(-cef_2 \frac{\varepsilon_{22}^{(3)}(l_3, s)}{M_{22}^{(2)}(l_2, s)})(\cdot), i = 1, 2$$

$$\mathcal{R}_{i1}(s,\mathcal{A}^e)(\cdot)=\left(M^{(2)}_{j1}(\zeta,s)-\frac{M^{(2)}_{j2}(\zeta,s)M^{(2)}_{21}(l_2,s)}{M^{(2)}_{22}(l_2,s)}\right)\varepsilon^{(1)}_{11}(l_1,s)(\cdot),i=3,4,j=1,2$$

$$\mathcal{R}_{i2}(s,\mathcal{A}^e)(\cdot)=\left(M^{(2)}_{j1}(\zeta,s)-\frac{M^{(2)}_{j2}(\zeta,s)M^{(2)}_{21}(l_2,s)}{M^{(2)}_{22}(l_2,s)}\right)\varepsilon^{(1)}_{12}(l_1,s)(\cdot),i=3,4,j=1,2$$

$$\mathcal{R}_{i3}(s,\mathcal{A}^e)(\cdot)=-\frac{M^{(2)}_{j2}(\zeta,s)}{M^{(2)}_{22}(l_2,s)}\varepsilon^{(2)}_{21}(l_2,s)(\cdot)+\varepsilon^{(2)}_{j1}(\zeta,s)(\cdot),i=3,4,j=1,2$$

$$\mathcal{R}_{i4}(s,\mathcal{A}^e)(\cdot)=-\frac{M^{(2)}_{j2}(\zeta,s)}{M^{(2)}_{22}(l_2,s)}\varepsilon^{(2)}_{22}(l_2,s)(\cdot)+\varepsilon^{(2)}_{j2}(\zeta,s)(\cdot),i=3,4,j=1,2$$

$$\mathcal{R}_{i5}(s,\mathcal{A}^e)(\cdot)=\left(M^{(2)}_{j1}(\zeta,s)-\frac{M^{(2)}_{j2}(\zeta,s)M^{(2)}_{21}(l_2,s)}{M^{(2)}_{22}(l_2,s)}\right)$$
$$M^{(1)}_{11}(l_1,s)cef_2\frac{\varepsilon^{(3)}_{21}(l_3,s)}{M^{(3)}_{22}(l_3,s)}(\cdot),i=3,4,j=1,2$$

$$\mathcal{R}_{i6}(s,\mathcal{A}^e)(\cdot)=\left(M^{(2)}_{j1}(\zeta,s)-\frac{M^{(2)}_{j2}(\zeta,s)M^{(2)}_{21}(l_2,s)}{M^{(2)}_{22}(l_2,s)}\right)$$
$$M^{(1)}_{11}(l_1,s)cef_2\frac{\varepsilon^{(2)}_{22}(l_3,s)}{M^{(3)}_{22}(l_3,s)}(\cdot),i=3,4,j=1,2$$

$$\mathcal{R}_{i1}(s,\mathcal{A}^e)(\cdot)=\left(M^{(3)}_{j1}(\zeta,s)+\frac{M^{(3)}_{j2}(\zeta,s)M^{(2)}_{21}(l_2,s)}{M^{(2)}_{22}(l_2,s)}\right)$$
$$\varepsilon^{(1)}_{11}(l_1,s)(\cdot)+M^{(3)}_{j2}(\zeta,s)\varepsilon^{(1)}_{21}(l_1,s)(\cdot),i=5,6,j=1,2$$

$$\mathcal{R}_{i2}(s,\mathcal{A}^e)(\cdot)=\left(M^{(3)}_{j1}(\zeta,s)+\frac{M^{(3)}_{j2}(\zeta,s)M^{(2)}_{21}(l_2,s)}{M^{(2)}_{22}(l_2,s)}\right)$$
$$\varepsilon^{(1)}_{12}(l_1,s)(\cdot)+M^{(3)}_{j2}(\zeta,s)\varepsilon^{(1)}_{22}(l_1,s)(\cdot),i=5,6,j=1,2$$

$$\mathcal{R}_{i3}(s,\mathcal{A}^e)(\cdot)=\frac{M^{(3)}_{j2}(\zeta,s)}{M^{(2)}_{22}(l_2,s)}\varepsilon^{(2)}_{21}(l_2,s)(\cdot),i=5,6,j=1,2$$

$$\mathcal{R}_{i4}(s,\mathcal{A}^e)(\cdot)=\frac{M^{(2)}_{j2}(\zeta,s)}{M^{(2)}_{22}(l_2,s)}\varepsilon^{(2)}_{22}(l_2,s)(\cdot),i=5,6,j=1,2$$

$$\mathcal{R}_{i5}(s,\mathcal{A}^e)(\cdot)=\varepsilon^{(3)}_{j1}(\zeta,s)(\cdot),i=5,6,j=1,2$$

$$\mathcal{R}_{i6}(s,\mathcal{A}^e)(\cdot)=\varepsilon^{(3)}_{j2}(\zeta,s)(\cdot),i=5,6,j=1,2$$

and

$$\varepsilon_{i1}^{(k)}(\zeta,s)(\cdot)=\int_0^{\zeta}M_{i2}^{(k)}(\zeta-\eta,s)H_{21}(\cdot)d\eta$$

$$\varepsilon_{i2}^{(k)}(\zeta,s)(\cdot)=\int_0^{\zeta}M_{i1}^{(k)}(\zeta-\eta,s)H_{12}(\cdot)d\eta, i=1,2, k=1,2,3$$

$$cef_1=(M_{21}^{(2)}(l_2,s)/M_{22}^{(2)}(l_2,s)-M_{21}^{(3)}(l_3,s)/M_{22}^{(3)}(l_3,s))/(M_{21}^{(1)}(l_1,s)$$
$$+M_{11}^{(1)}(l_1,s)(M_{21}^{(2)}(l_2,s)/M_{22}^{(2)}(l_2,s)+M_{21}^{(3)}(l_3,s)/M_{22}^{(3)}(l_3,s)))$$

$$cef_2=1/(M_{21}^{(1)}(l_1,s)+M_{11}^{(1)}(l_1,s)(M_{21}^{(2)}(l_2,s)/M_{22}^{(2)}(l_2,s)+M_{21}^{(3)}(l_3,s)/M_{22}^{(3)}(l_3,s)))$$

$$\varrho_1=cef_1\varepsilon_{11}^{(1)}(\zeta,s)+cef_2\varepsilon_{21}^{(1)}(\zeta,s)$$

$$\varrho_2=cef_1\varepsilon_{12}^{(1)}(\zeta,s)+cef_2\varepsilon_{22}^{(1)}(\zeta,s)$$